Ribonucleases and Ribonuclease Inhibitors:

Structure, Function, and Evolution

by

Jo Ellen Lomax

A dissertation submitted in partial fulfillment of

the requirements for the degree of

Doctor of Philosophy

(Cellular and Molecular Biology)

at the

UNIVERSITY OF WISCONSON–MADISON

2014

Date of final oral examination: 5/1/2014

The dissertation is approved by the following members of the Final Oral Committee:

Ronald T. Raines, *Henry Lardy Professor of Biochemistry*, Biochemistry and Chemistry
Alan D. Attie, *Jack Gorski Professor of Biochemistry*, Biochemistry
Timothy J. Kamp, Professor, Medicine
Anne E. Griep, Professor, Cell and Regenerative Biology
Nader Sheibani, Professor, Ophthalmology and Visual Sciences

RIBONUCLEASES AND RIBONUCLEASE INHIBITORS: STRUCTURE, FUNCTION, AND EVOLUTION

Jo Ellen Lomax
Under the supervision of Professor Ronald T. Raines
at the University of Wisconsin–Madison

Pancreatic-type ribonucleases (ptRNases) comprise a class of highly conserved, vertebrate-specific, secretory endoribonucleases. They mediate diverse biological actions by catalyzing the cleavage of RNA, and their activities are naturally regulated by a ubiquitous cytosolic protein, ribonuclease inhibitor (RI). The prototype of this enzyme family, mammalian ribonuclease 1 (RNase 1), has been extremely well characterized structurally; still, little is known about its biological function *in vivo*. The goal of this thesis is to understand the endogenous functions of RNase 1 by a) analyses of recombinant proteins, b) interpretation of evolutionary patterns across species, and c) characterizing the absence of RNase 1 in a genetic model.

Until recently, little interest has been given to the biology of RNase 1. However, understanding the physiological roles of RNase 1 is becoming increasingly important as engineered forms of the enzyme are progressing through clinical trials. In CHAPTER 1, I summarize the large body of evidence indicating an important role for RNase 1 in human disease, and I describe several therapeutic applications of RNase 1. In CHAPTER 2, I highlight the innate characteristics of RNase 1 that enable its use as a protein-based drug, as well as efficacious modifications to further expand and exploit its therapeutic potential.

Progress toward elucidating the endogenous functions of RNase 1 have been hindered by the historical view that all mammalian RNase 1 homologs are identical to the well-studied bovine

protein, pancreatic RNase A. In CHAPTER 3, I upend this supposition by demonstrating that human RNase 1 functions most similarly to a paralogous bovine RNase 1, bovine brain RNase. These data illuminate the functional evolution of RNase 1 across species and shed light on the non-digestive roles of RNase 1 in mammals. Ribonuclease inhibitor is also evolving novel functions. In CHAPTER 4, I describe the structures and functions of the first reported non-mammalian RI proteins. Analysis of these proteins suggests that mammalian RIs are evolving greater oxidation sensitivity, and that intraspecies RI•RNase complexes are co-evolving to maintain binding affinity.

Mammalian RNase 1 is a secreted protein and primarily functions in the extracellular space. As such, study of systemic RNase 1 physiology requires a model mammalian system. Therefore, in CHAPTER 5 I describe the creation and characterization of an *Rnase1* knockout mouse, the first-ever knockout for a canonical member of the mammalian ptRNase family. Preliminary analyses of *Rnase1*$^{-/-}$ mice indicate a role for RNase 1 in regulation of extracellular RNA, coagulation, and metabolic imbalance.

Finally, CHAPTER 6 outlines several future directions of study to better understand the functional relationships between ptRNases and ribonuclease inhibitor. I also speculate on novel therapeutic applications for RNase 1 as an anticoagulant. Taken together, this thesis presents evidence for the evolving functional roles of mammalian RNase 1 and ribonuclease inhibitor, demonstrating important biological functions conserved across species.

Acknowledgements

I would like to express my sincere thanks to the many people who have made the work in this thesis possible. First and foremost, I would like to thank Professor Ronald T. Raines for allowing me to be a part of his research group and giving me the opportunity to pursue research in a world-class laboratory. Through my tenure in the Raines lab, I have evolved into a strong, independent scientist and thinker, and my capacity for both interpreting and communicating scientific data have developed enormously.

I am grateful to my many Raines lab colleagues, past and present, who have often given me their time and attention. Specifically, I thank Chelcie Eller for her hard work and dedication to our many research collaborations. Thanks also to Emily Garnett for her excellent management and continuation of our transgenic mouse project. I also thank Trish Hoang, Kristen Andersen, Christine Bradford, Cindy Chao, Caglar Tanrikulu, Matt Aronoff, and Connor Feldman for their continual support and assistance.

Several aspects of this thesis were outside the range of my own expertise, and I greatly appreciate the technical and intellectual guidance given to me by my collaborators. I am grateful to the experts at the University of Wisconsin–Madison Transgenic Animal Facility for their guidance during the construction of our knockout mouse. Thanks to Dr. Pat Powers, Manu John, David "Tug" Peterson, and Ryan Wachowiak for their technical assistance. I am also grateful to the dedicated staff from the UW–Biochemistry Vivarium—especially Dave Nehls—for their excellent care of our mouse colony. Thanks also to the wonderful staff at the UW–Madison Research Animal Resource Center (RARC) for their expertise and guidance, including Dr. Ruth Sullivan for pathology assistance and Dr. Ryan Stoffel for veterinary assistance.

Special thanks are due to the numerous structural biologists I've had the pleasure to

collaborate with. I am grateful to Dr. Chris Bianchetti, Dr. Aram Chang, Dr. Craig Bingman, Professor George Phillips, and Professor Brian Fox for their technical expertise and support. I am also grateful for the equipment and funding provided by the Center for Eukaryotic Structural Genomics (CESG) and the Department of Energy.

During the course of assembling my ribonuclease "zoo", I've received tissue samples from many generous investigators. Thanks to Professor Mark Cook for *G. gallus* tissue, Professor Hasan Khatib for *B. taurus* tissue, Professor Yevgenya Grinblat for *D. rerio* tissue, Dr. David Blehert from the USGS National Wildlife Health Center for *M. lucifugus* tissue, and Angela and Ben Gruber for *S. carolinensis* tissue. Thanks also to Professor Chuck Czuprynski for bovine endothelial cells

I sincerely thank the members of my thesis committee for their time, continued encouragement, and helpful suggestions over the years. Thanks very much to Professor Alan Attie, Professor Anne Griep, and Professor Nader Sheibani. Special thanks are due to Professor Tim Kamp, who was also my undergraduate research mentor and started me on my path to success.

Thanks very much to my graduate program, Cellular and Molecular Biology, for assistance and guidance. Special thanks to Michelle Holland and Jessica Karis, as well as Colleen Clary from the Biochemistry Department, for administrative support. Thanks also to Doreen Forslund, Julie Kennedy, Laura Vanderploeg, and Robin Davies for their consistently helpful support in administrative and maintenance issues: the Raines lab runs much more efficiently thanks to their valiant efforts.

As always, thanks very much to my friends and family for their love and support, which helped me navigate the tempestuous waters of graduate school.

Table of Contents

List of Tables

List of Figures

List of Abbreviations

ε	extinction coefficient
6-FAM	6-carboxyfluorescien
6-TAMRA	6-carboxytetramethylrhodamine
ACN	acetonitrile
ALS	Amyotrophic lateral sclerosis
ANG	angiogenin
ASA	accessible surface area
ATCC	American Type Culture Collection
BCA	bicinchoninic acid
BFP	blue fluorescent protein
BODIPY	4,4-difluoro-4-bora-3a,4a-diaza-s-indacene
BRB	bovine brain ribonuclease
BSA	bovine serum albumin
BSR; BS–RNase	bovine seminal ribonuclease
cDNA	complementary deoxyribonucleic acid
CHO	Chinese hamster ovary
CPP	cell-penetrating peptide
Da	dalton
ddH_2O	distilled, deionized water
DEFIA	2',7'-diethylfluorescein-5-iodoacetamide
DMF	dimethylformamide
DMSO	dimethylsulfoxide
DNA	deoxyribonucleic acid
DOPC	1,2-dioleoyl-sn-glycero-3-ethylphosphocholine
DSF	differential scanning fluorimetry

dsRNA	double-stranded ribonucleic acid
DTNB	5,5’-dithiobis(2-nitrobenzoic acid)
DTT	dithiothreitol
EAR	eosinophil-associated ribonuclease
ECP	eosinophil cationic protein; RNase 3
EDN	eosinophil-derived neurotoxin; RNase 2
EDTA	ethylenediaminetetraacetic acid
ETOH	ethanol
exRNA	extracellular ribonucleic acid
FACS	fluorescence-activated cell sorting
FBS	fetal bovine serum
FPLC	fast performance liquid chromatography
GFP	green fluorescent protein
h	hour
HCl	hydrochloric acid
HEPES	2[4-(2-hydroxyethyl)-l-piperazinyl]ethanesulfonic acid
HPLC	high-performance liquid chromatography
IC_{50}	half maximal inhibitory concentration
IFN	interferon
IPTG	isopropyl-1-thio-ß-D-galactopyranoside
k_a	kinetic association rate constant
k_{cat}	first-order enzymatic rate constant
k_d	kinetic dissociation rate constant
K_d	equilibrium dissociation constant
kDa	kilodalton
K_i	inhibitor dissociation constant
K_M	Michaelis constant

λ_{em}	emission wavelength
λ_{ex}	excitation wavelength
LB	Luria-Bertani medium
lncRNA	long non-coding ribonucleic acid
LRR	leucine-rich repeat
MALDI-TOF	matrix-assisted laser desorption/ionization time-of-flight
MES	2-(7V-morpholino)-ethanesulfonic acid
MEOH	methanol
min	minute
mRNA	messenger ribonucleic acid
miRNA	micro ribonucleic acid
NaCl	sodium chloride
NaOH	sodium hydroxide
ncRNA	non-coding ribonucleic acid
nt	nucleotide
OD	optical density
ONC	onconase
OVS	oligo(vinylsulfonic acid)
PCR	polymerase chain reaction
PBS	phosphate-buffered saline
PDB	protein data bank
PEG	polyethylene glycol
p*I*	isoelectric point
pKa	log of the acid dissociation constant
poly(A:U)	polyadenylic–polyuridylic acid
poly(C)	polycytidylic acid
poly(I:C)	polyinosinic–polycytidylic acid

ptRNase	pancreatic-type ribonuclease
qPCR	quantitative polymerase chain reaction
RFP	red fluorescent protein
RI	ribonuclease inhibitor
RMSD	root mean square deviation
RNA	ribonucleic acid
RNAi	ribonucleic acid interference
RNase	ribonuclease
ROS	reactive oxygen species
rRNA	ribosomal ribonucleic acid
s	second
snRNA	small nuclear ribonucleic acid
snoRNA	small nucleolar ribonucleic acid
ssRNA	single-stranded ribonucleic acid
SDS–PAGE	sodium dodecyl sulfate-polyacrylamide gel electrophoresis
t	time
TB	terrific broth medium
TLR	toll-like receptor
T_m	melting point
TNB	2-nitro-5-thiobenzoate
Tris	2-amino-2-(hydroxymethyl)- 1 ,3 -propanediol
tRNA	transfer ribonucleic acid
UV	ultraviolet
vWF	von Willebrand factor
WPB	Weibel–Palade body
Z	net molecular charge (Arg + Lys - Asp - Glu)

CHAPTER 1

Introduction:

Understanding Ribonuclease 1 and Ribonuclease Inhibitor *in vitro* and *in vivo*

1.1 Overview

RNA, along with DNA and proteins, comprises one of the three essential macromolecules of life. Since the 1950s, RNAs—namely messenger RNA (mRNA), ribosomal RNA (rRNA), and transfer RNA (tRNA)—have been known as keystones of gene expression and protein synthesis. Still, the mysteries of RNA continue to expand. The 1980s saw the surprising discoveries of catalytic RNA molecules (ribozymes), as well as novel non-coding RNA (ncRNA), such as small nuclear RNA (snRNA) and small nucleolar RNA (snoRNA). More recently, the field of ncRNA research has exploded with the discoveries of microRNA (miRNA), small interfering RNA (siRNA), and long non-coding RNA (lncRNA), and we now recognize that up to 97% of the eukaryotic transcriptome is non-coding.[1] These ncRNAs are not restricted to the intracellular space; indeed, small intact RNAs of different types have been detected in many body fluids.[2] While extracellular RNAs were first thought to be molecular debris released by cell lysis, there is now evidence that at least a fraction of circulating RNAs are actively secreted.[69] Far beyond the mere mechanics of transcription and translation, RNA accomplishes a remarkable variety of regulatory functions in most, if not all, cellular activities, ranging from gene expression to epigenetic modifications to the pathogenesis of various diseases.[3] The importance of RNA in diverse biological processes is becoming increasing evident.

In light of the dynamic array of RNA functions, the broad spectrum of RNA processing enzymes is not surprising. A single cell has been estimated to express as many as 20 distinct ribonucleases (RNases) with overlapping specificities.[4] Most of these RNases are intracellular and are remarkably conserved across all kingdoms of life. The catalytic ribozymes RNase MRP, RNase P, and RNase Z serve to process and mature tRNAs and other small ncRNAs.[5,6] The exosome-associated PH-like RNases perform multiple RNA-processing and turnover functions.[7]

RNase III family enzymes, including Drosha and Dicer, can process double-stranded RNA and play central roles in the biogenesis of miRNAs and siRNAs, as well as mRNA processing and rRNA maturation.[8] T2-type RNases function to regulate self and non-self RNAs in the endosomes and lysosomes and assist in rRNA turnover.[9] Members of the RNase H family function to cleave the RNA of RNA/DNA hybrids that form during replication and repair and prevent genomic instability.[10] RNase L is a latent cytosolic endoribonuclease that is activated by the cytokine interferon (IFN) and plays an essential role in the IFN-induced antiviral response in mammals.[11]

Apart from the intracellular RNases, there exist ribonucleases that are specially packaged and excreted from the cell. These secreted RNases are predicted to function in the extracellular space. Bacteria, fungi, and plants all possess multiple secreted RNases that serve various roles in host defense, self-incompatibility, and stress response.[12-14] Vertebrate animals, on the other hand, possess a distinct, conserved family of secreted RNases not known to occur in any other taxon. This unique group of enzymes is termed the pancreatic-type RNases (ptRNases) or, alternatively, the vertebrate secretory RNases. These enzymes are not homologous to any other class of eukaryotic RNases, and together constitute an extensive superfamily of proteins that has been the subject of intense biochemical, structural, and evolutionary studies for over half a century. They are united by a common structure, size, and enzymatic ability and, despite their diversity, they are all bound and inhibited by a conserved cytosolic protein, ribonuclease inhibitor (RI). Members of this enzyme superfamily demonstrate functions ranging from innate immunity to angiogenesis to neuroprotection and efforts are being undertaken to exploit these proteins as biologic drugs.

Herein, I review the current knowledge of this particular enzyme family, with emphasis on the history, biology, and utility of the prototypical member conserved across mammals, Ribonuclease 1 (RNase 1). Of all the ptRNases, RNase 1 has the most diverse and robust tissue expression. It also shows immense promise as a putative anticancer agent. Despite its abundance, evolutionary conservation, and therapeutic potential, its biological functions *in vivo* remain poorly understood.

1.2 Ribonuclease 1: A historical perspective

1.2.1 RNase A and the golden age of biochemistry

Much of what is known about RNase 1 has come from the painstaking characterization of the bovine homolog, RNase A (Figure 1.1). RNase A is considered to be the best characterized enzyme of the 20th century, and few enzymes have contributed so much to our knowledge of protein structure and function.[15] Its legendary status arose somewhat serendipitously, due to its extreme stability, high expression in the bovine pancreas, and subsequently easy purification. Case in point, RNase A can be purified to near homogeneity by boiling pancreatic tissue in sulfuric acid, thereby precipitating out almost all other macromolecules.[16] Following the pioneering work of Jones and Kunitz in the 1920s and 1930s,[16,17] the Armour meatpacking company forever changed the field of biochemistry by partnering with Harvard University in one of the original industrial–academic collaborations. Utilizing their huge surplus of bovine byproducts, the Armour company was able purify and crystallize over a kilogram of pure RNase A protein and distribute it—free of charge—to researchers around the world.

The ready availability of a pure, homogenous protein sample (quite difficult to obtain at the time) ushered in a wave of post-war scientific achievements, leading to the so-called "golden age of biochemistry".[18] These accomplishments included the first purification of a macromolecule by

ion-exchange chromatography (1951), the first NMR study of a protein (1957), the first amino acid sequence of an enzyme (1960), the first well-characterized enzyme mechanism (1961), the first chemical synthesis of an enzyme (1963), and the first x-ray crystal structure of an enzyme (1967). RNase A would go on to contribute to four Nobel prizes in Chemistry, forever shaping such fundamental biochemical landscapes as protein folding, thermodynamics, and structure prediction.[15]

As fascination with the physical and chemical properties of RNase 1 skyrocketed, interest in its potential biology tumbled. In his oft-cited report in *Nature*, Barnard declared RNase 1 to possess little relevant function outside of ruminant digestion, where he purported it served to degrade and recycle RNA produced by symbiotic gut bacteria. Indeed, he went on to label RNase 1 as "generally vestigial" with "very minor value to the animal".[19] So went the general consensus about RNase 1 biology for the next 40 years.

1.2.2 RNase 1 as a non-specific biomarker for disease

The use of RNase A as a model protein for biochemical studies crept steadily forward throughout the 1970s and 1980s; however, new interest in RNase 1 was forming in the medical community. Human RNase 1, the predominant ribonuclease in serum, urine, and cerebrospinal fluid, showed promise as a putative biomarker for various cancers. With robust catalytic activity, the presence of RNase 1 could easily be measured in body fluids simply by measuring degradation of an added RNA substrate. Excitement brewed for RNase 1 as a marker for pancreatic cancer, with multiple reports citing significant increases in ribonucleolytic activity in the sera of afflicted patients.[20-24] However, enthusiasm began to fade when further studies found significant increases in RNase activity from patients suffering from a large variety of cancers (Table 1.1). Further, increased RNase activity was present in the body fluids of patients with

myriad pathological conditions, ranging from infectious, degenerative, and autoimmune diseases to physical injury and metabolic conditions (Table 1.1 and Figure 1.2). Thus, RNase 1 was deemed a failed biomarker due to its lack of specificity for a single condition. Despite the overwhelming data implicating RNase 1 as a more general agent involved in inflammation and disease—and therefore deserving of further study—interest again waned in the enzyme and it fell back into obscurity.

Regardless of the missed opportunity to better understand the role of RNase 1 in disease, valuable knowledge did result from the clinical experiments of the 1970s and 1980s. A huge volume of clinical and animal data was amassed, allowing unprecedented insight into the biological activities of RNase 1. Further, efforts to better characterize the enzyme lead to discoveries about its genetic origins. Previously, it was believed that the RNase activity detected in various tissues originated from multiple separate enzymes differentially localized throughout the body. However, with the advent of southern blot analysis, it was determined that only one gene for RNase 1 could be detected in human DNA, indicating that all of the RNase 1 enzymes measured were actually the products of the same gene.[25,26] Emerging DNA technology also lead to increased phylogenetic studies of RNase 1 and its enzyme family members, resulting in the expansion of the pancreatic-type superfamily to include a diverse range of related proteins.

1.2.3 Discovery of ribonuclease inhibitor

A critical step in understanding the workings of pancreatic-type ribonucleases was the discovery of a potent, protein RNase inhibitor present in the cytosol of all mammalian cells. Ribonuclease inhibitor (RI) was first identified from the high-speed supernatant fraction of guinea pig liver homogenate, and was later found to be present in all tissues and cell types.[26] Its activity could be inactivated by proteases, heat, sulfhydryl-group modification, and changes in

pH. Initial attempts to isolate the protein were hampered by its sensitivity to air oxidation and freeze-thaw cycles; eventually, the invention of RNase-affinity chromatography allowed RI to be purified to homogeneity, enabling its biochemical characterization.[27-29]

Ribonuclease inhibitor from multiple mammalian species was found to bind extremely tightly to mammalian ptRNases, completely inhibiting their ribonucleolytic activity. Surprisingly, RI was not found to interact with any of the intracellular RNases present in cells, implying a specific functional role in regulating ptRNases. The abundance of such an effective inhibitor in the mammalian cytosol insinuated that pancreatic-type ribonucleases might exert their primary functions in either cellular compartments that exclude RI, or in the extracellular environment. Circumvention of the endogenous RI within human cells became a primary goal during the efforts to create cytotoxic variants of RNases (see below).

1.3 The vertebrate secretory RNase family tree

The pancreatic-type ribonucleases (ptRNases) comprise a class of highly conserved secretory endoribonucleases that mediate diverse biological actions by catalyzing the cleavage of RNA. The family has been well characterized structurally; however, it is functionally quite diverse and not particularly well understood. These secreted RNases are the only enzyme family that is vertebrate-specific.[30] All family members are extracellular proteins, are generally cationic, and share specific elements of sequence signature, a disulfide-bonded tertiary structure, and the ability to degrade RNA. Overall they display little substrate specificity, aside from a preference for pyrimidine nucleobases. Moreover, they possess small size, high stability, and are purported to serve a variety of diverse biological roles *in vivo*.[31] Phylogenetic reconstructions of ptRNases indicate that the family is rapidly evolving and expanding, and that many members are under positive selection for increased diversification (Figure 1.4).[30,32] Surprisingly, despite their

diversity, all human ptRNases that have been characterized (RNases 1–8) bind extremely tightly to human RI.[33] Accordingly, almost all of the putative biological actions attributed to these RNases hinge upon their ribonucleolytic activity, suggesting a regulatory role for RI toward the entire ptRNase family.

In humans, thirteen different ptRNases have been identified, and the genes are all located in a cluster on chromosome 14 (Figure 1.3).[34] For other mammals, the number is slightly different: 19 ptRNases in cattle (present on chromosome 10),[35] ~25 ptRNases in mice (present on chromosomes 14 and 10),[36] and ~19 ptRNases in rats (present on chromosome 15);[34] however, most mammalian ptRNases fall into one of several categories (Figure 1.4). Here, we review the recognized groups of mammalian ptRNases (excluding RNase 1, which we describe later), as well as the more divergent non-mammalian RNases.

1.3.1 The eosinophil-associated ribonucleases (RNases 2 and 3)

Eosinophils are a specialized type of white blood cell functioning in the innate immune system. In response to chemokine signals produced during infection, allergic reaction, or autoimmune response, eosinophils migrate into various epithelial tissues and release a number of effector proteins to neutralize pathogens.[37,38] Two of the major proteins in human eosinophil secretory granules are the closely related pair of ribonucleases, RNase 2 (also known as eosinophil-derived neurotoxin; EDN) and RNase 3 (also known as eosinophil cationic protein; ECP). Human RNase 2 has antiviral properties, and can also induce the recruitment and activation of dendritic cells.[39,40] Human RNase 3 possesses antibacterial, anti-helminthic, antiviral, and cytotoxic activities *in vitro*.[41,42] Interestingly, both RNases 2 and 3 require their ribonuclease activity to manifest the majority of their host defense properties.[43]

RNases 2 and 3 are among the most rapidly evolving genes in primates, and their homologs in rodents are evolving at an even faster rate.[43,44] The rodent eosinophil associated ribonucleases (EARs) are also found in the granules of eosinophils. They have close sequence similarity to human RNase 2 and 3, and have been previously proposed to play a role in host defense. At least 13 EAR proteins have been identified in mice and 8 have been identified in rats.[34] However, aside from their presence in eosinophils and their patterns of expression, their physiological roles are not very well understood. Various reports have noted antimicrobial and antiviral activity for various EARs, as well as chemotactic activity on dendritic cells. The large expansion of EARs in rodents might be attributable to differential evolution: Mice have evolved in a significantly different ecological niche than humans, where they have been exposed to different pathogens. They also have a significantly smaller size and shorter lifespan, which necessitate a divergent immune system.[45]

1.3.2 Ribonuclease 4 and the Angiogenins

Among the members of the vertebrate secretory RNases, ribonuclease 4 (RNase 1.4) is the most conserved across different mammalian species. While it is evolutionarily most similar to RNase 1, RNase 4 displays different substrate specificity—strongly preferring uridine to cytidine nucleobases—as well as lower overall catalytic activity. Its uniquely adapted active site pocket, together with its remarkable interspecies similarity, suggests a unique, conserved biological function in mammals. RNase 4 has highest expression in the liver, but is also secreted by a variety of cell types and circulates in plasma.[46,47] Interestingly, RNase 4 is often co-expressed with RNase 5, suggesting complementary or supplementary activities. Indeed, a recent study identified RNase 4 as possessing similar biological properties to RNase 5, including moderate angiogenic, neurogenic, and neuroprotective functions.[48]

Human ribonuclease 5 (RNase 5), also known as angiogenin, is a particularly dynamic member of the ptRNase family. It is expressed from many different tissues, and is present in the serum, yet possesses extremely low catalytic activity. RNase 5 seems to exert much of its biological function intracellularly. It is a potent inducer of new blood vessel formation *in vivo*, which requires its transport into the nucleus and subsequent action as a transcription factor.[49,50] The mechanism of RNase 5 nuclear transport, its RNA substrates within the cell, as well as its ability to evade the ribonuclease inhibitor, are not understood. Recently, mutations in RNase 5 were associated with the pathogenesis of amyotropic lateral sclerosis (ALS), and recombinant RNase 5 was shown to promote neurogeneration and neuroprotection.[51-54] RNase 5 also demonstrates antimicrobial activity *in vitro*.[55] In rodents and cattle, the gene encoding Angiogenin has undergone rapid expansion and these species contain multiple copies of Ang-like enzymes.[34,35] The biological imperative for this expanded rodent subgroup is not known.

1.3.3 Ribonucleases 6, 7, and 8

Ribonuclease 6 (RNase 6) was the sixth member of the human RNase family to be characterized and its biological roles have yet to be determined. Expression of RNase 6 has been detected in many tissues, with highest expression in the lung. It is also expressed by both neutrophils and monocytes, suggesting a possible role in host defense. RNase 6 possesses low ribonucleolytic activity, but little is known regarding its substrate preference.[31,56]

Conversely, ribonuclease 7 (RNase 7) has been well documented as an important antimicrobial agent in the human epithelium. RNase 7 is expressed in various epithelial tissues and organs, with highest expression in the skin. It is also present in the urine and urinary tract. It demonstrates strong antibacterial activity against a wide range of microbes, and the expression of

RNase 7 increases during infection, suggesting a regulated role in host defense.[55,57-59] The activities of RNase 7 are known to be dynamically controlled by ribonuclease inhibitor *in vivo*.[60]

Ribonuclease 8 (RNase 8) is another somewhat mysterious member of the ptRNase family. Phylogenetically, RNase 8 is very similar to RNase 7, suggesting the pair of enzymes might have originated from a relatively recent gene duplication. However, although they show a very high similarity in structure, their physiological functions seem to be quite different. RNase 8 has most of all the structural characteristics of mammalian ribonucleases, except for two rearranged cysteine residues. These differences may imply a novel formation of disulfide bonds, and subsequently a divergent fold from other paralogous proteins. RNase 8 expression has been detected in the placenta, spleen and lung. The enzyme possesses low catalytic activity, and may possess antimicrobial activity, although conflicting reports exist.[31,61,62]

1.3.4 Ribonucleases 9–13

The sequencing of the human genome lead to the discovery of several non-canonical members of the ptRNase superfamily. These proteins are less conserved than RNases 1–8 (only 15–30% identical) and are missing some key structural elements, such as conserved active-site residues and cysteines. Possibly, RNases 9–13 possess little to no ribonucleolytic activity, and may have divergent tertiary structures from the canonical ptRNases. They do, however, possess predicted peptide secretion sequences, suggesting they are secretory proteins. Intriguingly, non-canonical ptRNases possess a wide *p*I range, with some proteins having strongly negative charge (Figure 1.3). How such anionicity affects biological function, or ribonuclease inhibitor binding, is not known. Despite their divergence from other ptRNases, these proteins are conserved across mammals, suggesting an important biological role (Figure 1.4).

Ribonucleases 9 and 10 are expressed almost exclusively in the male reproductive tract, with highest expression in the epididymis.[63,64] Recent characterizations of knockout mouse models suggest that these enzymes play a role in sperm maturation and fertility. While RNase 9 is not necessary for fertility, its absence does impair sperm development.[65] Conversely, RNase 10 was found to be critical for sperm maturation and male fertility, as its absence in mouse model resulted in sterility.[66]

Much less is known about ribonucleases 11–13, the most recently identified members of the ptRNase family.[34] Although their expression levels vary by tissue type, data suggest that RNases 11-13 are expressed ubiquitously, suggesting important biological roles.[67] Based on expression of recombinant proteins, RNase 12 appears to have at least some ribonucleolytic activity.[67] RNase 13 was recently identified as corresponding to executive functioning resilience in patients with neurocognitive disorders.[68]

1.3.5 Non-mammalian ptRNases and the origin of the superfamily

While the majority of work has been focused on the characterization of mammalian ptRNases, recent efforts have begun to characterize homologous proteins in non-mammalian species (Figure 1.4). Thus far, the family has only been found in vertebrates, as database searches against the genomes of *Caenorhabditis elegans* and *Drosophila melanogaster,* as well as the urochordate *Ciona intestinalis* did not yield any significant matches.[34] Multiple homologous secretory RNases have been identified in amphibian species, specifically the northern leopard frog (*Rana pipiens*) and the bullfrog (*Rana catesbiana*).[69-71] These enzymes display much lower ribonucleolytic activity than most mammalian ptRNases. They are also resistant to inhibition by the mammalian ribonuclease inhibitor, imbuing them with cytotoxic activity against mammalian cells.[72]

Secretory ribonucleases have also been identified in avian and reptilian species, specifically three enzymes in chicken (*Gallus gallus*) and at least one enzyme in iguana (*Iguana iguana*).[34,73,74] Some of these enzymes were found to possess antimicrobial and angiogenic properties. Similarly, ptRNases have been identified in several bony fish species, including zebrafish (*Danio rerio*) and Atlantic salmon (*Salmo salar*). While having low overall ribonucleolytic activity, several of these fish enzymes also demonstrate antimicrobial and angiogenic properties.[75-78] Presently, efforts to locate ptRNase homologs in cartilaginous fish genomes, such as sharks, have been unsuccessful.[77]

Characterizing diverse lineages of the ptRNase family can help predict the evolutionary origins of secretory ribonucleases in vertebrates. Given the shared sequence structure and function of many non-mammalian RNases to the mammalian angiogenins, it is likely that RNase 5 represents the most ancient form of the mammalian enzyme, and that all other members arose during mammalian evolution. An intriguing hypothesis is that the superfamily originated as a host-defense/pro-growth mechanism during early vertebrate evolution and underwent massive functional expansion in mammals, resulting in the family's current diversity.

1.4 Ribonuclease 1: More than just a digestive enzyme

As the ptRNase family expanded to include enzymes with novel biological functions, the original family member, RNase 1, became increasingly obsolete. The assumption remained that RNase 1, the so-called "pancreatic ribonuclease", was a superfluous digestive enzyme. Still, mammalian pancreatic ribonuclease is expressed in a wide variety of tissues and is evolving rapidly.[26,79,80] While it is highly expressed in the pancreas and salivary glands of ruminants and species with ruminant-like digestion, its expression is much more ubiquitous in non-ruminant mammals. It has been speculated that ruminants have evolved a duplicate version of RNase 1

specifically adapted for digestion;[81] indeed, many ruminants and ruminant-like species possess multiple genes encoding slightly different versions of RNase 1.[35,82] Humans, mice, and most other mammalian species instead have only one such gene and the major function of the enzyme is not a digestive one.

RNase 1 is the most catalytically active of all the ptRNases and displays greater substrate versatility than most other ribonucleolytic enzymes.[83] Human RNase 1 is particularly elastic, efficiently hydrolyzing double-stranded (ds) RNA substrates as well as single-stranded substrates.[84,85] This intriguing property might be due to the presence of additional noncatalytic basic residues that cooperatively contribute to the binding and destabilization of the double-helical RNA molecule. These residues are present in the human protein and other closely related species, but absent in other mammalian homologs.[86]

Studies of RNase 1 *in vitro* and observations *in vivo* have provided clues about its potential biological role. In addition to its broad expression in almost all tissues examined, RNase 1 has been isolated from a large variety of bodily fluids.[79,87] RNase 1 circulates freely in the blood, at a concentration of approximately 400 ng/mL, and is the only known ribonuclease in plasma with high, nonspecific ribonucleolytic activity.[88-90] In culture, RNase 1 has been shown to activate dendritic cells—leading to the production of a variety of inflammatory cytokines, chemokines and growth factors—as well as suppress the replication of HIV in lymphocytes.[39,91] The ability of RNase 1 to degrade dsRNA may speak to a putative antiviral function, as most viruses produce antigenic dsRNA at some point in their replication. Indeed, serum RNase 1 activity increases during infection with RNA-viruses, including influenza and tick-borne encephalitis (Table 1.1). Thus, like its paralogous cousins, RNase 1 may play important roles in host defense.

1.4.1 RNase 1 is secreted from vascular endothelial cells in a regulated manner

The presence of RNase 1 in mammalian serum supports a role in host defense. Further, analyses of RNase 1 glycosylation patterns indicate the source of serum RNase1 to be vascular endothelial cells, which have been shown to secrete large amounts of RNase1 in culture.[92-95] These cells line the interior surface of blood vessels and are in direct contact with antigens and signaling molecules circulating in the blood. As a result, they modulate multiple biologic pathways, including coagulation and inflammation.[96] Endothelial cells from large and small blood vessels secrete the enzyme at a high rate, suggesting RNase 1 is expressed by several types of endothelium and is not organ specific.[95] Combining the measured rate of RNase 1 secretion for cultured cells with the estimated surface area of the endothelial lining in humans (~1000 m^2) predicts that up to many milligrams of RNase 1 might be secreted in the human body every day.[97,98]

RNase 1 secretion from endothelial cells is highly regulated. In response to stimuli such as thrombin or endotoxin, vascular endothelial cells can quickly release contents from cytosolic storage compartments into the blood.[99] These storage granules, known as Weibel-Palade bodies (WPBs), contain various proteins that regulate both hemostasis and inflammation, including von Willebrand factor (vWF), a procoagulant that mediates platelet aggregation, and P-selectin, an adhesion receptor that triggers leukocyte migration.[96] Interestingly, RNase1 co-localizes with both vWF and P-selectin in endothelial Weibel-Palade bodies, and can be spontaneously released by treatment with a known exocytosis-inducing agent.[89] Consequently, in response to pathogens or other antigenic stimuli, RNase 1 could be quickly secreted into blood, thereby serving to counteract the agent.

1.4.2 RNase 1 might exert its biological function through degradation of extracellular RNA

Serum levels of RNase 1 increase in many diseases (Table 1.1), and RNase 1 treatment has been shown to alleviate symptoms of inflammation and hypercoagulation *in vivo* (Table 1.2). The common link connecting these myriad pathological conditions may be the presence of excess extracellular RNA in the bloodstream (Figure 1.2). Extracellular RNA (exRNA) is a recently identified novel cofactor in human blood, contributing to coagulation, blood vessel permeability, cell-cell signaling, tumor progression and inflammation.[100-106] While the source of exRNAs remains unclear, they are believed to be small (<200nt) and are sometimes complexed with various proteins, lipids or metallic ions, which contribute to their stability and longevity in the blood.[2,100,107,108] Increased levels of exRNAs—often found in patients suffering from cancer and sepsis—may contribute to the hypercoagulable state often observed in various disorders.[103] exRNA can promote coagulation by activating enzymes in the clotting cascade, as well as providing a physical scaffold for clot formation.[109,110] exRNAs can also act as antigenic agents that promote inflammation and immune response. They are recognized by toll-like receptors (TLR) 3, 7 and 8, which are expressed inside the endosomes of endothelial and immune cells. Upon endosomal uptake of exRNA, TLR3 recognizes double-stranded RNA, and TLRs 7 and 8 recognize single-stranded RNA, leading to signaling cascades that result in the induction of various proinflammatory cytokines and chemokines.[111-113]

As the only known serum protein with high activity against nonspecific RNA, RNase 1 is a likely candidate to regulate exRNA *in vivo*. Indeed, exRNA degradation by RNase 1 may constitute a novel mechanism of vascular homeostasis. Importantly, treatment with exogenous RNase 1 reduced clot formation and alleviated symptoms in mouse models of both arterial thrombosis and stroke (Table 1.2).[109,114] Thus, RNase 1 might act as an extracellular RNA

scavenger contributing to the normalization of serum viscosity as well as nonspecific response to pathogenic RNA.

1.4.3 Differential glycosylation of RNase 1 might regulate its functions in vivo

RNase 1 is one of the most heavily glycosylated of all of the secretory RNases. Human RNase 1 possesses three sites for N-linked glycosylation (Asn-34, Asn-76, and Asn-88), whereas other mammalian species have fewer or greater number of sites.[30] Characterization of RNase 1 secreted from different tissues and cell types—including tumors—reveal completely different glycosylation patterns.[115-118] In human RNase 1, Asn-34 is almost always glycosylated in all tissues, while Asn-76 and Asn-88 have carbohydrates in about half and a minor part of molecules, respectively.[93] Glycosylation can confer particular advantages to RNases. Glycans, especially sialic-acid moieties, increase the circulating half-life of RNases.[119] *In vitro*, glycosylation has been shown to protect ptRNases from proteases, oxidation, and heat denaturation.[120-122] Potentially, glycosylation is under positive selection toward both increasing sites of attachment, as well as greater heterogeneity in sugar moieties.

Glycosylation could potentially confer an additional advantage to RNases *in vivo*. Based on structural analyses and molecular modeling, N-glycosylation of human RNase 1 at Asn-88 should endow RNase 1 with the ability to evade the mammalian ribonuclease inhibitor. An endogenous RI-evasive RNase could have enormous repercussions *in vivo*, as engineered variants of ptRNases are toxic to cancer cells (see below). Thus, glycosylation might be a natural mechanism to imbue ptRNases with novel biologic functions, such as an innate anti-cancer ability.

1.5 RNases as therapeutics

Uncovering new biological roles for ptRNases is a crucial step toward exploiting their unique biology therapeutically. Currently, engineered forms of RNase 1 are progressing through a phase I clinical trial for patients with solid tumors.[123-125] Efforts are also underway to utilize RNase 5 as a putative treatment for ALS and other disorders.[50] However, we currently lack understanding of several key mechanisms associated with these enzymes. Thus, it is imperative to continue to dissect the endogenous functions of these proteins *in vivo*, so that we might improve upon existing therapeutics or derive novel drugs for disease.

1.5.1 ptRNases as ideal protein drug candidates

Protein-based drugs are emerging as ideal drug candidates, providing a level of target-specificity and affinity not achievable with small molecules. Still, many proteins suffer from low stability and are readily degraded, overshadowing their applicability as effective therapeutics.[126] Secreted ribonucleases are especially well suited for exploitation as therapeutic agents.[127] They are small, extremely stable even in the harshest conditions, and can readily internalize into mammalian cells. Moreover, secreted RNases are not hampered by problems of production, storage, or administration. They are produced readily in microbial hosts and maintain their integrity in all extracellular fluids and tissues. Amazingly, ptRNases seemingly self-target and preferentially enter cancer cells over non-cancerous cells.[128,129] Moreover, ptRNases remain intact and active during endocytosis, and naturally translocate into the cytosol, thereby bypassing the need for artificial drug delivery strategies.[130] Coupled with engineered modifications to enhance cytotoxicity, ptRNases are excellent candidates for proteins drugs.

1.5.2 Therapeutic ptRNases: extracellular and intracellular action

The unique properties of ptRNases imbue them with multiple therapeutic modes of action. Indeed, RNase 1 can exert therapeutic effect both extracellularly and intracellularly, and both wild-type and engineered forms of RNase 1 have shown remarkable potential as therapeutic agents (Table 1.2). Outside of cells, circulating RNase 1 can degrade antigenic exRNA throughout the vasculature, thereby reducing the volume of immunogenic substances in the blood. However, RNase 1 is naturally drawn to the surface of cells, especially cancer cells. The cell surface is highly anionic due to the abundance of sulfate, phosphate, and carboxylate groups of its carbohydrates and lipids, and tumor cells are even more negatively charged than are homologous normal cells.[118] It is probable that positively charged RNase 1 binds to the cell surface through favorable Coulombic interactions.[131,132] After binding to the cell surface, RNase 1 is internalized through energy-dependent endocytosis, where it can continue to degrade exRNA, thus reducing the signaling cascades produced by endosomal toll-like receptors (Figure 1.5).[128] Indeed, RNase 1 might be specially adapted for activity inside endosomes, as it remains active and stable even under acidifying conditions, and can degrade multiple types of RNA. RNase 1 can also manifest therapeutic activity inside of cells. If RNase 1 is made resistant to the cytosolic ribonuclease inhibitor, either via naturally occurring mechanisms (glycosylation) or through rational engineering, it can degrade intracellular RNAs like tRNA, mRNA, and rRNA, resulting in apoptosis (Figure 1.5).[133] Thus, the therapeutic potential of RNase 1, as well as other ptRNases, is vast and dynamic.

1.5.3 Onconase and the era of RNase-based cancer therapeutics

The antitumoral activity of pancreatic-type ribonucleases was initially observed with Onconase® (ONC), an amphibian homolog of RNase 1 from the oocytes of the northern leopard frog, *Rana pipiens*. ONC has been postulated to play a role in host defense of developing embryos. It is both cytotoxic and cytostatic toward cultured tumor cells and inhibits the growth of xenograft tumors in mice.[134,135] ONC was granted both fast-track and orphan-drug status by the FDA.[136,137] Unfortunately, ONC was shown to cause renal toxicity in humans,[138] and the dose of ONC in a Phase 3 trial against malignant mesothelioma was much too low to achieve meaningful efficacy.[139]

Mammalian-based ptRNase protein drugs have had much more clinical success (Table 1.2), as they are markedly less immunogenic than ONC and are more efficient catalysts of RNA cleavage.[72,140-142] Mammalian ribonucleases can be endowed with cytotoxicity by evasion of RI binding through chemical modifications and site-directed mutagenesis. For example, cytotoxic variants of bovine RNase 1 have been created by disrupting the shape-complementarity within the RI•RNase molecular interface. In addition, cationization, multimerization, as well as conjugation to other proteins have also resulted in cytotoxic variants of mammalian ribonucleases through RI- evasion (Table 1.2).[33] An RI-evasive human RNase 1 variant is currently progressing through clinical trials, where it has shown dose-dependent amelioration of cancer progression without adverse off-target effects.[123-125] Hence, the development of future generations of mammalian ribonuclease-based anticancer agents is underway.

1.6 Ribonuclease Inhibitor

A key element in understanding the biological actions of RNase 1 and other ptRNases is to understand the biological activities of ribonuclease inhibitor (RI). RI is a ~50 kD, cytosolic

protein that tightly binds many members of the ptRNase family, but does not interact with either cytosolic RNases or highly divergent ptRNases, such as those from amphibians.[27] RI is tightly conserved in mammals, with homologs sharing significant sequence and structure similarity. Structurally, RI homologs consist entirely of leucine-rich repeats (LRRs), which give the proteins an overall horseshoe shape (Figure 1.6).[29] The LRR segments of RI evolved rapidly by exon duplication around the time of ribonuclease expansion, suggesting coevolution of the protein families.[143,144] RI has been detected in all cells, and the cytosolic concentration of RI has been estimated to be approximately 4 μM.[145] This relatively high protein concentration, coupled with the ubiquitious expression of RI mRNA in mammalian tissues, suggests an important biological role.

1.6.1 Ribonuclease inhibitor as an intracellular "sentry" to regulate ptRNases

Previous *in vitro* experiments with RI have led to several hypotheses about the role of RI *in vivo*. RNase A variants engineered to evade RI binding show a marked increase in cytotoxicity against various human tumor lines, and RNAi knockdown of RI increases these cytotoxic effects.[146] These findings, coupled with RI's cytosolic localization and ability to bind ptRNases with high affinity, suggest that RI exists as a sort of "sentry" within cells, protecting them from exogenous invasion by secretory RNases. Indeed, wildtype RNase A injected into frog oocytes—which do not contain a closely related homolog of RI—proved to be more potent than the toxin ricin at inhibiting protein synthesis and promoting cell death.[147] Moreover, *in vitro* overexpression of RI in various human cell lines provided protection against cytotoxic RNase A variants, further indicating the important link between the presence of RI and protection against ptRNases.[145]

Apart from providing protection from ptRNases, RI could also function to regulate their physiological activities. Particularly, RI may regulate the activities of RNase 5 (angiogenin). Angiogenin induces neovascularization of endothelial cells at femtomolar concentrations, and contributes to the growth and metastasis of solid tumors.[148] Angiogenin must enter the cell to exert its actions; therefore, any intracellular inhibitor that could regulate or terminate its activity should bind to angiogenin with very high affinity. Human RI binds human angiogenin with a subfemtomolar dissociation constant, suggesting a possible regulatory role.[148] *In vitro*, RI is effective at inhibiting angiogenin-mediated neovascularlization by abolishing both angiogenic and ribonucleolytic activities of angiogenin.[149] Further, low doses of human RI administered to xenografted mice inhibited the growth of various types of tumors and increased the lifespan of the recipient animals.[150] Therefore, a possible biological role of RI is to regulate angiogenesis through direct interaction with angiogenin.[151]

1.6.2 Ribonuclease inhibitor as a modulator of intracellular redox homeostasis

The overall cytosolic abundance of RI, as well as the presence of RI in some enucleated cells, suggests that RI may play a biological role apart from interaction with ptRNases. RI homologs contain 29-32 reduced cysteine residues. These cysteines are not involved in disulfide bond formation and are therefore readily oxidized. The presence of these highly conserved cysteine residues in RI homologs suggests a role in protection against cellular oxidative stress.[152] Previous *in vitro* analysis demonstrated that bovine RI could effectively scavenge a variety of reactive oxygen species (ROS) even more effectively than tea polyphenols, which are considered powerful antioxidants.[153] ROS are potentially damaging, transient chemical species formed in all cells as unwanted byproducts of normal aerobic metabolism. The role of ROS in human disease is becoming increasingly recognized, as they can attack biological molecules and induce cell or

tissue damage.[153] RI has been implicated as an important, possibly key, physiological protector of cells from oxidative stress, as evidenced by increased oxidant-induced DNA damage in cultured cells deprived of RI.[154] Overexpression of RI in rat glial cells resulted in increased cell survival after oxidative injury, suggesting an antioxidant role for RI. The same study found that administering excess human RI to mice protected against oxidative hepatic damage *in vivo.*[155] Interestingly, RI has been isolated from human erythrocytes and platelets. This finding is surprising considering that these cells are enucleated and no RNA metabolism by RNases is likely to occur.[156] High levels of RI relative to other tissues were observed in erythrocytes, an unexpected finding given RI's sensitivity to oxidation and the constant oxidative stress present in oxygen-transporting cells.[157] Therefore, a possible biological role for RI is to protect cells from oxidative damage by scavenging cytosolic reactive oxygen species.

1.7 Prospectus

Pancreatic-type ribonucleases, and RNase 1 in particular, have been extremely well characterized structurally. However, many mysteries remain regarding the biological functions of this enzyme family. For the past six decades, increased levels of serum RNase 1 have been associated with numerous diseases, disorders, and cancers. More recently, RNase 1 has shown promise as an emerging chemotherapeutic agent. Beyond RNase 1, RNase 5 has been associated with neurodegenerative disorders like ALS and Parkinson's disease, and RNases 2 and 3 have been associated with infectious diseases and asthma. Therefore, it is imperative to understand the underlying mechanisms of action of these enzymes so that we might better design therapeutic strategies to both target and exploit their functionalities.

The central aim of this thesis is to demonstrate the dynamic biological potential of RNase 1 by illustrating its remarkable properties *in vitro* and *in vivo*. Specifically, we address the functional evolution and adaptation of RNase 1 across mammals, and use these data to speculate on the changing roles of RNase 1 in vertebrates. We also establish a genetic model to study the systemic role of RNase 1 in a mammal. Importantly, we also focus on the functional evolution of ribonuclease inhibitor, demonstrating the emergence of new dynamic properties. Taken together, this thesis provides an intriguing view into the structure, function, and evolution of both RNase 1 and ribonuclease inhibitor, and paves the way for further discoveries and insights into this remarkable protein duo.

Figure 1.1

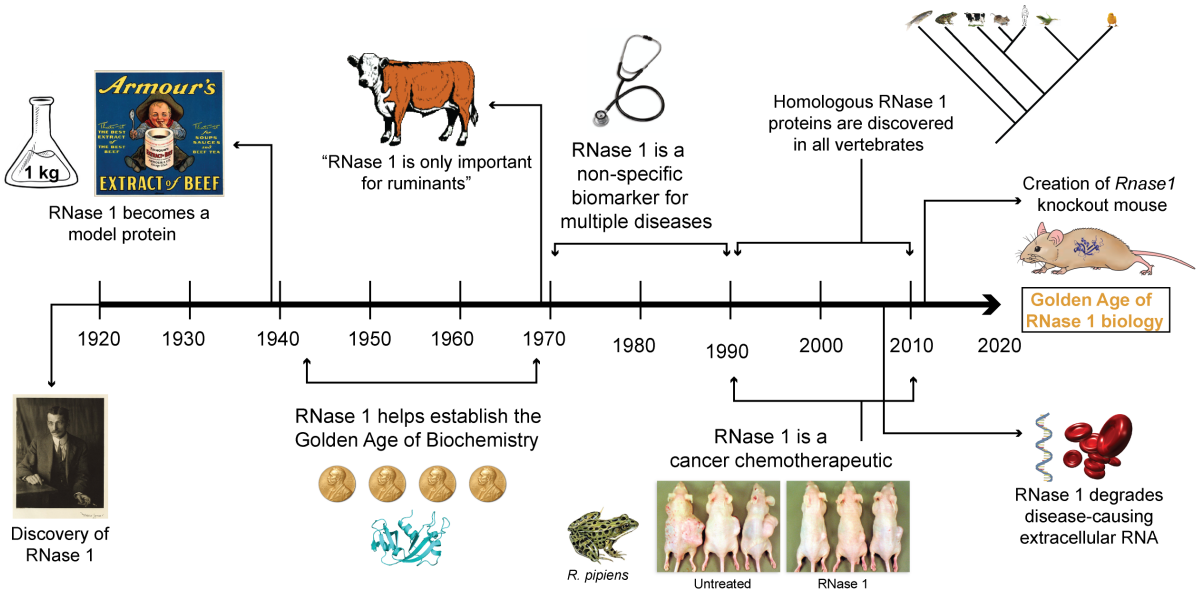
1 kg
Armour's
EXTRACT of BEEF
RNase 1 becomes a model protein
"RNase 1 is only important for ruminants"
RNase 1 is a non-specific biomarker for multiple diseases
Homologous RNase 1 proteins are discovered in all vertebrates
Creation of Rnase1 knockout mouse
Golden Age of RNase 1 biology
1920
1930
1940
1950
1960
1970
1980
1990
2000
2010
2020
Discovery of RNase 1
RNase 1 helps establish the Golden Age of Biochemistry
R. pipiens
RNase 1 is a cancer chemotherapeutic
Untreated
RNase 1
RNase 1 degrades disease-causing extracellular RNA

Figure 1.1 Ribonuclease 1: A historical perspective

History of the biochemical, medical, and evolutionary achievements associated with Ribonuclease 1 (RNase 1), beginning with its initial discovery and characterization and ending with the current work described in this thesis, including the generation of an *Rnase1* knockout mouse.

Figure 1.2

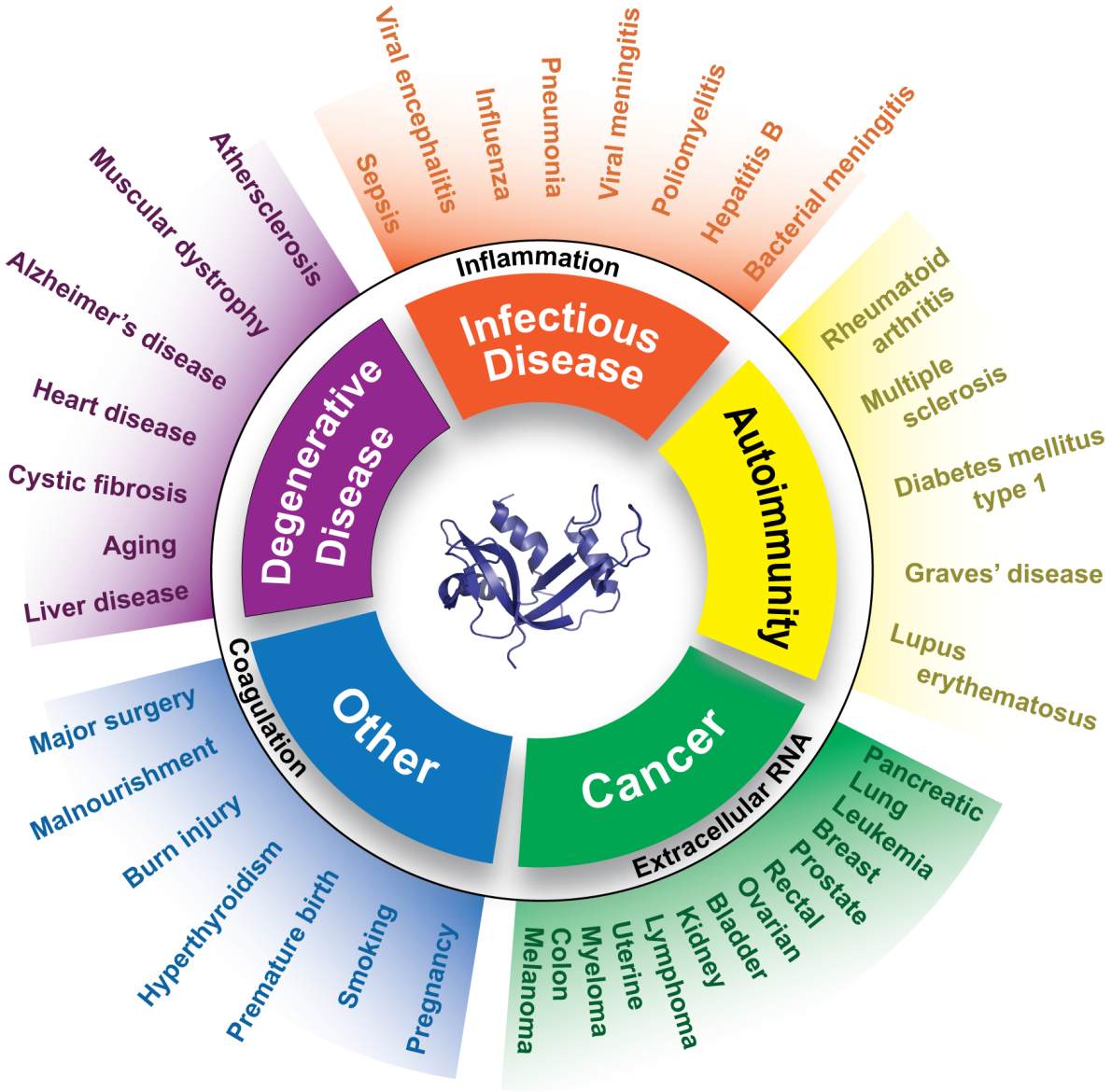
Inflammation
Infectious Disease
Autoimmunity
Cancer
Extracellular RNA
Other
Coagulation
Degenerative Disease
Viral encephalitis
Sepsis
Influenza
Pneumonia
Viral meningitis
Poliomyelitis
Hepatitis B
Bacterial meningitis
Rheumatoid arthritis
Multiple sclerosis
Diabetes mellitus type 1
Graves' disease
Lupus erythematosus
Pancreatic
Lung
Leukemia
Breast
Prostate
Rectal
Ovarian
Bladder
Kidney
Lymphoma
Uterine
Myeloma
Colon
Melanoma
Pregnancy
Smoking
Premature birth
Hyperthyroidism
Burn injury
Malnourishment
Major surgery
Liver disease
Aging
Cystic fibrosis
Heart disease
Alzheimer's disease
Muscular dystrophy
Atherosclerosis

Figure 1.2 Multiple diseases are associated with increased serum ribonuclease 1

Summary of the pathological conditions associated with increased levels of serum ribonuclease 1. All diseases displayed represent inflammatory states often associated with hypercoagulability and increased extracellular RNA production. RNase 1 (center), is released by vascular endothelial cells in response to antigenic RNA stimulation, and may serve to degrade extracellular RNA and suppress both hypercoagulation and inflammation

Table 1.1 Pathological conditions associated with elevated RNase 1 levels in body fluids

Degenerative Disease	Infectious Disease	Autoimmunity	Cancer	Other
Cystic fibrosis[158]	Sepsis[159-161]	Multiple sclerosis[162]	Uterine cancer[163]	Old age (<70 years) [164,165]
Liver cirrhosis[21,162,166]	Viral meningitis[167]	Rheumatoid vasculitis[92,168]	Rectal cancer[163,166]	Burn injury[169,170]
Muscular dystrophy[171]	Hepatitis B[172]	Rheumatoid arthritis[173]	Lung cancer[163,174,175]	Nephrectomy[176]
Acute myocardial infarction[177-179]	Influenza[180]	Diabetes mellitus type 1[181]	Pancreatic cancer[20-24,166]	Thyrotoxicosis & hyperthyroidism[164,181]
Congestive heart failure[178,179]	Bronchopneumonia[182]	Graves' disease[183]	Prostate cancer[184]	Thymectomy [185]
Alzheimer's disease[186]	Tick-borne viral encephalitis[187]		Renal cell carcinoma[184]	Smoking[175,188]
Degenerative brain disease[167]	Poliomyelitis[189,190]		Bladder cancer[184]	Brain trauma[191]
Chronic pancreatitis[24,192,193]	Coxsackie virus-induced meningitis[194]		Multiple myeloma[188,195,196]	Hemodialysis[197]
Kidney disease[178,195]	Japanese encephalitis virus[198]		Leukemia[162,188,196,199]	Thyroiditis & hypothyroidism[181]
	Bacterial meningitis[167]		Colon cancer[21,166]	Premature infants[181]
	Trichomonal vaginitis[200]		Ovarian cancer[201,202]	Pregnancy[203]
	Systemic lupus erythematosus[195]		Melanoma[188]	Starvation & malnourishment[160,203,204]
			Lymphoma[188,196]	Following major surgery[205]
			Hodgkin's disease[188]	Stabbing injury[162]
			Gall bladder and bile duct cancer[166]	Injection of cortisone and other hormones[206-208]
			Breast cancer[88,196]	X-ray irradiation[209]
			Brain tumor[210]	

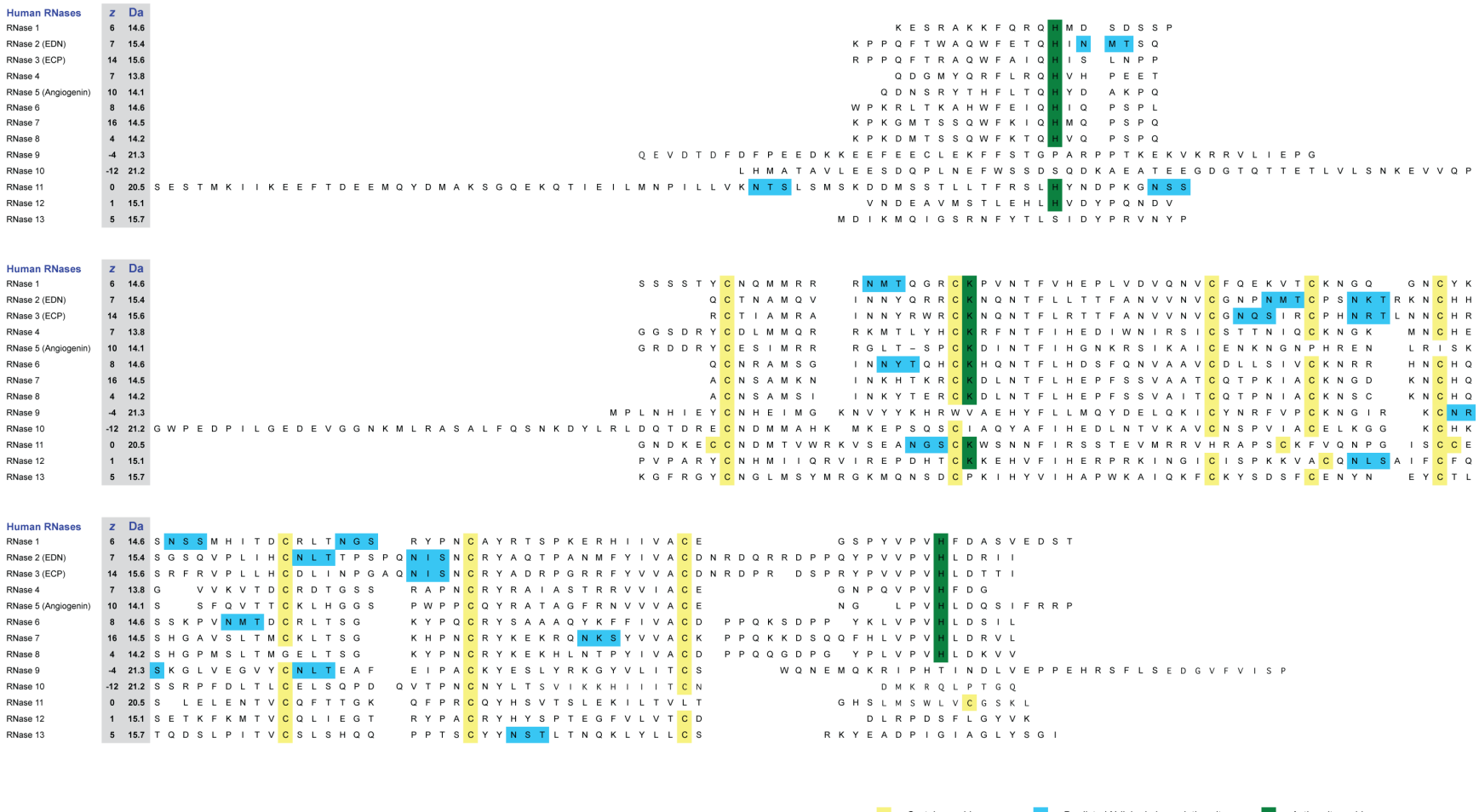
Human RNases
z
Da
RNase 1 6 14.6
RNase 2 (EDN) 7 15.4
RNase 3 (ECP) 14 15.6
RNase 4 7 13.8
RNase 5 (Angiogenin) 10 14.1
RNase 6 8 14.6
RNase 7 16 14.5
RNase 8 4 14.2
RNase 9 -4 21.3
RNase 10 -12 21.2
RNase 11 0 20.5
RNase 12 1 15.1
RNase 13 5 15.7
Cysteine residue
Predicted N-linked glycosylation site
Active site residue

Figure 1.3 Protein sequence alignment of human secretory ribonucleases

Alignment of the canonical (RNases 1–8) and non-canonical (RNases 9–13) human pancreatic-type ribonucleases showing conserved and divergent catalytic active site residues, structural cysteine residues, and predicted N-linked glycosylation sites.

Figure 1.4

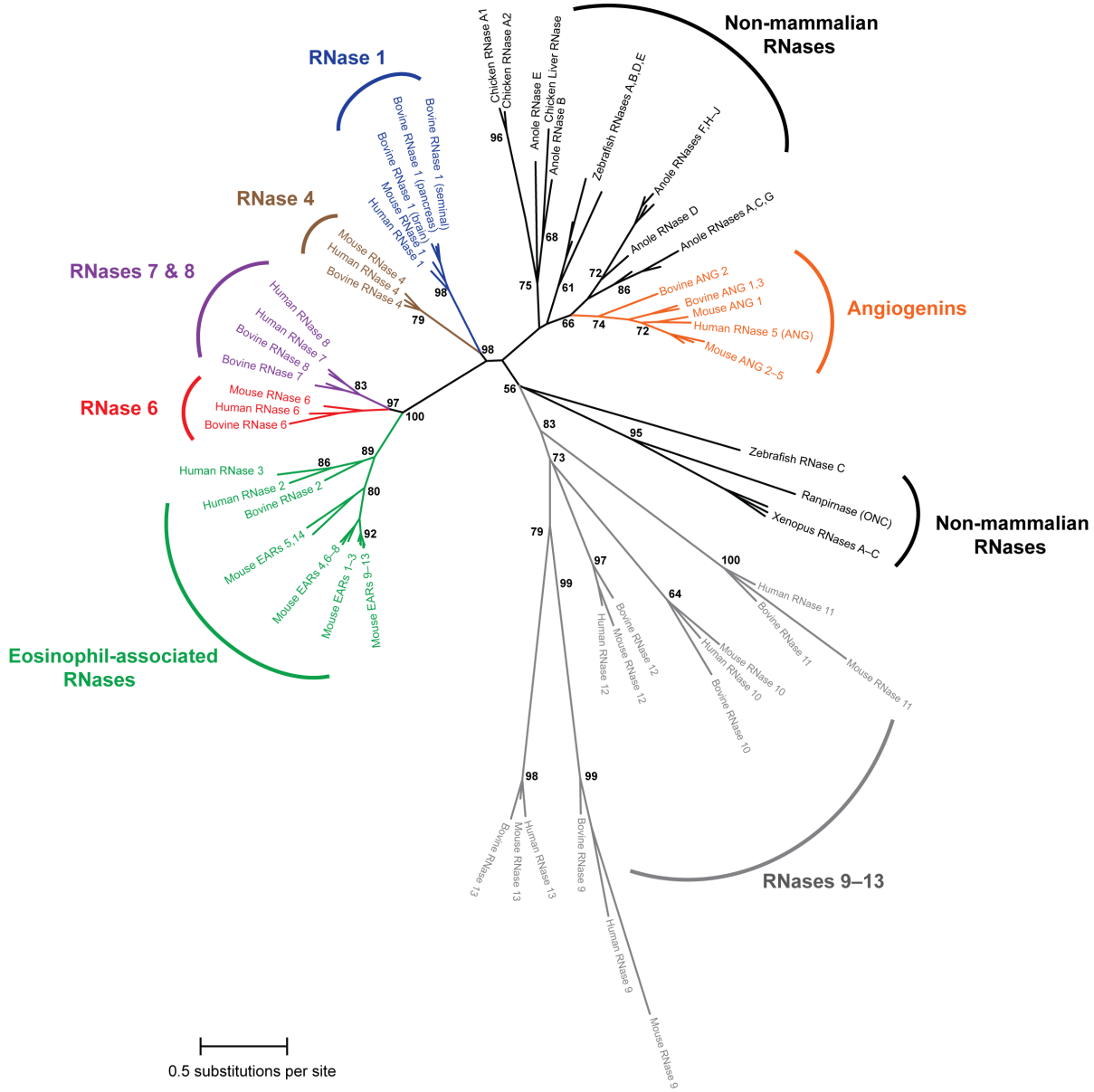
RNase 1
RNase 4
RNases 7 & 8
RNase 6
Eosinophil-associated RNases
Non-mammalian RNases
Angiogenins
Non-mammalian RNases
RNases 9–13
Bovine RNase 1 (seminal)
Bovine RNase 1 (pancreas)
Mouse RNase 1
Human RNase 1
Mouse RNase 4
Human RNase 4
Bovine RNase 4
Human RNase 8
Human RNase 7
Bovine RNase 8
Bovine RNase 7
Mouse RNase 6
Human RNase 6
Bovine RNase 6
Human RNase 3
Human RNase 2
Bovine RNase 2
Mouse EARs 5,14
Mouse EARs 4,6–8
Mouse EARs 1–3
Mouse EARs 9–13
Chicken RNase A1
Chicken RNase A2
Anole RNase E
Chicken Liver RNase
Anole RNase B
Zebrafish RNases A,B,D,E
Anole RNases F,H–J
Anole RNase D
Anole RNases A,C,G
Bovine ANG 2
Bovine ANG 1,3
Mouse ANG 1
Human RNase 5 (ANG)
Mouse ANG 2–5
Zebrafish RNase C
Ranpirnase (ONC)
Xenopus RNases A–C
Human RNase 11
Bovine RNase 11
Mouse RNase 11
Mouse RNase 12
Human RNase 12
Bovine RNase 12
Mouse RNase 10
Human RNase 10
Bovine RNase 10
Bovine RNase 13
Human RNase 13
Mouse RNase 13
Bovine RNase 9
Human RNase 9
Mouse RNase 9
0.5 substitutions per site

Figure 1.4 Evolutionary relationships between vertebrate secretory ribonucleases
Phylogenetic tree showing the evolutionary relationships between mammalian and non-mammalian pancreatic-type ribonucleases. RNase protein sequence alignments were made using MUSCLE[211] with manual adjustments. A maximum–likelihood phylogenetic tree was generated in MEGA5.2[212] using the Whelan and Goldman (WAG)[213] substitution model and 1000 bootstrap replicates. Non-uniformity of evolutionary rates was modeled using a discrete Gamma distribution,[214] assuming for the presence of invariable sites. Bootstrap values >50 are reported.

Figure 1.5

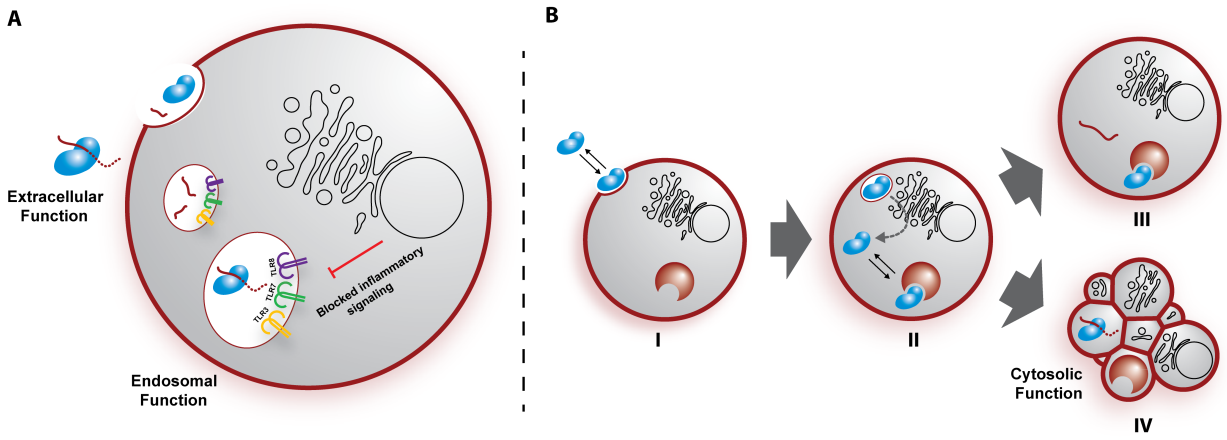
A
Extracellular Function
Endosomal Function
TLR3
TLR7
TLR8
Blocked inflammatory signaling
B
I
II
III
IV
Cytosolic Function

Figure 1.5 The multi-modal therapeutic actions of pancreatic-type ribonucleases

A. RNase 1 can manifest therapeutic activity outside the cell by degrading extracellular RNA targets. Upon association with the cell membrane and endosomal uptake, RNase 1 can continue to degrade antigenic RNA, thereby attenuating toll-like receptor inflammatory signaling cascades. *B*. RNase 1 can also act intracellularly. Upon cellular association (I) and endosomal translocation (II), RNase 1 can evade the cytosolic ribonuclease inhibitor by either natural or artificial means, resulting in the uncontrolled degradation of cytosolic RNAs and cellular apoptosis (IV).

Table 1.2 Disease models or clinical trials demonstrating therapeutic ability of RNase 1

Wild-type RNase 1 protein

Disease model/outcome	Protein
Increased survival and ameliorated symptoms of tick-borne encephalitis in human clinical trials[187]	Native bovine RNase 1 (isolated from pancreas)
Low-level treatment inhibits the development of metastasis of a lung tumor xenograft up to 90%[215]	Recombinant bovine RNase 1
Overexpression in a mouse model alleviated the symptoms of systemic lupus erythematosus[216]	Recombinant bovine RNase 1
Prevented clot formation in a mouse model of aortic thrombosis[109]	Recombinant bovine RNase 1
Attenuated brain edema and infarct size in a mouse model of stroke[114]	Recombinant bovine RNase 1
Decreased plaque formation and leukocyte recruitment in mouse model of atherosclerosis[217]	Recombinant bovine RNase 1
Attenuated myocardial cytokine production and leukocyte infiltration, and conferred significant cardiac protection against myocardial ischemia–reperfusion injury[218]	Recombinant bovine RNase 1
Toxic to Kaposi's sarcoma (KS) cell lines.[219]	Native human RNase 1 (isolated from urine)
Significantly reduced tumor burden in xenograft mouse cancer model[105]	Recombinant bovine RNase 1

Engineered variant RNase 1 protein

Disease model/outcome	Protein
Cytotoxic to various human cancer cell lines[129,145,146]	RI-evasive variants of bovine RNase 1
Cytotoxic to various human cancer cell lines[220,221]	RI-evasive variants of human RNase 1
Reduced tumor burden in patients with solid tumors in a Phase I trial[123-125]	RI-evasive variant of human RNase 1 (QBI-139)
Reduced tumor burden in xenograft mouse cancer model[222]	Covalently trimerized bovine RNase 1
Reduced tumor burden in xenograft mouse cancer model [223]	Human RNase 1 with pendant polyethylene glycol
Inhibited tumor growth in a xenograft cancer mouse model[224,225]	Human RNase 1–antibody fusion
Cytotoxic to transformed fibroblast cell lines[226,227]	Bovine RNase 1 with chemical cationization

Figure 1.6

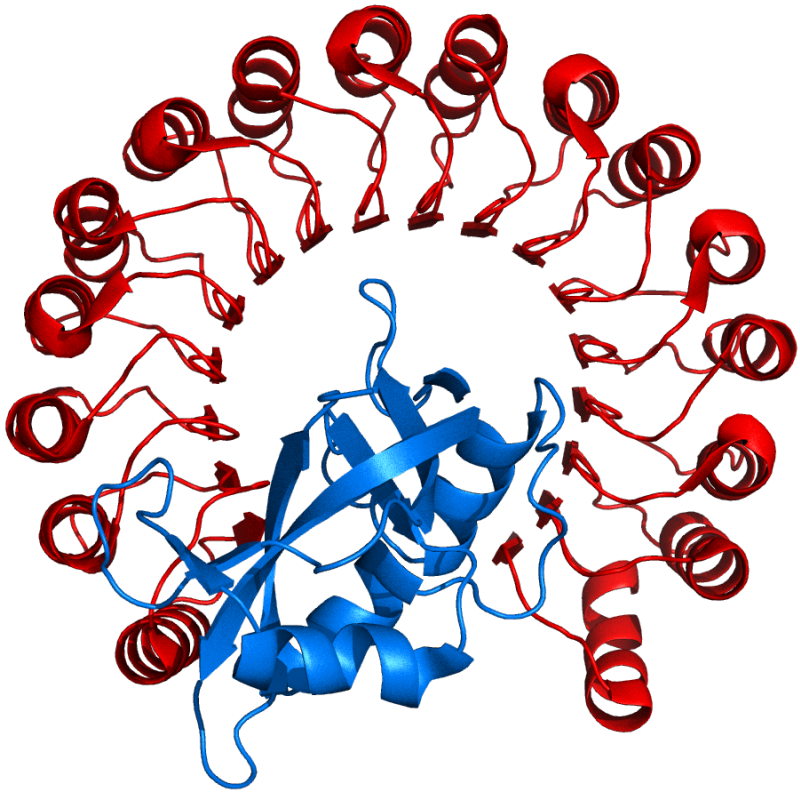

.

Figure 1.6 Human ribonuclease inhibitor (RI) bound to human RNase 1

The three-dimensional crystal structure of human ribonuclease inhibitor (red) complexed to human ribonuclease 1 (blue) (PDB 1z7x). Ribonuclease inhibitor is constructed entirely of conserved leucine-rich repeat units that are arranged in a horseshoe shape, and correspond to structural units consisting of a β-strand and an α-helix

CHAPTER 2

Rational Design and Evaluation of Mammalian Ribonuclease Cytotoxins

2.1 Abstract

Mammalian pancreatic-type ribonucleases (ptRNases) comprise an enzyme family that is remarkably well suited for therapeutic exploitation. ptRNases are robust and prodigious catalysts of RNA cleavage that can naturally access the cytosol. Instilling cytotoxic activity requires endowing them with the ability to evade a cytosolic inhibitor protein (RI) while retaining other key attributes. These efforts have informed our understanding of ptRNase-based cytotoxins, as well as the action of protein-based drugs with cytosolic targets. Further, we have gained particular insight into the mechanisms governing the extremely tight interaction between ptRNases and RI. Here, we address the most pressing problems encountered in the design of cytotoxic ptRNases, along with potential solutions. In addition, we describe assays that can be used to evaluate a successful design *in vitro*, *in cellulo*, and *in vivo*. The emerging information validates the continuing development of ptRNases as chemotherapeutic agents.

2.2 Introduction

Once, the utility of recombinant DNA technology in generating drugs was limited to producing wild-type human proteins in heterologous hosts. Now, protein engineering is being used to tailor proteins for specific clinical applications. The resulting biologic drugs can provide a level of target-specificity not achievable with small molecules.[126]

The mammalian pancreatic-type ribonucleases (ptRNases) are especially well suited for exploitation as chemotherapeutic agents. These enzymes circumvent the pitfalls that plague many other protein-based drugs, such as high molecular mass, instability, and immunogenicity. ptRNases comprise a highly conserved family of small (~13 kDa), secreted proteins that catalyze the degradation of RNA with extremely high efficiency.[15,150] Incredibly, mammalian cells internalize these enzymes readily (Figure 2.1); thus, ptRNases are not restricted to the extracellular or cell-surface targets of most other protein-based agents.[228] Moreover, whereas many promising proteins never achieve success in the clinic because they are hampered by problems with production, storage, and administration,[126] ptRNases are produced readily in microbial hosts, have unusually high conformational stability, and maintain their integrity in extracellular fluids and tissues.

Recently, ptRNases have garnered much attention because several, including the dimeric bovine seminal ribonuclease (BS-RNase) and an amphibian ortholog, onconase (ONC), have proven to be natural cytotoxins for human cancer cells. ONC is currently in a Phase IIIb confirmatory clinical trial as a second-line chemotherapeutic agent for malignant mesothelioma and has been granted both orphan-drug and fast-track status by the U.S. Food and Drug Administration.[134,229] Despite their inherent cytotoxicity, both BS-RNase and ONC are of limited clinical utility. For example, ONC is compromised by dose-limiting renal toxicity and high

immunogenicity relative to mammalian ribonucleases.[72,230] Moreover, cytotoxic variants of mammalian ptRNases have greater specificity than ONC for cancer cells.[129] Efforts to exploit naturally occurring microbial and fungal ribotoxins have been plagued by similar immunogenicity and low specificity.[231,232] Hence, the future of ptRNases as chemotherapeutic agents appears to rely on the strategic development of the mammalian homologues.[233]

Although mammalian ptRNases possess the necessary stability, catalytic activity, and non-immunogenicity to warrant consideration as potential chemotherapeutic agents, their success is limited by two substantial barriers: internalization into the cytosol of target cells and inhibition by the cytosolic ribonuclease inhibitor protein (RI), which binds with femtomolar affinity to most ptRNases but not BS-RNase or ONC (Figure 2.2).[27] To design ptRNase-based agents, we have sought to understand the underlying biophysical and biochemical basis for their mechanism of action—as well as their extremely tight binding to RI—and then to translate that knowledge into optimized proteins.

A useful ptRNase-based cytotoxin must catalyze the degradation of RNA within target cells. To do so, it must gain entry to the cytosol, evade RI there, and retain its catalytic activity throughout the process. Here, we report on our current understanding of these requirements and our strategies for engineering ptRNases that achieve maximal therapeutic efficacy. We also provide details on the assays that we use to evaluate relevant attributes of putative ptRNase cytotoxins. Although we focus on the well-known enzymes from cow (RNase A) and human (RNase 1), the methodologies are applicable to other ptRNases as well.

2.3 Attributes of Cytotoxic ptRNases

2.3.1 Catalytic activity and proteolytic stability

Two important attributes of a cytotoxic ptRNase are its ability to catalyze RNA cleavage and to resist proteolysis. Mammalian ptRNases can catalyze the cleavage of the P–$O^{5'}$ bond of RNA on the 3′ side of pyrimidine nucleosides with a second-order rate constant ($k_{cat}/K_M = 3.3 \times 10^9$ $M^{-1}s^{-1}$)[234] that is among the highest known for an enzyme-catalyzed reaction. This activity leads to cellular apoptosis,[235] and is essential for ptRNase-mediated cytotoxicity.[236] Proteins with high thermostability tend to have low susceptibility to proteolytic degradation.[237] This premise holds true for ptRNases, as installing an additional disulfide bond in RNase A significantly increases its thermostability, resistance to proteolysis, and cytotoxicity.[238] Accordingly, when choosing residues to alter within ptRNases, care must be taken to avoid interference with active-site residues, cysteine residues that participate in disulfide bonds, and other residues critical to structure and function (Figure 2.3).[239] Although no consensus exists regarding the minimal requirements for either parameter, decreasing catalytic activity or thermostability leads to decreases in cytotoxicity.[240,241] Catalytic activity can be measured by using a fluorogenic substrate, such as 6-carboxyfluorescein–dArUdAdA–6-carboxytetramethylrhodamine;[242,243] thermostability can be monitored by ultraviolet or circular dichroism spectroscopy, or by following the incorporation of a fluorescent dye upon thermal denaturation.[244]

2.3.2 Cellular internalization

ptRNases are especially well suited as biologic drugs due to their endogenous ability to enter cells without requiring any additional delivery strategy. Still, ptRNase internalization remains an inefficient process, and could limit cytotoxicity. To design a ptRNase-based drug that is

equipped for more efficient internalization, it is important to understand the pathway by which ptRNases enter cells (Figure 2.1).

Mammalian ptRNases undergo endocytosis through an adsorptive process that is non-saturable, non-receptor-mediated, and dynamin-independent.[128] Certain anionic cell-surface molecules facilitate Coulombic interactions with cationic ptRNases, which are highly positively charged (Table 2.1). Analyses *in vitro* and *in cellulo* reveal that RNase A interacts tightly with abundant anionic cell-surface glycosaminoglycans such as heparan sulfate and chondroitin sulfate, as well as sialic acid-containing glycoproteins. The uptake of RNase A correlates with cell-surface anionicity and could endow mammalian ptRNases with selective cytotoxicity for cancerous cells.[132] Following endocytosis, a very small fraction of the endosomal ptRNase is able to translocate into the cytosol and catalyze RNA degradation.

Specific modifications to a ptRNase can exploit the Coulombic interactions that likely facilitate RNase internalization.[33] Recent work has demonstrated that the amount of positive charge, as well as the distribution of that charge, can affect ptRNase adsorption.[245] For example, replacing two anionic surface residues, Glu49 and Asp53 (Figure 2.3), with arginines ("arginine grafting") results in enhanced internalization and cytotoxicity of an RNase A variant.[246] Similarly, chemical cationization of ptRNases by amidation of carboxyl groups with either ethylenediamine or polyethylenimine leads to enhanced internalization and cytotoxicity.[227] ptRNases can also be fused to cationic cell-penetrating peptides (CPPs) such as nonaarginine to increase internalization.[246,247] These cationic moieties need not be appended to ptRNases, as the addition of a cationic poly(aminoamine) dendrimer in *trans* increases the internalization and cytotoxicity of a ptRNase.[248] We note, however, that increasing the positive charge of a ptRNase can have the adverse effect of increasing its affinity for RI, which is highly anionic.[131]

2.3.3 Evading the ribonuclease inhibitor protein

Ribonuclease inhibitor (RI) is a ~50-kDa protein found exclusively in the cytosol of mammalian cells. Multiple biological roles for RI have been proposed, including protecting cells from internalized secretory ptRNases and maintaining cellular redox homeostasis.[27,154] Despite the uncertainty surrounding its precise physiological role(s), RI binds to members of the mammalian ptRNase superfamily with a 1:1 stoichiometry, completely inhibiting their catalytic activity by steric occlusion of the enzymic active site (Figure 2.2). Because ribonucleolytic activity is necessary to induce cellular apoptosis, a cytotoxic ptRNase must evade RI. Nevertheless, as the noncovalent complexes formed between RI and its ligands are among the tightest known in biology, instilling RI-evasion is a difficult task.

The goal of RI-evasion strategies is to modify the ptRNase so as to perturb only its interaction with RI. Many strategies are possible.[33] Recent analyses of various crystallized RI·ptRNase complexes indicate that although the interaction of RI with various ptRNases is similar, evasion strategies should be optimized to recognize the subtle differences that exist in the binding interfaces. Computational analyses can be used to identify which residues of a ptRNase make the most contacts with RI.[129] These residues can then be targeted for substitution through site-directed mutagenesis. We have found that introducing electrostatic and steric incompatibilities in these regions destabilize the RI·RNase complex, and that disruption is often best achieved by replacing small neutral or anionic residues in a ptRNase with arginine (Figure 2.3). Arginine, as the most polar and second largest amino acid, can generate electrostatic repulsion and steric strain while increasing positive molecular charge, thereby enhancing internalization.

Our initial engineering efforts yielded a prototype ptRNase cytotoxin, G88R RNase A. The

modification of a single residue imbued native RNase A with 10 thousand-fold lower affinity for RI and cytotoxicity.[146] Guided by computational algorithms, we have designed second-generation variants of RNase A and RNase 1 that evade RI more efficiently. For example, D38R/R39D/N67R/G88R RNase A demonstrates 20 million-fold lower affinity for RI than does native RNase A with little change to catalytic activity or thermostability (Table 2.1). This variant is more toxic to human cancer cells than ONC.[129] In addition to mutating the RI-binding interface of RNase A, we find that appending a folate moiety to glycine 88 can engender RI-evasion through steric repulsion. The pendant folate molecule can additionally provide enhanced targeting and uptake to cells overexpressing the cell surface folate receptor, as is common with many types of cancer cells.[249] A similar phenomenon is observed by attaching a pendant poly(ethylene glycol) (PEG) moiety to RNase A at the same position. Beyond RI-evasion, an RNase A–PEG conjugate displayed markedly lower renal clearance and increased tumor growth inhibition in mouse models of human tumors.[223]

Human RNase 1 proved to be a greater challenge, as it binds to RI with 10^2-fold higher affinity than does RNase A. Although R39D/N67D/N88A/G89D/R91D RNase 1 has 6 billion-fold lower affinity for RI than does wild-type RNase 1,[221] this variant is not as cytotoxic as D38R/R39D/N67R/G88R RNase A. An alternative strategy to engender RI-evasion is to bypass RI contact altogether. The human ptRNase variant PE5 carries a non-contiguous nuclear localization signal and has been shown to possess potent cytotoxicity that is dependent upon its nuclear uptake.[250]

BS-RNase is a naturally dimeric homologue of RNase A that evades RI. But upon entry into the cytosol, the dimer dissociates and the resulting monomers are inhibited by RI.[251] Recently, the endogenous properties of BS-RNase have been recapitulated by creating genetically encoded

or chemically conjugated multimers of ptRNases that are unable to dissociate *in cellulo.*[133,222,252] Still, aspects of the mechanism of action of these multimers remain unclear. Multimeric ptRNases can be more cytotoxic than BS-RNase despite being less RI-evasive. Hence, the enhanced cytotoxicity demonstrated could be due, in part, to improved interaction of the multimers with the negatively charged cell membrane, thereby favoring endocytosis.[222,252,253] High cytosolic localization of tandem RNase A dimers supports this hypothesis.[133]

2.4 Assays to Evaluate the Cytotoxicity of ptRNases

Just as effort has gone into the rational design of cytotoxic ptRNases, so too has substantial work been done to develop assays to measure and characterize the cytotoxicity of ptRNase-based chemotherapeutic agents. Cytotoxic ptRNases should be characterized thoroughly *in vitro* before being tested *in vivo*. Below, we describe the state-of-the-art in quantifying important parameters of ptRNase-mediated cytotoxicity, including cellular internalization, evasion of RI, inhibition of tumor cell proliferation *in vitro*, and inhibition of tumor growth *in vivo*. Several of these assays involve the use of fluorophores that can be tethered to ptRNases in a site-specific, non-perturbative manner.

2.4.1 Utility of small-molecule fluorophores

The constitutive fluorescence of traditional fluorophores (*e.g.*, fluorescein) can lead to high background that obscures valuable information. To overcome this limitation, we designed fluorogenic label **1** (Figure 2.4), which consists of a rhodamine 110 core enshrouded by an esterase-inducible "trimethyl lock" and a maleimido group for conjugation. Fluorescence is unmasked only in the presence of intracellular esterases. Hence, the endocytic uptake of ptRNase–**1** conjugates can be monitored by either fluorescence microscopy or flow cytometry.[254]

We designed a second fluorescent label that is likewise amenable to thiol-reactive, site-specific conjugation. We had observed that the fluorescence of fluorescein-labeled RNase A decreases upon binding to RI because the protonated, non-fluorescent form of fluorescein is stabilized by the anionic RI.[255] The discrepancy between the phenolic pK_a = 6.30 of fluorescein and physiological pH diminishes the sensitivity of this assay. To address this problem, we synthesized 2′,7′-diethylfluorescein, which has two electron-donating ethyl groups and a phenolic pK_a of 6.61. Fluorescent probe **2** (2′,7′-diethylfluorescein-5-iodoacetamide; Figure 2.4), which contains an iodoacetamido group for conjugation, enables a highly sensitive assay for the interaction of RI and ptRNases.[256]

2.4.2 Site-specific conjugation of ptRNases to fluorophores

Fluorescently labeled ptRNases have proven to be remarkably adaptable tools for a variety of assays. Nonetheless, as mammalian ptRNases contain multiple amino groups—including an essential one for catalysis in an active-site lysine residue—using amine-reactive reagents to cross-link or conjugate ptRNases can result in heterogeneity and inactivation.[257] To overcome this problem, we install cysteine residues at inconsequential positions in ptRNases, allowing for site-specific conjugation to fluorophores.

Both RNase A and RNase 1 contain eight cysteine residues that form four disulfide bonds in the native enzyme. To enable attachment of a thiol-reactive fluorophore, we introduce a cysteine residue at or near position 19 using site-directed mutagenesis. Position 19 is an optimal location because attachment of fluorophore groups there does not interfere with catalytic activity, RI binding, or cell-surface interactions (Figure 2.3). Further, this residue is in a solvated loop that is

inconsequential for protein stability.[255] Free-cysteine variants are produced and purified by methods described previously for other ptRNase variants,[146] with the following modifications.

To ensure that the free cysteine residue does not suffer irreversible oxidation to a sulfinic or sulfonic acid, O_2(g) must be removed from the buffers used in the purification process. Following initial purification, the free thiol group at position 19 is protected as a mixed disulfide by reaction with a 4-fold molar excess of 5,5′-dithiobis(2-nitrobenzoic acid) (DTNB). Immediately following purification by gel-filtration chromatography, pooled protein fractions are adjusted to become 8% (w/v) in 1.0 M Tris–HCl buffer, pH 8.0, containing EDTA (10 mM). DTNB was dissolved in a small quantity of ethanol, then brought to 5 mM with 20 mM HEPES–NaOH buffer, pH 8.0. Upon addition of DTNB to the protein solution, a yellow color is observed due to the production of 2-nitro-5-thiobenzoic acid (NTB). The resulting mixture is dialyzed against several liters of 20 mM sodium acetate buffer, pH 5.0, overnight at 4 °C to remove unreacted NTB. NTB-protected ribonucleases are then purified further with cation-exchange chromatography and stored at 4°C until needed for conjugation.

Immediately prior to fluorophore attachment, NTB-protected ptRNases are deprotected with a 4-fold molar excess of dithiothreitol (DTT) and desalted by chromatography. Deprotected ptRNases are incubated for 6 h at 25°C with a 10-fold molar excess of fluorophore in phosphate-buffered saline (PBS). *N*,*N*-Dimethylformamide (DMF) or dimethyl sulfoxide (DMSO) can be added to the reaction mixture (≤10% v/v) to increase fluorophore solubility. Following the conjugation reaction, the solution is dialyzed against 20 mM sodium acetate buffer, pH 5.0, and then purified again with reverse-phase HPLC to separate labeled and unlabeled protein. The molecular mass of each conjugate is verified by mass spectrometry prior to its use in assays.

2.4.3 Assessing cellular internalization with fluorescence spectroscopy

The internalization of a ptRNase–**1** conjugate into live cells can be visualized with fluorescence microscopy. The rate of ptRNase internalization can be quantified with flow cytometry. These analyses can be used with both adherent and nonadherent cell lines.

To quantify internalization, mammalian cells from nearly confluent flasks are collected by centrifugation and resuspended at a density of 10^6 cells/mL in fresh medium that is appropriate to the cell type. A ptRNase–**1** conjugate is added (to 10 μM) to 250 μL of medium containing 10^6 cells/mL of cells. An unlabeled ptRNase can serve as a negative control. The cells are incubated at 37°C for known times, typically ≤2 h. During this timeframe, we have observed that only a small fraction of labeled ptRNases are taken up by cells; therefore, we assume that the rate of internalization is not limited by substrate concentration. Further, we do not observe any significant exocytosis of labeled ptRNases by confocal microscopy.[254] To quench internalization, cells are collected by centrifugation at 1000 rpm for 5 min at 4°C, washed once with ice-cold PBS, and resuspended in 250 μL of PBS. Samples are kept on ice until their analysis. The fluorescence of unmasked **1** can be detected by flow cytometry using a 530/30-nm band-pass filter. Total cell viability can be determined by staining with propidium iodide, which can be detected through a 660-nm long-pass filter. The mean channel fluorescence intensity of 20,000 viable cells are determined for each sample and used for subsequent analyses. To determine the steady-state rate constant (k_I) for ptRNase internalization, fluorescence intensity data is fitted to Eq. (2.1), where F_{max} is the fluorescence intensity upon reaching the steady state and k_I is the first-order rate constant for ptRNase internalization into cells.

$$F = F_{max}(1 - e^{-k_I t}) \tag{2.1}$$

2.4.4 Evaluating RI evasion with fluorescence spectroscopy

Traditionally, the stability of an RI·RNase complex has been determined by measuring the inhibition of catalytic activity. The K_i values obtained by this method are lower than the concentration of wild-type RNase 1 used in the experiment itself. Accordingly, these values can only be an upper limit for the true K_d value. To more accurately measure the binding of ptRNases to RI, the dissociation rate of an RI·ptRNase complex is determined by monitoring the release of a ptRNase–**2** conjugate over time (Figure 2.5). To calculate the value of K_d of an RI·ptRNase complex, the value of k_a is assumed to be similar to that for the association of hRI with angiogenin or RNase A. These k_a values are within twofold of each other and are close to the diffusion limit.[258] Thus, the k_a value of homologous ptRNases is assumed to be equivalent to RNase A.

The dissociation rate of the complex between RI and a ptRNase–**2** conjugate can be determined by following the increase in fluorescence upon complex dissociation (Figure 2.5). A ptRNase–**2** conjugate (100 nM) in PBS containing tris(2-carboxyethyl)phosphine (100 μM) and bovine serum albumin (0.10 mg/mL; Sigma Chemical) is added to a 96-well microtiter plate, and the initial fluorescence is measured with a plate reader. RI is then added at equimolar concentrations and incubated with labeled ptRNase at 25°C for 5 min. A 50-fold molar excess of human angiogenin or RNase 1 (5 μM) is added to scavenge dissociated complex, and the change in fluorescence is measured at various time points. For endogenous RI•ptRNase complexes, the time scale of the experiment may extend to several months to achieve relevant data. Protein plates may be stored at 4°C and measurements can be taken every 24-48 hours. To insure that the proteins maintain their folded conformation for the duration of the experiment, additional data points should be monitored under the same conditions, only without the addition of the 50-fold

molar excess of angiogenin. To account for indeterminant error, data are the mean (± SE) from six solutions normalized for the fluorescence of four solutions of labeled ptRNase (100 nM) in the absence of RI. Fluorescence data are fitted to Eq. (2.2) to determine the dissociation rate constant (k_d), wherein F_0 is the fluorescence before the addition of angiogenin, and F_∞ is the fluorescence before RI addition. The equilibrium dissociation constant (K_d) for the RI·ptRNase complex can be determined with Eq. (2.3) and the known value for the association rate constant of RNase A ($k_a = 3.4 \times 10^8$ $M^{-1}s^{-1}$).[258]

$$F = F_0 + (F_\infty - F_0)(1 - ek_d t) \tag{2.2}$$

$$K_d = \frac{k_d}{k_a} \tag{2.3}$$

2.4.5 Measuring inhibition of tumor-cell proliferation in vitro

Multiple assays exist for measuring the effects of ribonucleases on cultured cells *in vitro*. We choose to use the following cell-proliferation assay because of its very high reproducibility. Cytotoxicity is evaluated by measuring the incorporation of [*methyl*-^{3}H]thymidine into newly synthesized DNA of either adherent or non-adherent cells. Although this assay measures the synthesis of DNA that is necessary for cell proliferation, the data also report on cell death. As revealed by trypan blue dye exclusion, the number of nonviable cells increases upon treatment with a toxic ptRNase.[220] A significant portion of these treated cells also display enhanced labeling with the apopotic marker Annexin V (Chao and Raines, unpublished results). Microscopic analyses of treated cells indicate an apoptotic morphology, including the formation of apoptotic bodies, nuclear condensation, and fragmentation. The extent of cell viability and

apoptotic morphology correlates well with [*methyl*-^{3}H]thymidine incorporation.[145] Thus, we believe that ptRNases render apoptosis upon target cells, and that our assay of the inhibition of DNA synthesis reports on cytotoxicity.

Cells, such as human erythroleukemia line K-562 (ATCC; Manassas, VA), are grown in Roswell Park Memorial Institute (RPMI) 1640 medium (Mediatech, Herndon, VA) supplemented with fetal bovine serum (FBS; 10% v/v), penicillin (100 units/mL), and streptomycin (100 μg/mL), and maintained at 37°C in a humidified atmosphere containing CO_2(g) (5% v/v). Aliquots (95 μL) of cultured cells (10^5 cells/mL) are placed in a microtiter plate, and sterile solutions (5 μL) of a ptRNase in PBS are added to the aliquots. Cells are incubated in the presence or absence of ribonucleases for 44 h, followed by a 4-h pulse with [*methyl*-^{3}H]thymidine (0.2 μCi per well). Cells are then harvested onto glass fiber filters by using, for example, a PHD cell harvester (Cambridge Technology, Watertown, MA) and lysed by the passage of several milliliters of water through the filters. The filter retains DNA and other cellular macromolecules, while small molecules, including unincorporated radiolabel, pass through. After washing extensively with water, the filters are dried with methanol and counted by using a liquid scintillation counter. Results from the cytotoxicity assay are reported as the percentage of [*methyl*-^{3}H]thymidine incorporation into the DNA of PBS-treated control cells. All assays should be repeated at least three times to lessen indeterminate error. Values of IC_{50}, which is the concentration of ribonucleases that decreases cell proliferation to 50%, are calculated by fitting the data using nonlinear regression to a sigmoidal dose–response curve (Eq. 2.4), in which y is the DNA synthesis following the [*methyl*-^{3}H]thymidine pulse and h is the slope of the curve.

$$y = \frac{100\%}{1+10^{(\log(IC_{50})-\log[\text{ribonuclease}])h}} \tag{2.4}$$

2.4.6 Measuring inhibition of tumor-cell proliferation in vivo

The most compelling method to measure the therapeutic effects of a cytotoxic ptRNase comes from *in vivo* analysis of tumor growth inhibition. This assay utilizes human tumor xenografts grown in the flanks of nude mice. Here, we describe our method for analyzing the effect on the growth of these tumors. We use the human tumor cell lines DU145 (prostate cancer) and A549 (non-small cell lung cancer) for their ability to proliferate in mice, their low rate of spontaneous regression, and their known sensitivity to RI-evasive variants of RNase A.[129] Moreover, each line represents a clinically relevant target that is used often in the testing of new chemotherapeutic agents.

DU145 cells are grown in Dulbecco's modified Eagle's medium (ATCC) containing FBS (10% v/v); A549 cells are grown in F12K medium (ATCC) containing FBS (10% v/v). Cells ($\sim 10^6$) are implanted into a rear flank of 5−6 week old male homozygous (*nu*/*nu*) nude mice. Tumors are allowed to grow to a volume of ≥ 75 mm^3 before the initiation of treatment. All test compounds are diluted in sterile PBS. All treatments are administered either by intraperitoneal injection (i.p.) or orally with a gavage needle (p.o.) for comparator chemotherapeutics, with the volume of administered solution based upon the body weight of the animal (10 μL/g). It is important to establish a dose and administration schedule that is effective with a specific cytotoxic ptRNase and tumor cell type. We have found that for mice bearing DU145 prostate carcinoma tumors, a dose of 15 mg/kg (i.p., qd × 5) of several monomeric ptRNase variants is optimal for eliciting maximum inhibition of tumor growth while minimizing off-target effects, as monitored by change in body weight. Similarly, we have found that frequent administration (qd × 5) achieves maximal tumor growth inhibition as compared to a single large dose (1 × wk). On the other hand, trimeric conjugates of cytotoxic RNase A variants can be administered less

frequently and at a lower dose with comparable effect.[222] We speculate that the increased hydrodynamic radii of these trimeric conjugates results in enhanced persistence in circulation, as is observed with ptRNase-PEG conjugates.[223] Animal body weights should be monitored continually throughout the experiment as an indicator of drug tolerance.

Treatment with all agents should be ongoing throughout the entire experiment, with a control set of animals treated with vehicle alone. Comparators can include approved chemotherapeutic agents, such as docetaxel (15 mg/kg; i.p., 1 × wk), cisplatin (6 mg/kg; i.p., 1 × wk), and erlotinib (100 mg/kg; p.o., 2 × wk). Tumor size should be measured twice-weekly using calipers, and tumor volume (mm^3) can be estimated by using the formula for a spheroid (Eq. 2.5). The percent tumor growth inhibition (%*TGI*) is then calculated with Eq. (2.6).

$$\text{volume} = \frac{l \times w^2}{2} \tag{2.5}$$

$$\%\text{TGI} = \left(1 - \left(\frac{(\text{volume}_{\text{final}} - \text{volume}_{\text{initial}})_{\text{treated}}}{(\text{volume}_{\text{final}} - \text{volume}_{\text{initial}})_{\text{control}}}\right)\right) \times 100 \tag{2.6}$$

2.5 Prospectus

We have engineered mammalian ptRNases into useful cytotoxins. Through the use of novel, sensitive assays, we have been able to reveal the contribution of various parameters toward cytotoxicity. Still, mechanistic issues remain unclear, involving ptRNase translocation from endosomes to the cytosol and the specific RNA targets of ptRNases. Novel assays to illuminate these issues—and exploit them therapeutically—are being developed in our laboratory. Further work is directed at enhancing the circulating half-life of ptRNases *in vivo* using pegylation or glycosylation.

ptRNases have shown exceptional applicability as model proteins for multi-faceted drug design. The potential therapeutic value of ptRNases has been extended beyond cancer with the creation of zymogens that can be engineered to be disease-specific. To date, protease-activatable ptRNase zymogens have been developed to combat malaria, hepatitis C, and HIV.[259-261] Another member of the ptRNase family, angiogenin, has been designed as a hyperactive variant capable of enhanced neovascularization.[148] Continued efforts to engineer this remarkable family of proteins will no doubt add even more therapeutic value.

Table 2.1 Salient Modifications of ptRNases that Enhance Cytotoxicity

Ribonuclease	T_m (°C)[a]	Ribonucleolytic Activity (%)[b]	K_i or K_d (n*M*)[c]	IC_{50} (μ*M*)[d]	*Z*[e]	Ref.
Wild-type RNase A	64	100	44×10^{-6}	>25	+4	129
G88R RNase A	60	142	2.8	6.2	+5	146
A4C/G88R/V188C RNase A	69	94	0.65	3	+5	238
D38R/R39D/N67R/G88R RNase A	56	75	1.4×10^{3}	0.19	+6	129
E49R/D53R/G88R RNase A	54	5	2.6	1.9	+9	246
E49R/D53R/G88R RNase A–R_9	49	7	3.0	0.58	+18	246
$(RNase A)_2$ [SGRSGRSG linker]	61	1.2	ND	12.9	+10	252
$(D38R/R39D/N67R/G88C RNase A)_3$	ND	17	ND	1.0	+16	222
Wild-type RNase 1	57	100	29×10^{-8}	>25	+6	221
R39D/N67R/N88R/G89D/R91D RNase 1	53	81	28	5.69	+3	221
PE5 (RNase 1–NLS)	46	ND	ND	4.6	+6	250
Onconase	90	100	$\geq 10^{3}$	0.27	+5	129

[a] Values of T_m are the temperature at the midpoint of thermal denaturation, which can be monitored by ultraviolet or circular dichroism spectroscopy.
[b] Values of ribonucleolytic activity are relative to the wild-type enzyme.
[c] Values of the equilibrium dissociation constant (or inhibition constant) are for the complex with human RI.
[d] Values of IC_{50} are for the incorporation of [*methyl*-^{3}H]thymidine into the DNA of K-562 human leukemia cells.
[e] Values of *Z* refer to the net molecular charge: Arg + Lys – Asp – Glu – Pyr (where "Pyr" refers to a pyroglutamate residue, which is found at the N-terminus of onconase).

Figure 2.1

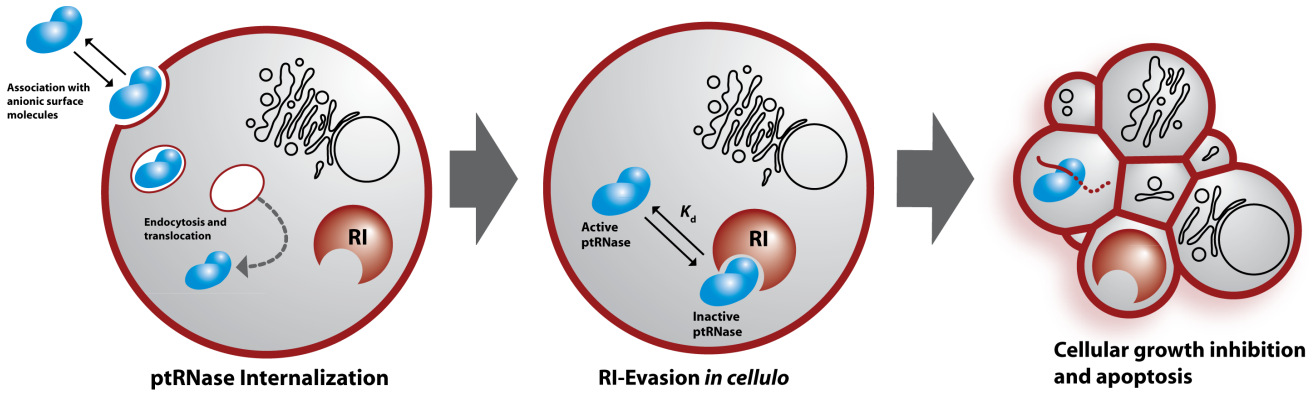
Association with anionic surface molecules
Endocytosis and translocation
RI
ptRNase Internalization
Active ptRNase
K_d
RI
Inactive ptRNase
RI-Evasion *in cellulo*
Cellular growth inhibition and apoptosis

Figure 2.1 Putative mechanism of ribonuclease cytotoxicity

The internalization pathway of ptRNases involves association with glycans on the cell membrane, absorptive endocytosis, and interaction with cytosolic RI. Upon evasion of RI, cytotoxic ptRNases can degrade cellular RNA and induce apoptosis.

Figure 2.2

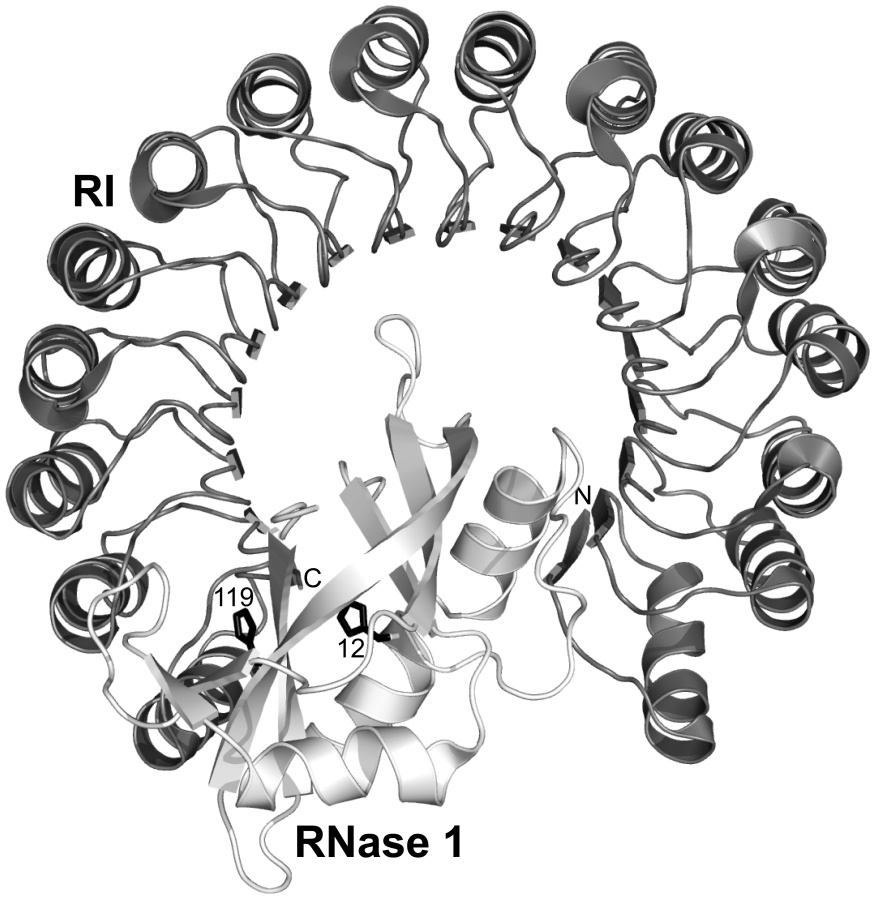

Figure 2.2 The structure of human RI complexed with human RNase 1

Three-dimensional structure of the human RI·RNase 1 complex (Protein Data Bank entry 1z7x). The active-site histidine residues 12 and 119 of RNase 1 are depicted explicitly, and the N and C termini of RI are labeled. The complex has $K_d = 2.9 \times 10^{-16}$ *M*.[221]

Figure 2.3

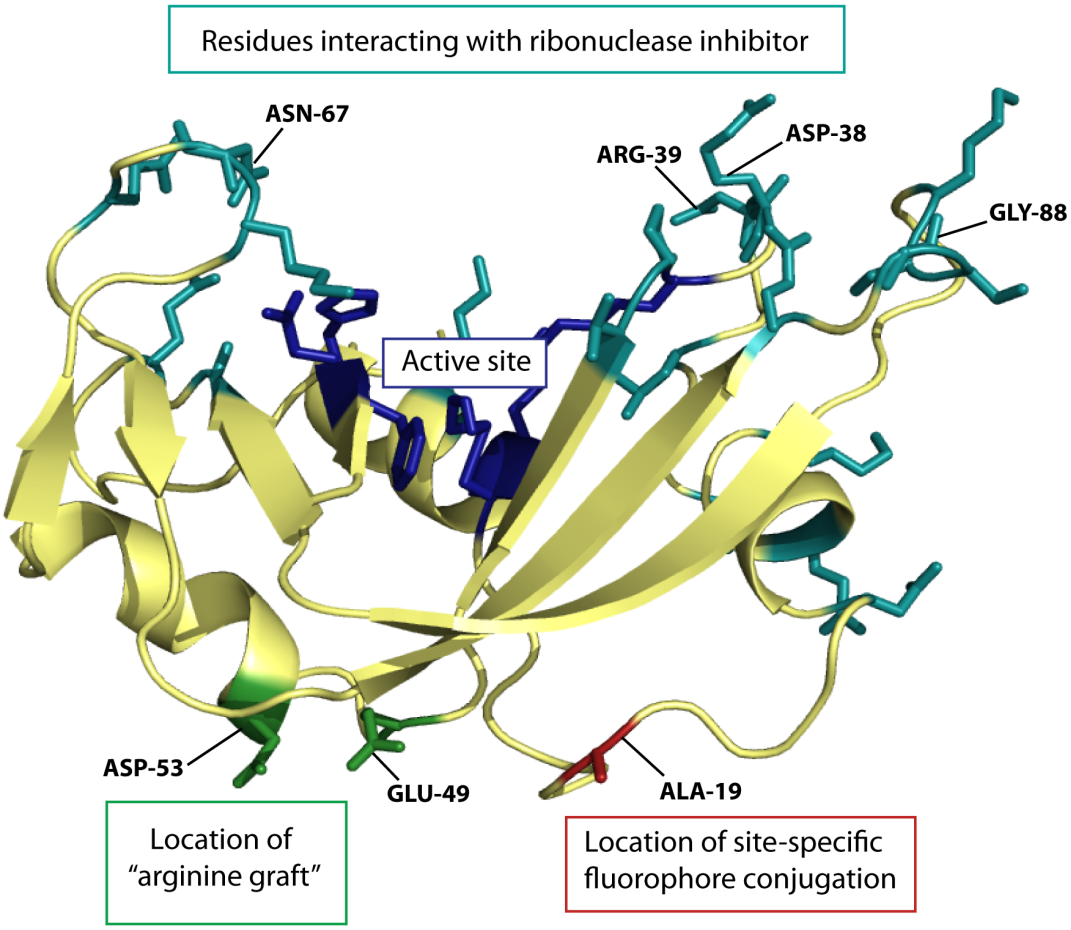
Residues interacting with ribonuclease inhibitor
ASN-67
ARG-39
ASP-38
GLY-88
Active site
ASP-53
GLU-49
ALA-19
Location of "arginine graft"
Location of site-specific fluorophore conjugation

Figure 2.3 Key functional residues in RNase A

Three-dimensional structure of RNase A showing residues important in the design and evaluation of an RNase A-based cytotoxin.

Figure 2.4

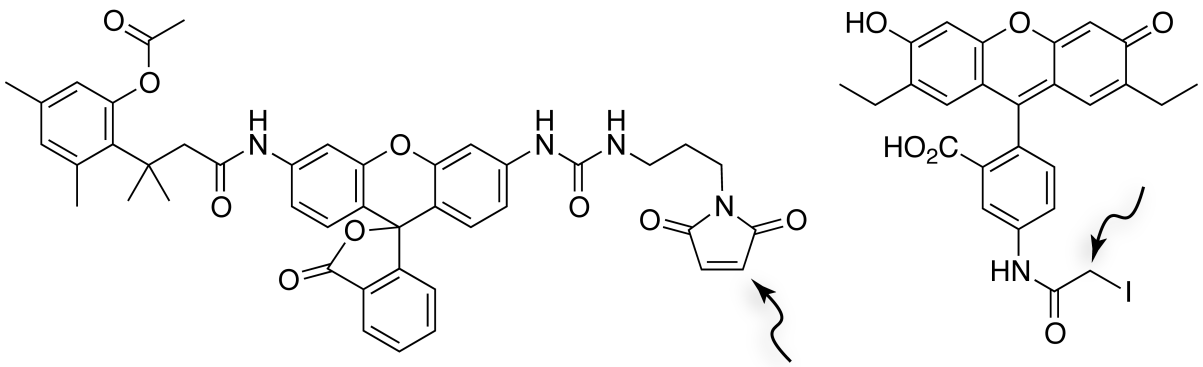

1 **2**

Figure 2.4 Chemical structures of fluorescent probes used in RNase conjugations Structures of fluorogenic label **1** for monitoring endocytosis[254] and fluorescent probe **2** for monitoring protein–ligand interactions.[256] The arrows indicate electrophilic carbons that can form thioether linkages with cysteine residues.

Figure 2.5

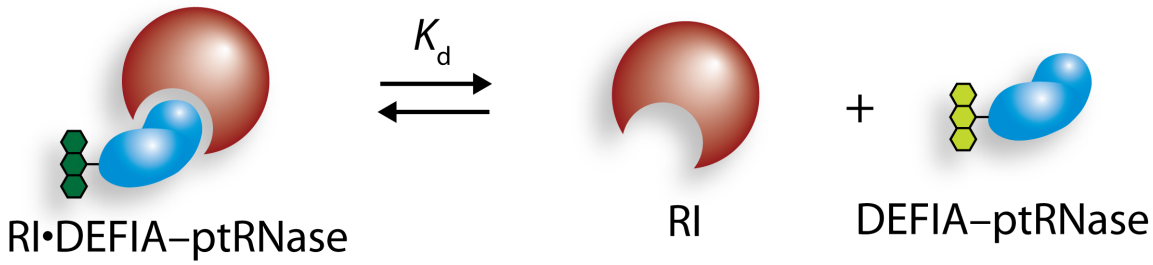

Figure 2.5 Mechanism of fluorescent probe quenching

Assay for evaluating K_d, which is the equilibrium dissociation constant of an RI·ptRNase complex.[256] Dissociation of the complex leads to an increase in fluorescence. The assay can also be used to evaluate the affinity of an unlabeled competitor ptRNase with a K_d value that is higher than the labeled ptRNase.

CHAPTER 3

Bovine Brain Ribonuclease is the Functional Homolog of Human Ribonuclease 1

Contribution: I produced all proteins used in this study, performed pH–rate titrations, RI-binding experiments, phylogenetic calculations and wrote the entire manuscript. Double-stranded RNA, glycan-binding and flow cytometry experiments were performed by Chelcie H. Eller.

Prepared for submission as:

Lomax J.E.[*], Eller C. H.[*], and Raines, R.T. (2014) Bovine brain ribonuclease is the functional homolog of human ribonuclease 1. ([*]denotes equal contribution)

3.1 Abstract

Mounting evidence suggests that human pancreatic ribonuclease (RNase 1) plays important roles *in vivo*, ranging from regulating blood clotting and inflammation to directly counteracting tumorigenic cells. Understanding these putative roles has relied on continual comparisons of human RNase 1 to bovine RNase A, an enzyme that appears to function primarily in the ruminant gut. Our results imply a different physiology for human RNase 1. We demonstrate distinct functional differences between human RNase 1 and bovine RNase A. Moreover, we characterize another RNase 1 homolog, bovine brain ribonuclease, and find pronounced similarities between that protein and human RNase 1. Specifically, we report that human RNase 1 and bovine brain ribonuclease have a similar thermostability, activity against single- and double-stranded RNA substrates, pH–rate profile, affinity for cell-surface glycans, and ability to enter cells. Our results suggest that brain ribonuclease—not RNase A—is the true bovine homolog of human RNase 1, and provide fundamental insight into the ancestral roles and functional adaptations of RNase 1 in mammals.

3.2 Introduction

Pancreatic ribonuclease (RNase 1) is a small, secreted, RNA-degrading enzyme conserved in mammals. Its biological purpose is unknown. Until recently, all assumptions about its physiology were based on studies of a well-known bovine homolog, RNase A. This protein is secreted primarily from the bovine exocrine pancreas, and is believed to degrade mRNA from symbiotic bacteria in the rumen, a harsh environment with a normal pH range of 5.8–6.4 and temperatures from 38–42°C.[19,262] Indeed, RNase A seems well-suited for this role, possessing extremely high catalytic activity against single-stranded (ss)RNA at acidic pH, as well as remarkable thermostability and acid-tolerance.[15]

Studies of RNase 1 in other species suggest a biological function apart from digestion. Observations in rats demonstrated that RNase 1 levels do not change following periods of fasting or consumption, as with other digestive enzymes.[263] In humans, pancreatectomy does not affect circulating RNase 1 levels,[264] and we now recognize the primary source of RNase 1 in human blood to be the vascular endothelium.[94] Recent work suggests that RNase 1 degrades extracellular RNA, potentially regulating hemostasis, inflammation, and innate immunity.[89,109,114,217,265] Data *in vitro*[33,221] and *in vivo*[223,266,267] have implicated human RNase 1 as having an endogenous anti-cancer function, and clinical trials for a variant of this enzyme are underway.[123,124] Taken together, these data imply a much broader physiological role for mammalian RNase 1 than digestion.

The discrepancies between bovine RNase A and mammalian homologs might reside in the peculiar evolution of RNase 1 in ruminants. Whereas most mammals possess a single *RNASE1* gene, evolutionary analyses predict that bovine *RNASE1* underwent two major gene duplication events around 30 million years ago, resulting in paralogous genes encoding three distinct

proteins: RNase A, seminal ribonuclease (BSR), and brain ribonuclease (BRB). Intriguingly, BSR naturally dimerizes upon folding, whereas all other homologs exist as monomers. Orthologs of these three ribonucleases have been identified in many ruminant species. Although many BSR genes show pseudogene features (including stop-codon insertion, loss of catalytic residues, or loss of dimerization), BRB genes do not, implying a necessary function for the BRB protein.[268-270]

Of the three bovine ribonucleases, only BRB is not well characterized. Aside from classic work on RNase A[15], D'Alessio, Matoušek, and others have established that BSR possesses interesting biological functions not associated with digestion.[271,272] Indeed, BSR has cytotoxic, aspermagenic, and immunosuppressive activity, likely related to the need to protect sperm cells from the female immune system. BSR is, however, only expressed in the seminal vesicles and testes of *Bos taurus*, limiting the potential to extrapolate its functions and properties to other mammalian RNase 1 homologs. In contrast, BRB (which was named for its initial discovery and purification from bovine brain)[273,274] is expressed not only in brain, but in all tissues examined, including endometrium, lymph node, small intestine, liver, and kidney.[35] The widespread expression pattern of BRB closely resembles that for human and mouse *RNASE1* genes.[79] Further, phylogenetic analyses imply that BRB is evolutionarily older than both RNase A and BSR, suggesting greater similarity to the ancestral form of RNase 1 in ruminants.[275] RNase A shares greater overall sequence identity with human RNase 1 than does BRB (Table 3.1). Nevertheless, conclusions based on sequence similarity are not nearly as powerful or as precise as those based on experimental data.

We have performed the first detailed biochemical characterization of BRB. Our data upend the relationship between human RNase 1 and bovine RNase A; instead, the true functional

homolog of human RNase 1 in the cow appears to be BRB. Moreover, our findings support the hypothesis that RNase 1 is not merely a digestive enzyme.

3.3 Materials and Methods

3.3.1 Equipment

All fluorescence and absorbance measurements were made with a Tecan M1000 fluorescence plate reader, unless stated otherwise. All data were fitted and analyzed with the program Prism 5 (GraphPad), unless stated otherwise.

3.3.2 Cloning, Expression, and Purification of Proteins

The signal peptide prediction program Signal P was used to predict and exclude peptide leader sequences from recombinant proteins. DNA constructs for human RNase 1 (residues 28-156), bovine RNase A (residues 26-150), bovine BSR (residues 26-150) and bovine RI (residues 1-456) were previously prepared. [143,276] The gene encoding bovine brain RNase (Gene ID: 280720) was amplified from a bovine brain cDNA library (Zyagen) using primers 5' ATTATAATACATATGAAGGAATCTGCGGCCGCCAA (with NdeI) and 3' ATTAATATTGAGCTCTCAGAGAAGCCTGTGTGGAG (with XhoI) and inserted into the pET22b (Novagen) expression vector for tagless expression in BL21(DE3) *E. coli.* Variant proteins RNase 1 P19C, RNase 1 H12A, RNase A A19C, BSR C31A/C32A, BSR C31A/C32A/P19C and BRB S19C were generated using site-directed mutagenesis. Ribonucleases were purified as inclusion bodies, and variants containing a free cysteine residue were labeled with either diethylfluorescein[256] or BODIPY FL (Molecular Probes) as described.[277] Bovine RI was purified via RNase A-affinity chromatography as described.[143] Dimeric BSR was

isolated as a monomer and allowed to dimerize upon refolding as described.[251] Following purification, protein solutions were dialyzed against PBS and filtered prior to use. The molecular masses of ribonuclease conjugates were confirmed by MALDI–TOF mass spectrometry. Protein concentration was determined by using a bicinchoninic acid assay kit (Pierce) with wild-type RNase A as a standard.

3.3.3 T_m Determination of ribonucleases

Thermal unfolding of ribonucleases was monitored in the presence of a fluorescent dye using differential scanning fluorimetry (DSF). DSF was performed using a ViiA 7 Real-Time PCR machine (Applied Biosystems) as described.[278,279] Briefly, a solution of protein (30 μg) was placed in the wells of a MicroAmp optical 96-well plate, and SYPRO Orange dye (Sigma Chemical) was added to a final dye dilution of 1:166 in relation to the stock solution of the manufacturer. The temperature was increased from 20°C to 96°C at 1°C/min in steps of 1°C. Fluorescence intensity was measured at 578 nm, and the resulting data were analyzed with Protein Thermal Shift software (Applied Biosystems). A solution with no protein was used for background correction. Values of T_m were calculated from ∂fluorescence/∂T and are the mean of three independent experiments.

3.3.4 Inhibitor Dissociation Rate

The equilibrium dissociation rates of the RI·ribonuclease complexes were determined as described.[127] Briefly, RI and diethylfluorescein-labeled ribonucleases were mixed in equimolar ratios, and the resulting solution was incubated at 25°C for 5 min. A 50-fold molar excess of human RNase 1 was added to scavenge dissociated RI. Complex dissociation was measured by

monitoring the increasing fluorescence of dissociated ribonuclease over time. Data were analyzed as described,[127] and values of K_d are the mean of at least three independent experiments.

3.3.5 Cytotoxicity

The effect of ribonucleases on the proliferation of K-562 human leukemia cells was assayed as described.[127] Briefly, K-562 cells were incubated with a ribonuclease for 44 h, and the incorporation of radioactive thymidine into the cellular DNA was quantified by liquid scintillation counting. Values of IC_{50}, which is the concentration of RNase that decreases cell proliferation by 50%, were calculated by fitting the data using nonlinear regression analysis, and are the mean of at least three independent experiments.

3.3.6 pH Dependence of Enzyme Activity

The pH dependence of ribonucleolytic activity with a ssRNA substrate was determined by measuring the initial velocity of cleavage of 6-FAM–dArU$(dA)_2$–6-TAMRA (IDT)[242] (0.2 μM) at pH 4.0–9.0. Assays were carried out in 96-well plates (Corning) at 25°C in various ribonuclease-free buffers: 0.10 M NaOAc, 0.10 M NaCl (pH 4.0–5.5); 0.10 M BisTris, 0.10 M NaCl (pH 6.0–6.5); 0.10 M Tris, 0.10 M NaCl (pH 7.0–9.0). All assays were performed in triplicate with three different enzyme preparations. Values of optimal pH were calculated by fitting of normalized initial velocity data from solutions of various pH to a bell-shaped distribution. Values of k_{cat}/K_M at the optimal pH were determined from initial velocity data, as described.[242]

3.3.7 Double-stranded RNA Degradation

Steady-state kinetic parameters for a double-stranded (ds)RNA substrate were determined by following changes in absorbance upon enzymatic degradation, as described.[84] Poly(A:U) (Sigma Chemical) was dissolved in reaction buffer (0.10 M Tris–HCl, 0.10 M NaCl, pH 7.4) and serially diluted two-fold in a 96-well plate (Corning). After equilibration at 25°C, a baseline at A_{260} was established, and the initial substrate concentration was determined using $\varepsilon_{260} = 6.5\ \mathrm{mM^{-1}cm^{-1}}$ for poly(A:U). Ribonucleases were added to varying substrate concentrations and mixed, and the change in absorbance at 260 nm was monitored over time. Initial reaction velocities were determined using $\Delta\varepsilon_{260} = 3.4\ \mathrm{mM^{-1}cm^{-1}}$ for poly(A:U). All assays were performed in triplicate with three different enzyme preparations. Values of V_{max} and K_M were calculated by fitting data to the Michaelis–Menten equation.

dsRNA degradation was also assessed with a stable fluorescent hairpin substrate with the sequence: 5,6-FAM–CGATC(rU)ACTGCAACGGCAGTAGATCG (IDT). This substrate had a single RNA nucleotide near the fluorescently labeled 5′ end. The substrate was dissolved in water and annealed by first heating to 95°C and then slowly cooling to room temperature. A solution of substrate (50 nM) was added to a solution of ribonuclease (1 μM), and the resulting mixture was incubated for 5 min. The reaction was quenched by the addition of 40 units of rRNasin (Promega), and the products were subjected to electrophoresis on a 20% w/v native acrylamide gel at 10 mAmp. Formation of cleavage product was monitored by excitation of FAM at 495 nm and emission at 515 nm on a Typhoon FLA 9000 scanner (GE Healthcare). Band density was quantified from FAM fluorescence with ImageQuant software (GE Healthcare). The gel was then incubated in SYBR Gold (Invitrogen) and imaged for total nucleic acid.). All assays were performed in triplicate with three different enzyme preparations.

3.3.8 Binding of Ribonucleases to Glycans

Soluble glycans, including heparin, chondroitin sulfate A, chondroitin sulfate B, and chondroitin sulfate C (Sigma Chemical), were diluted across a 96-well plate in 5-fold dilutions in 1× PBS, pH 7.4. Ribonuclease–BODIPY conjugates were added to a final concentration of 50 nM, and the resulting solutions were incubated for 30 min at room temperature. Polarization was monitored by excitation at 470 nm and emission at 535 nm, and data were normalized to a solution lacking carbohydrate and fitted by nonlinear regression.

3.3.9 Cellular Internalization of Ribonucleases

The uptake of a fluorescently labeled ribonuclease by mammalian cells was followed by flow cytometry, as described.[127] Human K-562 cells were grown in RPMI media (Invitrogen) containing FBS (10% v/v) and pen/strep (Invitrogen). Cells were maintained at 37°C in 5% CO_2. Cells were plated at 2×10^6 cells/mL in a 96-well plate. Ribonucleases in PBS were added to 5 μM, and the resulting solution was incubated for 4 h. Cells were collected by centrifugation at 1000 rpm for 5 min, washed twice with PBS, exchanged into fresh medium, and collected on ice. The total fluorescence of live cells was measured using a FacsCalibur flow cytometer (BD Bioscience). Fluorescence data between experiments were normalized by calibrating each run with fluorescent beads. Data were analyzed with FlowJo software (Tree Star).

3.3.10 Liposomal Disruption Assay

Liposomes were constructed as described[280] using 1,2-dioleoyl-*sn*-glycero-3-ethylphosphocholine (DOPC; Avanti Polar Lipids). Lyophilized lipids were resuspended in 25 mM Tris–HCl buffer, pH 7.0, containing NaCl (80 mM), 8-aminonaphthalene-1,3,6-

trisulfonic acid (12.5 mM), and *p*-xylene bis(pyridinium bromide) (45 mM).[281] The lipid suspension was subjected to five freeze–thaw cycles and extruded through polycarbonate filters to form unilamilar vesicles of diameter ~100–150 nM as determined by dynamic light scattering (data not shown). Liposomes were diluted to 700 μM and incubated with 5 μM ribonuclease in a 96-well plate. Ribonuclease-induced leakage of the entrapped vesicle content was monitored by measuring the de-quenching of the fluorescence of 8-aminonapthalene-1,3,6-trisulfonic acid over time.[281] Percent leakage was calculated by normalizing to end-point disruption with Triton-X 100.

3.3.11 Sequence Alignment and Phylogenetic Tree Reconstruction

Protein sequence alignments were made using MUSCLE[282] with manual adjustments. A neighbor-joining phylogenetic tree was generated in MEGA5.2 using the Jones–Taylor–Thornton (JTT) substitution model with uniform site substitution rates[283] and 1000 bootstrap replicates.

3.4 Results

Recombinant BRB had never been characterized prior to our work. Indeed, only preliminary studies had even been performed on this enzyme.[284,285] To enable relevant comparisons, we also analyzed previously characterized recombinant proteins, including human RNase 1, bovine RNase A, and both monomeric (mBSR) and dimeric (dBSR) forms of bovine seminal RNase (BSR). Until now, these enzymes had never been compared in a single, controlled study using the same methods and substrates. We chose to include a monomeric form of BSR (C31A/C32A)[251] to establish any differences in biochemical properties conferred by dimerization.

3.4.1 Initial Characterizations of BRB

We began our study by analyzing biochemical properties of BRB that had been investigated for other homologous ribonucleases, including thermostability, inhibitor binding, and cytotoxicity (Table 3.1). Analysis of aligned sequences demonstrated that BRB has less overall sequence identity and similarity to human RNase 1 than to either RNase A or BSR. Yet, when the divergent, 17-residue C-terminal tail of BRB was excluded from analysis, the ensuing BRBΔ125–141 displayed identity (70%) and similarity (82%) to human RNase 1 as high or higher than those of RNase A and BSR. Like human RNase 1, BRB was found to be less thermostable than either RNase A or BSR. BRB was found to bind tightly to its endogenous inhibitor, bovine RI, as in previous studies with homologous RNases using human RI.[143,251,286] As some homologous ribonucleases, including dBSR,[271,272] manifest potent cytotoxic activities, we also determined the effect of BRB on the proliferation of human cells. As with human RNase 1, RNase A, and mBSR, we found that BRB did not demonstrate any significant cytotoxic activity.

3.4.2 Human RNase 1 and BRB Show a Pronounced Shift in Catalytic pH Optimum

Previous studies have shown that orthologous ribonucleases can exhibit different pH optima for catalysis.[287] Our results reveal similar contrasts. Whereas RNase A has its highest activity at pH 6.1, both human RNase 1 and BRB have their highest activity at pH 7.2 (Figure 3.1A). Additionally, RNase A is ~5-fold more active against ssRNA at optimal pH than either human RNase 1 or BRB (Figure 3.1B). Interestingly, we also report a distinct shift in pH optimum between monomeric and dimeric forms of BSR: mBSR shows its highest activity at pH 6.5,

whereas dBSR shows its highest activity at pH 7.1 (Figure 3.1A). Further, we note a drastic drop in catalytic efficiency for dBSR over its monomeric form (Figure 3.1B).

3.4.3 Human RNase 1 and BRB Can Degrade Double-Stranded RNA with High Efficiency

Although all pancreatic-type ribonucleases can degrade ssRNA substrates, a small subset display high activity toward dsRNA.[84] We examined the ability of ribonucleases to degrade dsRNA using poly(A:U) as substrate. We found that human RNase 1 degraded this dsRNA substrate with >2000-fold higher efficiency than that of RNase A. Tellingly, we found that BRB degraded poly(A:U) with efficiency ~200-, 7-, and 2-fold higher than those of RNase A, mBSR and dBSR, respectively (Figure 3.2A). The trend for human RNase 1 and dBSR agrees with previous reports.[84,288,289] An active-site variant, H12A RNase 1, demonstrated little measurable activity against the substrate. We also assessed the ability of RNase B (Sigma Chemical), which is a naturally occurring glycoform of RNase A, to degrade poly(A:U), and found no significant change in activity from RNase A (data not shown).

Because the heterogeneous nature of poly(A:U) does not allow for controlled secondary structure, we sought to create a novel dsRNA substrate to confirm our findings with poly(A:U). We designed a simple hairpin that contains a single ribonucleotide embedded within a DNA oligonucleotide and labeled on the 5′ end with a fluorophore. We monitored the formation of the fluorescent 6-mer cleavage product of ribonuclease catalysis by electrophoresis using a native polyacrylamide gel (Figure 3.2B). Densitometric analysis of substrate and cleavage products mirrored the same trend observed with the poly(A:U) substrate. Specifically, human RNase 1 demonstrated the most product formation, followed by BRB, then dBSR, mBSR and RNase A (Figure 3.2C). Again, H12A RNase 1 demonstrated little activity.

3.4.4 Human RNase 1 and BRB Bind Cell-Surface Molecules and Readily Internalize into Mammalian Cells

We used fluorescence polarization (FP) to compare the affinity of human and bovine ribonucleases toward common cell-surface glycans. A representative fit of fluorescent data is shown in Figure 3.3A. We found that both human RNase 1 and BRB had significantly higher affinity for all glycans tested than did either mBSR or RNase A. Average K_d values determined from at least three independent FP experiments are displayed as a heatmap (Figure 3.3B), and show that human RNase 1 and BRB exhibited nanomolar affinity for various carbohydrates.

Next, we determined if greater cell-surface glycan association enhanced the uptake of human RNase 1 and BRB into mammalian cells. A representative sample of raw fluorescence data acquired by flow cytometry is shown in Figure 3.3C. Averaged, normalized data from three independent experiments indicated that both human RNase 1 and BRB were internalized to a significantly greater extent than were either mBSR or RNase A (Figure 3.3D).

3.4.5 Human RNase 1 and BRB Disrupt Liposomes Better than RNase A and mBSR

We sought to determine if increased cellular uptake of ribonucleases correlated with their ability to disrupt lipid membranes. We saw significant differences between human RNase 1, BRB, and dBSR as compared to RNase A and mBSR, mimicking the trend of cellular internalization (Figure 3.3E). Still, the rates of liposomal disruption were relatively low compared to enzymes such as lysozyme, which exhibits ~12-fold higher disruption efficiency than human RNase 1 (data not shown). The hydrophoboic C-terminal tail did not endow BRB with a marked ability to disrupt liposomes.

3.5 Discussion

Mounting evidence suggests that mammalian RNase 1 plays important roles *in vivo*, ranging from regulating blood clotting and inflammation to directly counteracting tumorigenic cells. Yet, progress toward understanding these putative roles has been stymied by the continual comparisons of human RNase 1 to bovine RNase A. Although RNase A is perhaps the most important model protein in biological chemistry,[15,290,291] RNase A is the product of but one of three *RNASE1* duplicates in the bovine genome. Its expression is limited *in vivo*, and its evolution is recent. Despite these shortcomings, RNase A has been considered the archetypal RNase 1 enzyme, with its properties globally ascribed to all homologous proteins. Thus, the prevailing view of RNase 1 has been of a digestive enzyme possessing little importance beyond the ruminant gut.

Our data stand in stark contrast to this hypothesis. We find distinct differences between human RNase 1 and RNase A. Moreover, we have characterized an additional bovine variant, BRB, and find pronounced similarities between this unappreciated protein and human RNase 1. We have demonstrated that human RNase 1 and BRB share a similar thermostability, activity against single- and double-stranded substrates, pH optimum for catalysis, affinity for cell-surface glycans, and rate of cellular internalization. These features set apart human RNase 1 and BRB from either BSR or RNase A (Figure 3.5). Coupled with previous reports of the widespread tissue expression of BRB in cows,[35] our results suggest that BRB—not RNase A—is the true functional homolog of human RNase 1.

Our treatise is consistent with phylogenetic analyses, which suggest BRB resulted from an earlier genetic duplication than did either BSR or RNase A and thus resembles more closely the ancestral form of RNase 1 in ruminants.[275] Laboratory reconstructions of proposed “ancient”

bovine ribonucleases support this claim, showing that "ancestral" forms of bovine RNase 1 display properties more similar to BRB than RNase A, including decreased thermostability and increased activity toward dsRNA.[292,293] Compellingly, the timeline of the divergence of RNase A corresponds to the Oligocene cooling epoch, which resulted in the rise of grasslands and the emergence of ruminant digestion. Hence, RNase A most likely represents a specialized digestive form of RNase 1 that arose simultaneously with foregut fermentation.[270,292] A similar phenomenon is known to have occurred in colobine monkeys, where a secondary form of RNase 1—with properties distinct from the original enzyme—evolved to participate in ruminant-like digestion.[287] Taken together, extant evidence indicates that RNase A is not the prototype for mammalian RNase 1 in terms of function.

The question remains: if not digestion, what is the biological purpose of RNase 1? A conclusive answer to this question hinges upon future analysis of *in vivo* models. Still, our work does provide a basis for speculation. The ability of human RNase 1 and BRB to degrade dsRNA is of special interest because of its immunological implications. Most viruses produce dsRNA at some point during their replication. In mammalian cells, dsRNA is a potent antigen recognized by sensors such as Toll-like receptor (TLR) 3, through which dsRNA can trigger the transcription-based antiviral interferon response.[294] By degrading this antigenic stimulant, RNase 1 could play a crucial role in regulating antiviral immunity. Whereas the potential importance of dsRNA degradation by RNase 1 is clear, the mechanism of catalysis is not. The RNase 1 active site cannot simultaneously accommodate two nucleic acid strands; thus, the putative mechanism invokes the unwinding of the double helix by cationic residues near the enzymic active site. Arg-32[84,268] and Lys-102[289] have been implicated, in particular. Both of these cationic residues are present in human RNase 1 and BRB, but absent in BSR and RNase A.

Yet, other residues that could be important for dsRNA degradation by human RNase 1—including Arg-4, Lys-6, Lys-62, and Lys-74[288,289]—are not found in BRB, leaving unknown the precise basis for dsRNA degradation.

Intriguingly, the Toll-like receptors that respond to ssRNA and dsRNA (TLR7/TLR8 and TLR3, respectively) are all localized within endosomes.[295-297] Our current work demonstrates that both human RNase 1 and BRB internalize into mammalian cells significantly better than do either RNase A or mBSR. We have shown previously that RNase 1 internalization involves endocytosis;[128,132,298] thus, human RNase 1 and BRB might be especially well adapted to enter endosomes, where they could degrade antigenic RNA and regulate signaling cascades. Their increased cellular uptake could hinge upon increased interactions with negatively charged cell-surface glycans. Indeed, our data show that human RNase 1 and BRB bind much more tightly to an assortment of sulfated glycans, especially heparin, than does RNase A. This interaction is not merely based on Coulomb's law, as mBSR ($Z = +9$) binds much more weakly than does human RNase 1 ($Z = +6$). Accordingly, we posit that human RNase 1 and BRB contain putative heparan sulfate-binding motifs. For example, the BBXB motif, where B represents a basic residue, has been shown to be a common heparan sulfate-binding motif in proteins.[299-301] Human RNase 1 and BRB both contain three cationic regions that are similar to a BBXB motif and are absent from both mBSR and RNase A (Figure 3.4B). These unique areas of positive charge might account for many of the distinct properties shared by these enzymes, including dsRNA degradation, increased cellular internalization, and increased lipid disruption.

An unexpected result in our study is the pronounced divergence in pH optimum for catalysis among ribonucleases (Figure 3.1). We found RNase A to have a pH-optimum of 6.0, a value that closely reflects classic studies[302] and makes RNase A well-suited for the acidic environment of

the bovine rumen. Conversely, human RNase 1 and BRB had a pH-optimum of 7.3 and 7.4, respectively, which are close to the physiological pH of many bodily fluids, including blood (~7.4). These data correlate with observations that human RNase 1 circulates freely throughout the body in all fluids tested.[79] We speculate that differences in pH-optimum between homologs could be due to slight perturbations in the pK_a values of the active-site histidine residues. We were surprised to observe a large difference in optimum-pH (~1.3 pH units) for catalysis by the native dimeric form of BSR and the artificial monomer. The dimeric structure of BSR is also necessary for its other putative biological functions, including its immunosuppressive and antitumor activity.[271,286] The dimer is known to swap its N-terminal helices,[303,304] thereby forming a chimeric active site that could have higher histidine pK_a values. Thus, its unique quaternary structure appears to equip BSR for catalysis in the cytosol as well as in bovine seminal fluid, where the typical pH is 6.8–7.2.[305] The necessity for a dimeric form of BSR explains why BSR exists as a pseudogene in species where the cysteine residues required for dimerization have been lost.

Many questions remain regarding the biology of mammalian RNase 1, and BRB in particular. An ongoing mystery is how glycosylation of RNase 1 influences its endogenous functions. Analyses of human tissues and fluids indicate that various tissue sources produce differentially glycosylated forms of RNase 1;[93,94] BRB has also been shown to have *N*-linked glycans that are highly heterogeneous and distinct from those attached to RNase A.[306] A second perplexity surrounds BRB: what is the purpose of its extended, hydrophobic C-terminal tail? Although all ruminant brain ribonucleases possess a similar tail, the amino-acid sequences of these regions are not conserved, and seem to have arisen through multiple substitutions and deletions.[269,284] The tail is known to be *O*-glycosylated at two sites,[273] but the significance of

these oligosaccharide chains is not known. We speculated that the hydrophobic tail allows BRB to preferentially disrupt lipid membranes; however, our results showed that BRB did not have significantly different activity toward liposomes than either human RNase 1 or dBSR. Previous studies have shown that proline-rich motifs can be associated with facilitating protein–protein interactions, specifically transient interactions such as recruitment of multiple factors.[307] Thus, the proline-rich C-terminal tail of BRB could act as a protein scaffold to recruit other proteins.

In conclusion, we have presented data that establish functional relationships between human and bovine homologs of mammalian RNase 1. Our data provide fundamental insight into the biological role of RNase 1 in mammals, suggesting a physiology not associated with digestion. Further studies, including analyses of mammalian animal models, are necessary for a complete description of the most significant biological functions of RNase 1 in humans and other mammals. Finally, we note that our understanding of BRB has been hindered by its appellation, which incorrectly implies an association only with the brain, just as our understanding of human RNase 1 has been obfuscated by its undue association with the pancreas.

Table 3.1 Biochemical properties of human and bovine ribonucleases

Ribonuclease	MW (kDa)	Z^a	% Identity to RNase 1	% Similarity to RNase 1[b]	T_m (°C)[c]	K_d (fM)[d]	IC_{50} (μM)[e]
RNase 1 (*H. sapiens*)	14.7	+6	100	100	55.5 ± 0.5	0.12 ± 0.1	>30
BRB (*B. taurus*)	15.8	+11	61	72	52.2 ± 0.4	0.35 ± 0.21	>30
mBSR (*B. taurus*)	13.7	+9	70	80	60.1 ± 0.5	1.94 ± 0.72	>30
dBSR (*B. taurus*)	27.5	+18	70	80	62[f]	>2 x 10^{9}[g]	1.3 ± 0.1[h]
RNase A (*B. taurus*)	13.7	+4	68	82	63.9 ± 0.4	0.16 ± 0.12	>30

[a] Value is for the net molecular charge: Arg + Lys – Asp – Glu

[b] For % similarity calculations: K = R; D = E; C = G = H = N = Q = S = T = Y; A = F = I = L = M = P = V = W

[c] Value is the temperature at the midpoint of thermal denaturation, determined by incorporation of a hydrophobic dye and quantitation by differential scanning fluorimetry [279]

[d] Value is for the complex with bovine ribonuclease inhibitor, determined as previously described [127,143]

[e] Value is for the incorporation of [*methyl*-^{3}H]thymidine into the DNA of K-562 human leukemia cells, determined as previously described [127]

[f] Value was determined with circular dichroism spectroscopy [308]

[g] Value is for the complex with human ribonuclease inhibitor [286]

[h] From [251]

ND, not determined

Figure 3.1

A

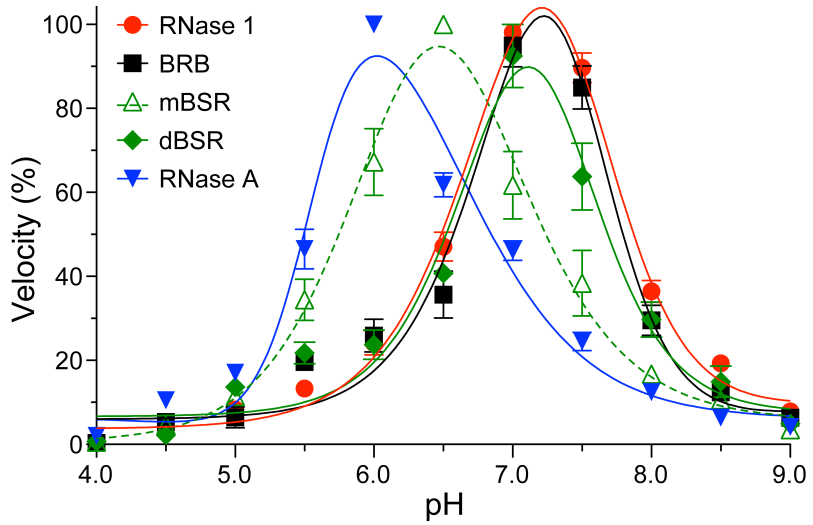

B

	pH Optimum	k_{cat}/K_M (10^6 $M^{-1}s^{-1}$) at pH Optimum
RNase 1	7.3	2.8 ± 1.6
BRB	7.4	2.2 ± 1.4
dBSR	7.2	0.3 ± 0.1
mBSR	6.3	4.9 ± 1.7
RNase A	6.0	11.5 ± 1.5

Figure 3.1 Effect of pH on catalysis by human and bovine RNases

A. pH–Rate profiles using the normalized initial velocity for cleavage of single-stranded RNA. Values (± SE) are the mean from at least three independent experiments. *B*. pH optima for catalysis as calculated from the data in panel *A*, and values (± SE) of k_{cat}/K_M at that pH.

Figure 3.2

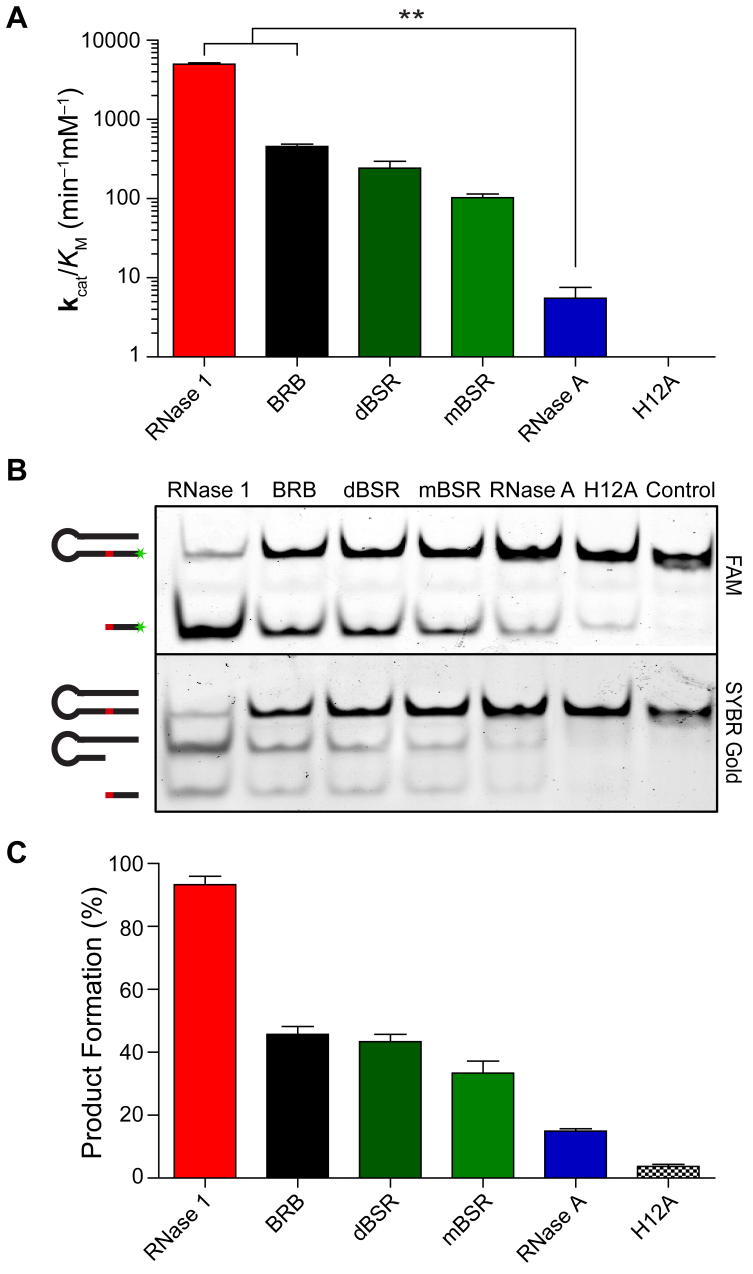
A
**
10000
1000
100
10
1
k_{cat}/K_M (min^{-1}mM^{-1})
RNase 1
BRB
dBSR
mBSR
RNase A
H12A
B
RNase 1
BRB
dBSR
mBSR
RNase A
H12A
Control
FAM
SYBR Gold
C
Product Formation (%)
100
80
60
40
20
0
RNase 1
BRB
dBSR
mBSR
RNase A
H12A

Figure 3.2 Catalysis of double-stranded RNA cleavage by human and bovine RNases *A*. Values k_{cat}/K_M for the cleavage of poly(A:U). Values (± SE) are from at least three independent experiments. $^{**}p < 0.01$. *B*. Native polyacrylamide gel showing cleavage of a DNA hairpin containing a single RNA residue (red) and labeled on the 5′ end with FAM (green). SYBR Gold enables imaging of all nucleic acids. *C*. Extent of FAM-labeled product formation for the data in panel *B*. Values (± SE) are the mean from four native gels.

Figure 3.3

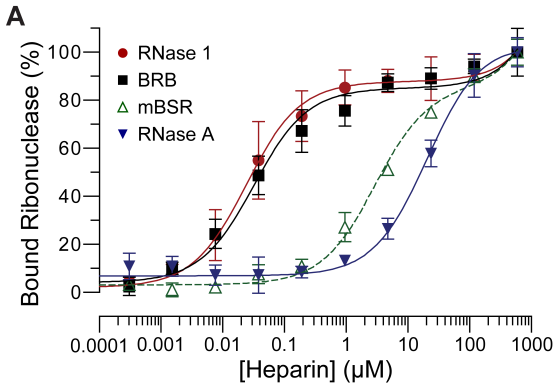
A
Bound Ribonuclease (%)
RNase 1
BRB
mBSR
RNase A
[Heparin] (μM)

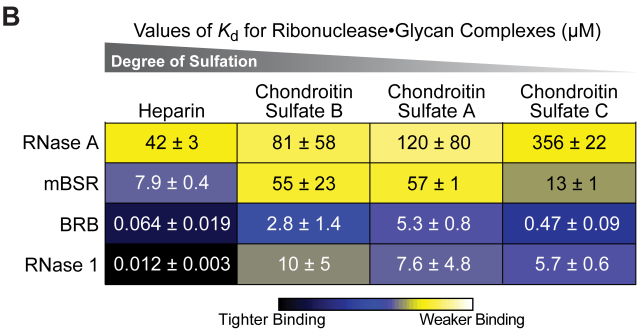
B
Values of K_d for Ribonuclease•Glycan Complexes (μM)
Degree of Sulfation
Heparin
Chondroitin Sulfate B
Chondroitin Sulfate A
Chondroitin Sulfate C
RNase A
42 ± 3
81 ± 58
120 ± 80
356 ± 22
mBSR
7.9 ± 0.4
55 ± 23
57 ± 1
13 ± 1
BRB
0.064 ± 0.019
2.8 ± 1.4
5.3 ± 0.8
0.47 ± 0.09
RNase 1
0.012 ± 0.003
10 ± 5
7.6 ± 4.8
5.7 ± 0.6
Tighter Binding
Weaker Binding

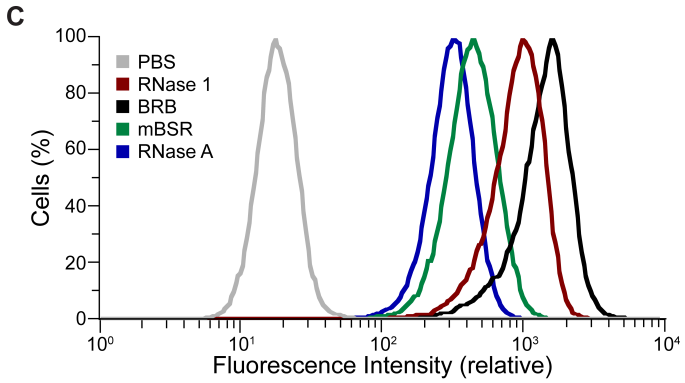
C
Cells (%)
PBS
RNase 1
BRB
mBSR
RNase A
Fluorescence Intensity (relative)

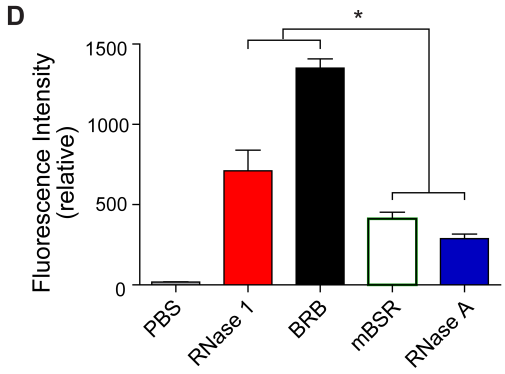
D
Fluorescence Intensity (relative)
PBS
RNase 1
BRB
mBSR
RNase A

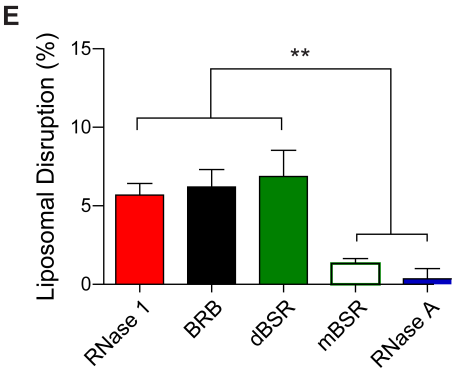
E
Liposomal Disruption (%)
RNase 1
BRB
dBSR
mBSR
RNase A

Figure 3.3 Cellular interactions of human and bovine RNases

A. Representative isotherms for binding of BODIPY-labeled ribonucleases to heparin as determined by fluorescence polarization. *B*. Heatmap indicating the relative affinity for various cell-surface glycans, determined as in panel *A*. Values (± SE) are the mean from at least three independent experiments. Blue tones represent nM affinity; yellow tones represent μM affinity. *C*. Representative flow cytometry data on the uptake of BODIPY-labeled ribonucleases into K-562 cells after 4 h. *D*. Uptake of BODIPY-labeled ribonucleases into K-562 cells after 4 h, determined as in panel *C*. Values (± SE) are the mean from four independent experiments. *$p < 0.05$. *E*. Disruption of phosphatidylcholine liposomes by ribonucleases, as measured by the release of an encapsulated dye. Values (±SE) are the mean from at least three independent experiments. **$p < 0.01$.

Figure 3.4

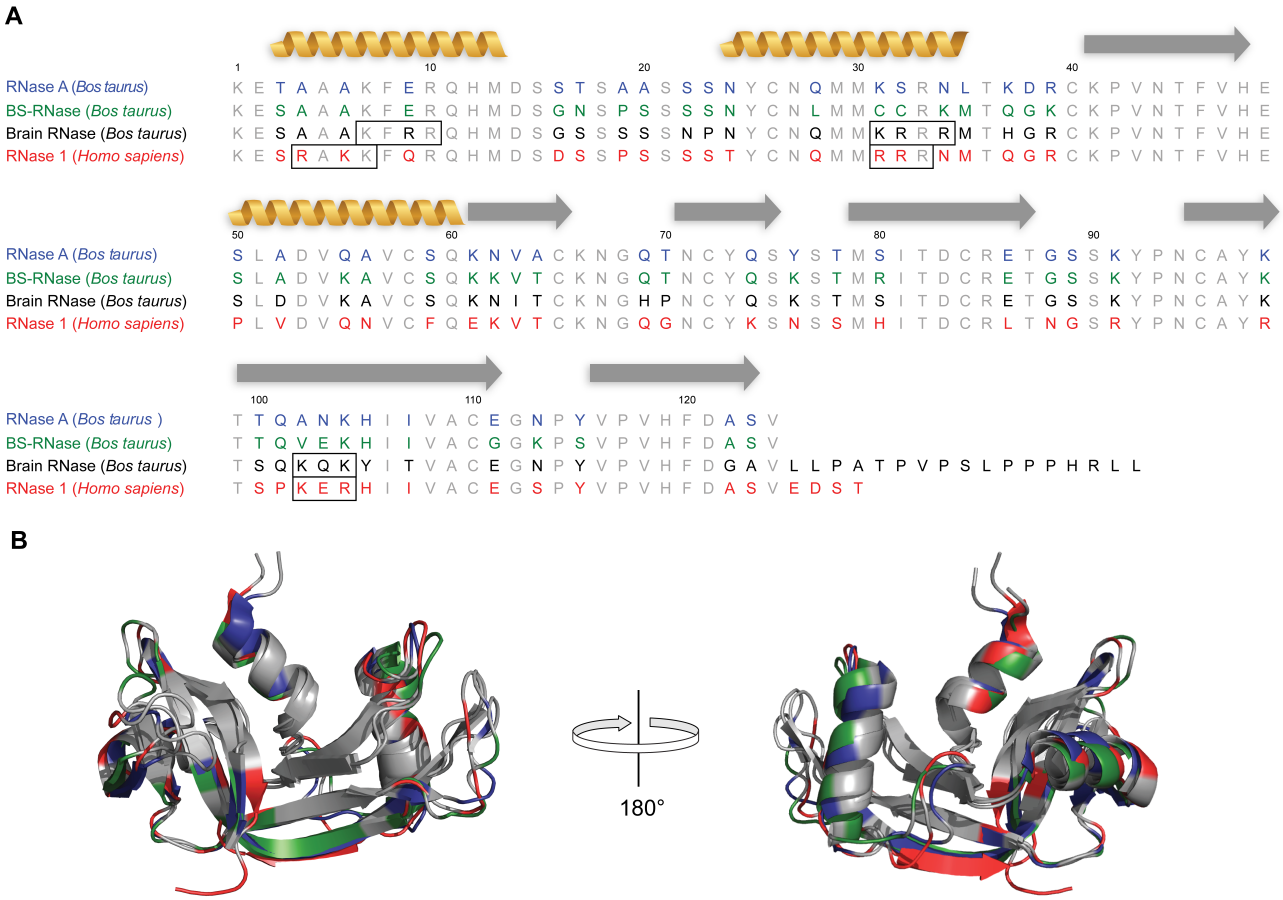
A
RNase A (Bos taurus)
BS-RNase (Bos taurus)
Brain RNase (Bos taurus)
RNase 1 (Homo sapiens)
B
180°

Figure 3.4 Sequence and structural alignment of human and bovine RNases

A. Grey residues indicate residues conserved in all proteins; colored residues indicate divergence. Black boxes indicate putative heparan sulfate-binding domains. Yellow coils denote α-helices; gray arrows denote β-sheets. *B*. Backbone overlay of human RNase 1 (red; PDB entry 1z7x), mBSR (green; 1bsr), and RNase A (blue; 1fs3).

Figure 3.5

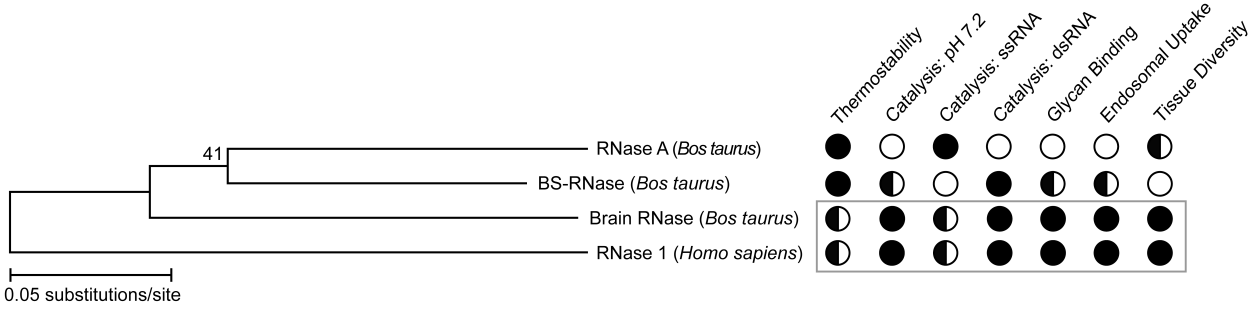
Thermostability
Catalysis: pH 7.2
Catalysis: ssRNA
Catalysis: dsRNA
Glycan Binding
Endosomal Uptake
Tissue Diversity
41
RNase A (Bos taurus)
BS-RNase (Bos taurus)
Brain RNase (Bos taurus)
RNase 1 (Homo sapiens)
0.05 substitutions/site

Figure 3.5 Biochemical and phylogenetic summary of data for human and bovine RNases Bootstrap values >40 are indicated in the phylogenetic tree. Solid circles indicate a high level of functionality; half-open circles indicate a medium level, and open circles indicate a low level. Tissue expression data for human and bovine ribonucleases are from ref. 79 and 35, respectively.

Figure 3.6

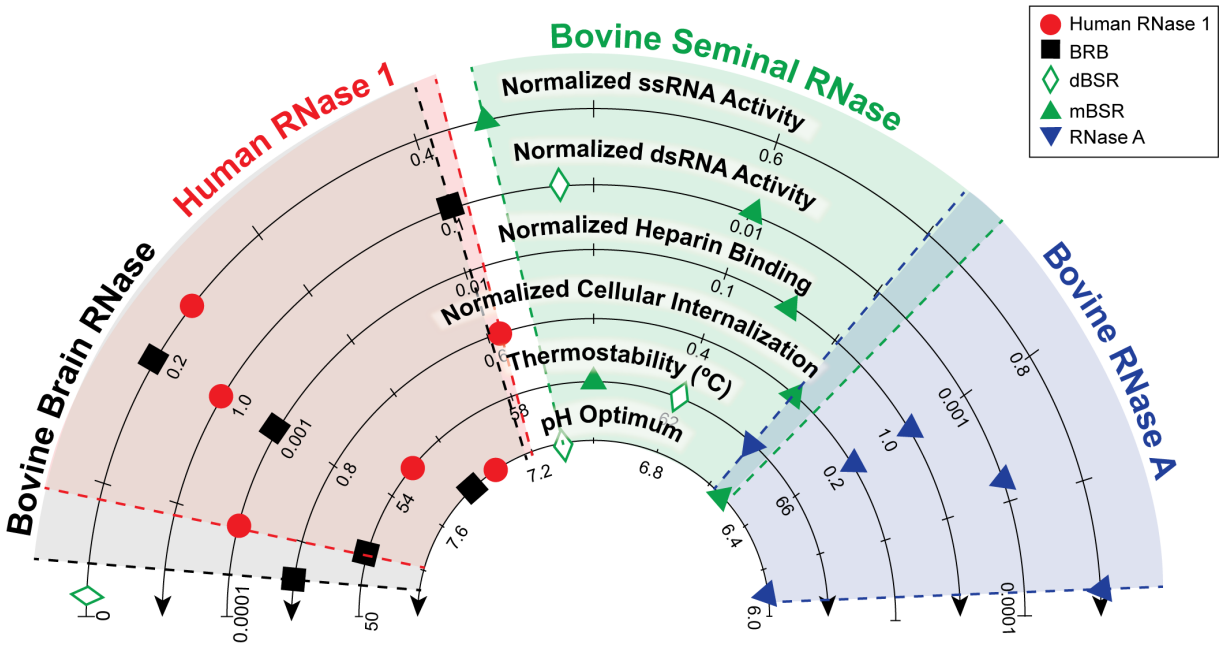
Human RNase 1
BRB
dBSR
mBSR
RNase A
Bovine Seminal RNase
Human RNase 1
Bovine Brain RNase
Bovine RNase A
Normalized ssRNA Activity
Normalized dsRNA Activity
Normalized Heparin Binding
Normalized Cellular Internalization
Thermostability (°C)
pH Optimum

Figure 3.6 Schematic representation of biochemical data for human and bovine RNases Normalized data are fit along a linear range with an indicated directionality. Colored shapes indicate data obtained for each RNase from assays presented throughout this manuscript, whereas colored shaded regions indicate the range of all values for a particular RNase.

Figure 3S.1

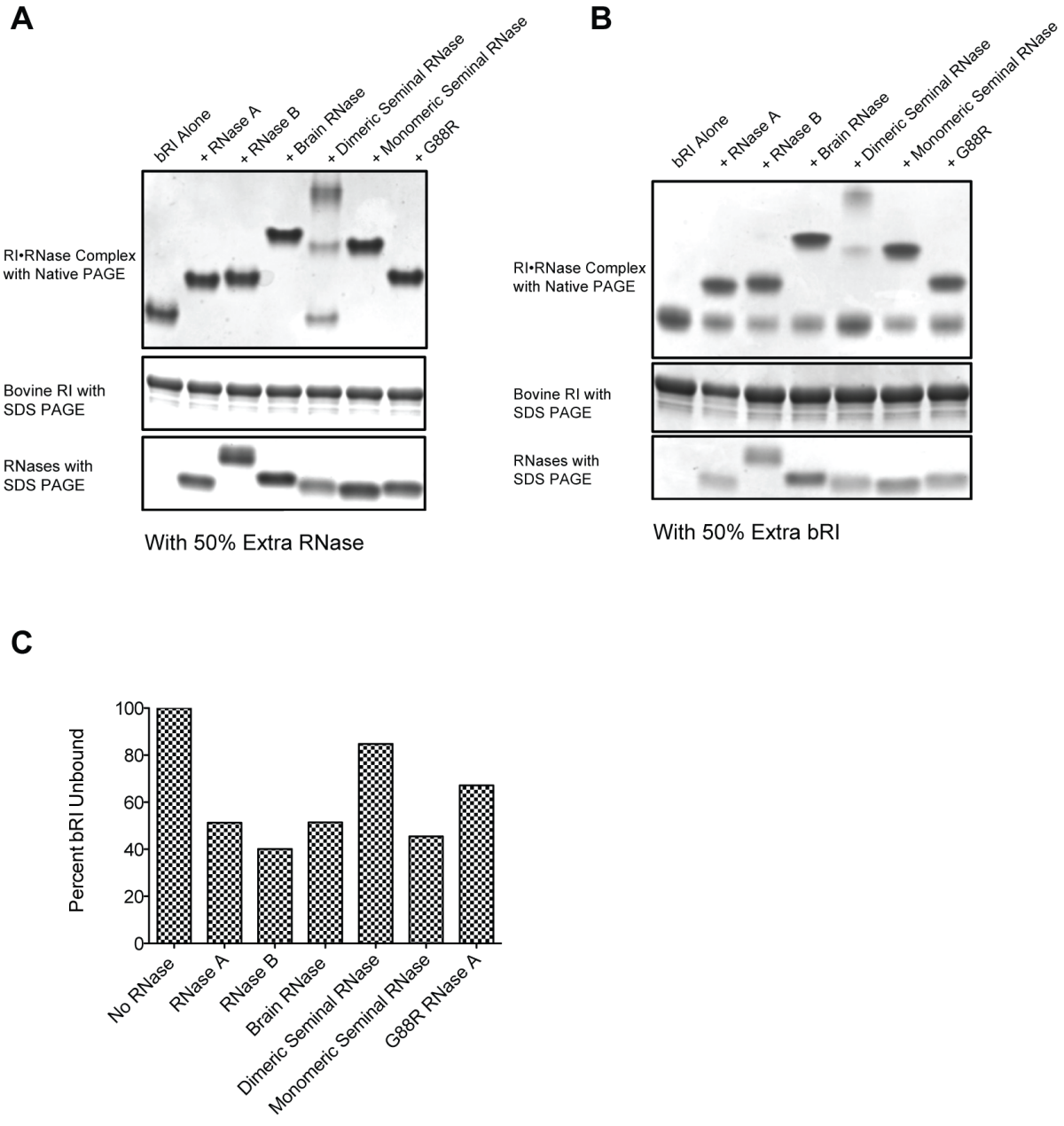
A
bRI Alone
+ RNase A
+ RNase B
+ Brain RNase
+ Dimeric Seminal RNase
+ Monomeric Seminal RNase
+ G88R
RI•RNase Complex with Native PAGE
Bovine RI with SDS PAGE
RNases with SDS PAGE
With 50% Extra RNase
B
bRI Alone
+ RNase A
+ RNase B
+ Brain RNase
+ Dimeric Seminal RNase
+ Monomeric Seminal RNase
+ G88R
RI•RNase Complex with Native PAGE
Bovine RI with SDS PAGE
RNases with SDS PAGE
With 50% Extra bRI
C
Percent bRI Unbound
100
80
60
40
20
0
No RNase
RNase A
RNase B
Brain RNase
Dimeric Seminal RNase
Monomeric Seminal RNase
G88R RNase A

Figure 3S.1 Native gel shift showing binding affinity for bovine RNases and bovine RI

A. Native gel shift showing the binding affinity of various bovine RNases to bovine RI. RNases were added in 50% molar excess to RI. Middle and lower panels show loading volumes of RNases and RI as a control. *B*. Native gel shift with 50% molar excess of RI, allowing for the detection and quantification of unbound RI. *C*. Densitometric quantification of unbound RI fraction is panel B

Figure 3S.2

A

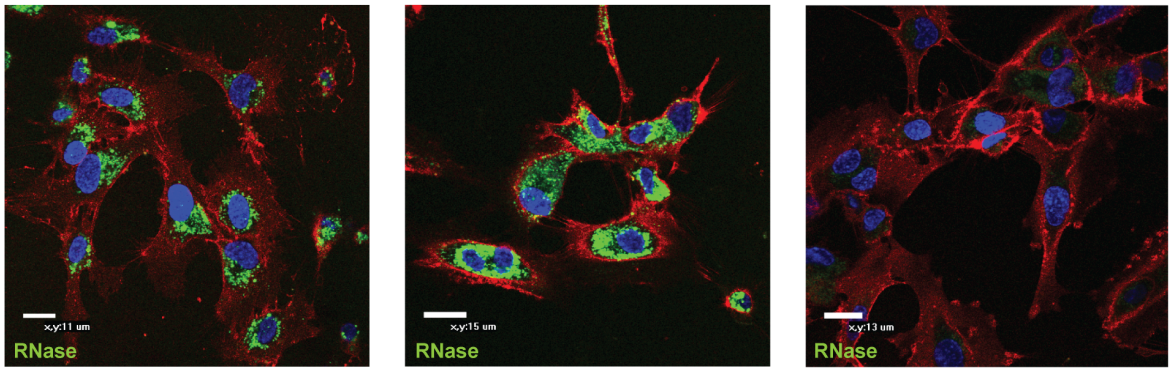

Human RNase 1 (human endothelial cells)

Bovine Brain RNase (bovine endothelial cells)

Bovine RNase A (bovine endothelial cells)

B

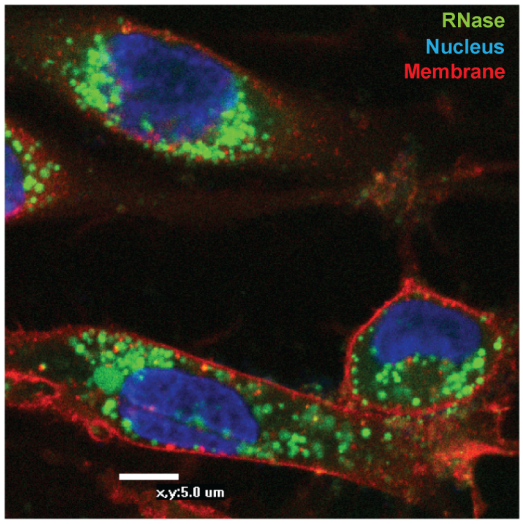

Bovine Brain RNase (bovine endothelial cells)

C

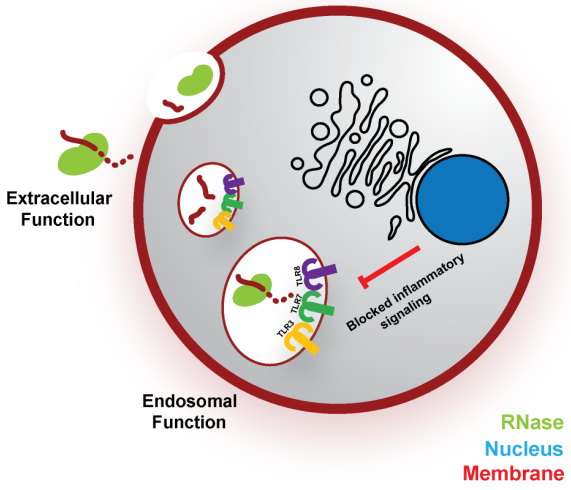

Figure 3S.2 Confocal microscopy showing endosomal uptake of ribonucleases

A. Confocal micrographs showing endosomal uptake of fluorescently labeled ribonucleases. *Left panel*: human RNase 1 is readily endocytosed into human umbilical vascular endothelial cells (HUVEC). *Middle panel*: bovine brain RNase is readily endocytosed into bovine brain endothelial cells (BBE). *Right panel*: bovine RNase A is not readily endocytosed into BBE cells. *B*. Zoomed-in image showing florescent punctae (endosomes containing fluorescently-labeled RNases). *C*. Cartoon model demonstrating putative role of RNases to degrade antigenic RNA in the endosomes and attenuate inflammatory signaling from toll-like receptors.

CHAPTER 4

Functional Evolution of Ribonuclease Inhibitor: Insights from Birds and Reptiles

Contribution: I produced all proteins used in this study and performed all biochemical characterizations. Protein crystal generation, X-ray diffraction, and structure determination was performed by Chris M. Bianchetti and Aram Chang.

Prepared for submission as:

Lomax J.E., Bianchetti, C.M. Chang, A, Phillips, G., Fox, B., Raines, R.T. (2014)

4.1 Abstract

Ribonuclease inhibitor (RI) is a conserved protein of the mammalian cytosol. RI binds with high avidity to diverse secretory ribonucleases (RNases) and inhibits their enzymatic activity. Although secretory RNases are found in all vertebrates, no homologs of RI have been characterized from non-mammalian species, and the existence of non-mammalian RI has been questioned. Here, we report on the identification and characterization of RI homologs from chicken and anole lizard. These proteins bind to RNases from multiple species, but exhibit much greater affinity for their cognate RNases than for mammalian RNases. To understand the mechanism governing the differential binding affinity between proteins from diverse species, we determined the crystal structures of mouse, bovine, and chicken RI•RNase complexes to a resolution of 2.20Å, 2.21Å, and 1.92Å, respectively. A combination of bioinformatics, computational biology, and structural analysis allowed for the identification of two potential residues that may contribute to the contrasting binding strength. Our study also reveals startling differences in oxygen sensitivity between mammalian and non-mammalian RIs, suggesting evolution toward greater thiol reactivity in RIs from mammalian species. Taken together, our results highlight the structural and functional evolution of ribonuclease inhibitor and shed light on its dynamic role in vertebrate biology.

4.2 Introduction

Understanding the sequence–structure–function relationships of proteins, as well as how evolution has guided and shaped these relationships, is a central aim of biology. A protein that is particularly worthy of study—due to its unique structure, fascinating biology, and emerging evolution—is ribonuclease inhibitor (RI).

RI is a highly conserved, 50-kDa protein present in the cytosol of all mammalian cells. Its name originates from its ability to inhibit the ribonucleolytic activity of a large variety of secretory ribonucleases (RNases).[27] The structure of RI is composed entirely of leucine-rich repeats (LRR), a domain specifically associated with protein–protein and protein–ligand interactions.[309] Crystal structures of both free[310] and RNase-bound[221,311-313] RI have yielded a wealth of information about the LRR fold and its interaction with ligands. Beyond its unique shape, RI also possesses a large number of conserved cysteine residues, which must each be in their reduced form to maintain form and function.[152,314] Indeed, oxidation of even a single cysteine leads to a cooperative "all-or-none" cascade of disulfide-bond formation, resulting in the complete inactivation of RI.[315] Tellingly, treatment of cultured cells with oxidants is sufficient to cause the rapid disappearance of RI.[152]

Despite vast knowledge about its structure, the biological function of RI remains enigmatic. Based on its extremely tight affinity for diverse secretory RNases,[33] RI could serve to regulate the localization and function of RNases *in vivo*. Engineering RNases to evade RI binding imbues them with latent cytotoxicity for human cells,[129] and overproduction of RI makes cells less susceptible to cytotoxic RNases.[145] Recent studies indicate RI might dynamically regulate the function of the secretory RNase angiogenin,[50,151] as well as the secreted skin ribonuclease, RNase 7.[60]

In addition to controlling the activity of RNases, RI could play a role in maintaining intracellular redox homeostasis. The cytosolic localization of RI, coupled with its many free cysteine residues, suggests that RI might scavenge reactive oxygen species (ROS).[153,154,316] ROS encompass a variety of highly reactive chemical species including superoxide anion, hydroxyl radical, and hydrogen peroxide.[317] The role of ROS and oxidative stress in various human diseases, cancer and aging is becoming increasingly recognized.[318] Knockdown of RI in various human cell lines leads to enhanced susceptibility to oxidant-induced DNA damage.[154] Similarly, overproduction of RI can protect cells against the effects of oxidative stress.[155] *In vivo*, oxidation of RI has been linked to the progression of pancreatitis,[319] as well as to the effectiveness of certain cancer treatments.[320] Intriguingly, RI is present in red blood cells, which contain neither a nucleus nor RNA. RI might play a role in protecting red blood cells from oxidative-stress-related ageing and turnover.[156,157]

An overarching mystery in RI biology has been its apparent absence from non-mammalian species. Secretory ribonucleases are known to be present in all vertebrates.[32,321] Inhibition of ribonucleolytic activity has been previously detected in cellular lysates from non-mammalian hosts.[29] Yet, the source of this inhibition has never been characterized, and no specific non-mammalian RI homologs have been isolated.

We have identified and characterized homologous ribonuclease inhibitors from two non-mammalian species: chicken and anole lizard. Our efforts provide much insight into the evolution of RI structure and function, and on its biological role. We show pronounced differences in oxidation sensitivity across homologs, suggesting a dynamic evolutionary shift between mammals and non-mammals. Our observation that RI occurs in a wide range of animals indicates an essential role for this protein.

4.3 Materials and Methods

4.3.1 Materials and Instrumentation

E. coli BL21(DE3) cells and the plasmid pET22b(+) were from EMD Millipore. 6-FAM–dArU$(dA)_2$–6-TAMRA, a fluorogenic ribonuclease substrate, as well as DNA oligonucleotides for PCR, sequencing, and mutagenesis were from Integrated DNA Technologies. Protein purification columns were from GE Healthcare. Costar 96-well NBS microtiter plates were from Corning Life Sciences. Restriction and PCR enzymes were from Promega. All other chemicals were of commercial grade or better and were used without further purification.

The molecular mass of each RI and ribonuclease was determined by matrix-assisted laser desorption/ionization-time-of-flight (MALDI–TOF) mass spectrometry using a Voyager-DE-PRO Biospectrometry Workstation (Applied Biosystems). MALDI–TOF mass spectrometry experiments were performed at the campus Biophysics Instrumentation Facility. All fluorescence and absorbance measurements were made using a Tecan M1000 fluorimeter plate reader, unless stated otherwise. All data were fit and analyzed using the graphing software package Prism 5 (GraphPad), unless stated otherwise.

4.3.2 Ribonuclease Inhibitor cloning and purification

Human RI[221] and bovine RI[143] constructs were inserted previously into the pET22b expression vector for tagless expression in BL21(DE3) *E. coli*. The gene encoding mouse RI (Gene ID: 107702) was amplified from *Mus musculus* liver cDNA and inserted in the pET22b vector. The sequences of chicken RI (Gene ID: 423111) and anole RI (Gene ID:100553617) were identified by their hypothetical annotation in the GenBank database. The genes encoding chicken RI and anole RI were amplified from *Gallus gallus* liver cDNA and *Anolis carolinsis*

liver cDNA (Reptile Rapture, Madison, WI), respectively, and inserted into pET22b with an N-terminal, protease-cleavable 6× His tag. All primers used for cloning are listed in Table S1.

Human, bovine, and mouse RI were purified via RNase A–affinity chromatography and ion–exchange chromatography as described previously.[143,221] Chicken RI and anole RI were produced as described previously,[143] with the following modifications. In lieu of RNase A–affinity chromatography, chicken and anole RI were purified over a nickel column and eluted over a linear gradient of imidazole. They were then purified again over an anion–exchange column to yield highly pure protein. The N-terminal 6× His purification tag was cleaved by incubation with TEV protease,[322] yielding native RI proteins with a single N-terminal glycine residue. Molecular masses of RI proteins were confirmed by MALDI–TOF mass spectrometry. Protein concentration was determined by using a Bradford assay kit (Pierce) with BSA as a standard.

4.3.3 Ribonuclease cloning and purification

Human RNase 1[143], bovine RNase A[143] and frog RNase (*Rana pipiens*)[132] constructs were inserted previously into the pET22b expression vector for tagless expression in BL21(DE3) *E. coli*. The gene encoding mouse RNase 1 (Gene ID: 19752) was amplified from *Mus musculus* pancreas cDNA and inserted into pET22b. The gene encoding chicken RNase A-1[74] (Gene ID: 396194) was amplified from *Gallus gallus* liver cDNA and inserted into pET22b. The novel anole RNase used in this study, referred to as "anole RNase 1", was identified by BLAST analysis using human RNase 1 as an input. This RNase was the most evolutionarily similar to human RNase 1 from all returned BLAST hits, as determined by phylogram analysis (data not shown), and possessed the identifier "LOC100555482 ribonuclease-like". The gene encoding anole RNase 1 (Gene ID: 100555482) was amplified from *Anolis carolinsis* liver cDNA and

inserted into pET22b. The gene encoding zebrafish RNase 3/4[77,78] (Gene ID: 100101462) was amplified from *Danio rerio* cDNA and inserted into pet22b. The program Signal P was used to predict and exclude peptide leader sequences for all proteins. All primers used for cloning are listed in Table S1.

To enable site-specific fluorescent labeling of ribonucleases, cysteine residues were introduced by site-directed mutagenesis into loop regions that are distal to both the enzymic active site and RI-binding interface. The ensuing variants were P19C human RNase 1, S19C mouse RNase 1, A19C bovine RNase 1, T17C chicken RNase A-1, S20C anole RNase 1, A14C zebrafish RNase 3/4, and S61C frog RNase. RNases were purified as inclusion bodies and free-cysteine protein variants were labeled with diethylfluorescein[256] as described.[127,143,323] Molecular masses of RNase conjugates were confirmed by MALDI–TOF mass spectrometry. Protein concentration was determined by using a bicinchoninic acid (BCA) assay kit (Pierce) with wild-type RNase A as the standard.

4.3.4 RI·RNase dissociation rate

For the tightest-binding RI·RNase complexes ($K_d \leq 10^{-15}$), the dissociation rate constant (k_d) was determined by following the release of diethylfluorescein (DEFIA)-labeled ribonuclease from the RI·RNase complex over time, as described previously.[127] Briefly, RI and a DEFIA-labeled RNase were mixed in equimolar ratios, and the resulting solution was incubated at 25 °C for 5 min. A 50-fold molar excess of human RNase 1 was added to scavenge dissociated RI. Complex dissociation was measured by monitoring the increasing fluorescence of dissociated RNase over time (≥60 days). A value of K_d for each complex was determined as described previously.[127] These values represent the mean from at least three independent experiments.

For weaker-binding complexes ($K_d \geq 10^{-9}$), an RI-saturation binding assay was used, as

described previously.[255] Briefly, fluorescence spectroscopy was used to monitor the binding of an RI to a DEFIA-labeled ribonuclease, availing the decrease in fluorescence upon binding to RI. Data were normalized to unbound DEFIA-RNase and fitted with nonlinear regression analysis to obtain a value of K_d for each complex. These values are the mean from at least three independent experiments.

4.3.5 T_m Determination

Thermal unfolding of RIs (unbound and bound to an RNase) was monitored in the presence of a fluorescent dye using differential scanning fluorimetry (DSF). DSF was performed using a ViiA 7 Real-Time PCR machine (Applied Biosystems) as described.[244,324] Briefly, a solution of protein (10 μg) was placed in the wells of a MicroAmp optical 96-well plate, and SYPRO Orange dye (Sigma Chemical) was added to a final dilution of 1:333 in relation to the stock solution of the manufacturer. The temperature was increased from 20–96 °C at 1 °C/min in steps of 1 °C. Fluorescence intensity was measured at 578 nm, and the resulting data were analyzed with Protein Thermal Shift software (Applied Biosystems). A solution with no protein was used for background correction. Values of T_m were calculated from curves of ∂fluorescence/∂T and are the mean from three independent experiments.

4.3.6 RI·RNase complex purification

Mouse, bovine, and chicken RI·RNase complexes were purified for crystallization as described previously.[221] Briefly, purified RNase (~50 mg/ml) and RI (~10 mg/ml) were mixed at a 1.2:1.0 molar ratio, and this solution was incubated at 25 °C for 20 min to allow for complex formation. The solution was then purified using anion-exchange chromatography to remove any

unbound RNase. Purified complex was dialyzed for 16 h at 4 °C against 20 mM Hepes–NaOH buffer (pH 7.5) containing DTT (10 mM) and glycerol (2% v/v), and concentrated to ~10 mg/ml. Aliquots were flash frozen and stored at −80 °C.

4.3.7 Crystallization of RI·RNase complexes

All RI·RNase complexes were screened for initial crystallization conditions using a Mosquito nanoliter liquid handling robot (TTP LabTech), and the resulting crystals were optimized using the hanging drop vapour diffusion method at 20 °C. Crystals for bovine RI·RNase were observed in the PACT premier HT screen (Molecular Dimensions) and grew to maximum size within a week.[325] Optimized bovine RI·RNase crystals that were used for structure determination were grown by mixing 1 μL of protein solution with 1 μL of 25% w/v PEG 1500 and 100 mM malic acid/MES/Tris (MMT) buffer (pH 4.0). Initial chicken RI·RNase crystals were observed in the PEGRx HT screen (Hampton research) and grew to maximum size within 24 h.

Crystals used to determine the chicken RI·RNase structure were grown by mixing 1 μL of protein solution with 1 μL of 21% w/v PEG 1500 and 100 mM sodium citrate buffer (pH 3.5). Mouse RI·RNase crystals were observed in the IndexHT screen (Hampton research) and were optimized further. The crystals that were used to determine the mouse RI·RNase structure were grown by mixing 1 μL of protein solution with 1 μL of 25% w/v PEG 3350 and 100 mM sodium citrate buffer (pH 3.5). All RI·RNase crystals were frozen directly in liquid N_2 before data collection. The bovine, chicken, and mouse crystals were cryoprotected by the addition of ethylene glycol to 15%, 15%, and 20% v/v, respectively, to the solutions described above.

4.3.8 Structure Determination of RI·RNase complexes

Diffraction images for bovine RI·RNase, chicken RI·RNase, and mouse RI·RNase were collected at the Life Sciences Collaborative Access Team 21-ID-G, 21-ID-G, and 21-ID-D beamlines, respectively, at the Advanced Photon Source, Argonne National Laboratory. All the RI·RNase structures presented here were solved by molecular replacement with Phaser[326] using PDB entries 1dfj[144] and 1z7x[221] as a starting model for bovine, and chicken and mouse, respectively. All RI·RNase structures were completed with altering rounds of model building in Coot[327] and refinement in Phenix.[328] Model quality was assessed with Molprobity[329] before deposition to the PDB. Structural images were generated with PyMOL (The PyMOL Molecular Graphics System, Version 1.5.0.4 Schrödinger, LLC). Data collection, refinement, and model statistics are presented in Table 2. All structures used in this study were analyzed with the program PDBsum[330] to identify intermolecular hydrogen bonds and van der Waals contacts. PDBsum uses the algorithm HBPLUS[331] to identify hydrogen bonds ($r_{X\cdots X}$ <3.3 Å). Structures were also analyzed using the Knowledge-based FADE and Contacts (KFC2) server.[332,333]

4.3.9 Oxidative stability of RI·RNase complexes

The stability of RI·RNase complexes to oxidation by hydrogen peroxide (H_2O_2) was assessed by following the release of diethylfluorescein-labeled ribonuclease upon RI dissociation, as described.[143] Briefly, fresh H_2O_2 (30% v/v, Fisher Scientific) was diluted serially in reaction buffer (20 mM HEPES–HCl buffer, pH 7.0, containing 50 mM KCl) to produce a final range of 30–0.001% v/v H_2O_2. Desalted RI (100 nM) and ribonuclease (100 nM) were combined in 50 µL of reaction buffer across a 96-well plate and incubated for 20 min at 25 °C to allow for complex formation. Initial fluorescent readings were taken, and 50 µL of H_2O_2 serial dilutions were added

to each well containing the RI·RNase complex. Plates were incubated at 37 °C for 1 h, and final fluorescent readings were taken. Data were normalized to control wells containing only labeled RNase at each H_2O_2 concentration and fitted using nonlinear regression to generate H_2O_2 IC_{50} values for complex dissociation. Values represent the mean from at least three independent experiments.

The release of active ribonuclease from the RI·RNase complex in response to H_2O_2 treatment was measured by assessing the ability of ribonucleases to cleave a fluorogenic RNA substrate, as described previously.[242] Briefly, RIs and RNases were incubated in equimolar ratios (50 nM for human, mouse, bovine, and chicken; 500 nM for anole) in 50 μL of reaction buffer and allowed to form RI·RNase complexes. Initial fluorescent readings were recorded, and 50 μL of H_2O_2 serial dilutions (see above) were added to each well containing a RI·RNase complex. Plates were incubated at 37 °C for 1 h, and final fluorescent readings were recorded. Data were normalized to control wells containing only labeled RNase at each H_2O_2 concentration and fitted with nonlinear regression analysis to generate values of IC_{50} for complex dissociation. These values represent the mean from at least three independent experiments.

4.3.10 Quantification of RI thiol groups and cysteine solvent-exposed surface area

Accessible protein sulfhydryl groups were quantified by UV spectroscopy using Ellman's Reagent (Pierce) according to the manufacturer's protocol. Briefly, 10 μM RI was eluted from PD-10 columns (GE Healthcare) to remove all traces of reducing agents. A 250-μL aliquot of desalted RI (10 μM) was added to 2.5 mL of reaction buffer (0.10 M sodium phosphate buffer, pH 8.0, containing 1 mM EDTA) and 50 μL of Ellman's Reagent solution (4 mg/mL in reaction buffer). The resulting solutions were incubated for 15 min at 25 °C, and their absorbance was

recorded at 412 nm and converted to absolute values using *N*-acetylcysteine as the standard (0–0.1 mM). Samples were analyzed in triplicate and values represent the mean from three independent experiments.

The solvent-accessible surface area of cysteine residues in RI crystal structures was calculated with PyMOL.[334]

4.3.11 Ribonuclease Inhibitor Phylogenetic Tree Reconstruction

Annotated ribonuclease inhibitor protein sequences were obtained from the National Center for Biotechnology Information (NCBI) database. Only 100% complete sequences were used for analysis. RI protein sequence alignments were made using MUSCLE[211] with manual adjustments. A maximum–likelihood phylogenetic tree was generated in MEGA5.2[212] using the Jones–Taylor–Thornton (JTT)[335] substitution model and 1000 bootstrap replicates. Non-uniformity of evolutionary rates was modeled using a discrete Gamma distribution,[214] assuming for the presence of invariable sites. Bootstrap values >50 are reported.

4.3.12 Native gel-shift analysis of RI·RNase complexes

Ribonuclease inhibitors and ribonucleases from endogenous species were incubated together in a 1:1.2 molar ratio at 25 °C for 20 min to allow for complex formation. A 10-µL aliquot of protein solution was combined with 2 µL of a 6× loading dye, and the resulting mixtures were loaded immediately onto a non-denaturing 12% w/v polyacrylamide gel (BioRad). Gels were run in the absence of SDS at 20–25 mA for ~3 h at 4 °C and stained with Coomassie Brilliant Blue G-250 dye (Sigma Chemical).

4.3.13 RI inhibition of endogenous ribonucleolytic activity

Ribonuclease inhibitors were diluted to 10 μM in PBS, and diluted serially across a 96-well plate to yield a final range of 0.001 pM–1 μM RI. A fluorogenic RNA substrate was added to each well (0.2 μM of 6-FAM–dArU$(dA)_2$–6-TAMRA from IDT)[242] and baseline fluorescent readings were recorded. Ribonucleases were added to a final concentration of 50 pM (human, bovine, mouse, chicken) or 500 pM (anole), and the initial velocity of substrate cleavage was measured by following the increase in fluorescence over time. After 10 min, substrate cleavage was saturated by the addition of 5 μM bovine RNase A. Values of k_{cat}/K_M were determined for each RI concentration as described previously,[242] and these values were normalized to those in the absence of RI. Values represent the mean of at least three independent experiments.

4.3.14 Ribonuclease phylogenetic tree reconstruction

Ribonuclease protein sequence alignments were made using MUSCLE[211] with manual adjustments. A maximum–likelihood phylogenetic tree was generated in MEGA5.2[212] using the Whelan and Goldman (WAG)[213] substitution model and 1000 bootstrap replicates. Non-uniformity of evolutionary rates was modeled using a discrete Gamma distribution,[214] assuming for the presence of invariable sites. Bootstrap values >40 are reported.

4.4 Results

4.4.1Production of ribonuclease inhibitor from mouse, chicken, and anole

Prior to our work, the presence of a homologous ribonuclease inhibitor (RI) in a non-mammalian species had never been confirmed. We located avian and reptile homologs of RI, and produced these proteins heterologously in *Escherichia coli*. In addition, we produced the mouse homolog of RI, which had never been characterized. To enable comparisons, we produced the

previously characterized human and bovine RI proteins.[143] All RI homologs have similar molecular weight, contain unusually high cysteine and leucine content, and have a strong overall negative charge (Table 1). Mammalian RI homologs share relatively high sequence identity and similarity to each other. Avian and reptile RI homologs are more similar to each other than to any of the mammalian RIs (Table S3). Our initial characterization determined that RI from each species bound tightly to its cognate ribonuclease in a 1:1 ratio and completely inhibited ribonucleolytic activity (Figure S1a and S1b).

4.4.2 Contrasts between intra- and inter-species RI·RNase binding affinity

To quantify the stability of both endogenous RI·RNase complexes as well as inter-species complexes, we used binding assays that employ a fluorescently labeled RNase (Figure 1). From these data, we determined equilibrium dissociation constants for each RNase paired with each RI in our study (Figure 1c; Table S2). We found that each endogenous RI·RNase complex was extremely tight ($K_d \leq$ fM). Additionally, the mammalian RIs bind tightly to mammalian RNases, and avian and reptile RIs bind tightly to avian and reptile RNases. Interestingly, complexes formed between evolutionarily distant classes (*i.e.*, mammalia versus aves or reptilia) were ~7–8 orders of magnitude weaker than endogenous complexes (Figure 1c; Table S2). Surprisingly, none of the RIs in our study exhibited detectable binding to RNases from either frog or fish.

4.4.3 Increased thermostability of RI complexes correlates to binding strength

We next determined if differences in the affinity of RI for an RNase correlated to differences in the thermostability of the RI·RNase complex. To do so, we measured the thermal denaturation of RI in both an unbound and RNase-bound state. For each species, the thermostability of RI

increased dramatically (>21 °C) when bound to its cognate RNase (Figure 2a and 2b). We also determined the shift in T_m for each RI bound to every RNase in our study. We found that changes in RI thermostability upon RNase binding correlated well with the measured K_d for that RNase (Figure 2c). Similarly, there was no change in RI thermostability when incubated with either frog or fish ribonuclease.

4.4.4 Structural characterization of endogenous RI·RNase complexes

Intrigued by the large differences in binding affinity between mammals and non-mammals, we sought structural explanations to account for the change in K_d. Accordingly, we determined high-resolution crystal structures for three complexes: mouse RI·mouse RNase, bovine RI·bovine RNase, and chicken RI·chicken RNase (Table 3; Figure S2). We were unable to generate diffraction-quality crystals for the anole RI·anole RNase complex.

The overall structures of the RI homologs bear striking resemblance to each other, as well as to the previously characterized structures of human and porcine RI (Figure S2).[221,310] The structures are repetitive and symmetrical, and have a vast surface area that is largely concave. The conserved LRR units are arranged in a horseshoe shape, and correspond to structural units consisting of a β-strand and an α-helix. Each RI molecule binds to its cognate ribonuclease in a similar position and orientation.

4.4.5 Analyses of binding interface regions highlight key differences across classes

Beyond the outward similarities of each RI·RNase complex, we probed for subtle differences at the interface region between the two bound proteins. We found each interface to contain a similarly large amount of buried surface area (Table 3). The number and character of interface

residues were similar across the complexes, with the exception of that in the chicken complex, which has more non-polar residues and fewer uncharged residues than do the mammalian complexes (Table 3). Shape complementarity (S_c) calculations appeared to correlate with buried surface area and followed a general trend, with the human interface having the greatest complementarity, followed by mouse, bovine, and chicken. The human complex has the greatest number of both hydrogen bonds and non-bonded interactions, whereas the chicken complex has the fewest. As a comparison, we also analyzed the inter-species porcine RI·bovine RNase complex.[311] Interestingly, this non-endogenous complex displays less buried surface area, the lowest S_c value, and fewer hydrogen bonds and non-bonded interactions than any of the endogenous complexes (Table 3).

Upon mapping the interface residues of each complex onto protein sequence alignments, we discovered the interface residues contributed by both RIs and RNases were highly conserved across homologs (Figures 3 and S3). We analyzed each RI·RNase interface for the presence of predicted "hot spots"—residues predicted to have a large contribution to binding energy.[333,336] We found two hotspot regions in chicken RI that are particularly divergent from those in mammalian RIs: Arg321 and Tyr40 (human RI nomenclature) (Figure 3). Analysis of these regions at the atomic level indicated that Arg321 and Tyr407 might play a role in the differential RI binding described above. Arg321 in chicken RI forms a hydrogen bond with the carbonyl of Leu86 in chicken RNase (human RNase nomenclature). Due to the substitution of Lys in mammalian RIs this interaction is lost. Additionally, the positioning of Lys321—which is structurally conserved in human, cow, and mouse RI—could present a steric hindrance upon chicken RNase binding (Figure 4b). Similar to Arg321, Tyr407 in chicken RI makes a hydrogen bonding interaction with its endogenous RNase (carbonyl of Leu43) that is not observed in the

cow and mouse RI•RNase structures. The larger Tyr residue, which is highly conserved in non-mammalian RIs, could present a significant steric clash during the formation of a cow RI•chicken RNase or mouse RI•chicken RNase complex (Figure 4c). Thus, these two substitutions result in the loss of two direct RI•RNase interactions in the chicken structure and generate potential steric clashes during the formation of non-endogenous RI•RNase complexes. Interestingly, these two residues are present in anole RI as well. We compared the protein sequences of 15 mammalian RI homologs and 9 non-mammalian RI homologs and found that these residues were highly conserved across non-mammalian species, but completely absent from mammalian species (Figure 4a).

4.4.6 RI·RNase complexes are differentially sensitive to oxidation

Upon oxidation, RI undergoes rapid unfolding and inactivation, subsequently releasing bound ribonuclease.[27] To determine the oxidative stability of each RI complex, we assessed the ability of hydrogen peroxide to disrupt RI·RNase complexes using two distinct assays. Upon measuring the dissociation of a fluorescently labeled RNase, we found that human RI was the most sensitive to oxidation, with H_2O_2 IC_{50} values 7-, 13-, 46-, and 56-fold lower than mouse, bovine, chicken, or anole RI, respectively (Figure 5a). Oxidation of each endogenous RI·RNase complex yielded a catalytically active RNase. Upon measuring the release of fully active RNase, we found that human RI was again most sensitive to oxidation, with H_2O_2 IC_{50} values 10-, 12-, 147-, and 213-fold lower than mouse, bovine, chicken, or anole RI, respectively (Figure 5b).

4.4.7 Cysteine solvation correlates to RI oxygen sensitivity

To explain the extreme differences in oxidation sensitivity measured for RI homologs, we computationally analyzed the crystal structures of human, mouse, bovine, and chicken RI, and calculated the solvent-exposed surface area for each cysteine residue. We found that human RI contained the highest overall cysteine solvent accessibility, followed by mouse, bovine, and chicken RI (Figure 6a). Next, we empirically measured the amount of reactive thiol content for each RI protein using an assay based on the reduction of DTNB. Our experimental results matched closely with the computational data: human RI had the highest reactive thiol content, followed by mouse, cow, chicken, and anole RI (Figure 6b).

Finally, we mapped the relative solvent accessibility of the cysteine residues for each RI homolog (Figure 6c). We determined that there were four cysteines with the high overall solvent-exposed surface area: Cys12, Cys96, Cys220, and Cys409. Of these four cysteines, human RI contains all four, mouse RI contains three, bovine RI contains three, chicken RI contains one, and anole RI contains zero (Figures 3 and 6c). We expanded our analysis to include 15 mammalian and 9 non-mammalian RI homologs. We determined that although all mammalian RI homologs possessed at least three highly solvated cysteine residues, non-mammalian RI homologs only contained one or none (Figure 7).

4.5 Discussion

Secretory ribonucleases have been characterized from every class of vertebrates.[34,337] Typically, these proteins have high, non-specific activity against RNA substrates, circulate freely in extracellular fluids, and can enter cells spontaneously.[128,338] A potent, cytosolic inhibitor for such RNases is critical. Indeed, mammalian ribonuclease inhibitor (RI) was discovered and

characterized over fifty years ago.[36,339] Still, multiple early studies proclaimed the total absence of RI in avian, reptile, and amphibian tissues (for reviews, see ref. [28,29]). Our data stand in stark contrast to this proclamation. We have identified and characterized ribonuclease inhibitors from both chicken and anole lizard. We find many similarities between these proteins and their more characterized mammalian counterparts, as well as key differences.

Importantly, we determined that non-mammalian ribonuclease inhibitors bind their cognate ribonucleases with tight affinity, similar to that of mammalian inhibitors. This observation implies that a critical role for non-mammalian RIs—like mammalian RIs— is to regulate the biological activity of secretory ribonucleases. Further evidence for this hypothesis is the apparent co-evolution of RIs from different species to bind to their endogenous RNases. We find that proteins bind as tightly or tighter to their cognate partner than to any inter-species partner (regardless of p*I* or overall charge), suggesting the presence of subtle changes in the binding interface to promote better molecular recognition.

Our observation that avian and reptile RI binds ~10^8-fold more weakly to mammalian RNases (and vice versa) has other implications. These data explain the previous difficulties in detecting and purifying non-mammalian RIs, which do not bind tightly to the bovine RNase used in early detection assays and affinity chromatography. Whereas nanomolar binding affinities are seemingly tight, in the RI·RNase system they are biologically irrelevant. Mammalian RNases engineered to evade mammalian RI possess nanomolar binding affinity, yet are highly toxic to human cells. For many of these cytotoxic variants, substituting a single interface residue resulted in enormous changes in binding strength.[129,146]

Accordingly, accounting for the specific changes that have lead to the diversity between species, as well as conclusively demonstrating co-evolution between intraspecies binding

partners, is difficult and imprecise. The similarity of the various RI·RNase binding interfaces suggests that the changes that drive the divergent binding are subtle. This notion corresponds well with the hypothesis of interface "hot spots", or the small subset of residues that are predicted to account for most of the binding affinity between two proteins.[336,340] Tellingly, detailed dissection of the binding interface between human RI and human angiogenin revealed that, although the binding affinity relied upon relatively few key contacts, multiple residues function cooperatively, suggesting a complicated landscape and highlighting the difficultly of rigorously assigning the sources of binding energy.[341] Still, as difficult as they are to study, co-evolutionary changes in protein–protein interactions do occur, and are an important driver of speciation.[342,343]

Surprisingly, we were unable to detect binding between ribonucleases from fish and frog and any of the RI molecules in our study. An exhaustive search of amphibian and fish genomes did not yield any viable candidate RI homologs. Nonetheless, it is possible that RI is quite divergent in these classes. Fish and frog RNases share low sequence identity and similarity to other secretory RNases (Table S4). Early studies in bullfrogs indicated the presence of a cytosolic protein that could inhibit the activity of bullfrog RNase (but not bovine RNase), and was sensitive to thiol-reactive agents. The estimated size of the complex between this molecule and RNase was, however, ~130–140 kDa, which is much larger than ~65 kDa size noted for mammalian RI·RNase complexes.[69,339,344] This dissimilarity could reflect intrinsic differences in the amphibian RI homolog, such as in molecular weight or binding stoichiometry. New methods, such as affinity chromatography using frog or fish RNase, could be necessary to identify these more divergent RI homologs.

The apparent evolving oxidation sensitivity of mammalian RI homologs implies the emergence of new functionality. Indeed, RI has been identified as a potential keystone in the maintenance of cellular redox homeostasis.[154,155] The ability of oxidized RI to release functional, active ribonuclease is particularly fascinating. Potentially, the intracellular redox state could serve as a trigger to release a caged ribonuclease. Previous studies have shown that partially oxidized RI can allow partial RNase activity.[345] Thus, cells might have a "redox switch" that regulates RNases. Under oxidative stress, the manifestation of ribonucleolytic activity could induce apoptosis. This hypothesis has important implications, given the well-characterized association of oxidative stress with aging, cancer, and other diseases.

In conclusion, we have confirmed the existence of avian and reptile homologs of ribonuclease inhibitor that display characteristics unique from mammalian homologs. The observations that non-mammalian RIs exhibit extremely tight binding to their endogenous RNases, but remarkably lower sensitivity to oxidation, suggest that the primary role of non-mammalian RI might be to regulate the biological activities of secretory ribonucleases. Intriguingly, these data also imply that mammalian RIs have not only retained and even improved upon their avid RNase binding, but also evolved greater sensitivity to oxidation. This redox reactivity might be driving new biological roles—such as scavenging intracellular free radicals—or might be adding complexity to existing roles, such as triggering the release of active RNases as a cellular stress-response mechanism. Further *in vivo* characterizations are necessary to continue probing the dynamic biology of ribonuclease inhibitor.

Table 4.1 Properties of homologous ribonuclease inhibitors

Species	MW (Da)	No. residues	No. leucine residues (%)	No. cysteine residues (%)	Z^a	T_m [b]	GenBank Accession No.
Human (*H. sapiens*)	49973	461	92 (20%)	32 (6.9%)	–22	51.7 ± 1.1	**NP_976323**
Mouse (*M. musculus*)	49816	456	92 (20%)	30 (6.6%)	–20	48.8 ± 0.5	**NP_001165571**
Bovine (*B. taurus*)	48850	456	98 (22%)	29 (6.4%)	–22	52.5 ± 0.9	**NP_001030396**
Chicken (*G. gallus*)	49846	456	81 (18%)	30 (6.6%)	–20	52.2 ± 0.4	**NP_001006473**
Lizard (*A. carolinensis*)	49581	456	78 (17%)	29 (6.4%)	–10	50.0 ± 0.7	**XP_003214831**

[a] Values of Z refer to the net molecular charge: Arg + Lys – Asp – Glu

[b] Values of T_m are the temperature at the midpoint of thermal denaturation, as determined by incorporation of a hydrophobic dye and quantitation by differential scanning fluorimetry (DSF)

Table 4.2 Summary of crystal parameters, data collection, and refinement statistics

	Mouse RI·Mouse RNase	Bovine RI·Bovine RNase	Chicken RI·Chicken RNase
Crystal parameters			
Space group	$P2_1$	I222	$P2_12_12_1$
Unit-cell parameters (Å)	a = 72.40 b = 125.34 c = 123.06 β = 94.72°	a = 117.79 b = 123.55 c = 179.30	a = 52.66 b = 84.54 c = 121.66
Data collection statistics			
Wavelength (Å)	0.9794	0.97857	0.97857
Resolution range (Å)	50.00–2.20 (2.25–2.20)	50.00–2.21 (2.25–2.21)	50.00–1.82 (1.85–1.82)
Completeness (%)	97.9 (88.2)	100.0 (99.4)	99.4 (99.8)
R_{merge}*	0.145 (0.478)	0.084 (0.747)	0.134 (0.687)
Redundancy	4.2 (2.6)	7.2 (5.6)	4.0 (3.7)
Mean I / sigma (I)	9.9 (2.1)	22.72 (2.31)	9.16 (1.69)
Refinement and model statistics			
Resolution range (Å)	34.38–2.20	49.24–2.21	39.83–1.92
No. of reflections (work / test)	102210 / 1897	57584 / 1930	39152 / 2064
R_{cryst}[§]	0.183 (0.234)	0.176 (0.218)	0.207 (0.234)
R_{free}[¶]	0.233 (0.338)	0.226 (0.298)	0.254 (0.263)
RMSD bonds (Å)	0.003	0.008	0.009
RMSD angles (°)	0.679	1.192	1.158
Average B-factor (Å^2)	25.5	20.5	30.7
No. of protein atoms	17650	8698	4404
No. of waters	882	562	233
Ramachandran plot (%)			
Favorable	97.20	97.65	96.83
Allowed	2.80	2.35	3.17
Disallowed	0.00	0.00	0.00
PDB ID	3tsr	4peq	4per

* $R_{merge} = \sum_h \sum_i | I_i(h) - \langle I(h) \rangle | / \sum_h \sum_i I_i(h)$, where $I_i(h)$ is the intensity of an individual measurement of the reflection and $\langle I(h) \rangle$ is the mean intensity of the reflection.

§ $R_{cryst} = \sum_h ||F_{obs}| - |F_{calc}|| / \sum_h |F_{obs}|$, where F_{obs} and F_{calc} are the observed and calculated structure-factor amplitudes, respectively.

¶ R_{free} was calculated as R_{cryst} using randomly selected unique reflections that were omitted from the structure refinement.

Table 4.3 Computational analysis of the interface in RI•RNase complexes

			No. of Contacts Residues[c]		Character of Interface Residues[c] [No. (%)]				
Endogenous RI·RNase Complex	Buried ASA[a] (Å^2)	S_c[b]	From RI	From RNase	Non-polar	Uncharged Polar	Charged	Hydrogen Bonds[d] (Å)	Non-bonded contacts[e]
Human[f]	2801	0.688	28	23	17 (33%)	14 (27%)	20 (39%)	19 (2.79)	177
Mouse[g]	2650	0.645	23	25	15 (30%)	18 (36%)	16 (33%)	13 (2.92)	126
Cow[h]	2793	0.605	28	25	15 (28%)	17 (32%)	21 (40%)	15 (2.90)	150
Chicken	2757	0.599	26	20	21 (46%)	7 (15%)	18 (39%)	12 (2.90)	118
Pig·Cow[i]	2582	0.590	26	23	14 (29%)	13 (27%)	22 (45%)	8 (3.01)	90

[a] Buried accessible surface area (ASA) was calculated with the program PDBsum.
[b] The value of S_c reports on geometrical shape complementarity, where $S_c = 1.0$ for two perfectly complementary surfaces and $S_c = 0$ for two completely dissimilar surfaces.[346] S_c values were calculated with SC v6.4.
[c] Contact residues were identified by PDBsum as non-polar (A,F,G,I,L,M,P,V,W,Y), uncharged polar (C,N,Q,S,T), or charged (D,E,H,K,R).
[d] Hydrogen bonds were calculated by the HBPLUS[331] algorithm of PDBsum ($r_{X\ldots X}$ <3.3 Å).
[e] Non-bonded contacts were calculated by HBPLUS[331] and defined as any contacts between proteins involving either a carbon or a sulfur atom, where the interaction distance is ≤3.9 Å.
[f] Calculations were performed with chain Y (hRI) and chain Z (RNase 1) from PDB 1Z7X due to the presence of bound citrate in the active site of RNase 1 in the other complex in the asymmetric unit.
[g] Calculations represent the average values across four complexes in the asymmetric unit.
[h] Calculations represent the average values between two complexes in the asymmetric unit.
[i] Shading denotes non-endogenous complex between two different species.

Figure 4.1

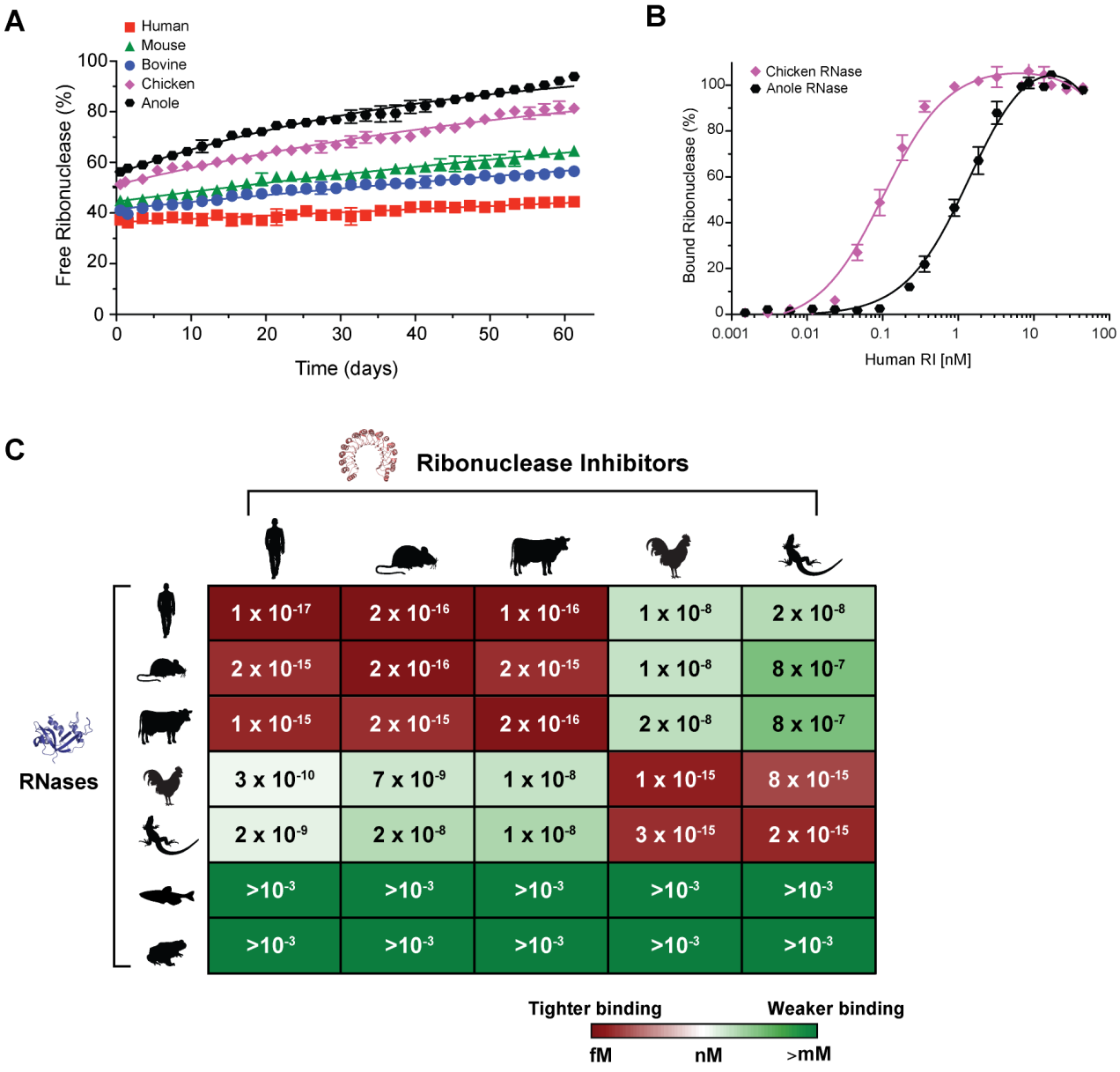
A
Human
Mouse
Bovine
Chicken
Anole
Free Ribonuclease (%)
Time (days)
B
Chicken RNase
Anole RNase
Bound Ribonuclease (%)
Human RI [nM]
C
Ribonuclease Inhibitors
RNases
1 x 10-17
2 x 10-16
1 x 10-16
1 x 10-8
2 x 10-8
2 x 10-15
2 x 10-16
2 x 10-15
1 x 10-8
8 x 10-7
1 x 10-15
2 x 10-15
2 x 10-16
2 x 10-8
8 x 10-7
3 x 10-10
7 x 10-9
1 x 10-8
1 x 10-15
8 x 10-15
2 x 10-9
2 x 10-8
1 x 10-8
3 x 10-15
2 x 10-15
>10-3
>10-3
>10-3
>10-3
>10-3
>10-3
>10-3
>10-3
>10-3
>10-3
Tighter binding
Weaker binding
fM
nM
>mM

Figure 4.1 Fluorescent assays to evaluate RI•RNase complexes

Fluorescent assays to evaluate the binding affinity of endogenous and inter-species RI·RNase complexes. *A*. Representative normalized fluorescence data showing the gradual dissociation of labeled ribonucleases from their endogenous RI binding partners over time. Data were fitted to derive k_d values for each RI·RNase pair. *B*. Representative normalized fluorescence data showing inter-species RI·RNase complex formation with increasing concentration of RI. Data were fitted to derive K_d values for each RI·RNase pair. *C*. Heat map summarizing the intra- and inter-species binding affinities for various RI·RNase complexes. Red indicates lower K_d values; green indicates higher K_d values.

Figure 4.2

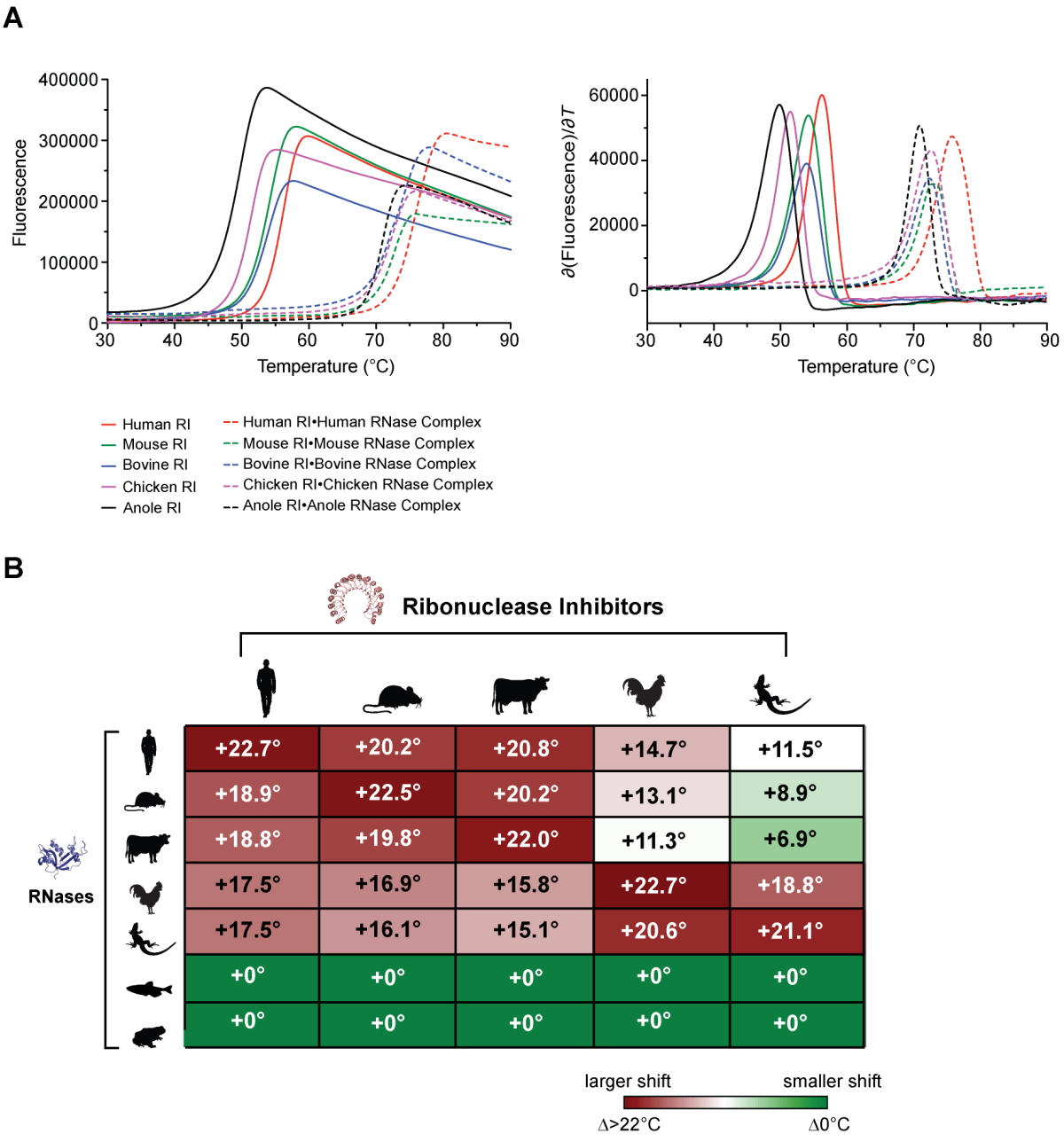
A
Fluorescence
400000
300000
200000
100000
0
30
40
50
60
70
80
90
Temperature (°C)
∂(Fluorescence)/∂T
60000
40000
20000
0
Temperature (°C)
Human RI
Mouse RI
Bovine RI
Chicken RI
Anole RI
Human RI•Human RNase Complex
Mouse RI•Mouse RNase Complex
Bovine RI•Bovine RNase Complex
Chicken RI•Chicken RNase Complex
Anole RI•Anole RNase Complex
B
Ribonuclease Inhibitors
RNases
+22.7° +20.2° +20.8° +14.7° +11.5°
+18.9° +22.5° +20.2° +13.1° +8.9°
+18.8° +19.8° +22.0° +11.3° +6.9°
+17.5° +16.9° +15.8° +22.7° +18.8°
+17.5° +16.1° +15.1° +20.6° +21.1°
+0° +0° +0° +0° +0°
+0° +0° +0° +0° +0°
larger shift
smaller shift
Δ>22°C
Δ0°C

Figure 4.2 Assessing the thermostability of RI•RNase complexes

A. Raw fluorescent data showing the thermal unfolding of RI, unbound and bound to RNase, as measured through incorporation of a hydrophobic fluorescent dye. *Left panel*, thermal melting curves; *right panel*, derivative melting curves showing ∂fluorescence/∂T. *B*. Heat map summarizing the change in RI thermostability conferred upon binding various RNases. Numbers represent ΔT_m from the unbound to the bound state.

Figure 4.3

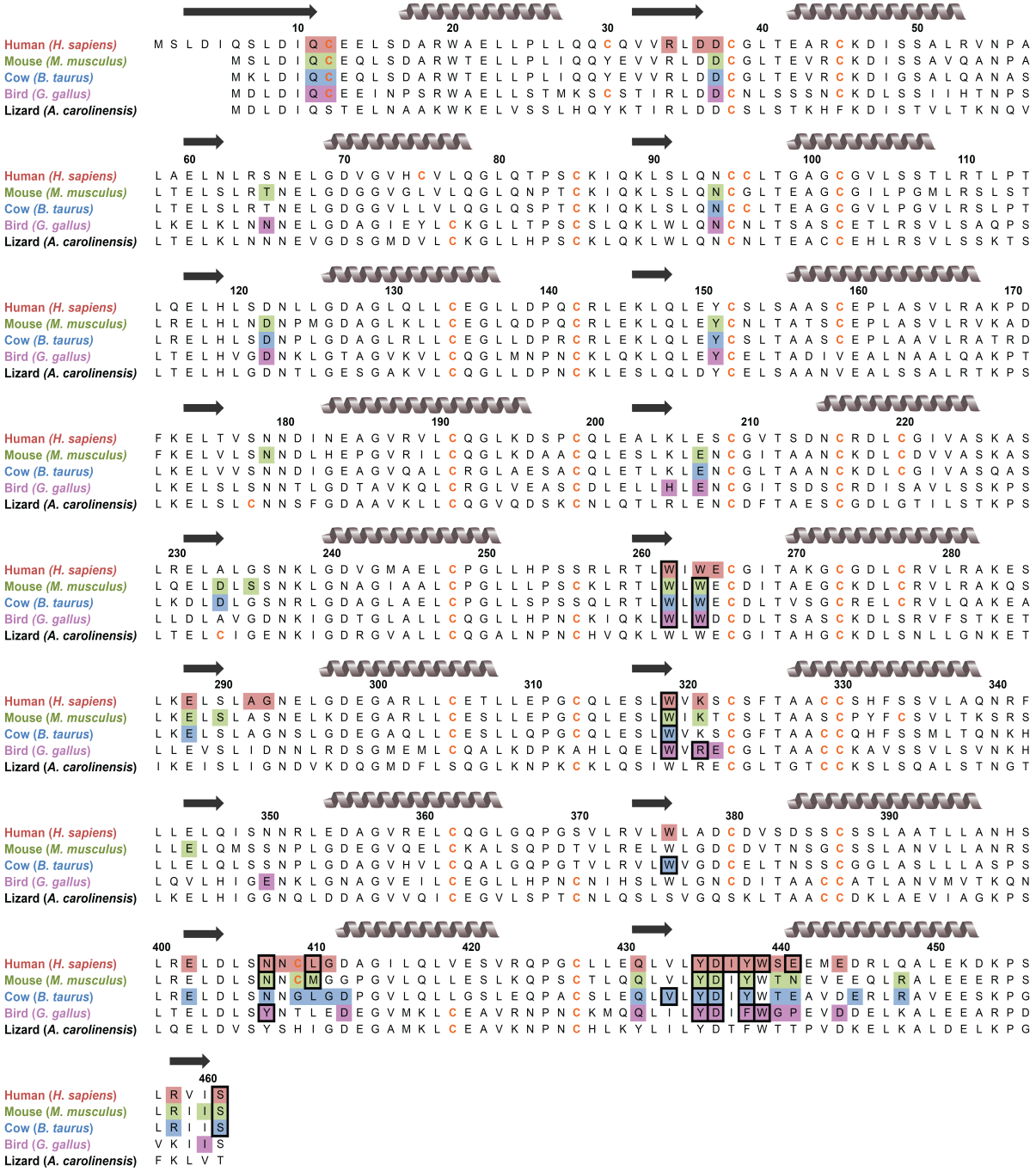
Human (H. sapiens)
Mouse (M. musculus)
Cow (B. taurus)
Bird (G. gallus)
Lizard (A. carolinensis)

Figure 4.3 Protein sequence alignment of homologous ribonuclease inhibitors
Residues participating in binding to endogenous RNases (as identified by crystal structure analysis) are shaded. Black boxes indicate predicted "hotspots" for binding affinity.[333] Gray coils represent α-helices and black arrows represent β-sheets.

Figure 4.4

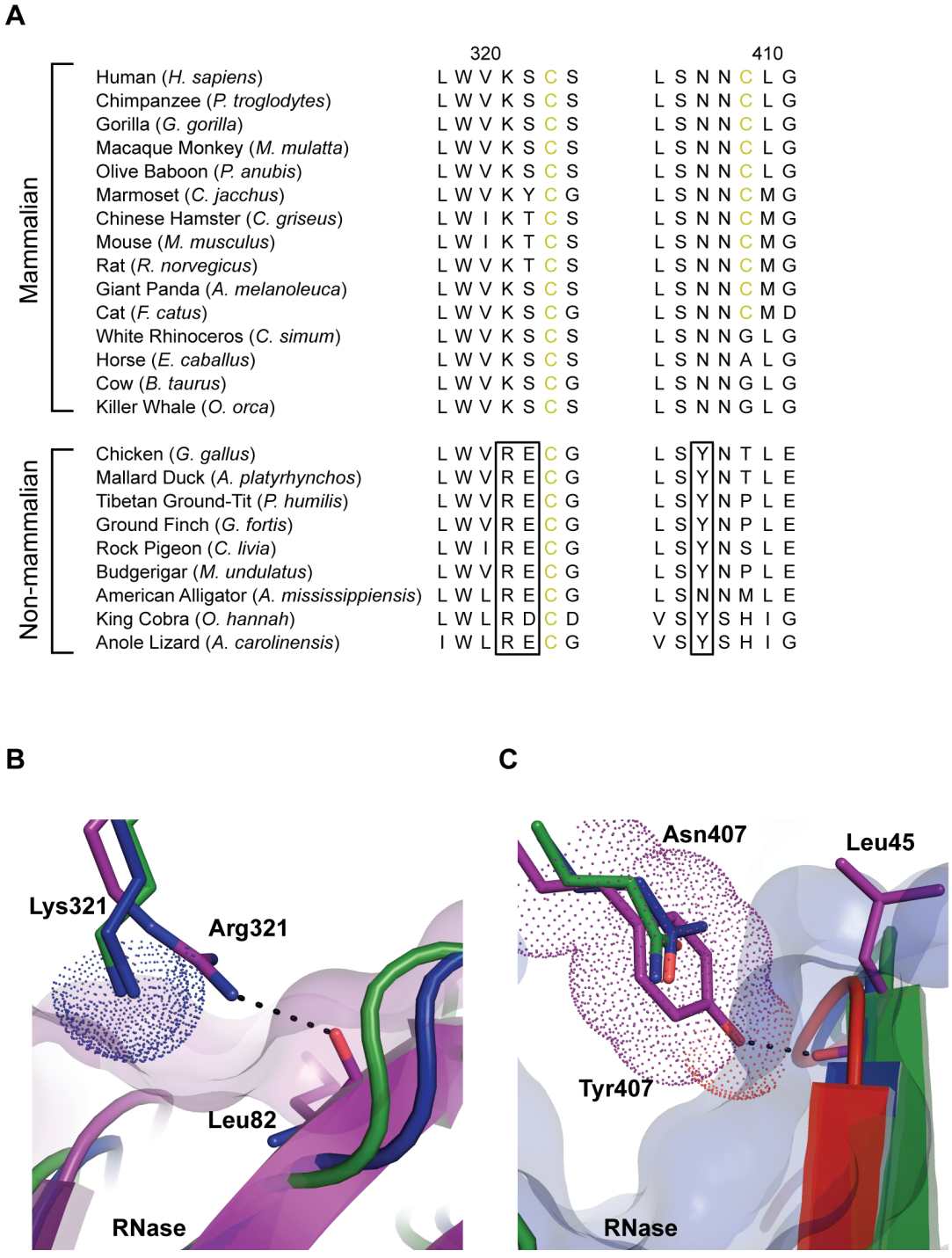
A
320
410
Mammalian
Human (H. sapiens) L W V K S C S L S N N C L G
Chimpanzee (P. troglodytes) L W V K S C S L S N N C L G
Gorilla (G. gorilla) L W V K S C S L S N N C L G
Macaque Monkey (M. mulatta) L W V K S C S L S N N C L G
Olive Baboon (P. anubis) L W V K S C S L S N N C L G
Marmoset (C. jacchus) L W V K Y C G L S N N C M G
Chinese Hamster (C. griseus) L W I K T C S L S N N C M G
Mouse (M. musculus) L W I K T C S L S N N C M G
Rat (R. norvegicus) L W V K T C S L S N N C M G
Giant Panda (A. melanoleuca) L W V K S C S L S N N C M G
Cat (F. catus) L W V K S C G L S N N C M D
White Rhinoceros (C. simum) L W V K S C S L S N N G L G
Horse (E. caballus) L W V K S C S L S N N A L G
Cow (B. taurus) L W V K S C G L S N N G L G
Killer Whale (O. orca) L W V K S C S L S N N G L G
Non-mammalian
Chicken (G. gallus) L W V R E C G L S Y N T L E
Mallard Duck (A. platyrhynchos) L W V R E C G L S Y N T L E
Tibetan Ground-Tit (P. humilis) L W V R E C G L S Y N P L E
Ground Finch (G. fortis) L W V R E C G L S Y N P L E
Rock Pigeon (C. livia) L W I R E C G L S Y N S L E
Budgerigar (M. undulatus) L W V R E C G L S Y N P L E
American Alligator (A. mississippiensis) L W L R E C G L S N N M L E
King Cobra (O. hannah) L W L R D C D V S Y S H I G
Anole Lizard (A. carolinensis) I W L R E C G V S Y S H I G
B
Lys321
Arg321
Leu82
RNase
C
Asn407
Leu45
Tyr407
RNase

Figure 4.4 Evolutionary and structural analysis of RI•RNase complexes

Evolutionarily conserved structural differences in the binding interface between mammalian and non-mammalian RI•RNase complexes. *A*. Excerpted sections of RI amino acid sequence alignments for homologous mammalian and non-mammalian species. Black boxes highlight residues conserved in non-mammalian proteins that are absent from mammalian homologs. *B*. A structural alignment of the mouse (green), bovine (blue), and chicken (purple) RI•RNase complexes illustrates the affects of amino acid substitutions at position 321 and 407 (human RI•RNase numbering). The interaction of Arg321 in chicken RI with the backbone oxygen of Leu86 in chicken RNase is not present in mammalian RI•RNase complexes that contain Lys at this position. The surface of Lys321 (shown as dots) of the cow and mouse RI could potentially clash with a bound chicken RNase (transparent purple surface). *C*. Chicken RI contains a Tyr (surface shown as dots) at position 407 that interacts with Leu43 and could impinge on the surface of bovine RNase (transparent blue surface).

Figure 4.5

A

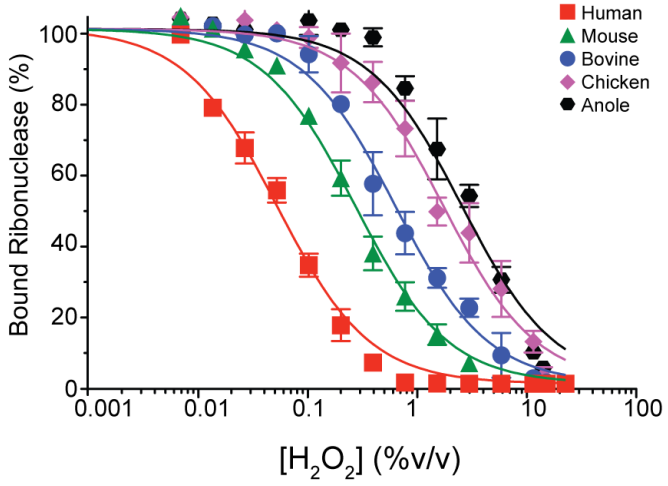

B

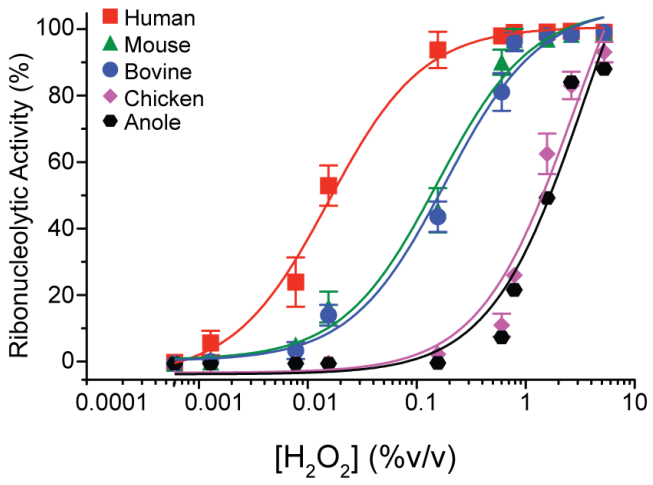

C

	Complex Dissociation	RNase Release
Complex	IC_{50} (% v/v H_2O_2)	IC_{50} (% v/v H_2O_2)
Human	0.059 ± 0.005	0.015 ± 0.003
Mouse	0.43 ± 0.04	0.15 ± 0.07
Bovine	0.76 ± 0.05	0.18 ± 0.07
Chicken	2.7 ± 0.5	2.2 ± 0.2
Anole	3.3 ± 0.4	3.2 ± 0.3

Figure 4.5 Comparison of RI•RNase oxidation sensitivity

Comparison of the oxidation sensitivity of homologous RI·RNase complexes.

A. The dissociation of fluorescently-labeled RNases upon treatment of RI·RNase complexes with increasing concentrations of H_2O_2. *B*. The release of active ribonucleases from RI·RNase complexes upon treatment with increasing concentrations of H_2O_2. *C*. H_2O_2 IC_{50} values derived from fitting the data in *A* and *B*.

Figure 4.6

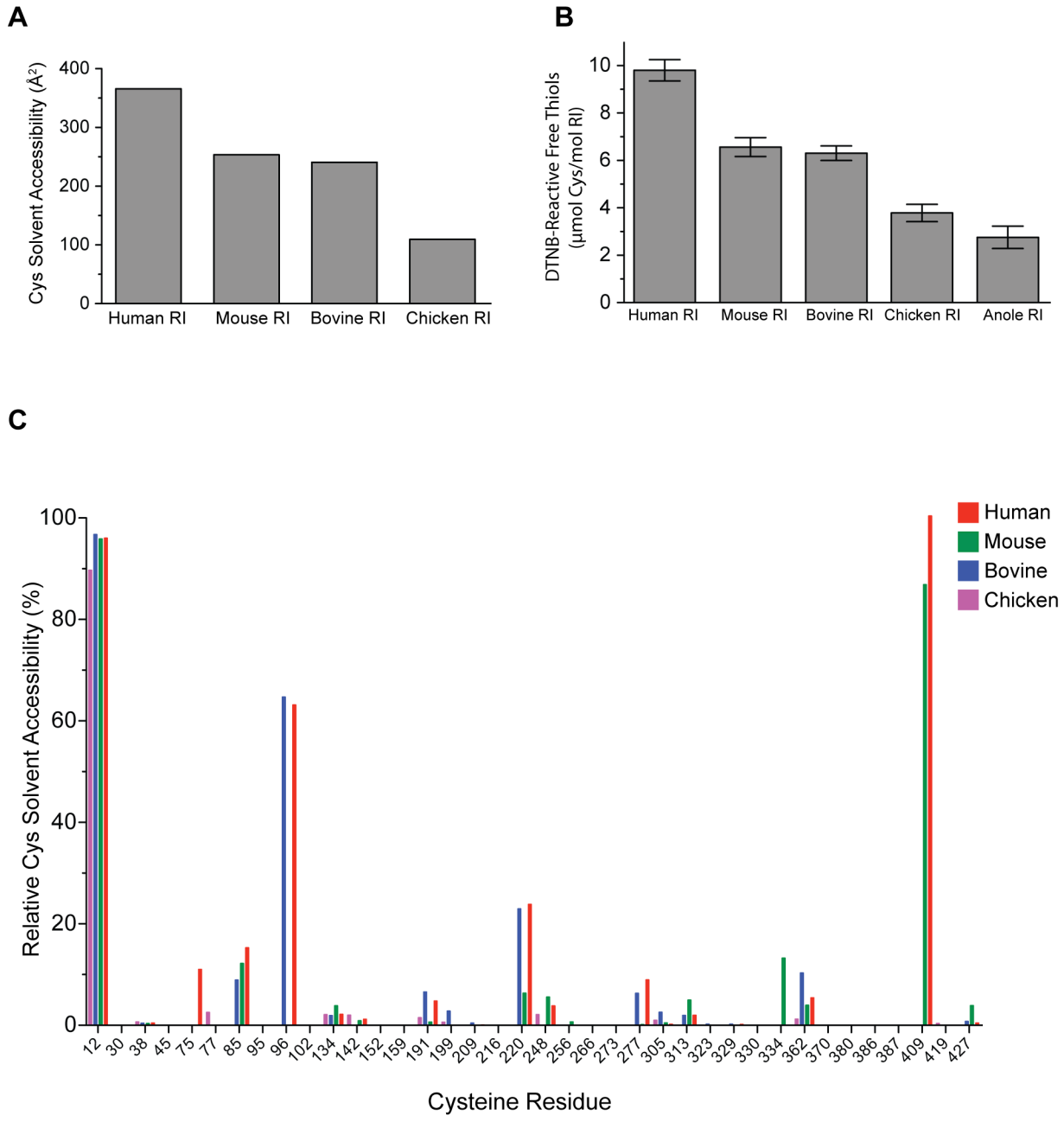
A
Cys Solvent Accessibility (Å²)
400
300
200
100
0
Human RI
Mouse RI
Bovine RI
Chicken RI
B
DTNB-Reactive Free Thiols (µmol Cys/mol RI)
10
8
6
4
2
0
Human RI
Mouse RI
Bovine RI
Chicken RI
Anole RI
C
Relative Cys Solvent Accessibility (%)
100
80
60
40
20
0
Human
Mouse
Bovine
Chicken
12 30 38 45 75 77 85 95 96 102 134 142 152 159 191 199 209 216 220 248 256 266 273 277 305 313 323 329 330 334 362 370 380 386 387 409 419 427
Cysteine Residue

Figure 4.6 Comparison of cysteine residues across RI homologs

A. Combined solvent-exposed surface area for cysteine residues, as calculated from crystal structures with Pymol. *B*. Quantitation of solvent-exposed thiol groups in recombinant proteins, based on reaction with DTNB. *C*. Relative solvent accessibility calculations for each cysteine residue in human, mouse, bovine and chicken RI.

Figure 4.7

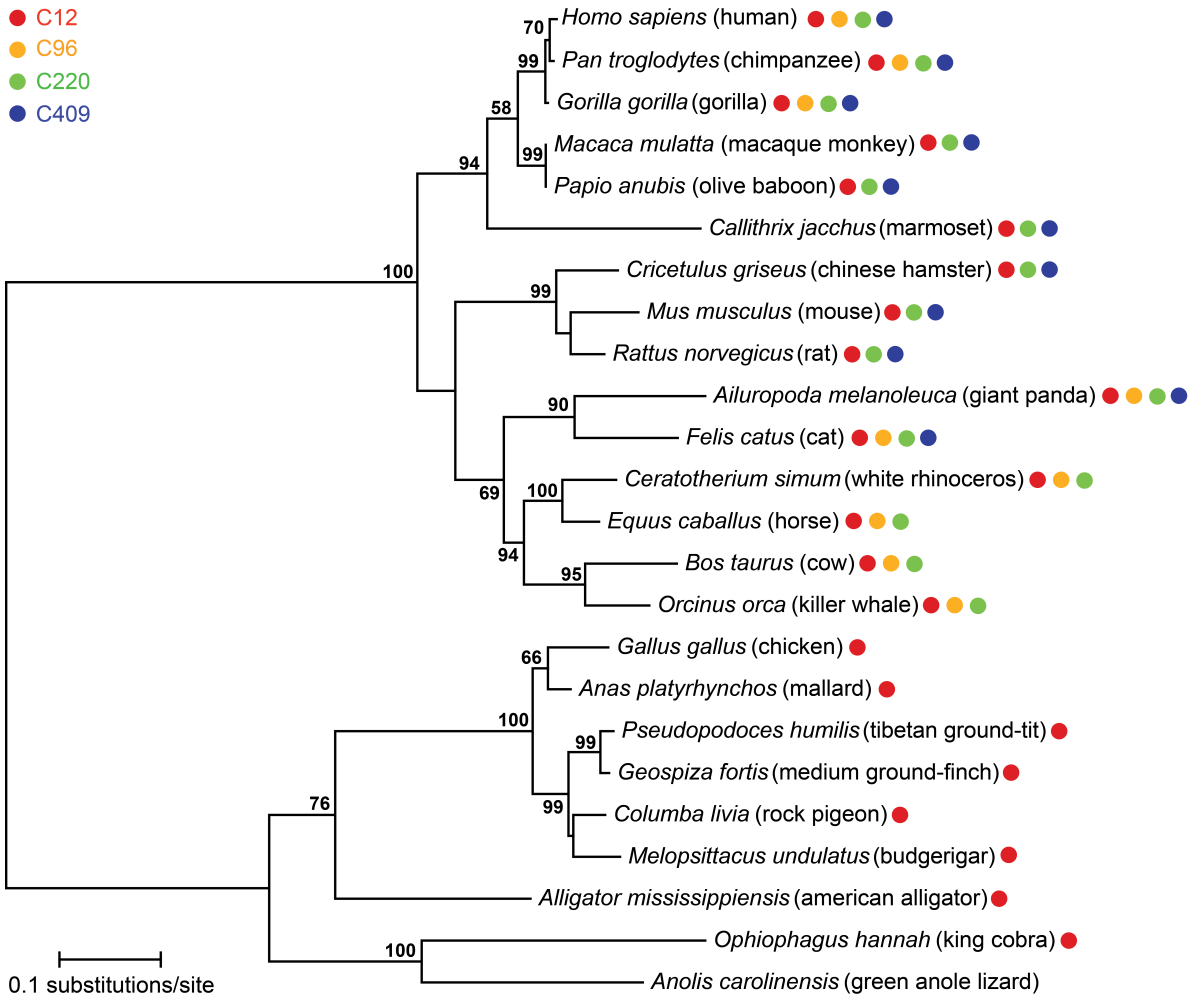
C12
C96
C220
C409
Homo sapiens (human)
Pan troglodytes (chimpanzee)
Gorilla gorilla (gorilla)
Macaca mulatta (macaque monkey)
Papio anubis (olive baboon)
Callithrix jacchus (marmoset)
Cricetulus griseus (chinese hamster)
Mus musculus (mouse)
Rattus norvegicus (rat)
Ailuropoda melanoleuca (giant panda)
Felis catus (cat)
Ceratotherium simum (white rhinoceros)
Equus caballus (horse)
Bos taurus (cow)
Orcinus orca (killer whale)
Gallus gallus (chicken)
Anas platyrhynchos (mallard)
Pseudopodoces humilis (tibetan ground-tit)
Geospiza fortis (medium ground-finch)
Columba livia (rock pigeon)
Melopsittacus undulatus (budgerigar)
Alligator mississippiensis (american alligator)
Ophiophagus hannah (king cobra)
Anolis carolinensis (green anole lizard)
70
99
58
99
94
100
99
90
69
100
94
95
66
100
99
99
76
100
0.1 substitutions/site

Figure 4.7 Comparison of RI solvated cysteine residues

Comparison of solvated cysteine residues across mammalian and non-mammalian RI homologs. A phylogenetic tree was reconstructed to visualize the evolutionary relationship among homologous RI proteins. Colored circles indicate the presence or absence of each of the four most highly solvated cysteine residues. Bootstrap values >50 are shown.

Table 4S.1 Oligonucleotides used in the cloning of novel ribonuclease and ribonuclease inhibitor genes

Gene	Restriction Enzyme	Primer Sequence
Mouse RNase 1 (forward)	*Nco*I	ATTATCATATGAGGGAATCTGCACAG
Mouse RNase 1 (reverse)	*Xho*I	AACTCGAGCTACACAGTAGCATCAAAG
Chicken RNase A-1 (forward)	*Nde*I	ATATAATCATATGGTTCCAACCTACCAAGATTTTTTGC
Chicken RNase A-1 (reverse)	*Sal*I	TATAATATGTCGACTCATGGAAAGGTGCCATCCAG
Anole RNase 1 (forward)	*Nde*I	AATATAATCATATGAGGGAAAGCCGTCATGAC
Anole RNase 1 (reverse)	*Sal*I	TTATAATATGTCGACCTAAAGAGGAGCTTTGAAG
Zebrafish RNase 3/4 (forward)	*Nde*I	CTATATATACATATGCAGTCTTATAATGACTTCAAAC
Zebrafish RNase 3/4 (reverse)	*Zho*I	CTATATATACTCGAGTTAAGAATTGTTGGAACGTC
Mouse RI (forward)	*Nde*I	CATATG ATGAGTCTTGACATCCAGTGTGAG
Mouse RI (reverse)	*Sal*I	GTCGAC CTTCCCTGAGGATCATTTCCTGA
Chicken RI (forward)	*Nde*I	CATGGACCTTGACATCCAGTGTGAGGAG
Chicken RI (reverse)	*Sal*I	ATTATTATATGTCGACTCATGAAATGATCTTCACATCAGG
Anole RI (forward)	*Nde*I	CATGGATCTTGACATCCAGTCTACCGAG
Anole RI (reverse)	*Sal*I	AATTATAATATGTCGACTCATGTAACCAATTTAAATCCAG

Table 4S.2 Dissociation rate constants and equilibrium dissociation constants for RI•RNase complexes

		Human RI (*H. sapiens*)	Mouse RI (*M. musculus*)	Bovine RI (*B. taurus*)	Chicken RI (*G. gallus*)	Lizard RI (*A. carolinensis*)
Human RNase 1 (*H. sapiens*)	k_d (s^{-1})[a]	$(1.2 \pm 0.5) \times 10^{-8}$	$(5.4 \pm 3.2) \times 10^{-8}$	$(4.1 \pm 1.4) \times 10^{-8}$	$(1.2 \pm 0.7) \times 10^{-8}$	$(2.3 \pm 0.2) \times 10^{-8}$
	K_d (M)[b]	$(3.5 \pm 1.4) \times 10^{-17}$	$(1.6 \pm 1.0) \times 10^{-16}$	$(1.2 \pm 1.0) \times 10^{-16}$		
Mouse RNase 1 (*M. musculus*)	k_d (s^{-1})	$(7.9 \pm 1.9) \times 10^{-7}$	$(6.5 \pm 4.4) \times 10^{-8}$	$(6.3 \pm 3.8) \times 10^{-7}$	$(1.3 \pm 0.9) \times 10^{-8}$	$(7.6 \pm 0.2) \times 10^{-7}$
	K_d (M)	$(2.3 \pm 1.9) \times 10^{-15}$	$(1.9 \pm 1.3) \times 10^{-16}$	$(1.8 \pm 1.1) \times 10^{-15}$		
Bovine RNase A (*B. taurus*)	k_d (s^{-1})	$(3.8 \pm 2.4) \times 10^{-7}$	$(5.9 \pm 1.6) \times 10^{-7}$	$(5.6 \pm 3.1) \times 10^{-8}$	$(1.9 \pm 1.2) \times 10^{-8}$	$(7.5 \pm 0.1) \times 10^{-7}$
	K_d (M)	$(1.2 \pm 1.1) \times 10^{-15}$	$(1.7 \pm 1.2) \times 10^{-15}$	$(1.7 \pm 1.2) \times 10^{-16}$		
Chicken RNase (*G. gallus*)	k_d (s^{-1})	$(3.1 \pm 0.7) \times 10^{-10}$	$(7.3 \pm 1.9) \times 10^{-9}$	$(1.2 \pm 0.5) \times 10^{-8}$	$(3.4 \pm 1.3) \times 10^{-7}$	$(2.7 \pm 1.5) \times 10^{-6}$
	K_d (M)[c]				$(1.0 \pm 0.8) \times 10^{-15}$	(8.0 ± 0.1) x 10^{-15}
Lizard RNase (*A. carolinensis*)	k_d (s^{-1})	$(1.6 \pm 0.4) \times 10^{-9}$	$(2.2 \pm 1.0) \times 10^{-8}$	$(3.9 \pm 0.1) \times 10^{-8}$	$(9.0 \pm 0.8) \times 10^{-7}$	$(5.4 \pm 3.1) \times 10^{-7}$
	K_d (M)				$(2.6 \pm 0.2) \times 10^{-15}$	$(1.6 \pm 1.1) \times 10^{-15}$
Frog RNase (*R. pipiens*)	K_d (M)	$>10^{-3}$	$>10^{-3}$	$>10^{-3}$	$>10^{-3}$	$>10^{-3}$
Fish RNase (*D. rerio*)	K_d (M)	$>10^{-3}$	$>10^{-3}$	$>10^{-3}$	$>10^{-3}$	$>10^{-3}$

[a] For intra-species complexes and high-affinity inter-species complexes, values of k_d (± SE) were determined by monitoring the release of diethylfluorescein-labeled ribonuclease from a RI·ribonuclease complex over time and fitting the resulting data as described previously.[127]

[b] For intra-species complexes and high-affinity inter-species complexes, values of K_d (± SE) were determined with the equation $K_d = k_d/k_a$ and the k_a value for human RI and RNase A.[347]

[c] For low-affinity inter-species complexes, values of K_d (±SE) were determined directly by measuring the fluorescent quenching of diethylfluorescein-labeled ribonucleases upon incubation with increasing concentrations of RI, and fitting the data as described previously.[255]

Table 4S.3 Percent identity/similarity and crystal structure RMSD between ribonuclease inhibitor homologs

	Human RI		Mouse RI		Bovine RI		Chicken RI		Anole RI	
Human RI[c]			82	**1.05**	83	**0.80**	66	**0.86**	64	**ND**
Mouse RI	73	**1.05**			84	**0.83**	65	**1.14**	66	**ND**
Bovine RI	74	**0.80**	77	**0.83**			66	**1.03**	65	**ND**
Chicken RI	49	**0.86**	49	**1.14**	49	**1.03**			76	**ND**
Anole RI	46	**ND**	45	**ND**	46	**ND**	60	**ND**		

[a] Gray shading denotes percent similarity of residues, as calculated by: G=A=V=L=I; F=Y=W; C=M; S=T; K=R=H; D=E=N=Q

[b] Bold typeface denotes RMSD values calculated with the program PyMOL.

[c] PDB 1z7x.

ND; not determined.

Table 4S.4 Percent identity/similarity and crystal structure RMSD between ribonuclease homologs

[a] Gray shading denotes percent similarity of residues, as calculated by: G=A=V=L=I; F=Y=W; C=M; S=T; K=R=H; D=E=N=Q

	Human RNase		Mouse RNase		Bovine RNase		Chicken RNase		Anole RNase		Frog RNase		Fish RNase	
Human RNase[c]			77	**0.29**	77	**0.36**	43	**0.85**	46	**ND**	33	**1.31**	30	**ND**
Mouse RNase	68	**0.29**			77	**0.38**	46	**0.83**	52	**ND**	35	**1.01**	32	**ND**
Bovine RNase	68	**0.36**	70	**0.38**			43	**0.82**	49	**ND**	37	**1.22**	34	**ND**
Chicken RNase	28	**0.85**	32	**0.83**	29	**0.82**			46	**ND**	33	**1.47**	32	**ND**
Anole RNase	38	**ND**	40	**ND**	38	**ND**	32	**ND**			37	**ND**	30	**ND**
Frog RNase[d]	21	**1.31**	22	**1.01**	23	**1.22**	18	**1.47**	22	**ND**			42	**ND**
Fish RNase	19	**ND**	20	**ND**	20	**ND**	21	**ND**	19	**ND**	26	**ND**		

[b] Bold typeface denotes RMSD values calculated with the program PyMOL.
[c] PDB 1z7x.
[d] PDB 3phn.
ND; not determined.

Table 4S.5 GenBank accession numbers for ribonuclease inhibitor and ribonuclease sequences

Ribonuclease Inhibitors		Ribonucleases	
Species	Accession Number	Species	Accession Number
H. sapiens	**NP_976323**	*H. sapiens*	**CAG29314**
P. troglodytes	**NP_001009060**	*M. musculus*	**EDL20847**
G. gorilla	**XP_004050395**	*B. taurus*	**NP_001014408**
M. mulatta	**XP_001116618**	*G. gallus*	**ABD60081**
P. anubis	**XP_003909365**	*A. carolinensis*	**XP_003223861**
C. jacchus	**JAB44758**	*D. rerio*	**ABQ23785**
C. griseus	**EGW05529**	*R. pipiens*	**AAL54383.1**
M. musculus	**NP_001165571**		
R. norvegicus	**BAJ22804**		
A. melanoleuca	**XP_002929526**		
F. catus	**XP_003993862**		
C. simum	**XP_004441085**		
E. caballus	**XP_001488525**		
B. taurus	**NP_001030396**		
O. orca	**XP_004278153**		
G. gallus	**NP_001006473**		
A. platyrhynchos	**EOB05008**		
P. humilis	**XP_005522432**		
G. fortis	**XP_005419558**		
C. livia	**XP_005509116**		
M. undulatus	**XP_005149280**		
A. mississippiensis	**XP_006263475**		
O. hannah	**ETE73461**		
A. carolinensis	**XP_003214831**		

Figure 4S.1

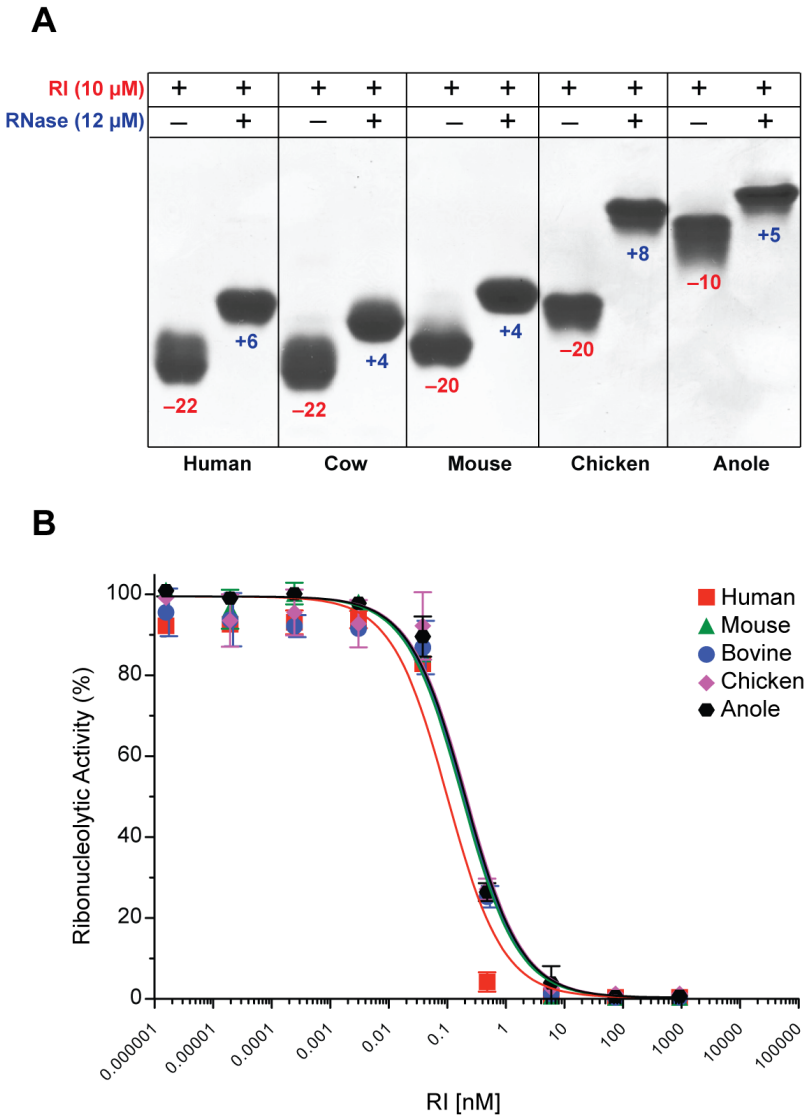
A
RI (10 μM)
RNase (12 μM)
+ + + + + + + + + +
– + – + – + – + – +
–22
+6
–22
+4
–20
+4
–20
+8
–10
+5
Human
Cow
Mouse
Chicken
Anole
B
Ribonucleolytic Activity (%)
100
80
60
40
20
0
0.000001
0.00001
0.0001
0.001
0.01
0.1
1
10
100
1000
10000
100000
RI [nM]
Human
Mouse
Bovine
Chicken
Anole

Figure 4S.1 Biochemical characterization of ribonuclease inhibitors

Ribonuclease inhibitors bind and inhibit their cognate ribonucleases with 1:1 stoichiometry.

A. Native gel demonstrating the shift in the p*I* of RI induced by binding to its RNase. Values of *Z* for each RI (red) and cognate ribonuclease (blue) are indicated for each species.

B. Ribonucleolytic activity of each RNase in panel A (human, bovine, mouse, chicken, 50 pM; anole, 500 pM) in the presence of increasing concentrations of its cognate RI.

Figure 4S.2

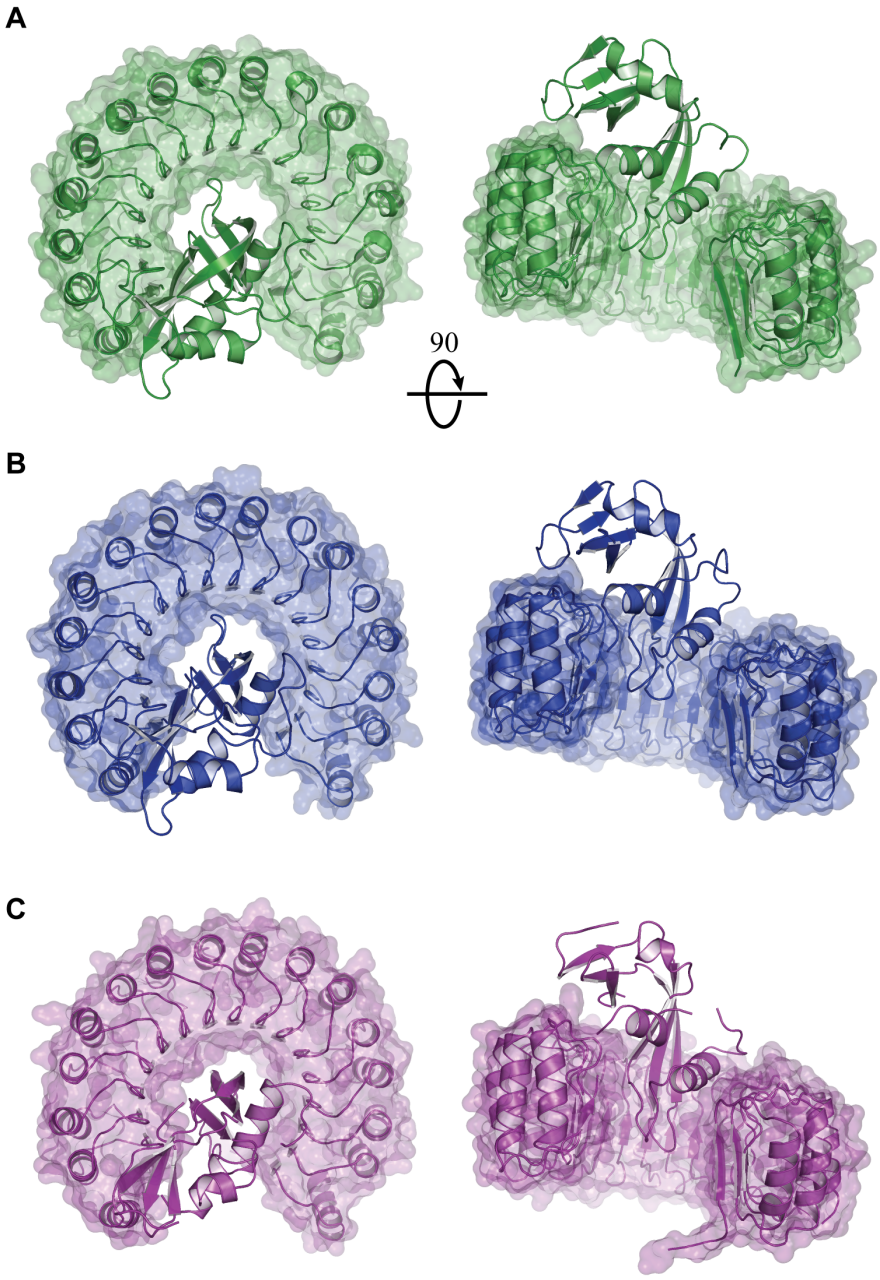

Figure 4S.2 Crystal structures of homologous RI•RNase complexes

A. Mouse ribonuclease inhibitor with mouse RNase 1 (PDB entry 3tsr). *B*. Bovine ribonuclease inhibitor with bovine RNase 1 (PDB entry 4peq). *C*. Chicken ribonuclease inhibitor with chicken RNase A-1 (PDB entry 4per).

Figure 4S.3

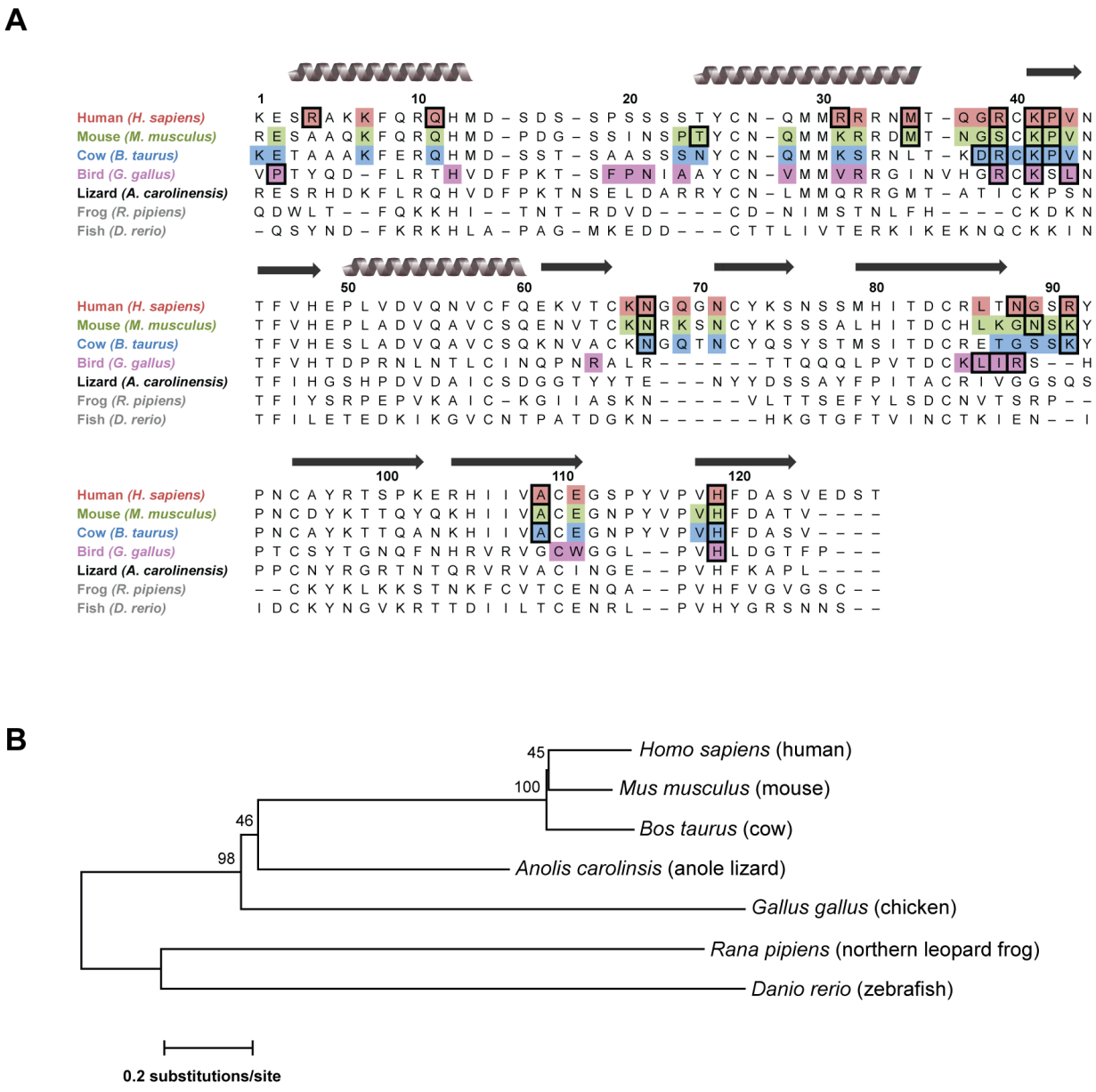
A
B
Human (H. sapiens)
Mouse (M. musculus)
Cow (B. taurus)
Bird (G. gallus)
Lizard (A. carolinensis)
Frog (R. pipiens)
Fish (D. rerio)
Homo sapiens (human)
Mus musculus (mouse)
Bos taurus (cow)
Anolis carolinsis (anole lizard)
Gallus gallus (chicken)
Rana pipiens (northern leopard frog)
Danio rerio (zebrafish)
45
100
46
98
0.2 substitutions/site

Figure 4S.3 Comparisons of homologous secreted ribonucleases

A. RNase protein sequence alignment showing endogenous RI–interface regions (shaded) based on analyses of crystal structures. Black boxes indicate predicted "hotspots" for binding affinity.[333] Gray coils represent α-helices; black arrows represent β-sheets. *B*. Maximum-likelihood phylogenetic tree showing the evolutionary relationship of homologous ribonucleases. Bootstrap values >40 are shown

Figure 4S.4

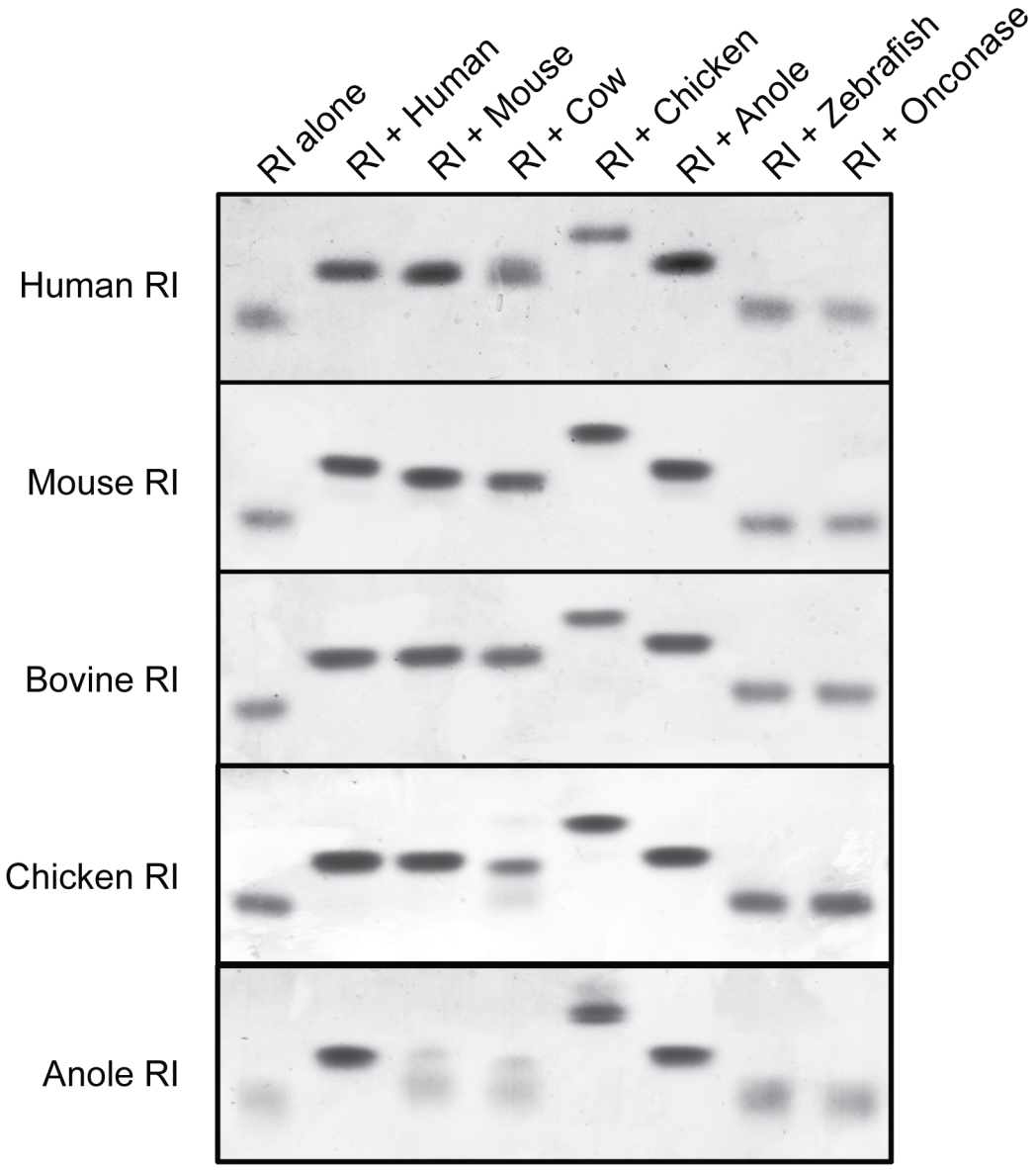
RI alone
RI + Human
RI + Mouse
RI + Cow
RI + Chicken
RI + Anole
RI + Zebrafish
RI + Onconase
Human RI
Mouse RI
Bovine RI
Chicken RI
Anole RI

Figure 4S.4 Native gel shift showing cross-species RI•RNase binding

CHAPTER 5

Construction and Characterization of a Conditional *Rnase1* Knockout Mouse

Contribution: I designed and constructed the conditional targeting vector, developed Southern blot probes, and performed screens of targeted ES cells. The UW–Madison Transgenic Animal Facility performed ES cell karyotyping and blastocyst injection. I performed all initial breeding, genotyping, and phenotypic analyses. Emily Garnett performed subsequent assays, including all metabolism cage studies. She is currently taking over the project.

5.1 Abstract

RNase 1 is emerging as an enzyme with important biological potential. Discounted for decades as a vestigial protein, its expression and activity have now been linked to myriad illnesses, including bacterial, viral, and autoimmune diseases, multiple forms of cancer, atherosclerotic plaque formation, hypercoagulability and stroke. Moreover, RNase 1 has been engineered as a potent anti-cancer chemotherapeutic agent that is progressing through clinical trials. Still, the exact mechanisms of its actions are poorly understood. As a secreted enzyme that functions systemically throughout the bodies of vertebrates, the actions of RNase 1 cannot be recapitulated in a petri dish. Hence, we have created the first whole-body knockout mouse for RNase 1. We have also engineered conditional capabilities into our targeted construct, allowing temporal and spatial control of *Rnase1* knockdown in various tissues. Our preliminary results suggest a role for RNase 1 in metabolism and coagulation. Our *Rnase1*$^{-/-}$ mouse will provide unprecedented insight into the biology of RNase 1. The ensuing knowledge will inform the development of new and improved ribonuclease-based chemotherapeutic agents, enhance their utility, and illuminate new physiology. Beyond RNase 1, our mouse could aid in understanding the inchoate field of extracellular RNA, shedding light on both the composition as well as the function of this enigmatic entity.

5.2 Introduction

Pancreatic ribonuclease (RNase 1) is a small, secreted, RNA-degrading enzyme conserved in mammals. Its biological purpose is unknown. Recombinant forms of RNase 1 have been engineered as potent chemotherapeutic agents, demonstrating antitumor properties *in vitro* and *in vivo*.[127,220,222,348] Moreover, recombinant RNase 1 is emerging as an ideal candidate for protein-based drug therapy, as it possesses remarkably high stability and low immunogenicity upon administration.[127,222] Beyond exploiting its potential as a useful drug, we seek to understand its endogenous role *in vivo*. We believe that this knowledge will not only allow for improved design of current RNase 1 therapeutics, but potentially open doors to novel applications of this versatile enzyme.

Based on its high expression in the pancreas of many species, RNase 1 has been considered to be a digestive enzyme.[19,31] Certain data challenge this convention and indicate a broader biological role. Unlike other hydrolytic digestive enzymes, levels of RNase 1 do not change in response to fasting or consumption.[263] Further, pancreatectomy in both rats and humans does not affect circulating levels of RNase 1.[23,349] Beyond the digestive tract, human RNase 1 has been detected in every bodily tissue examined, as well as multiple fluids including milk, urine, seminal plasma, cerebrospinal fluid, and blood.[79,87,350-352] Serum RNase 1 is elevated in many disease states, including bacterial and viral infection, multiple forms of cancer, and autoimmune disorders.[92,163,187,353-355] The enzyme is bound tightly and inhibited by a cytosolic inhibitor protein, ribonuclease inhibitor (RI), suggesting that RNase 1 functions in the extracellular environment.[221]

RNase 1 circulates freely in the blood, at a concentration of approximately 400 ng/mL.[88,89] Analyses of RNase 1 glycosylation indicate that the primary source of serum RNase 1 to be

vascular endothelial cells, which have been shown to secrete large amounts of RNase 1 in culture.[92-95] These cells line the interior surface of blood vessels and are in direct contact with antigens and signaling molecules circulating in the blood. As a result, they modulate multiple biologic pathways, including coagulation and inflammation.[96] In response to various stimuli, vascular endothelial cells can quickly release contents from cytosolic storage compartments into the blood.[99] These storage granules, known as Weibel–Palade bodies, contain various proteins that regulate both hemostasis and inflammation, including von Willebrand factor (vWF), a procoagulant that mediates platelet aggregation, and P-selectin, an adhesion receptor that triggers leukocyte migration.[96,356] Interestingly, RNase 1 co-localizes with both vWF and P-selectin in endothelial Weibel–Palade bodies, and can be spontaneously released by treatment with known exocytosis-inducing agents, including thrombin and endotoxin.[89] These data suggest that RNase 1 secretion from endothelial cells is regulated tightly.

A possible role for RNase 1 is to modulate the level of extracellular RNAs (exRNAs). Recently, small exRNAs have been identified as potent effectors in human blood. They have been shown to activate clotting cascade proteins during thrombosis, increase blood vessel permeability, and play a role in cell–cell signaling and tumorigenesis.[100-104] exRNA is secreted by tumorigenic cells, and can promote tumor progression.[105] Increased levels of exRNAs—often found in patients suffering from cancer and sepsis—could contribute to the hypercoagulable state often observed in various inflammatory disorders.[103] Cancer often shows co-morbidity with chronic inflammation and hypercoagulation; indeed, cancers are often thought of as “wounds that do not heal” because of the upregulation of various inflammatory, angiogenic, and cell-survival pathways.[357] exRNA may be the mechanistic link between these phenomena. Beyond cancer, exRNA has been shown to promote the formation of atherosclerotic plaques in mouse

arteries, as well as enhance morbidity in a mouse model of lupus.[216,358] Thus, exRNA presents a novel therapeutic target for treating a variety of disease states, ranging from cancer to hypercoagulation to autoimmunity; yet, its regulation remains mysterious. As the only known serum protein with high activity against nonspecific RNA, RNase 1 is a likely candidate to regulate exRNA *in vivo*. Indeed, exRNA degradation by RNase1 could constitute a novel mechanism of vascular homeostasis. Tellingly, multiple studies have demonstrated therapeutic effects from RNase treatment of various mouse models of disease.[105,109,114,216,218,358] Further, treatment with exRNA (but not DNA) induces the release of RNase 1 from cultured endothelial cells.[89]

Based on its evolutionary conservation among mammals, ubiquitous distribution throughout the body and intriguing immunologic and cytotoxic properties *in vitro*, we believe that RNase 1 possesses important biologic function. Nevertheless, as a secreted enzyme, RNase 1 could exert its functions systemically in the bodies of vertebrates. As such, its biological roles cannot be inferred or recapitulated in a petri dish. To elucidate the endogenous biological roles of RNase 1, we have used a reverse-genetics approach to create a conditional knockout mouse for the murine homolog, *Rnase1*. Use of conditional Cre/lox technology gives us ultimate flexibility in locational and temporal control of *Rnase1* deletion, providing vast possibilities for experimental design. We believe a thorough phenotypic characterization of this mouse model will provide novel insight into the as-yet-uncharacterized biology of RNase 1. This knowledge could directly impact the design of novel therapeutics, as well as illuminate poorly understood physiological mechanisms.

5.3 Methods and Results I: Construction of a conditional *Rnase1* KO mouse

5.3.1 Characterization of murine RNase 1 in vitro and in vivo

Before embarking on a reverse-genetics approach, we sought rigorous validation of mouse RNase 1 as a model for its human homolog. Prior to our work, no data existed on the expression of mouse *Rnase1*, nor had the protein been characterized or even produced by recombinant DNA methods. Accordingly, we analyzed 18 mouse tissues for *Rnase1* expression by RT-PCR using primers for *Rnase1* as well as mouse *Gapdh* as a control. All tissues examined were found to express *Rnase1* (Figure 1A).

Next, we expressed the cDNA for mouse RNase 1 and its cognate mouse ribonuclease inhibitor in our *E. coli* systems, and purified the resulting proteins.[146,221] Mouse RNase 1 shares ~70% protein sequence identity with human RNase 1. We found that mouse RNase 1 is thermostable (T_m = 65 °C) and has $k_{cat}/K_M = 1.7 \times 10^7$ $M^{-1}s^{-1}$ for cleavage of a standard substrate (6-FAM–dArUdAdA–6-TAMRA[243]), and that the mouse RI·RNase 1 complex has K_d = 0.19 fM. These values are all similar to those for the human proteins (Figure 1C). Finally, we used X-ray diffraction analysis to determine the structure of the mouse RI·RNase 1 complex at a resolution of 2.20 Å with *R*-value = 0.183 (Figure 1B). The structure of the mouse complex is virtually identical to that of the human complex and the backbone atoms of mouse and human RNase 1 have an rmsd of only 0.29 Å. Together, these structure–function data *in vitro*, coupled with the similarly broad expression pattern *in vivo*, give us confidence in mouse RNase 1 as a model for human RNase 1. A more thorough explanation of the production, characterization and structural analysis of mouse proteins can be found in CHAPTER 4.

5.3.2 Engineering the Rnase1 conditional targeting vector

Like the human gene encoding RNase 1, mouse *Rnase1* exists in a single copy in the mouse genome and does not have pseudogenes.[359] The *Rnase1* gene consists of two exons and one intron, with the entire coding sequence contained within exon 2. Due to its small size, we chose to target the entire *Rnase1* coding sequence (exon 2) for eventual deletion *in vivo* (Figure 2).

The recombineering strategy of Copeland and coworkers was used to construct the conditional knock-out (cKO) targeting vector for the mouse RNase 1 gene (Figure 3).[360] A bacterial artificial chromosome (BAC) clone containing ~100 kb of murine genomic DNA—including the entire *Rnase1* coding sequence—was obtained from a 129/SvJ embryonic stem (ES) cell library (Genome Systems Inc.). An 8.7-kb genomic fragment containing *Rnase1* exons 1 and 2 was isolated from the BAC clone and introduced into plasmid pL253 containing a thymidine kinase selection cassette (*MC1-TK*). A mini-targeting vector was constructed by cloning the following three PCR fragments into the vector pL452 (which contained a *lox*P site and the FRT-flanked pGK promoter/EM7 promoter-*Neo*-pGHpA cassette): (a) a 539 bp sequence immediately upstream of exon 2; (b) a *lox*P site and a 622-bp sequence containing exon 2 and (c) a 531-bp sequence immediately downstream of exon 2. The mini-targeting cassette was excised by digestion with XhoI and SacII and transformed into recombination-competent DY380 bacteria cells previously transformed with the 8.7 kb–pL253 (pL253-8.7) plasmid. Recombinants that integrated the pGK promoter/EM7 promoter-*Neo*-pGHpA cassette into pL253-8.7 were selected on kanamycin plates. Restriction mapping and DNA sequencing were performed to confirm the homologous integration of the mini-targeting cassette into the pL253-8.7 plasmid, creating the finished floxed *Rnase1* targeting vector (Figures 2, 3, and 4A).

5.3.3 Generation of gene-targeted murine embryonic stem cells

The targeting vector was linearized by digestion with Hind III and introduced by electroporation into murine SV/129 R1 embryonic stem (ES) cells. Cells that had integrated the targeting vector either by homologous or random integration were selected for by growth in media containing G418. Cells that integrated the HSV-TK cassette were selected against with gancyclovir. Neomycin/ganciclovir-resistant colonies (180) were picked, duplicated, and frozen in 96-well dishes. DNA was isolated from all clones, digested with AseI, and analyzed by Southern blot genotyping with 5′ and 3′ probes that were outside the region of homology (Figure 4B). Previously, we had designed and empirically tested these probes to ensure their specificity (data not shown). Of the initial 180 clones, three (1.7%) displayed proper vector targeting due to homologous recombination. Nonetheless, DNA sequence analysis confirmed that exon 2 was correctly flanked by two *loxP* sites in only one clone (0.6%). Karyotype analysis performed at the Molecular Cytogenetics Laboratory at Yale University (New Haven, CT) confirmed that the positive clone was karyotypically normal.

5.3.4 Blastocyst injection of gene-targeted clone and generation of chimeras

The single validated ES cell clone was expanded for four days on a LIF (leukemia inhibitory factor) producing feeder layer. ES cells were disaggregated into single-cell suspension, separated from the feeder cells, and microinjected into the blastocoel cavities of expanded C57BL/6 blastocysts. All ES cell work, including microinjection, was carried out by the University of Wisconsin Transgenic Animal Facility. Following microinjection, blastocysts were allowed to recover and transferred into the oviducts of pseudopregnant female mice. Chimeric pups were born 19 days later and the most highly chimeric males (based on coat color) were bred to C57BL/6 partners at six weeks of age. Germline transmission of the targeted allele resulted in the

production of multiple agouti F1 progeny. Transmission of the floxed *Rnase1* allele was confirmed by PCR analysis of genomic DNA isolated from tail biopsies (Figure 4C). All procedures involving animal care and handling were reviewed and approved by the Institutional Animal Care and Use Committee at the University of Wisconsin–Madison.

5.3.5 Breeding strategy to achieve Rnase1$^{-/-}$ mice

F1 mice heterozygous for the floxed *Rnase1* allele were intercrossed to yield homozygous *Rnase1*$^{flox/flox}$ mice. These mice were crossed to mice expressing germline Flp recombinase (Jackson Laboratory strain #009086) to excise fritted *Neo* from all tissues (Figure 5A). Subsequent breeding of heterozygous progeny generated mice homozygous for floxed *Rnase1*, but lacking *Neo*. To test for lethality of a null *Rnase1* phenotype, *Rnase1*$^{flox/flox}$ mice were crossed with mice expressing germline Cre recombinase (Jackson Laboratory strain #006054) to excise *Rnase1* from all tissues (Figure 5B). Subsequent breeding of heterozygous progeny yielded nullizygous *Rnase1*$^{-/-}$ mice (Figure 6). All genotyping was confirmed with PCR genotyping of genomic DNA derived from tail snips using primers specific to *Rnase1*, *Neo, Flp* and *Cre* (Table 1).

5.4 Methods and Results II: Characterization of an *Rnase1*$^{-/-}$ mouse

5.4.1 Genotyping of weanling mice

Tail biopsies (~0.5 cm of distal tail) were collected from weanling mice at 21 days old. Tail tissue samples were digested overnight in 650 µL of lysis buffer (10 mM Tris–HCl buffer, pH 7.5, containing 400 mM NaCl, 100 mM EDTA, and 0.6% w/v SDS) and 35 µL proteinase K (10 mg/mL). Following digestion, 350 µL of saturated aqueous NaCl was added to each solution, and the tubes were shaken by hand for 15 s and then subjected to centrifugation for 5 min at

14,000*g*. The supernatant was transferred to a new tube, and DNA was precipitated with 1 mL of ice-cold molecular biology-grade ethanol. The precipitated DNA was washed with 1 mL of 70% v/v ethanol and pelleted by centrifugation for 5 min at 14,000*g*. The pellet was air-dried briefly and resuspended in 100 µL of laboratory-grade water. The concentration and quality of the extracted genomic DNA was assessed on a NanoVue Plus spectrophotometer (GE Healthcare), and DNA stocks were stored at –80 °C.

Working stocks of 50 ng/µL genomic DNA were used for genotyping. Primers specific for each locus of interest (*i.e., Rnase1*, *Neo*, *Cre*, and *Flp*) were from Integrated DNA Technologies (IDT) (Table 1). Genotyping PCR reactions were carried out using GoTaq Green master mix (Promega). Reactions were run on 2% w/v agarose gels stained with ethidium bromide, and band sizes were visualized with a FOTODYNE Gel documentation system.

5.4.2 Rnase1$^{-/-}$ mice appear morphologically normal

Rnase1$^{-/-}$ mice were compared to wild-type control mice matched for age, gender and genetic background (*i.e*., litter-matched). Both male and female *Rnase1*$^{-/-}$ mice were found to be viable and showed no outward physical phenotype (Figure 7). Mating pairs of both *Rnase1*$^{+/-}$ and *Rnase1*$^{-/-}$ mice produced litter sizes similar to wild-type, with no divergence in the Mendelian ratios of offspring genotypes. No behavioral differences were noted between *Rnase1*$^{-/-}$ or wild-type animals.

5.4.3 Rnase1$^{-/-}$ mice show undetectable levels of Rnase1 expression in all tissues

Quantitative PCR analysis of tissues derived from *Rnase1*$^{-/-}$ mice revealed the absence of detectable *Rnase1* in all tissues (Figure 8B). Sixteen mouse tissues (~100 mg each) were extracted from either wild-type or *Rnase1*$^{-/-}$ mice and immediately submerged into RNA*later* solution. Tissues were blotted dry and minced into a Potter–Elvehjem tissue grinder (Wheaton).

1 mL of TRIzol reagent (Life Technologies) was added and samples were homogenized by hand on ice for ~5 min. RNA was extracted from homogenates via TRIzol extraction according to the manufacturer's protocol. RNA was eluted with DEPC-treated water and treated with DNase I (Promega) to remove any DNA contamination. The concentration and quality of the extracted RNA was assessed on a NanoVue Plus spectrophotometer (GE Healthcare), and samples were stored at –80 °C until further use. cDNA was generated using the High-Capacity cDNA Reverse Transcription Kit (Applied Biosystems) according to the manufacturer's instructions. qPCR was performed on an ABI 7500 Fast Real-Time PCR system (Applied Biosciences) using gene-specific primers for *Rnase1* and *Gapdh* and PerfeCTa SYBR Green FastMix Low ROX master mix (Quanta Biosciences).

5.4.4 Rnase1$^{-/-}$ mice show increased body weight compared to wild-type mice

Starting at 4 weeks of age, *Rnase1*$^{-/-}$ and matched wild-type controls were weighed once weekly. Pronounced differences in weight emerged at around 8 weeks of age, where male and female *Rnase1*$^{-/-}$ mice were ~33% and ~21% heavier than their wild-type counterparts, respectively (Figure 9A). This trend continued throughout the life of the animals, with *Rnase1*$^{-/-}$ mice consistently showing increased weight at all measured time points (Figure 9B).

5.4.5 Rnase1$^{-/-}$ mice show no significant differences in metabolic parameters

We attempted to explain the significant differences in body weight in *Rnase1*$^{-/-}$ mice by revealing differences in metabolic parameters, including various measurements of nutrient intake and excretion. Healthy adult mice (≥ 6 weeks of age) were placed individually into metabolism cages (Techniplast). Sterile water was provided in graduated water bottles, and standard ground mouse diet (LabDiet 5008) was provided in chow hoppers. At the beginning of each experiment, the weight of the mouse, the water bottle, and the chow hopper for each cage were recorded.

Cages were checked 8 h later to ensure mice could access chow and water appropriately; mice that were unable to access chow (due to size) were removed from metabolism caging and returned to normal housing. The weights of mice, food containers, and water bottles were recorded after 24 h, and urine and fecal collection receptacles were emptied. Food and water were replenished, and data were collected at both 48- and 72-h time points. After 72 h, mice were returned to normal housing.

We found no significant differences between *Rnase1*$^{-/-}$ and control groups in food intake, water intake, fecal output, or urine output (Figures 10A–D). We next probed for differences in the biochemical composition of urine and feces. Urine glucose concentration was assayed spectrophotometrically using the Infinity™ Glucose Oxidase Liquid Stable Reagent (Thermo Scientific), according to the manufacturer's instructions. Glucose standards were prepared in water. The assay was performed in a clear 96-well plate, with each reaction comprising 1 μL of undiluted sample or glucose standard and 150 μL of Infinity™ reagent. Each sample or standard was assessed in triplicate, and absorbance at 500 nm was measured with a Tecan M1000 plate reader. Urine and fecal protein concentration was assayed spectrophotometrically by the Pierce™ BCA Protein Assay Kit (Thermo Scientific), according to the manufacturer's instructions. Urine samples were diluted 1:100 in water, and each sample was assessed in duplicate. Fecal samples were generated by homogenizing 50 mg of feces in 1 mL water, then diluting 10–fold to yield a final concentration of 5 mg/mL. No significant differences in urine glucose concentration, urine protein content, or fecal protein content were found between *Rnase1*$^{-/-}$ and control groups (Figures 10E–G).

We speculated that mice with greater body weight might possess higher plasma lipid content. To determine if *Rnase1*$^{-/-}$ mice had higher cholesterol levels than wild-type mice, plasma

cholesterol was measured using the Amplex Red Cholesterol Assay kit (Invitrogen). Cholesterol standards were prepared in the included reaction buffer, and plasma samples were diluted 1:100 in the same buffer. Aliquots (50 μL) of samples or standards were incubated with 50 μL of working reagent in a black 96-well plate and incubated for 30 min at 37 °C. Fluorescence was measured with a Tecan M1000 plate reader. Preliminary data suggest no significant differences in plasma cholesterol levels between *Rnase1*$^{-/-}$ and wild-type mice (Figure 10H). Thus, *Rnase1*$^{-/-}$ mice do not shows symptoms of hypercholesterolemia, insinuating a normal ratio of low-density lipoprotein (LDL) to high-density lipoprotein (HDL) particles. Still, analysis of plasma lipoprotein fractions is necessary to conclude that the ratio of LDL to HDL is unaffected.

5.4.6 Rnase1$^{-/-}$ *mice show decreased plasma ribonucleolytic activity and increased plasma RNA content*

We were curious to probe for differences in both plasma RNase activity and plasma RNA content between *Rnase1*$^{-/-}$ and wild-type mice. To obtain plasma, mice were anaesthetized individually with isoflurane (4% v/v) using the open drop method. Loss of consciousness was verified by toe pinch. Mice were sacrificed by exsanguination, which was accomplished by brachial artery bleed. Blood was collected into EDTA–treated syringes and deposited into EDTA–treated microcentrifuge tubes. The tubes were kept on ice and subjected to centrifugation promptly for 10 min at 1,500*g*. Plasma was collected into a new tube and subjected to centrifugation again for 10 min at 1,500*g*. The upper ¾ portion of plasma was collected into a new tube, and stored at –80 °C for subsequent analysis.

Plasma samples were analyzed for ribonucleolytic activity against a standard substrate (6-FAM–dArUdAdA–6-TAMRA) as described previously.[243] Briefly, 1 μL of plasma was diluted into 198 μL of 0.10 M MES–NaOH (OVS-free[361]) buffer, pH 6.0, containing NaCl (0.10 M) and substrate (0.2 μM). The initial velocity of substrate cleavage was measured, and known

k_{cat}/K_M values for recombinant mouse RNase 1 were used to estimate the RNase 1 concentration in each plasma sample. We found that *Rnase1*$^{-/-}$ mice possessed significantly lower plasma ribonuclease content than matched wild-type controls. Yet, *Rnase1*$^{-/-}$ mice still showed measureable plasma ribonucleolytic activity (Figure 11A), suggesting the presence of plasma ribonucleases other than RNase 1.

We next measured the concentration of RNA in plasma samples from *Rnase1*$^{-/-}$ and wild-type mice. Plasma (1 µL) was added to a 10 µL DNase I (Promega) reaction and incubated at 37 °C for 30 min. A blank reaction, containing no plasma, served as a reference for absorbance measurements. The absorbance at 260 nm was analyzed using a NanoVue Plus spectrophotometer (GE Healthcare). We determined that *Rnase1*$^{-/-}$ mice had significantly higher levels of plasma RNA than did wild-type mice (Figure 11B).

5.4.7 Histopathological examination of Rnase1$^{-/-}$ *mouse tissues reveal no major differences*

We collaborated with the on-campus Research Animal Resources Center Veterinary Pathology Laboratory to perform histological examinations of *Rnase1*$^{-/-}$ and wild-type mice. Four litter-matched mice (1 KO male, 1 KO female, 1 WT male, and 1 WT female), aged 8 weeks, were given to Dr. Ruth Sullivan, D.V.M./Ph.D., for blind analysis. After detailed study of each tissue, Dr. Sullivan could find no significant differences between groups.

5.4.8 Rnase1$^{-/-}$ *mice show reduced clotting time and increased fibrinogen production*

We probed for differences in plasma coagulation parameters between *Rnase1*$^{-/-}$ and wild-type mice. Blood was collected and sent to IDEXX laboratories for *in vitro* coagulation assays, including measuring prothrombin time (PT) (which is the time for plasma to clot after addition of tissue factor) and the production of fibrinogen. Preliminary analyses of four samples indicate

pronounced differences between *Rnase1*$^{-/-}$ mice and wild-type controls, with *Rnase1*$^{-/-}$ mice showing greatly reduced prothrombin time (*i.e.*, faster clot formation) and greater fibrinogen production (Table 2). Measurements of partial thromboplastin time (PTT) did not show interpretable differences between groups (data not shown).

5.4.9 Rnase1$^{-/-}$ *mice show compensatory gene expression of paralogous ribonucleases*

We suspected that the expression of related mouse ribonucleases might be upregulated in *Rnase1*$^{-/-}$ mice. These compensatory changes might explain the surprising ribonucleolytic activity measured in plasma samples of *Rnase1*$^{-/-}$ mice. We used qPCR to probe the expression levels of paralogous ribonuclease-encoding genes in both wild-type and *Rnase1*$^{-/-}$ mice. Primers used for qPCR were designed using primer BLAST (NCBI) and checked for specificity using BLAST analysis, with the exception of primers to target EAR subfamilies A and B, which were described previously[362] (Table 1). qPCR was performed on an ABI 7500 Fast Real-Time PCR system (Applied Biosciences) using PerfeCTa SYBR Green FastMix Low ROX master mix (Quanta Biosciences) and the following reaction protocol: 95 °C:2 min; 40 cycles of 95 °C:30 s, 55 °C:30 s, 72 °C:30 s; 72 °C:30 s. A melting curve was performed at the end of the reaction to confirm primer specificity for each reaction.

Our preliminary findings suggest there is significant upregulation of RNase 1 paralogs in various tissues of *Rnase1*$^{-/-}$ mice (Figure 12A). Expression of mouse *Angiogenin1* was found to be ~500-fold higher in the pancreas of *Rnase1*$^{-/-}$ mice than wild-type mice. There was strong upregulation of mouse *Rnase4* expression in the brain, salivary gland, thymus, and testes (Figure 12A). Several mouse eosinophil-associated RNases also showed elevated expression in several tissues, as well as mouse *Rnase10*, which had elevated expression in the seminal vesicles

and testes of *Rnase1*$^{-/-}$ mice. Surprisingly, the expression of mouse ribonuclease inhibitor was also elevated in several tissues, especially pancreas (Figure 12A).

5.5 Discussion and Future Directions

Emerging evidence from *in vitro* studies, *in vivo* animal models, and cancer clinical trials suggests that RNase 1 is an important biological effector in mammalian systems. Still, understanding the precise mechanisms and actions of secreted ribonucleases is hindered by the absence of genetic models to probe systemic function. We have addressed a critical need in the RNase 1 field by creating a conditional knockout mouse for murine *Rnase1*. We have generated germline *Rnase1* knockouts and have begun preliminary phenotypic characterizations of these mice. We verified the total absence of *Rnase1* expression in all tissues, thus confirming the functionality of our system. Our mouse model is poised to be an invaluable resource toward understanding the putative biological roles of RNase 1, as well as probing the mechanisms underlying extracellular RNA (exRNA) function.

In support of our hypotheses, we find that *Rnase1*$^{-/-}$ mice have increased levels of exRNA, as compared to matched wild-type controls. These data strongly suggest a role for RNase 1 in regulating RNA in the blood. exRNA has been shown to promote the activation of FSAP (Factor VII-activating protease), a recently characterized extrinsic pathway coagulation factor. FSAP activates Factor VII, which induces downstream factors (including thrombin), ultimately culminating in the formation of a fibrin clot.[110] The activation of the extrinsic pathway can be assessed by measuring prothrombin time (PT), which measures the time needed for plasma to form fibrin clots after the addition of tissue factor. Interestingly, *Rnase1*$^{-/-}$ mice showed reduced

PT in preliminary experiments. These data indicate that *Rnase1*$^{-/-}$ mice exhibit a pro-thrombotic phenotype, perhaps as a consequence of excess exRNA.

RNase 1 and exRNA might constitute a novel set of pro- and anti-thrombotic regulators of the coagulation cascade. Presently, there are three major anticoagulation pathways: (1) tissue factor protein inhibitor (TFPI), which inhibits tissue factor; (2) antithrombin, which inhibits thrombin, as well as other serine proteases in the cascade; and (3) the protein C pathway, involving thrombomodulin binding to thrombin and altering its substrate specificity.[363] Intriguingly, RNase 1 shares many similarities with these known anticoagulant proteins. TFPI and thrombomodulin are both highly expressed by vascular endothelial cells, and their expression can be upregulated by treatment with thrombin. Like RNase 1, TFPI is known to bind tightly to cell-surface heparan sulfate; such binding to glycans anchors TFPI at the surface of the endothelium, where it is well poised to affect the nascent coagulation cascade. Further, TFPI circulates in the plasma at a low nanomolar concentration.[364,365] Taken together, RNase 1 is both expressed and localized in a manner similar to known anticoagulants. These observations provide strong evidence that a putative biological role for RNase 1 is to act as an anticoagulant via the regulation of extracellular RNA.

Beyond coagulation, exRNA has been implicated as a potent antigenic agent capable of provoking a strong immunogenic response. Indeed, exRNA has been postulated as a major contributor to the mechanistic interconnection between inflammation and coagulation. The Toll-like receptors that recognize and respond to exRNA (TLRs 3, 7, and 8) are all localized within endosomes. Upon binding to exRNA, these receptor proteins facilitate downstream signaling that results in the upregulation of hundreds of genes.[295-297,366] Previously, we have shown that RNase 1 associates with cell-surface glycans and internalizes into cells via endocytosis.[128,132,298] Hence,

RNase 1 might be especially well adapted to enter endosomes, where it could degrade antigenic RNA and regulate signaling cascades. Consequently, through regulating exRNA, RNase 1 may exert remarkable control over not only coagulation, but also inflammation.

Dysregulated inflammatory pathways can result in various pathologies, including obesity.[367,368] Indeed, clinical data suggests that chronic low-level inflammation can actually cause obesity.[369] Hence, the increased body weight of *Rnase1*$^{-/-}$ mice is particularly intriguing, especially when paired with preliminary measurements of increased plasma fibrinogen. Beyond being an essential factor in coagulation, fibrinogen has also been identified as one of several inflammation-sensitive plasma proteins. Increased levels of fibrinogen have been associated with increased risk of hypertension,[370] myocardial infaction,[371] thrombosis,[372] diabetes,[373] peripheral artery disease,[374] and weight gain.[369] Indeed, fibrinogen represents one of many cofactors that link the coagulation, inflammation, and metabolic systems. Taken together, the increased biomarkers for hypercoagulation, inflammation, and obesity presented by *Rnase1*$^{-/-}$ mice might indicate a role for RNase 1 in regulating metabolic syndrome. Mechanistically, clinical evidence suggests that the extrinsic coagulation pathway is upregulated in obesity and the metabolic syndrome, with obese patients have higher levels of Factor VII.[368,375]

An interesting avenue for future metabolic analysis is to probe for differences in the gut microbiome of *Rnase1*$^{-/-}$ mice. The microbiome represents a major intersection of the metabolic and immune systems, which are closely integrated and functionally dependent. The microbiome has been proposed to affect the host by regulating energy harvest and nutrient metabolism, modulating hormone secretion, and inducing inflammation. In turn, the innate immune system shapes commensal microbial communities: disruption of the innate immune system can result in alteration of gut microbial composition, diversity, and homeostasis. Altered composition of gut

microbiota has been linked to the pathogenesis of obesity, fatty liver disease, diabetes, and atherosclerosis, and could lead to increased susceptibility to autoimmune disorders such as inflammatory bowel disease, asthma, and allergic dermatitis.[376] Interestingly, recent analyses of extracellular human RNAs determined that many were sourced from the human gut microbiota.[377,378] Hence, extracellular RNA might again be the underlying factor connecting interrelated body systems.

In conclusion, our initial characterizations of *Rnase1*$^{-/-}$ mice have yielded preliminary data implicating RNase 1 in regulating the interconnected systems of coagulation, inflammation, and metabolism. Moving forward, more robust analyses are necessary, especially experiments designed to provoke and manifest subtle phenotypes. In particular, it will be interesting to immunologically challenge the *Rnase1*$^{-/-}$ mice, either with viral or bacterial pathogens, or with cancer. As RNase 1 is known to be upregulated in various disease states, its absence could indeed result in exacerbated morbidity or mortality. Further, it will be interesting to investigate the compensatory expression of paralogous ribonucleases suggested by our initial characterizations. Especially relevant is RNase 4, which is the most evolutionarily similar to RNase 1 (Figure 12B). Currently, little is known about the biochemistry or biology of human or mouse RNase 4. Additionally, utilizing the conditional nature of the *Rnase1* construct to generate adult-onset *Rnase1* ablation may yield a more robust phenotype. Through our novel mouse model, we are well poised to unlock the mysterious biology of RNase 1.

Figure 5.1

A

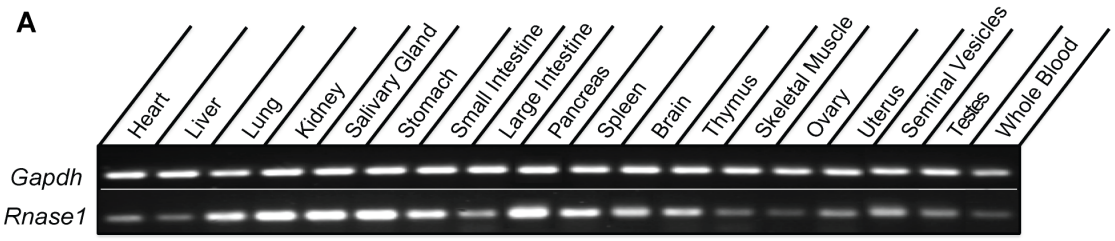

B

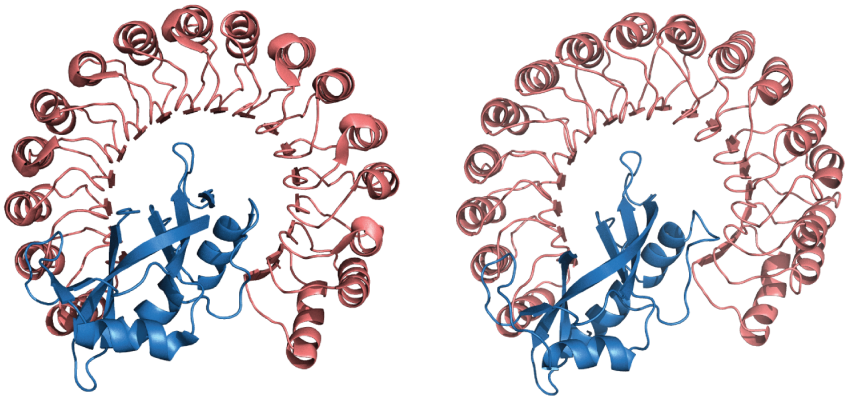

Human RNase 1 Complexed with Human Ribonuclease Inhibitor (PDB 1Z7X)

Mouse RNase 1 Complexed with Mouse Ribonuclease Inhibitor (PDB 3TSR)

C

	Human RNase 1	Mouse RNase 1
Molecular Weight (Da)	14705.5	14149.9
Charge (Z)	+6	+4
Catalytic Activity [k_{cat}/K_M (10^6 M^{-1} s^{-1})]	1.8 ± 0.5	17 ± 1.5
Inhibitor Binding [K_d (M)]	1.31×10^{-17}	1.93×10^{-16}

Figure 5.1 Comparison of mouse and human RNase 1 expression

A. RT-PCR analysis demonstrating that mouse *Rnase1* is expressed in a broad range of tissues. *B.* (*right*) Novel crystal structure of mouse RNase 1 in complex with mouse ribonuclease inhibitor; (*left*) crystal structure of human RNase 1 in complex with human ribonuclease inhibitor. *C.* Comparative biochemical values for human and mouse RNase 1, including catalytic activity and inhibitor binding affinity.

Figure 5.2

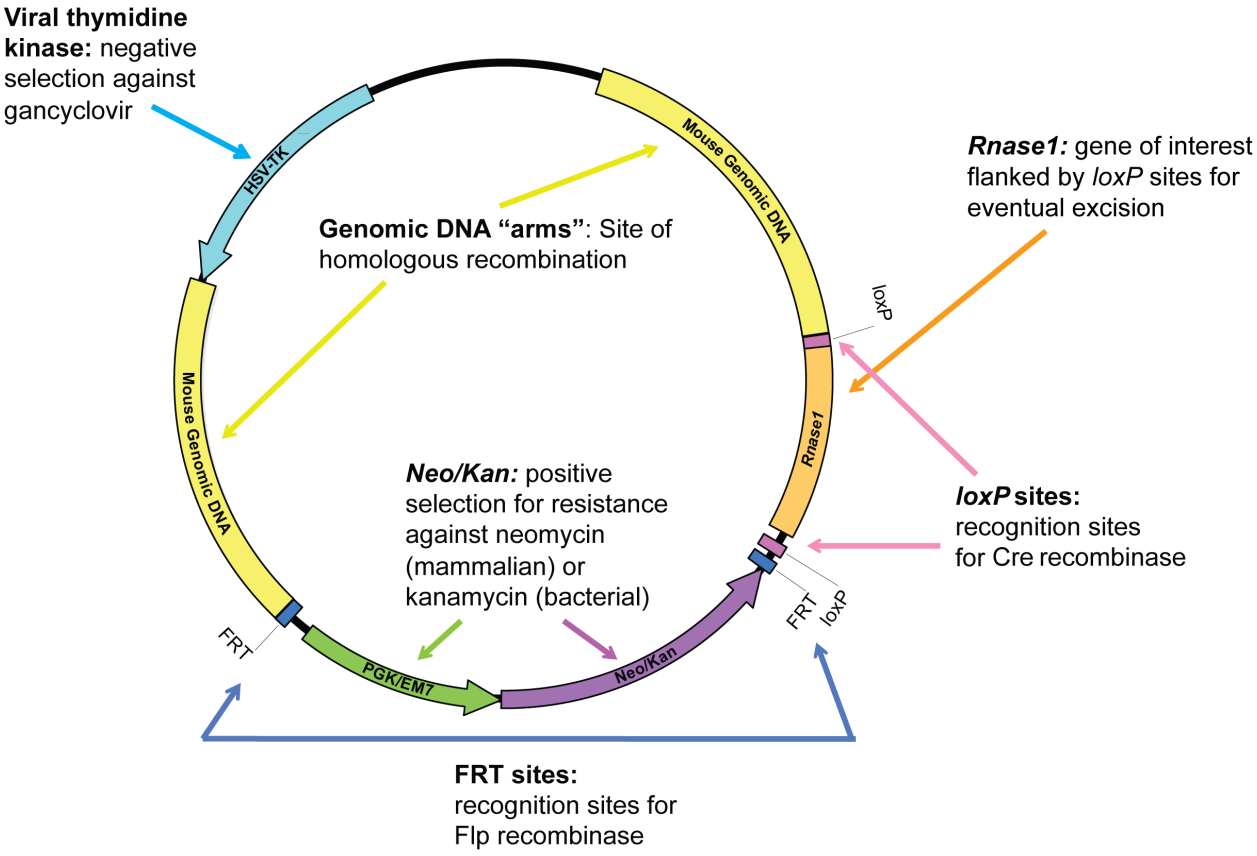
Viral thymidine kinase: negative selection against gancyclovir
HSV-TK
Mouse Genomic DNA
Genomic DNA "arms": Site of homologous recombination
Rnase1: gene of interest flanked by *loxP* sites for eventual excision
loxP
Rnase1
Mouse Genomic DNA
Neo/Kan: positive selection for resistance against neomycin (mammalian) or kanamycin (bacterial)
***loxP* sites:** recognition sites for Cre recombinase
FRT
loxP
FRT
PGK/EM7
Neo/Kan
FRT sites: recognition sites for Flp recombinase

Figure 5.2 Structure of the *Rnase1* targeting vector

General layout of the conditional *Rnase1* targeting vector, showing inclusion of positive and negative selection genes, targeting sequences for Cre and Flp recombinases, and large "arms" of mouse genomic DNA for homologous recombination.

Figure 5.3

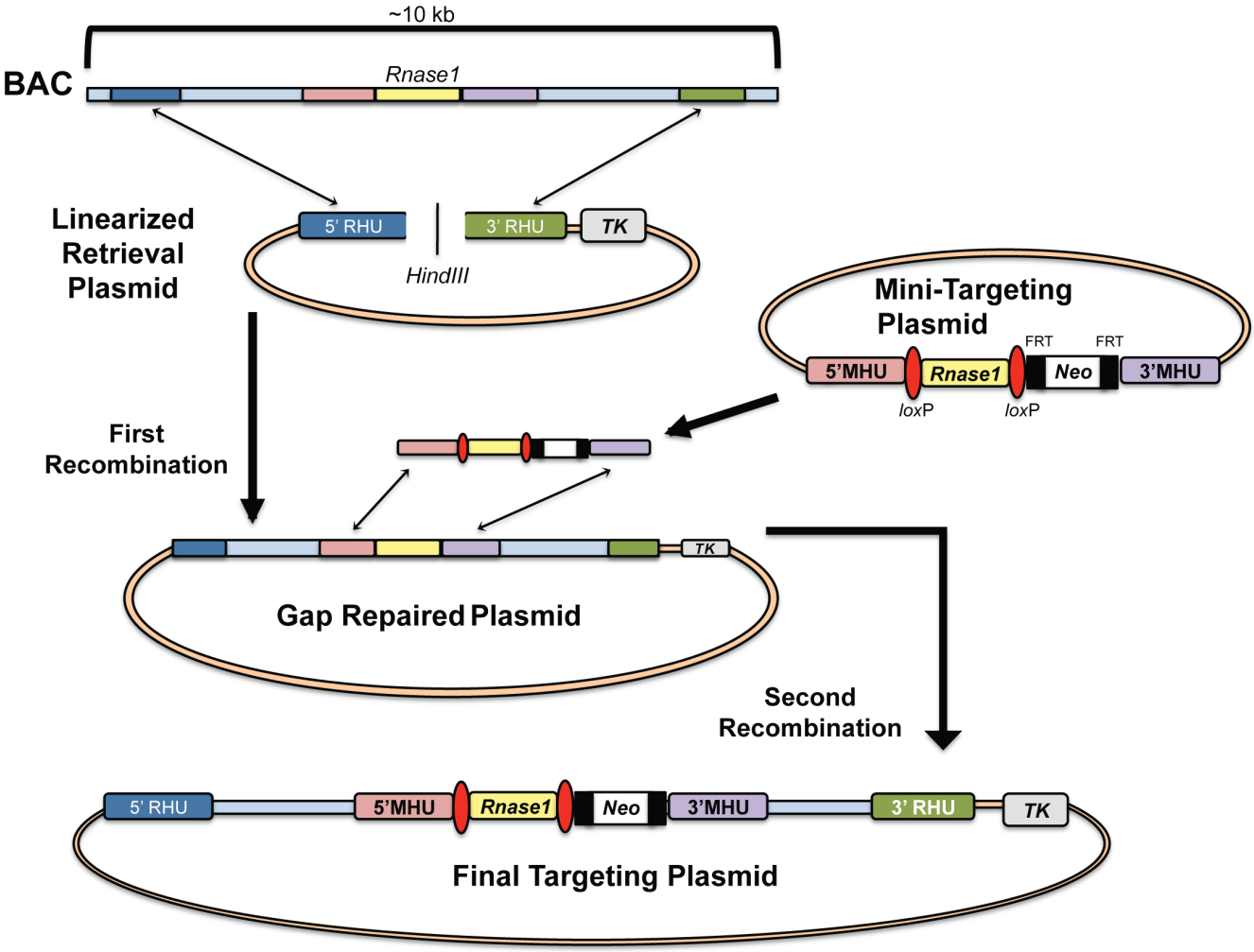
~10 kb
BAC
Rnase1
Linearized
Retrieval
Plasmid
5' RHU
3' RHU
TK
HindIII
Mini-Targeting
Plasmid
FRT
FRT
5'MHU
Rnase1
Neo
3'MHU
loxP
loxP
First
Recombination
TK
Gap Repaired Plasmid
Second
Recombination
5' RHU
5'MHU
Rnase1
Neo
3'MHU
3' RHU
TK
Final Targeting Plasmid

Figure 5.3 Recombineering method for constructing an *Rnase1* conditional targeting vector Final targeting plasmid was generated through a series of homologous recombination events. *Rnase1* genomic DNA was subcloned from a BAC via gap repair mediated by viral recombinases in *E. coli.* A mini-targeting plasmid was separately constructed that contained *lox*P-flanked Exon 2 for *Rnase1*, as well as a neomycin-resistance gene. This region of DNA from the mini-targeting plasmid was similarly subcloned into the gap-repaired plasmid, resulting in a final targeting plasmid that contained positive and negative selection markers (*neo* and *TK*, respectively), a *lox*P-flanked coding sequence for *Rnase1*, and large regions of genomic DNA that promote correct insertion of the targeting plasmid via homologous recombination in mouse embryonic stem cells.

Figure 5.4

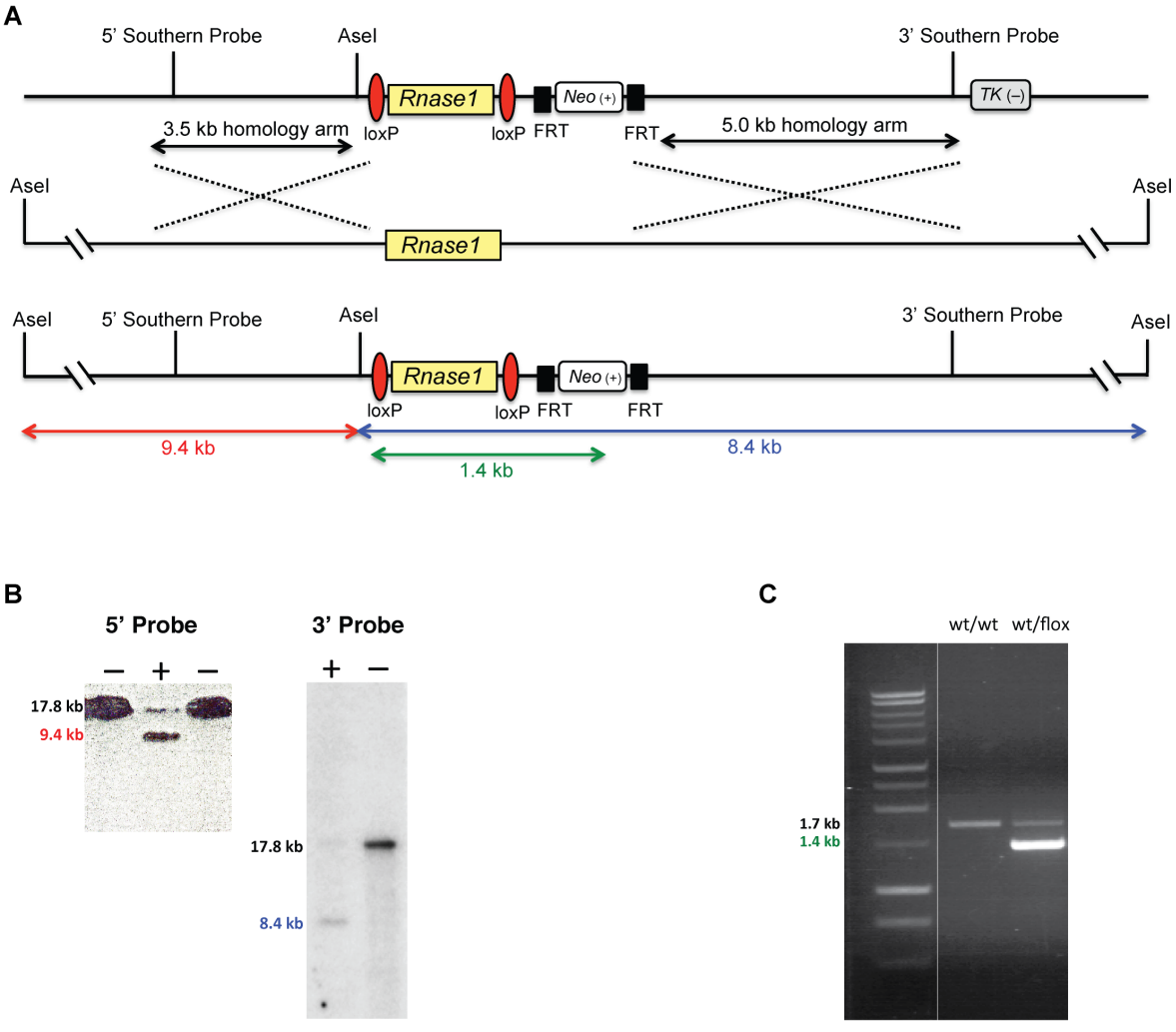
A
5' Southern Probe
AseI
3' Southern Probe
Rnase1
Neo (+)
TK (–)
3.5 kb homology arm
loxP
loxP
FRT
FRT
5.0 kb homology arm
AseI
AseI
Rnase1
AseI
5' Southern Probe
AseI
3' Southern Probe
AseI
Rnase1
Neo (+)
loxP
loxP
FRT
FRT
9.4 kb
8.4 kb
1.4 kb
B
5' Probe
3' Probe
– + –
+ –
17.8 kb
9.4 kb
17.8 kb
8.4 kb
C
wt/wt
wt/flox
1.7 kb
1.4 kb

Figure 5.4 Targeted gene disruption of *Rnase1*

A. The *Rnase1* targeting vector was constructed via homologous recombination in *E. coli*. The final targeting vector contained 3.5 kb of 5′ homology, the *Rnase1* gene flanked by *lox*P sites, an FRT-*Neo*-FRT cassette introduced into the 3' untranslated region of exon 2 of *Rnase1*, 5.0 kb of 3′ homology, and the TK cassette. *B.* Correctly targeted ES cell clones were identified by Southern blot using unique 3′ and 5′ probes to detect either wildtype (17.8 kb) or targeted (8.4 kb) bands following digestion with AseI. *C.* Germline transmission of the floxed *Rnase1* allele from chimeric founders to F1 progeny was confirmed via PCR genotyping with *lox*P and *Neo* specific primers. A 1.7-kb band corresponds to the unfloxed wildtype allele, and a 1.4-kb band corresponds to the floxed *Rnase1* allele.

Figure 5.5

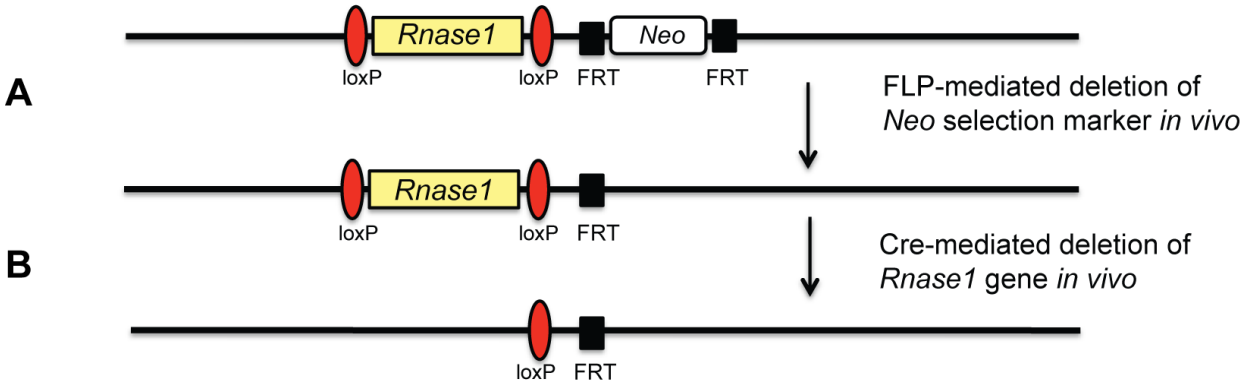
A
Rnase1
Neo
loxP
loxP
FRT
FRT
FLP-mediated deletion of
Neo selection marker in vivo
Rnase1
loxP
loxP
FRT
B
Cre-mediated deletion of
Rnase1 gene in vivo
loxP
FRT

Figure 5.5 Breeding strategy to mediate *in vivo* deletion of *Neo* and *Rnase1*

A. Mice bearing two copies of the floxed *Rnase1* allele were bred to mice expressing germline Flp recombinase. Expression of Flp mediates site-specific recombination at FRT sites, thereby deleting the neomycin selection marker (*Neo*). *B.* Mice bearing two copies of the floxed *Rnase1* allele (sans *Neo*) were bred to mice expressing germline Cre recombinase. Expression of Cre mediates site-specific recombination at *lox*P sites, thereby deleting the *Rnase*1 gene.

Figure 5.6

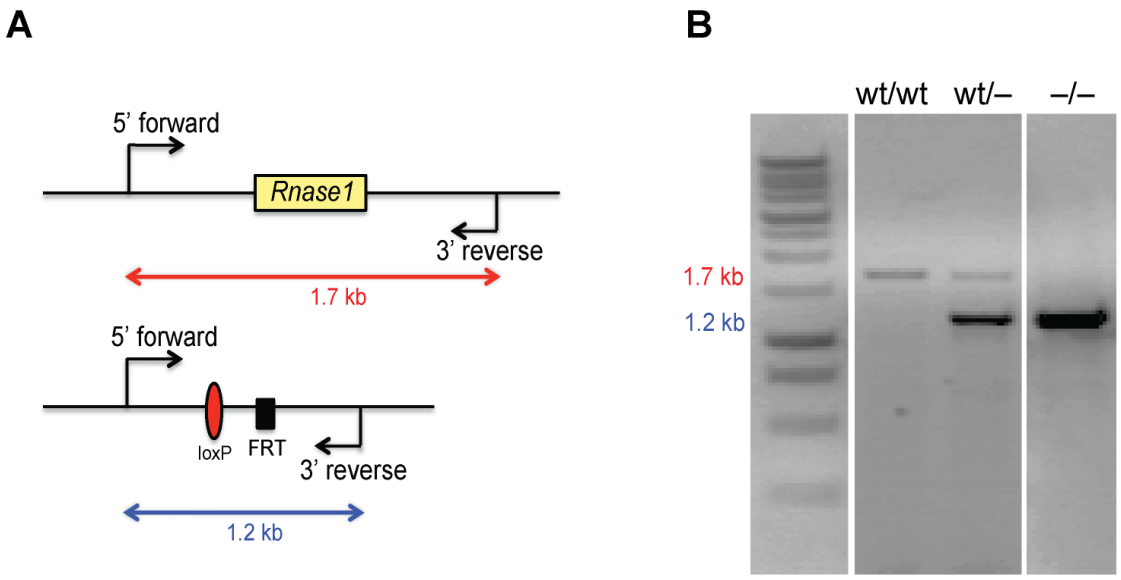
A
5' forward
Rnase1
3' reverse
1.7 kb
5' forward
loxP
FRT
3' reverse
1.2 kb
B
wt/wt
wt/–
–/–
1.7 kb
1.2 kb

Figure 5.6 PCR genotyping strategy to confirm *Rnase1* nullizygous mice

A. Forward and reverse primers were used to amplify upstream and downstream of the *Rnase1* locus. The same primer set yields two distinct bands for mice possessing either a WT allele or a *Rnase1*$^{-/-}$ excised allele. *B.* Ethidium bromide stained gel showing PCR genotyping for mice with either two copies (*Rnase1*$^{wt/wt}$), one copy (*Rnase1*$^{wt/-}$), or no copies of the *Rnase1* gene (*Rnase1*$^{-/-}$).

Table 5.1 Oligonucleotides used for genotyping and qPCR analysis

Locus	Sequence
Genotyping Primers	
Cre	F – GCATTACCGGTCGATGCAACGAGTGATGAG R – GAGTGAACGAACCTGGTCGAAATCAGTGCG
Flp	F – GTCCACTCCCAGGTCCAACTGCAGCCCAAG R – CGCTAAAGAAGTATATGTGCCTACTAACGC
Neo	F – TGCTCCTGCCGAGAAAGTATCCATCATGGC R – CGCCAAGCTCTTCAGCAATATCACGGGTAG
Rnase1	F – TGCAGGGACTAGGGTAGTGG R – CATGACACAGGACAGGAACG
qPCR Primers	
Gapdh	F – CTCCCACTCTTCCACCTTCG R - CCACCACCCTGTTGCTGTAG
Rnase1	F – CTGCAAGAACAGGAAGAGCAAC R – GAGTGGTCTTGTAGTCACAGTTGG
Rnase4	F – AACGGTTCCTTCGACAGCAT R – GCGTTTGCACTGGACAGAAG
Rnase5/Ang1	F – TCTGCAGGGTTCAGACATGT R - TCTGGGCTATGAGGGGAGAT
Rnase10	F – TGTAACGGTTCCCTGGTTGA R - GAGTGACTTGGCCTGGTTTG
EAR subfamily A	F – GCCTCATGCCTGGGACA R – GTGGAGTTCTGGGGTTACA
EAR subfamily B	F – CCTGCTGATGCTGGGACTT R - CATGCAACTCTGGGCTCACA
Rnh1	F – CCCAGCTGTAAGCTCAGGAC R – CTCTGCTTGGCTCTGAGGAC

Figure 5.7

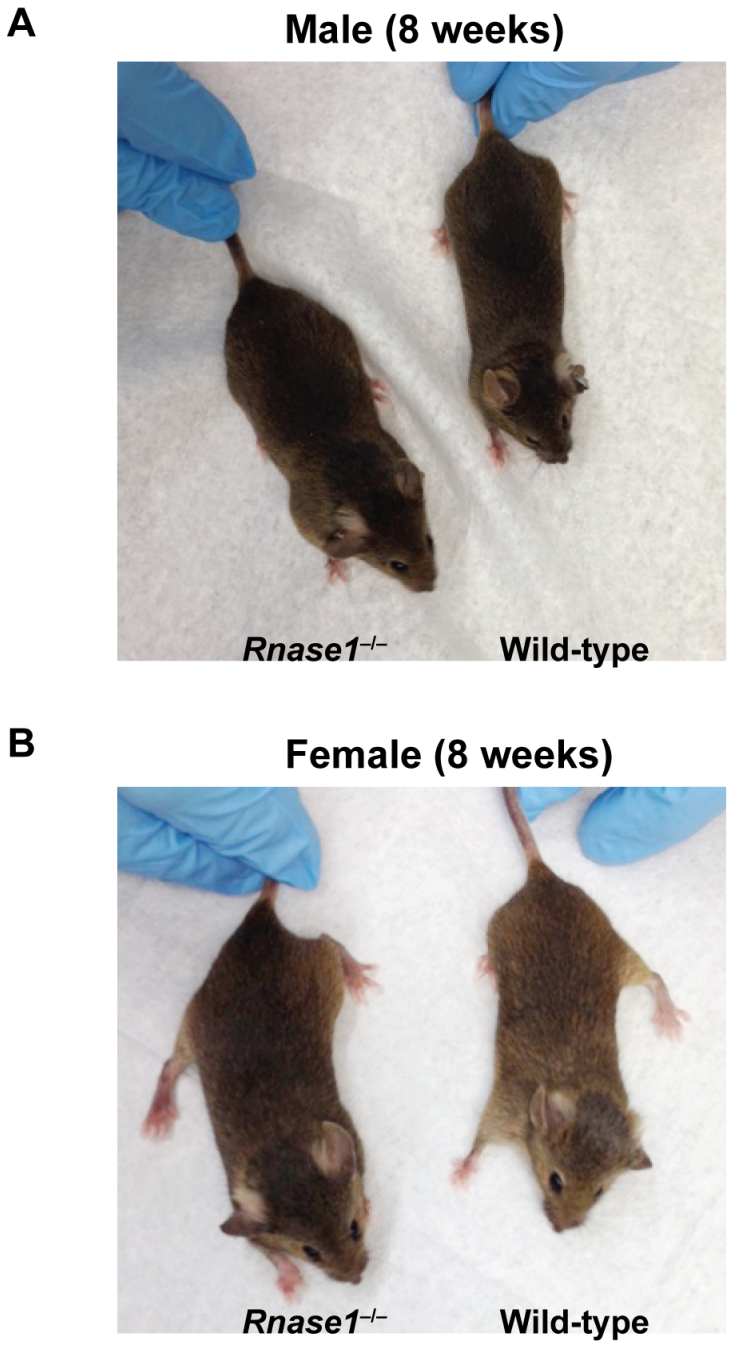
A
Male (8 weeks)
Rnase1−/−
Wild-type
B
Female (8 weeks)
Rnase1−/−
Wild-type

Figure 5.7 Phenotypic characterization of *Rnase1*$^{-/-}$ mice

Side-by-side photographs of wild-type and *Rnase1*$^{-/-}$ littermates. *A.* Male mice aged 8 weeks. *B.* Female mice aged 8 weeks.

Figure 5.8

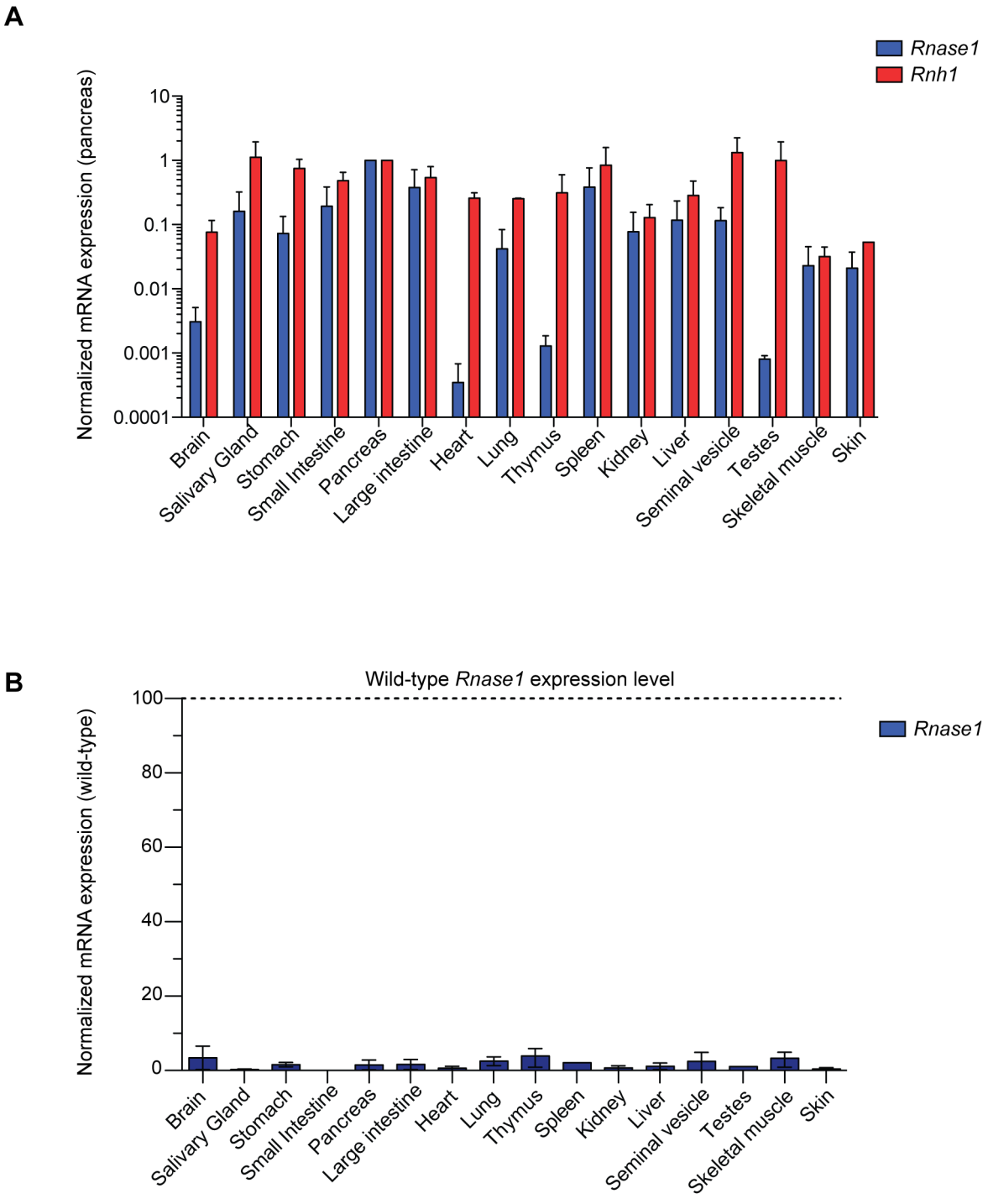
A
Rnase1
Rnh1
Normalized mRNA expression (pancreas)
10
1
0.1
0.01
0.001
0.0001
Brain
Salivary Gland
Stomach
Small Intestine
Pancreas
Large intestine
Heart
Lung
Thymus
Spleen
Kidney
Liver
Seminal vesicle
Testes
Skeletal muscle
Skin
B
Wild-type Rnase1 expression level
Rnase1
Normalized mRNA expression (wild-type)
100
80
60
40
20
0
Brain
Salivary Gland
Stomach
Small Intestine
Pancreas
Large intestine
Heart
Lung
Thymus
Spleen
Kidney
Liver
Seminal vesicle
Testes
Skeletal muscle
Skin

Figure 5.8 *Rnase1* gene expression profiles for wild-type and *Rnase1*$^{-/-}$ mice

A. Wild-type *Rnase1* and *Rnh1* expression in various mouse tissues (n = 3). Data are normalized to expression levels in the pancreas for each gene. *B.* Expression of *Rnase1* across various tissues in *Rnase1*$^{-/-}$ mice (n = 3). Data are normalized to wild-type expression levels of *Rnase1* in each tissue.

Figure 5.9

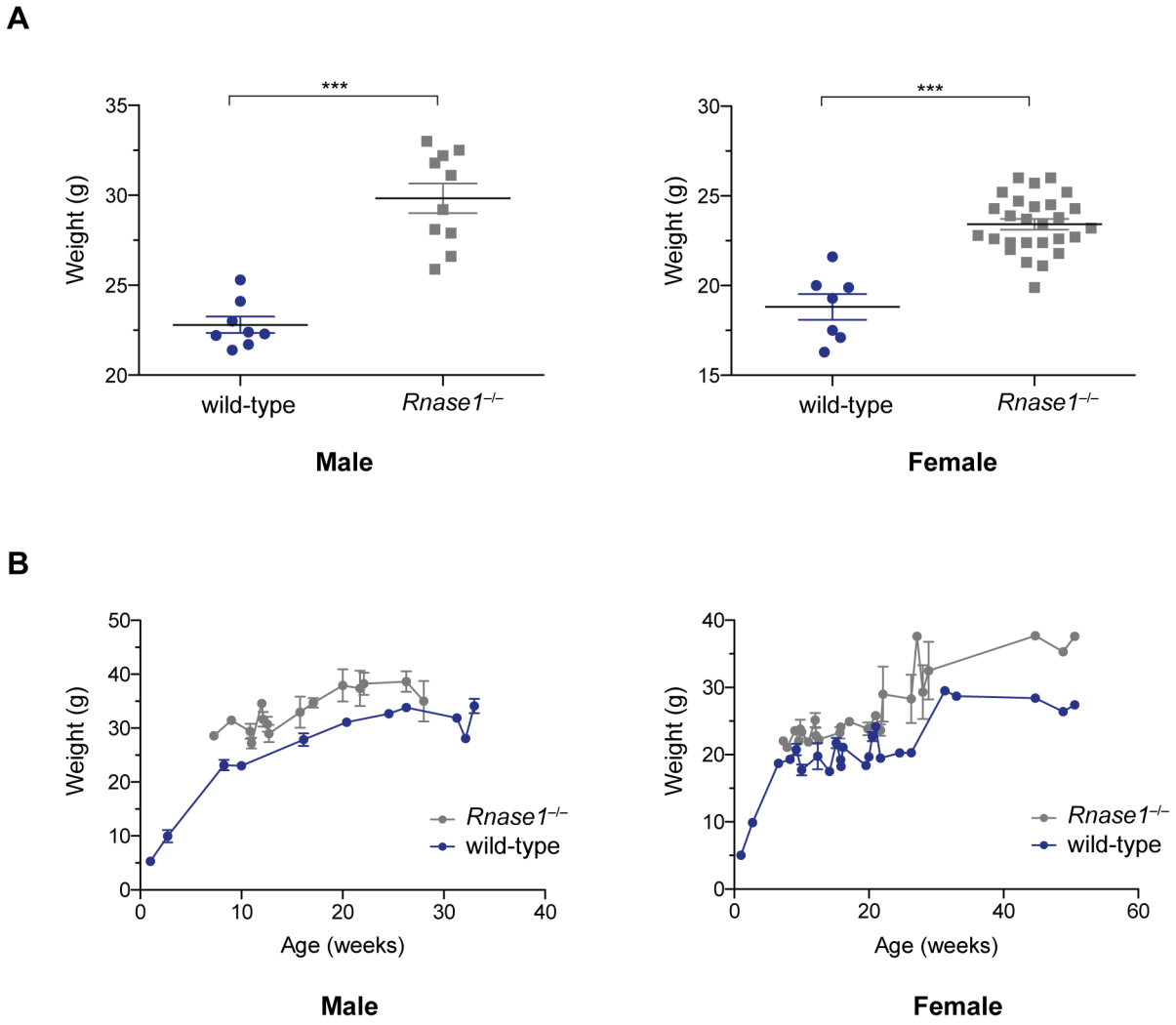
A
***
Weight (g)
35
30
25
20
wild-type
Rnase1−/−
Male
***
Weight (g)
30
25
20
15
wild-type
Rnase1−/−
Female
B
Weight (g)
50
40
30
20
10
0
0
10
20
30
40
Age (weeks)
Rnase1−/−
wild-type
Male
Weight (g)
40
30
20
10
0
0
20
40
60
Age (weeks)
Rnase1−/−
wild-type
Female

Figure 5.9 Increased body weights in *Rnase1*$^{-/-}$ mice

Differences in body weight between wild-type and *Rnase1*$^{-/-}$ mice. *A.* Body weight at 8 weeks of age for both male (*left*) and female (*right*) *Rnase1*$^{-/-}$ mice as compared to litter-matched, wild-type controls. *B.* Body weight at varying age for both *Rnase1*$^{-/-}$ and matched controls ($n \geq 3$ for each group). ***$p < 0.001$

Figure 5.10

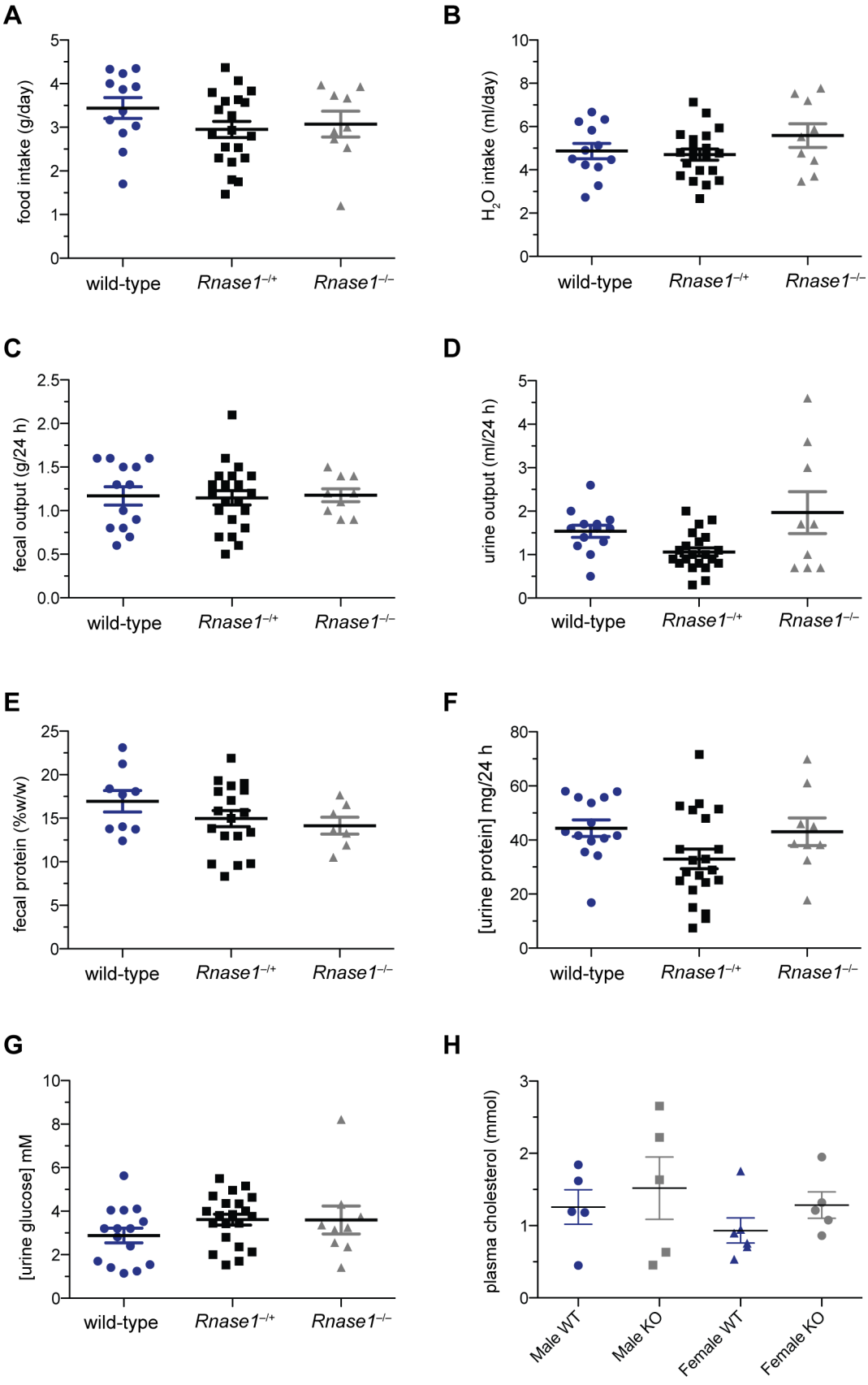
A
food intake (g/day)
0
1
2
3
4
5
wild-type
Rnase1−/+
Rnase1−/−
B
H2O intake (ml/day)
0
2
4
6
8
10
wild-type
Rnase1−/+
Rnase1−/−
C
fecal output (g/24 h)
0.0
0.5
1.0
1.5
2.0
2.5
wild-type
Rnase1−/+
Rnase1−/−
D
urine output (ml/24 h)
0
1
2
3
4
5
wild-type
Rnase1−/+
Rnase1−/−
E
fecal protein (%w/w)
0
5
10
15
20
25
wild-type
Rnase1−/+
Rnase1−/−
F
[urine protein] mg/24 h
0
20
40
60
80
wild-type
Rnase1−/+
Rnase1−/−
G
[urine glucose] mM
0
2
4
6
8
10
wild-type
Rnase1−/+
Rnase1−/−
H
plasma cholesterol (mmol)
0
1
2
3
Male WT
Male KO
Female WT
Female KO

Figure 5.10 Metabolic studies in *Rnase1*$^{-/-}$ mice

Aggregate data from metabolism cage studies measuring the following parameters: *A.* Food intake *B.* Water intake. *C.* Fecal output. *D.* Urine output. *E.* Fecal protein content *F.* Urine protein content *G.* Urine glucose content *H.* Plasma cholesterol content.

Figure 5.11

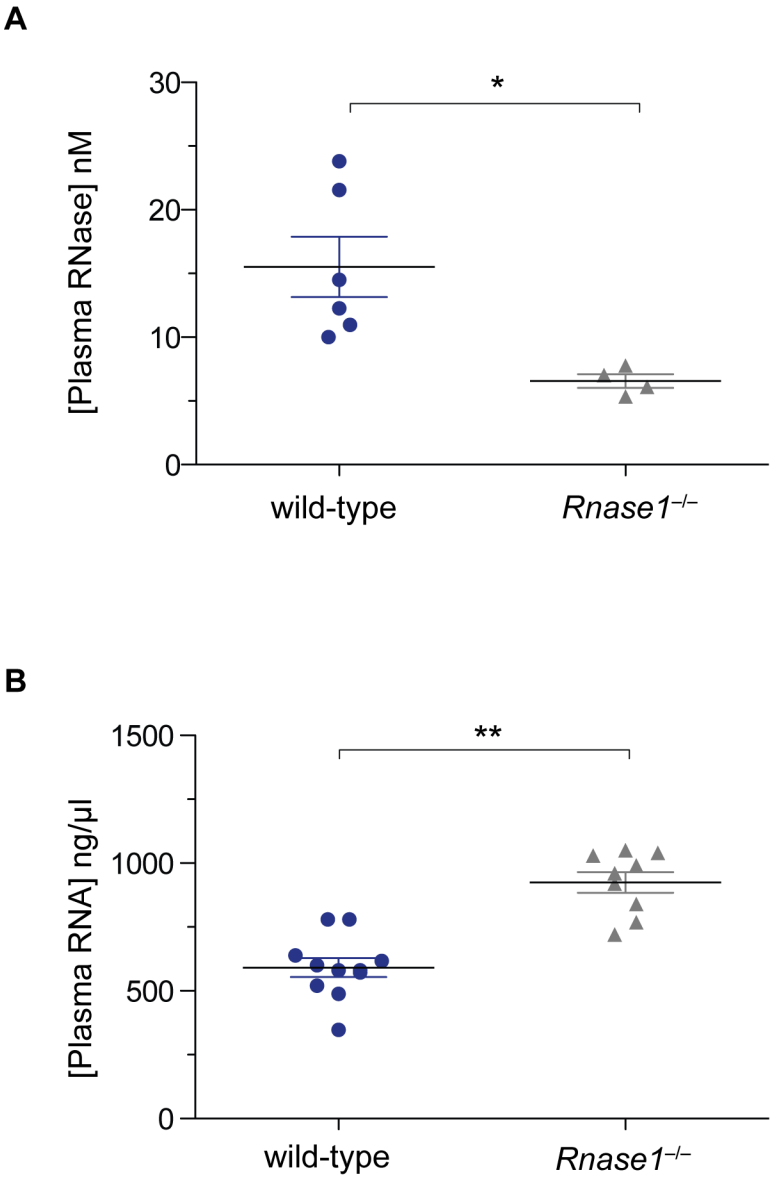
A
[Plasma RNase] nM
30
20
10
0
*
wild-type
Rnase1−/−
B
[Plasma RNA] ng/µl
1500
1000
500
0
**
wild-type
Rnase1−/−

Figure 5.11 Analysis of plasma RNase and RNA levels in wild-type and *Rnase1*$^{-/-}$ mice

A. Estimated concentration of plasma ribonuclease (based on activity) for both *Rnase1*$^{-/-}$ mice and matched wild-type controls. *B.* Concentration of RNA in DNase-treated plasma samples from both *Rnase1*$^{-/-}$ mice and matched wild-type controls. *$p < 0.05$; **$p < 0.01$

Table 5.2 Preliminary data describing coagulation parameters for *RNase1*$^{-/-}$ mice

	Prothrombin Time (s)		Fibrinogen Production (mg/mL)	
	wild-type	*Rnase1*$^{-/-}$	wild-type	*Rnase1*$^{-/-}$
Male	>70.0	28.8	<0.36	2.37
Female	>70.0	20.7	0.95	1.45

Figure 5.12

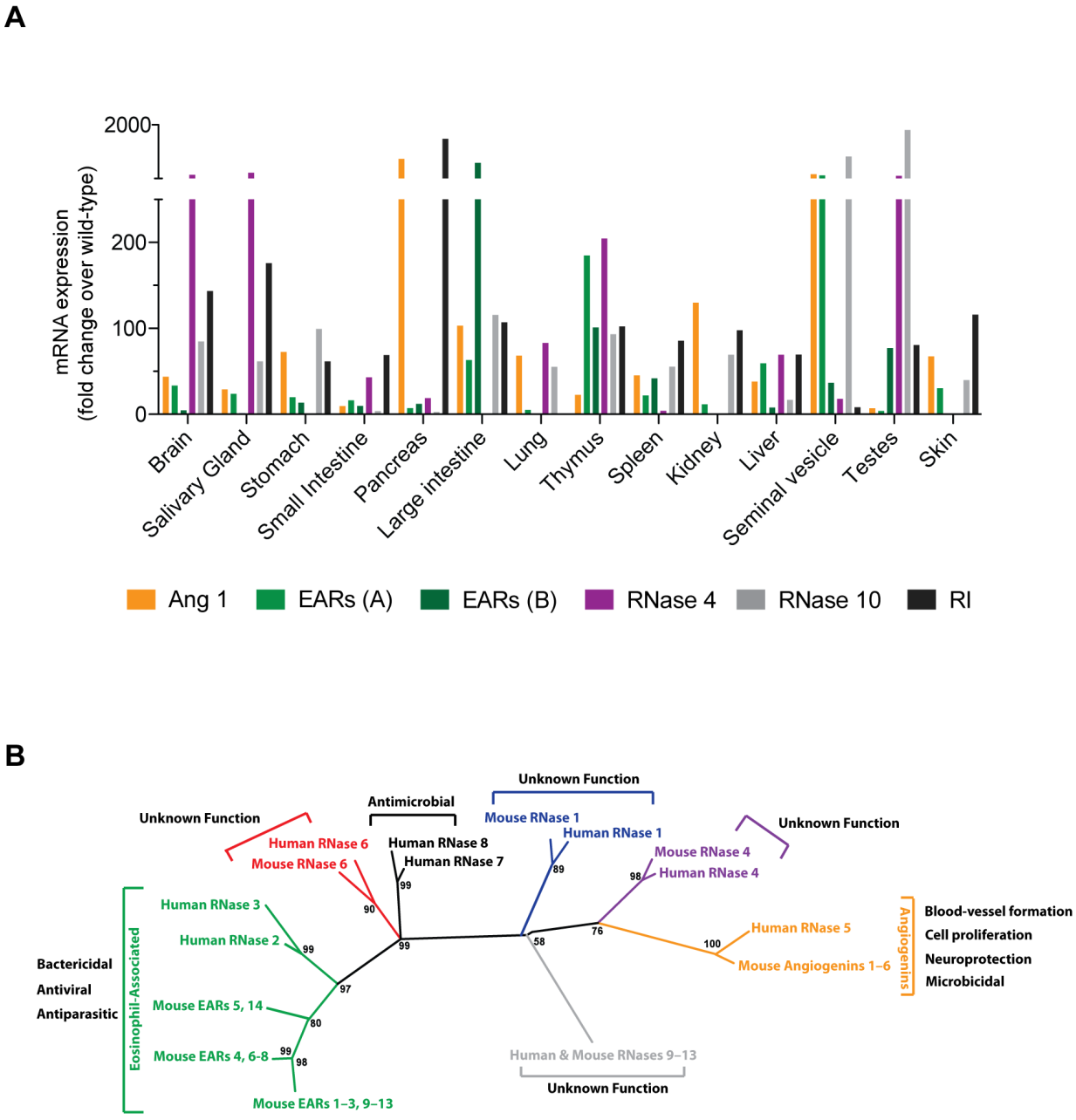
A
2000
200
100
0
mRNA expression
(fold change over wild-type)
Brain
Salivary Gland
Stomach
Small Intestine
Pancreas
Large intestine
Lung
Thymus
Spleen
Kidney
Liver
Seminal vesicle
Testes
Skin
Ang 1
EARs (A)
EARs (B)
RNase 4
RNase 10
RI
B
Unknown Function
Antimicrobial
Unknown Function
Unknown Function
Human RNase 6
Mouse RNase 6
Human RNase 8
Human RNase 7
Mouse RNase 1
Human RNase 1
Mouse RNase 4
Human RNase 4
Human RNase 3
Human RNase 2
Human RNase 5
Mouse Angiogenins 1–6
Mouse EARs 5, 14
Mouse EARs 4, 6-8
Mouse EARs 1–3, 9–13
Human & Mouse RNases 9–13
Unknown Function
Bactericidal
Antiviral
Antiparasitic
Eosinophil-Associated
Angiogenins
Blood-vessel formation
Cell proliferation
Neuroprotection
Microbicidal

Figure 5.12 Upregulation of various genes in KO mice as compared to WT mice

A. qPCR data showing the fold-change for various related murine secreted RNases and ribonuclease inhibitor for *Rnase1*$^{-/-}$ mice. Data are normalized to wild-type expression levels for each gene in each tissue. *B.* Phylogenetic tree showing the evolutionary relationship among paralogous ribonucleases in mice and humans

CHAPTER 6

Conclusions and Future Directions

6.1 Conclusions

Pancreatic-type ribonucleases, and RNase 1 in particular, have been extremely well characterized structurally. However, many mysteries remain regarding the biological functions of this enzyme family. Increased serum RNase 1 activity has been associated with multiple diseases states, and RNase 1 has demonstrated therapeutic potential against cancer, as well as other conditions. Therefore, it is imperative to understand the underlying mechanisms of action of this enzyme so that we might better design therapeutic strategies to both target and exploit its functionalities.

The central aim of this thesis was to demonstrate the dynamic biological potential of RNase 1 by illustrating its remarkable properties *in vitro* and *in vivo*. In CHAPTER 3, I determined that human RNase 1 and bovine RNase A are not functional homologs; importantly, these data imply a non-digestive physiology for human RNase 1. The ability of human RNase 1 to degrade a variety of double-stranded RNA substrates, as well as its strong affinity for cell-surface glycans, might have significant implications for its biology. RNase 1 may be evolutionarily designed to associate with cell membranes and enter endosomes, where it can degrade antigenic RNA substrates and attenuate inflammatory signaling.

RNase 1 might also be co-evolving with its endogenous inhibitor, RI. In CHAPTER 4, I characterize the first-ever non-mammalian RI homologs, along with their cognate ribonucleases. My data show that the interface regions in intraspecies RI•RNase complexes are evolving for greater molecular recognition. Also, mammalian RIs are evolving greater sensitivity to oxidation. This apparent “redox switch” may serve to regulate the release of latent RNases in the cytosol, thus constituting a novel mechanism for apoptosis. The ability to endogenously evade RI might imbue RNase 1 with novel biological function *in cellulo*.

Finally, in CHAPTER 5, I have created a vital resource to understand the endogenous role of RNase 1 by developing the first-ever *Rnase1*$^{-/-}$ mouse. Characterization of this null mouse model indicates a role for RNase 1 in coagulation and metabolic disregulation. These symptoms might be associated with increased extracellular RNA in the plasma of *Rnase1*$^{-/-}$ mice. Taken together, this thesis provides an intriguing view into the structure, function, and evolution of both RNase 1 and ribonuclease inhibitor, and paves the way for further discoveries and insights into this remarkable protein duo.

6.2 Future Directions

6.2.1 Visualizing the RI•RNase interaction in cellulo

Despite the incredible binding affinity measured between ptRNases and ribonuclease inhibitor *in vitro*, the interaction of these proteins has never been directly observed *in cellulo.* Since the role(s) of RI in several ribonuclease-mediated processes, such as angiogenesis, have not been fully elucidated, a sensitive method for detecting ribonuclease-RI complexes in live cells could shed light on the dynamic biological roles of RI and mammalian ribonucleases.

I sought to utilize the technology of bimolecular fluorescence complementation (biFC), which involves the reconstitution of fluorescence upon association of fragments of a fluorescent protein.[379] My theory was that by fusing two complementary fragments of a fluorescent protein to either RNase or RI, the fluorophore could be reconstituted upon RI•RNase complex formation. I initially attempted to use a split version of enhanced yellow fluorescent protein (YFP);[380] however, I found the fluorescence to be quite low *in cellulo*. Further, I encountered many problems trying to recombinantly produce a RNase–YFP fusion protein, as the over all size of the complementary YFP fragments are quite large in comparison to ribonuclease..

The new strategy that I would recommend to anyone interested in using biFC is to use a split

version of green fluorescent protein (GFP) that requires only a single beta-strand for complementation (*i.e.*, GFP11).[381] In this way, a much smaller segment can be fused to RNase, facilitating its recombinant production (Figure 6.1). To further enhance RNase 1 translocation and uptake, I recommend use of an arginine–grafted version of RNase 1.[246] One could also utilize a linker peptide infused with arginine residues to facilitate RNase translocation and subsequently enhance RI binding. A similar linker allowed genetically-dimerized RNase 1 variants better access to the mammalian cytosol.[252] Usefully, GFP has higher quantum yield that YFP and can be visualized more readily.

A second method to visualize RI•RNase interactions *in cellulo* is to exploit the small molecule FlAsHEDT$_2$, a latent fluorophore that is caged by arsenic.[382-384] Upon binding to the tetracysteine motif CCXXCC, the arsenical hairpins become dislodged and fluorescence is restored. I envision a system whereby the FlAsH–EDT$_2$ compound could be designed with a malemide handle for site-specific conjugation to RNases, which could then be added exogenously to cultured cells. The RI molecule could be modified with a C-terminal extension that contains a tetracysteine binding motif and could be overexpressed in cultured cells (Figure 6.2). Fluorescence would occur upon RI•RNase complex formation and could be visualized with confocal microscopy and/or quantified with flow cytometry. A cell line known for enhanced endocytosis, such as CHO-K1 cells, would facilitate RNase translocation. Similarly, the use of an Arg-grafted RNase could also enhance RNase translocation, thereby enriching for RI•RNase complex formation *in vivo*.

Figure 6.1

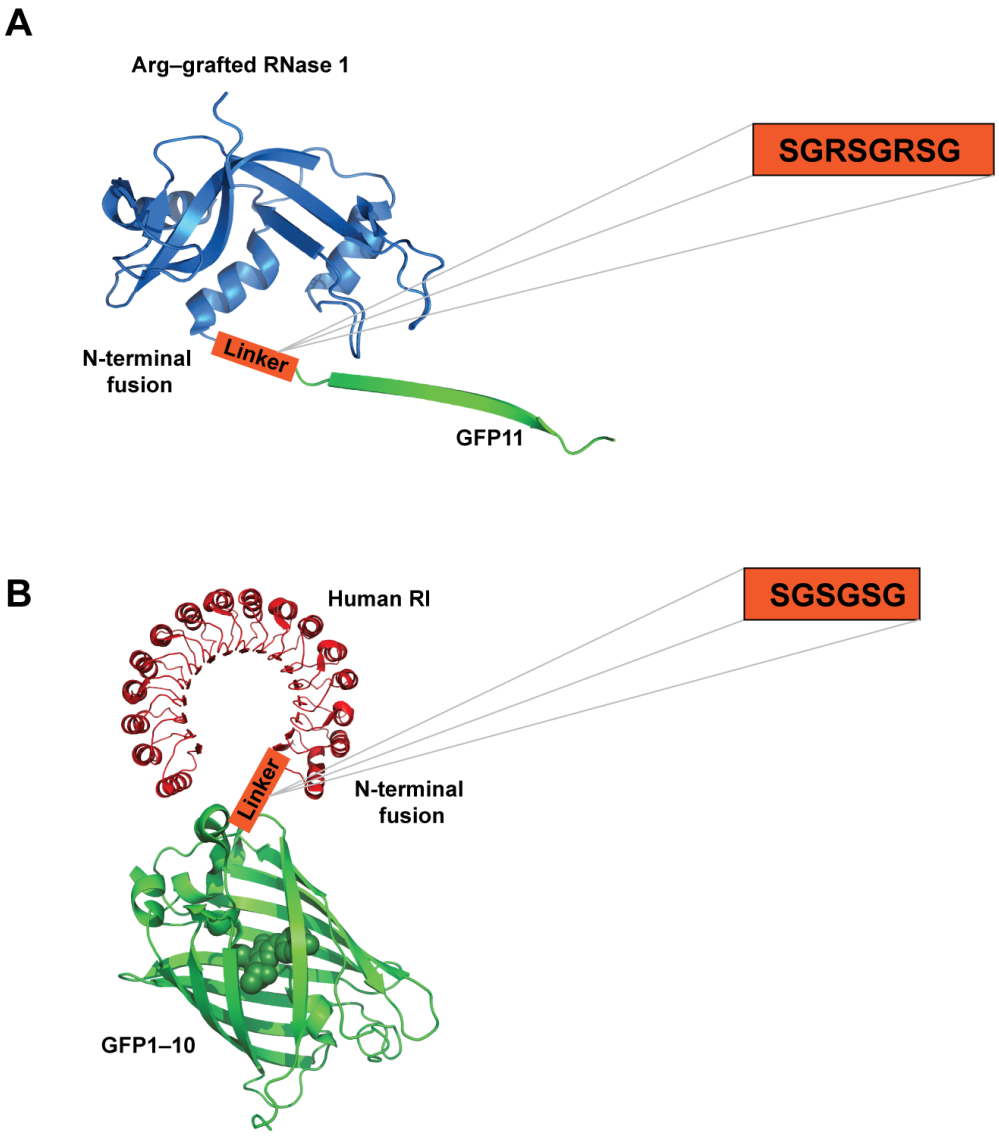
A
Arg–grafted RNase 1
SGRSGRSG
N-terminal fusion
Linker
GFP11
B
Human RI
SGSGSG
Linker
N-terminal fusion
GFP1–10

Figure 6.1 Strategy to visualize RI•RNase interaction in live cells using biFC

The endogenous protein–protein interaction between ribonucleases and RI might be possible through the use of bimolecular fluorescence complementation (biFC). *A*. Possible scheme for RNase 1 engineering, utilizing an Arg-grafted RNase 1 variant with an N-linked segment of GFP (GFP11). The linker also contains Arg residues to promote greater translocation. *B*. Possible scheme for human RI engineering, linking GFP(1–10) to the N-terminus of RI via a flexible linker.

Figure 6.2

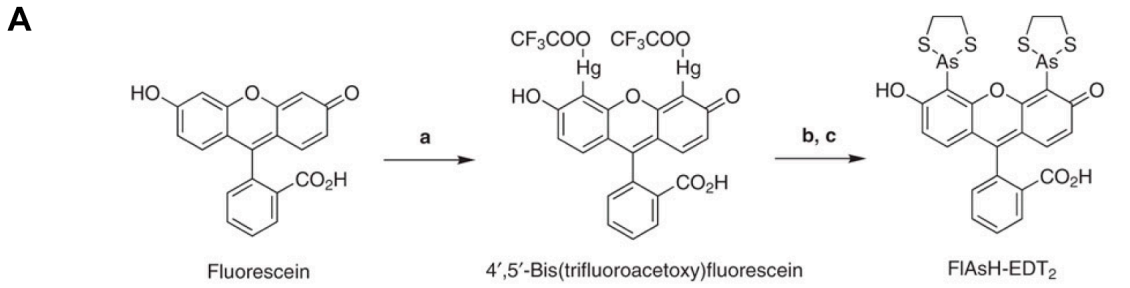

(a) HgO, TFA; (b) $AsCl_3$, $Pd(OAc)_2$, DIEA, NMP; (c) EDT, aqueous acetone

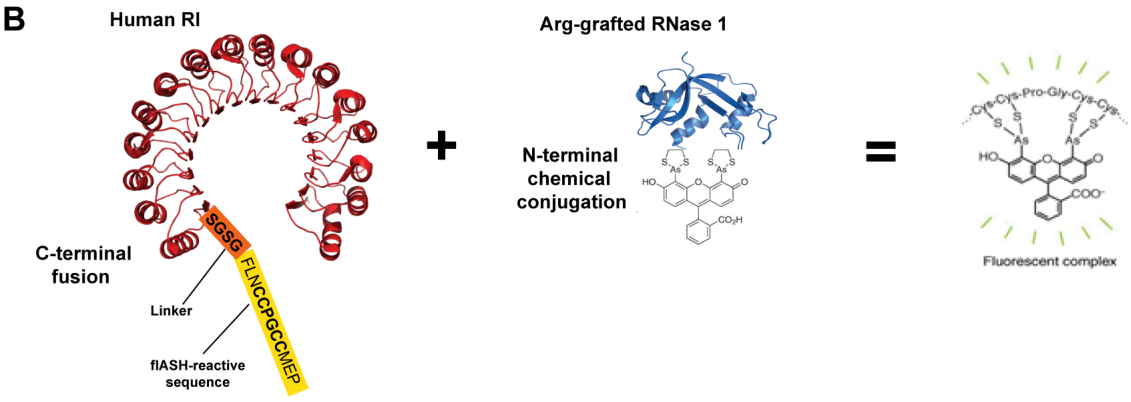

Figure 6.2 Strategy to visualize RI•RNase interaction in live cells using FlAsH–EDT_2

The endogenous protein–protein interaction between ribonucleases and RI might be possible through the use of bimolecular fluorescence complementation (biFC). *A*. Chemical synthesis of the caged fluorophore FlAsH–EDT_2. *B*. Possible scheme for human RI and RNase engineering. RNases could be site-specifically labeled with a modified version of FlAsH–EDT_2. RI could be modified to include a tetracysteine motif that has been optimized for visualization in mammalian cells.

6.2.2 Characterizing Ribonucleases 9–13

Ribonucleases 9–13 represent a non-canonical group of pancreatic-type ribonucleases that were recently discovered.[34] Little is known regarding their form or function. These RNases are missing some key structural and catalytic residues from the canonical ptRNases. Recent studies of RNases 9 and 10 indicate a role for these proteins in sperm maturation.[65,66] However, no published reports exist regarding RNases 11–13. Many questions surround these proteins. Specifically, do these RNases have catalytic activity? Where are they expressed and localized? Do they bind to ribonuclease inhibitor?

I attempted to answer these questions by assessing the expression of RNases 9–13 across multiple human tissues via reverse-transcription (RT) PCR. My results indicate that RNases 11–13 have low to moderate expression in multiple tissues, suggesting an important biological role (Figure 6.3). I cloned the genes encoding human RNases 9–13 into protein expression vectors and attempted to produce the proteins recombinantly in *E. coli*. However, the proteins did not express well in bacterial hosts. I also attempted to express the enzymes in genetically engineered bacteria with oxidizing cytosol (Origami® *E. coli*). However, these cells also failed to yield robust expression. Possibly, by empirically modifying existing purification techniques, or devising new expression conditions, folded RNase 9–13 proteins could be attained, purified to homogeneity, and biochemically characterized. Determining a structure for any of these non-canonical proteins would be especially interesting.

Figure 6.3

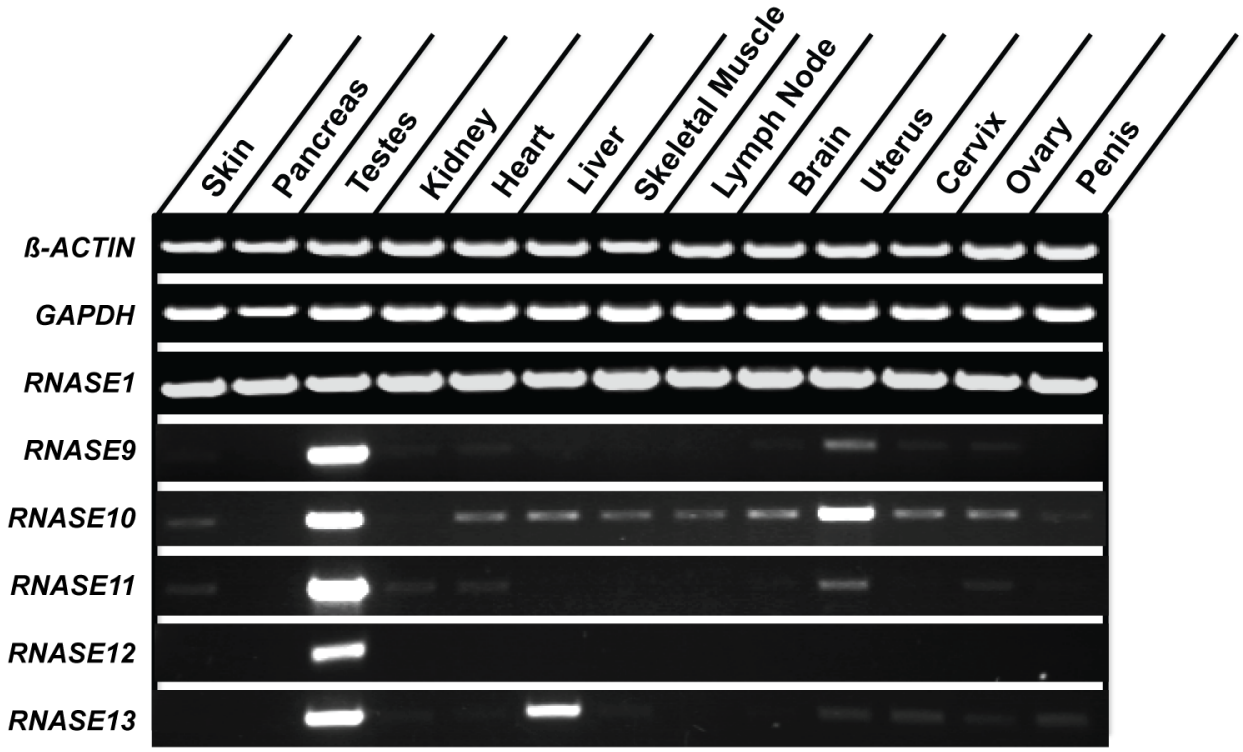
Skin
Pancreas
Testes
Kidney
Heart
Liver
Skeletal Muscle
Lymph Node
Brain
Uterus
Cervix
Ovary
Penis
ß-ACTIN
GAPDH
RNASE1
RNASE9
RNASE10
RNASE11
RNASE12
RNASE13

Figure 6.3 Expression patterns of human ribonucleases 9–13

The endogenous mRNA expression of the non-canonical human ptRNases 9–13 was analyzed with reverse-transcription PCR. Various human tissues total RNA samples were purchased and reverse-transcribed into cDNA. PCR primers specific to each gene of interest were used to determine amplification after 40 cycles. Human beta-actin and gapdh were used as housekeeping genes, and human RNase 1 was included as an additional control.

6.2.3 Engineering RNase 1 variants as anticoagulant drugs

Increased blood clotting in the veins and arteries leads to many fatal conditions, including deep vein thrombosis, pulmonary embolism, heart attack and stroke.[385-387] Current anticoagulant drugs are plagued by multiple problems, including nonspecific interactions that can lead to both drug inactivation and adverse side effects.[388] Better understanding of coagulation mechanisms is crucial for developing safer and more effective antithrombotic drugs.[96,388] There is significant interest in developing novel anticoagulant drugs to assist in treating various conditions; specifically, a drug is needed that can reduce clotting without leading to bleeding disorders. One such therapeutic may be pancreatic ribonuclease (RNase1). RNase 1 has a strong precedent as an effective protein scaffold for therapeutic modulation. RNase 1 is small, extremely stable, easily produced, and well tolerated in safety profiles.[127] Currently, RNase 1 is successfully progressing through a Phase I trial for patients with solid tumors. However, RNase 1 has the potential to be modified for other therapeutic purposes. Specifically, RNase 1 might be a successful anticoagulant.

RNase 1 demonstrates the ability to reduce clot and stroke formation *in vivo*, as well as prevent the formation of atherosclerotic plaques.[109,114,217] Potentially, if RNase 1 could be modified to both preferentially target clots or plaques, as well as remain in circulation longer, it might be better exploited toward anticoagulation therapy. To increase plasma retention, polyethylene glycol (PEG) moieties could be covalently attached to the protein. Such a modification has been shown to be effective in previous studies in enhancing plasma circulation times.[223] To better target clots and plaques, we could utilize novel clot-targeting peptides that have been identified from large-scale peptide arrays.[389-392] Many of these peptides are relatively small and could be genetically integrated into the sequence of RNase 1. Alternatively, the

peptides could be synthesized and covalently attached through site-specific linkage to an RNase 1 molecule. Potentially, *RNase1*$^{-/-}$ mice (which demonstrate a hypercoagulation phenotype) could be used as a model system in which to test putative therapeutic RNase 1 anticoagulants. Indeed, modified versions of RNase 1 could be compared with wild-type RNase 1 to see which versions can better rescue a pro-coagulation phenotype.

APPENDIX I

Rational Design of a Cysteine–Free Human Ribonuclease Inhibitor

Contribution: I performed evolutionary analyses, all molecular biology and protein purification, and all biochemical characterization of variant proteins. RosettaDesign calculations were performed by Caglar Tanrikulu in conjunction with Professor Julie Mitchell.

A1.1 Abstract

Human ribonuclease inhibitor (hRI) is a cytosolic protein that protects cells from the adventitious invasion of pancreatic-type ribonucleases (ptRNases). Human RI possesses many cysteine residues (32 in total), and oxidation of these residues results in the formation of disulfide bonds that inactivate RI in a rapid, cooperative process. Creation of an RI protein that is not sensitive to the damaging effects of oxidation, yet still maintains avidity for ptRNases, could be an extremely valuable research resource. I have attempted to create such an RI molecule through the rational replacement of the 32 cysteine residues present in the human RI protein. Through various computational means, I devised specific amino acid substitutions specially chosen for each position. This cysteine-free RI (CF–RI) expressed readily in *E. coli* cells, demonstrated low nanomolar binding affinity to RNase 1, and had reduced oxygen sensitivity as compared to wild-type (WT) RI. However, the CF–RI protein proved to be inherently unstable, thus hindering its purification; therefore, I have designed a series of chimeric CF/WT RI protein vectors that systematically replace certain segments of the CF–RI molecule. Through characterization of these chimeric proteins, the contribution of various cysteine positions to structure and stability can be determined, and better, more stable, versions of CF–RI can be developed.

A1.2 Introduction

Ribonuclease inhibitor (RI) protein is present in the cytosol of all mammalian cells and serves to regulate the activity of pancreatic-type ribonucleases (ptRNases). Recombinant RI is a valuable commodity for research labs studying RNA, as ptRNases present on human skin can introduce detrimental contamination into RNA reactions. However, RI is inherently unstable due to its large number of cysteine residues, each of which must stay reduced to maintain proper form and function of the protein.[27] This sensitivity to oxidation results in high production costs and short shelf life for recombinant human RI, leading to large expense for consumers. An RI protein that is resistant to oxidative damage, yet maintains tight binding affinity for ptRNases, would be highly useful to the greater biological community.

Beyond a laboratory tool, a cysteine-free RI molecule has the potential to elucidate novel biological mechanisms. Human RI contains 32 cysteine residues and is more sensitive to oxidation that other mammalian and non-mammalian ribonuclease inhibitors (see CHAPTER 4). There is speculation that these cysteine residues might play an important role in cellular physiology by modulating redox homeostasis in the cytosol. Indeed, multiple reports indicate that RI might scavenge reactive oxygen species, thus ameliorating cellular oxidative stress.[153-155] Potentially, intracellular analysis of a cysteine-free ribonuclease inhibitor might help illuminate the biological role of RI in redox physiology.

There have been several previous attempts to create variants of ribonuclease inhibitor that are less sensitive to oxidative unfolding. Replacing Cys328 and Cys329 with alanine residues had little effect on the affinity of RI for bovine RNase A, but increased its resistance to oxidation by 10- to 15-fold. Similar effects are observed for the single variants, C328A hRI and C329A hRI, suggesting that oxidative resistance arises from the inability to form a Cys328–Cys329 disulfide

bond.[314] Interestingly, C328 and C329 are buried cysteine residues with little relative solvent accessibility, yet can still confer protection against oxidation.

More recently, attempts to replace all cysteine residues in RI molecules have met with less success. An attempt to replace all cysteines with alanines in porcine RI resulted in a transcript that could not be expressed in *E. coli*.[393] Similarly, an attempt to use a semi-rational approach for residue replacement also yielded a gene that could not be expressed in bacterial hosts (G.A. Ellis, unpublished results).[394]

I have employed a hybrid rational design approach, whereby I utilize both computational modeling and evolutionary precedents to determine the best residues to substitute for each cysteine residue at a particular site. Through these methods, I have produced an RI variant devoid of cysteine residues that can be expressed in *E. coli.*

A1.3 Methods and Results

A1.3.1 Evolutionary prediction of cysteine residue substitutions

Ribonuclease inhibitor protein is found in all mammalian species. It has also been recently identified in many non-mammalian vertebrate species. I speculated that there might be evolutionarily-determined cysteine substitutions that would still maintain proper protein form and function. Accordingly, I collected the protein sequences from ~60 mammalian and non-mammalian RI homologs and aligned the sequences using the CLUSTAL algorithm (data not shown). From this alignment, I was able to determine substitutions for multiple human cysteine positions (Figure A1.1). However, in certain key positions—Cys37, Cys84, Cys94, Cys101, Cys141, Cys208, Cys272, Cys322, and Cys329—cysteines were uniformly maintained throughout evolution, suggesting that these cysteines may constitute an important structural or functional element at specific positions.

A1.3.2 Computational prediction of cysteine residue substitutions

In order to computationally predict the best residues to substitute for each cysteine position, I utilized two different computational algorithms. First, I used the Sorting Intolerant from Tolerant (SIFT) algorithm online server, which predicts whether an amino acid substitution will affect protein function. SIFT prediction is based on the degree of conservation of amino acid residues in sequence alignments derived from closely related sequences. To assess the effect of a substitution, SIFT assumes that important positions in a protein sequence have been conserved throughout evolution and therefore substitutions at these positions may affect protein function. Thus, by using sequence homology, SIFT predicts the effects of all possible substitutions at each position in the protein sequence.[395-398] Best-fit substitutions for each cysteine position were predicted by SIFT analysis (Figure A1.1).

Through collaboration with the lab of Professor Julie Mitchell, we utilized the RosettaDesign web server to perform fixed backbone protein design simulations. The RosettaDesign server identifies low energy amino acid sequences for target protein structures.[399,400] Given a target protein structure or complex, RosettaDesign searches for amino acid sequences that pack well, bury their hydrophobic atoms, and satisfy the hydrogen bonding potential of polar atoms. It has been optimized to return sequences within amino acid frequencies comparable to those found in naturally occurring proteins. To favor low energy designs, amino acid side chains are only allowed to adopt a discrete set of favorable conformations using a rotamer library. We ran three different RosettaDesign simulations to model best-fit cysteine substitutions using different constraints for each round (Figure A1.1). The first round used all possible residues, the second round constrained the possible substitutions to those residues most commonly used for substitution (ASTLV), and the third round constrained the possible substitutions to those

residues most commonly substituted across RI evolution at each cysteine position (obtained from above evolutionary analysis of protein sequence alignments).

Upon completion of both evolutionary and computational analyses, I made a best guess for each site, taking into account all of the possible predicted substitutions. The result was a rationally designed human RI molecule with zero cysteine residues (Figure A1.2).

A1.3.3 Molecular cloning, expression, and protein production of cysteine–free RI

In order to systematically study the various cysteine residues in human RI, I envisioned a modular system in which sections of variant CF–RI could be swapped with wild-type RI to create chimeric molecules. I designed versions of CF–RI and wild-type RI genes that contained seven silent mutations encoding restriction enzyme digestion sites (Figure A1.3). Each segment between restriction sites contained approximately 4–5 cysteine residues. The engineered genes for CF–RI (including all substitutions and silent restriction sites) and wild-type RI (including silent restriction sites) were ordered from Integrated DNA Technologies (IDT). Upon arrival, I inserted the genes into a pET22b protein expression vector (Novagen).

CF–RI was grown in BL21(DE3) *E. coli* (Novagen) at 37 °C to an optical density of 1.0, induced with 1 mM IPTG, and incubated at 16 °C overnight in a shaking incubator. Analysis of crude cell lysate showed a pronounced band at 50 kD for CF–RI expression, whereas previous versions of a cysteine-free RI protein failed to express (Figure A1.4). However, subsequent analysis of soluble and insoluble fractions indicated that most CF–RI expression was insoluble (data not shown). Attempts to purify CF–RI using an RNase A–affinity column were unsuccessful; therefore, I installed a TEV-cleavable 6X histidine tag on the N-terminus of CF–RI and proceeded to purify CF–RI over a nickel column and eluted it over a linear gradient of imidazole. I further purified CF–RI over an anion–exchange column. Rough estimates based on

SDS–PAGE gel indicated the protein was ~70% pure and had an overall yield of ~0.2 mg/L. It should be noted that subsequent attempts to produce pure recombinant CF–RI protein were not successful.

A1.3.4 Determination of CF–RI binding affinity to human RNase 1

In order to determine if CF–RI bound to various ptRNases, I first utilized a native gel–shift assay. Equimolar amounts of CF–RI and various mammalian and non-mammalian ribonucleases were incubated together at room temperature for 20 min. Non-denaturing sample dye was added, and protein solutions were run on a 12% non-denaturing polyacrylamide gel. Proteins were visualized using coommassie brilliant blue dye. As indicated by a pronounced p*I*-induced gel shift, CF–RI did bind to human, mouse, and bovine RNase 1, but not to frog onconase (Figure A1.5A).

In order to more quantitatively measure binding affinity, an RI-saturation binding assay was used, as described previously.[255] Briefly, fluorescence spectroscopy was used to monitor the binding of CF–RI to a DEFIA-labeled ribonuclease, availing the decrease in fluorescence upon binding to RI. Data were normalized to unbound DEFIA-RNase and fitted with nonlinear regression analysis to obtain a value of K_d for each complex. These values are the mean from at least three independent experiments. From these data, I determined that CF–RI bound to human RNase 1 with K_d ~10 nM (Figure A1.5B).

A1.3.5 Determination of CF–RI oxidative stability

The stability of the CF–RI·RNase 1 complex to oxidation by hydrogen peroxide (H_2O_2) was assessed by following the release of diethylfluorescein-labeled ribonuclease upon CF–RI dissociation, as described.[143] Briefly, fresh H_2O_2 (30% v/v, Fisher Scientific) was diluted serially in reaction buffer (20 mM HEPES–HCl buffer, pH 7.0, containing 50 mM KCl) to produce a

final range of 30–0.001% v/v H_2O_2. Desalted CF–RI (100 nM) and ribonuclease (100 nM) were combined in 50 μL of reaction buffer across a 96-well plate and incubated for 20 min at 25 °C to allow for complex formation. Initial fluorescent readings were taken, and 50 μL of H_2O_2 serial dilutions were added to each well containing the RI·RNase complex. Plates were incubated at 37 °C for 1 h, and final fluorescent readings were taken. Data were normalized to control wells containing only labeled RNase at each H_2O_2 concentration and fitted using nonlinear regression to generate H_2O_2 IC_{50} values for complex dissociation. Values represent the mean from at least three independent experiments. From these data I determined that CF–RI was approximately 10-fold less sensitive to oxidative unfolding.

A1.3.6 Generation and expression of CF/WT chimeric proteins

In order to systematically assess the contribution of various cysteines toward protein stability and oxidation sensitivity, I designed a modular system to generate chimeric proteins. By digesting CF and WT RI genes with various restriction endonucleases (Figure A1.3A), I was able to swap out vsections of CF–RI with WT-RI and produce seven different chimeric proteins (Figure A1.7A). These proteins all expressed robustly in *E. coli*. However, purifying these proteins proved extremely challenging; I was unable to purify any chimeric proteins to homogeneity, thus precluding their biochemical characterization.

A1.5 Discussion

I have rationally designed a variant form of human ribonuclease inhibitor that does not contain any cysteine residues, yet can still bind to its cognate ribonuclease (albeit with greatly reduced affinity). Of the many attempts to create such a version of RI, mine is the first variant that can be expressed and purified recombinantly from *E. coli*. This accomplishment is

noteworthy because it sets a precedent that a protein engineer can potentially change a very large number of residues while still maintaining form and function of the target protein. Further efforts are needed to create more stable cysteine-free RI variants with tighter affinity for ptRNases.

My struggles to purify CF–RI and CF/WT chimeras have demonstrated the pronounced instability and insolubility of these proteins in bacterial hosts. The inherent instability of the CF–RI protein might imply that certain cysteine residues are necessary for proper folding of the leucine-rich repeat structure of RI. Indeed, multiple buried cysteine residues are conserved in all RI homologs across both mammalian and non-mammalian species. Potentially, further efforts to optimize CF–RI could systematically restore some of these key residues. Previously (see CHAPTER 4), I have determined that four cysteine residues in human RI are particularly solvent exposed: Cys12, Cys96, Cys220, and Cys409. Potentially, modulating these residues would have the greatest impact of reducing RI sensitivity to oxidation. Alternatively, the modular nature of the CF/WT chimeric system could be utilized differently, whereby sections of CF–RI are swapped into the WT–RI structure. In this way, smaller perturbations to cysteine residues could be achieved, allowing for biochemical analysis of hybrid proteins without disruptive instability.

Taken together, my efforts to achieve a cysteine-free human ribonuclease inhibitor have demonstrated the feasibility of replacing a large number of protein residues in a single molecule. Through continued empirical determination of better cysteine replacement residues, and/or by systematically restoring key structural cysteines, we can achieve our greater goal of creating a functional RI that is oxidation resistant. A cysteine-free, oxidation insensitive RI molecule could have vast utility as a commercial anti-RNase agent, as well as aid in understanding the fundamental biological roles of the RI protein *in vivo*.

Figure A1.1

Position	%RSA	A	B	C	D	E	F
12	96	Y	A	G	S	S	S
30	0	Y	Y	A	A	A	Y
38	0.43	–	S	T	T	T	T
45	0	F	S	A	A	A	A
75	11	L	L	R	L	H	L
85	15	–	–	T	T	S	S
95	0	–	–	T	T	T	T
96	63	S	K	K	S	K	S
102	0	–	–	A	A	A	A
134	2.2	S	–	A	A	A	A
142	1.2	–	S	T	T	S	S
152	0	G	–	A	A	S	G
159	0	V	V	A	A	A	V
160	4.8	G	L	A	A	A	G
199	0	S	–	A	A	A	S
209	0	–	I	A	A	S	A
216	0	S	D	A	A	A	S
220	24	G	S	M	A	A	G
248	4.0	F	V	A	A	A	V
266	0	Y	S	A	A	S	S
273	0	–	–	A	A	A	A
277	9.0	S	A	A	A	A	S
305	0.20	S	A	A	A	A	A
313	2.0	S	A	D	A	A	S
323	0	–	–	T	T	T	T
329	0.15	S	A	S	S	S	S
330	0	–	–	A	A	A	A
362	5.4	S	–	A	A	A	S
380	0	S	–	D	S	S	S
387	0	–	–	A	A	A	A
409	100	G	S	A	A	A	G
427	0.42	S	–	D	A	A	S

Figure A1.1 Possible cysteine substitutions to create CF–RI

The finalized CF–RI sequence was an amalgamation of multiple computational and evolutionary mechanisms to predict the most appropriate substitutions for cysteine residues at each position. %RSA values refer to the relative solvent accessibility of each cysteine residue as calculated with Pymol. *A*. Evolutionarily conserved substitutions determined from multiple RI protein sequence alignments from many species. *B*. Predicted best-fit substitution from the computational program SIFT (sorting tolerant from intolerant).[395] *C*. Predicted substitutions from the RosettaDesign server, using all possible residues. *D*. Predicted substitutions from the RosettaDesign server, limiting substitutions to ASTLV. *E*. Predicted substitutions from the RosettaDesign server, limiting substitutions to residues naturally substituted at each position through evolution. *F*. Final set of substitutions for each cysteine position in CF–RI.

Figure A1.2


Human RI M S L D I Q S L D I Q C E E L S D A R W A E L L P L L Q Q C Q V V R L D D C G L T E A R C K D I S S A L R V N P A
cf-hRI - - - - - - - - - - - S - - - - - - - - - - - - - - - - - - - Y - - - - - - - T - - - - - - A - - - - - - - - - - -
Human RI L A E L N L R S N E L G D V G V H C V L Q G L Q T P S C K I Q K L S L Q N C C L T G A G C G V L S S T L R T L P T
cf-hRI - - - - - - - - - - - - - - - - - - - L - - - - - - - - - - S - - - - - - - - - - T S - - - - - A - - - - - - - - - - -
Human RI L Q E L H L S D N L L G D A G L Q L L C E G L L D P Q C R L E K L Q L E Y C S L S A A S C E P L A S V L R A K P D
cf-hRI - A - - - - - - - S - - - - - - - - - - G - - - - - - V - - - - - - - - - - -
Human RI F K E L T V S N N D I N E A G V R V L C Q G L K D S P C Q L E A L K L E S C G V T S D N C R D L C G I V A S K A S
cf-hRI - G - - - - - - - S - - - - - - - - - - A - - - - - - S - - - G - - - - - - - - -
Human RI L R E L A L G S N K L G D V G M A E L C P G L L H P S S R L R T L W I W E C G I T A K G C G D L C R V L R A K E S
cf-hRI - V - S - - - - - - A - - - S - - - - - - - - -
Human RI L K E L S L A G N E L G D E G A R L L C E T L L E P G C Q L E S L W V K S C S F T A A C C S H F S S V L A Q N R F
cf-hRI - A - - - - - - - S - - - - - - - - - - T - - - - - S A - - - - - - - - - - -
Human RI L L E L Q I S N N R L E D A G V R E L C Q G L G Q P G S V L R V L W L A D C D V S D S S C S S L A A T L L A N H S
cf-hRI - S - S - - - - - - A - - - - - - - - - - -
Human RI L R E L D L S N N C L G D A G I L Q L V E S V R Q P G C L L E Q L V L Y D I Y W S E E M E D R L Q A L E K D K P S
cf-hRI - - - - - - - - - G - S -
Human RI L R V I S
cf-hRI - - - - -

Figure A1.2 Finalized sequence of human cysteine-free (CF) RI

Figure A1.3

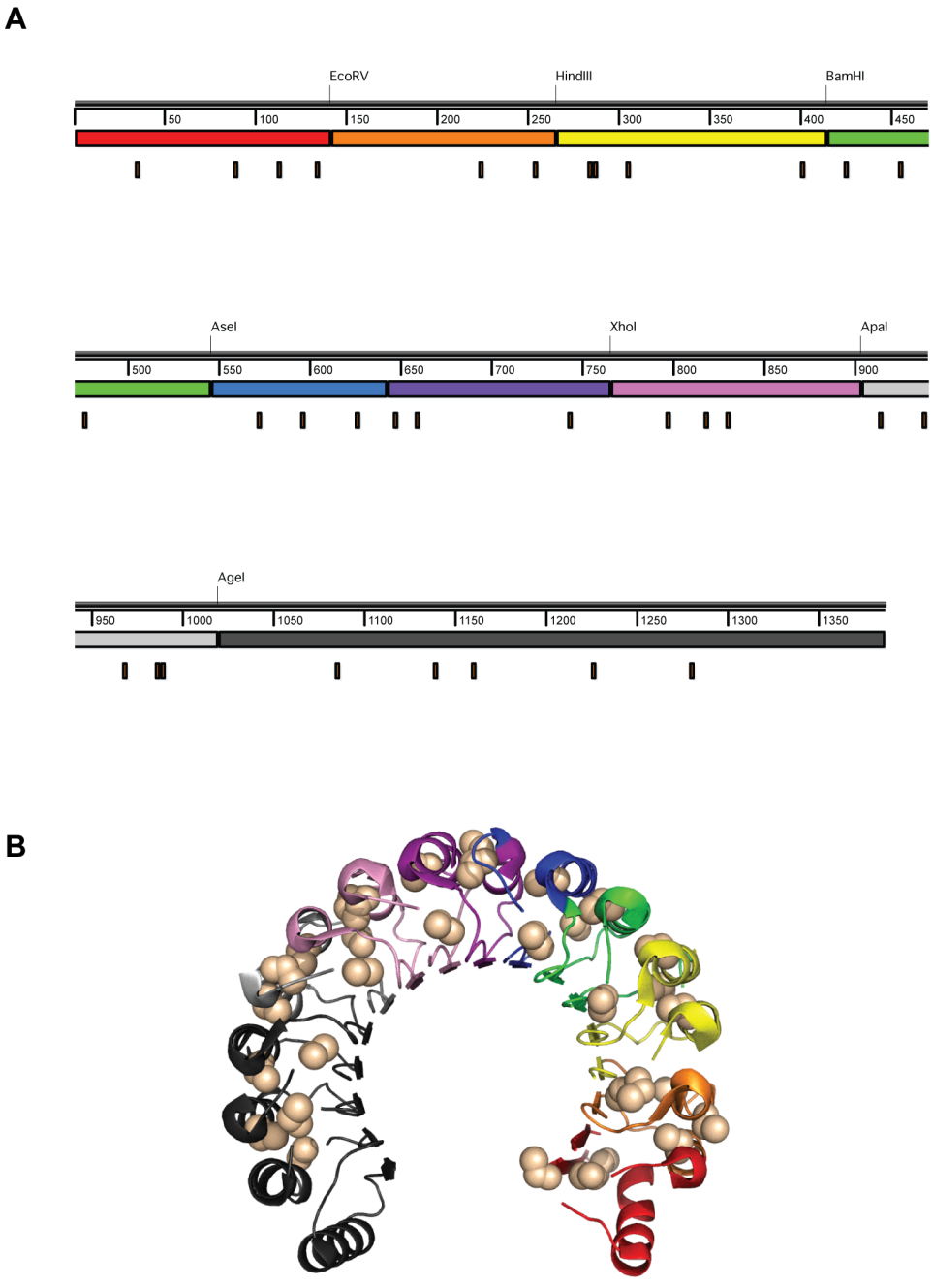
A
EcoRV
HindIII
BamHI
50
100
150
200
250
300
350
400
450
AseI
XhoI
ApaI
500
550
600
650
700
750
800
850
900
AgeI
950
1000
1050
1100
1150
1200
1250
1300
1350
B

Figure A1.3 Modular silent mutations in wild-type and cysteine-free RI

A. RI protein sequence map showing that seven silent mutations encoding restriction endonuclease recognition sites were installed into both WT–RI and CF–RI to allow for segmental swapping and creation of chimeric variant proteins. *B*. Color-coded segments mapped onto the three-dimensional structure of human RI.

Figure A1.4

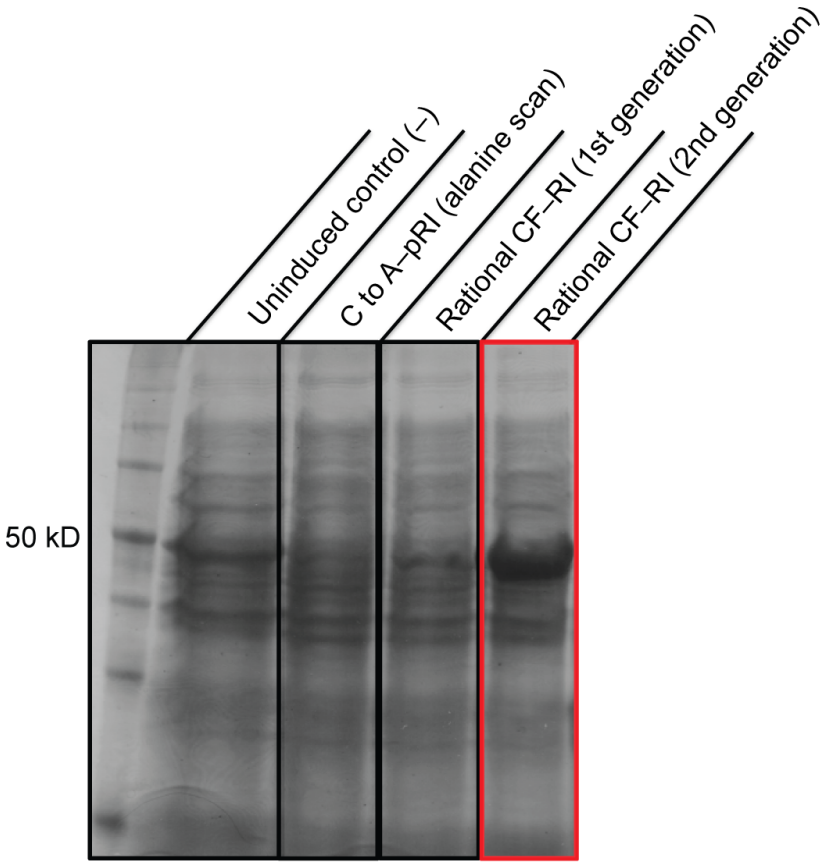
Uninduced control (–)
C to A–pRI (alanine scan)
Rational CF–RI (1st generation)
Rational CF–RI (2nd generation)
50 kD

Figure A1.4 Successful expression of cysteine-free RI in *E. coli*

CFRI (highlighted in red; lane 4) shows up as a dark expression band at ~50 kD on an SDS-PAGE expression gel of total cell lysate. Conversely, no expression is detected in either uninduced control cells (lane 1), a variant of porcine RI where all Cys residues are substituted with Ala (lane 2), or a semi-rational design of human RI replacing all Cys residues with mostly Ala (lane 3).

Figure A1.5

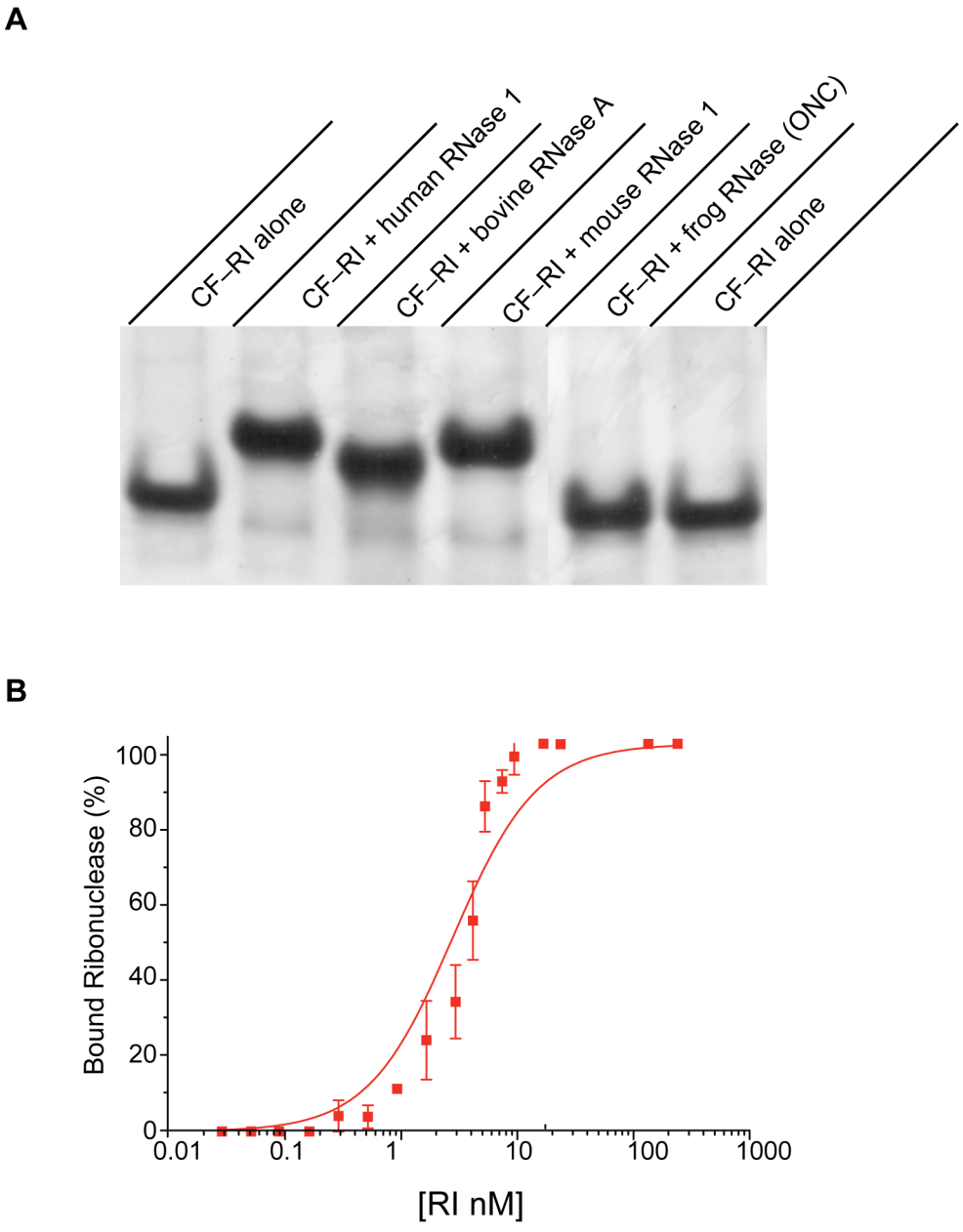
A
CF–RI alone
CF–RI + human RNase 1
CF–RI + bovine RNase A
CF–RI + mouse RNase 1
CF–RI + frog RNase (ONC)
CF–RI alone
B
Bound Ribonuclease (%)
100
80
60
40
20
0
0.01
0.1
1
10
100
1000
[RI nM]

Figure A1.5 CF–RI can bind to ptRNases with nanomolar affinity

A. Native gel–shift showing the ability of CF–RI to bind to various mammalian ptRNases, but not to frog RNase (ONC). Shifted bands indicate a change in p*I* that occurs upon the anionic CF–RI binding to the cationic RNase. *B*. Saturation binding curve demonstrating the relatively tight (K_d ~ 10 nM) binding affinity for CF–RI to human RNase 1. Important to note, the K_d measured for CF–RI•RNase 1 is approximately seven orders of magnitude weaker than wild-type RI.

Figure A1.6

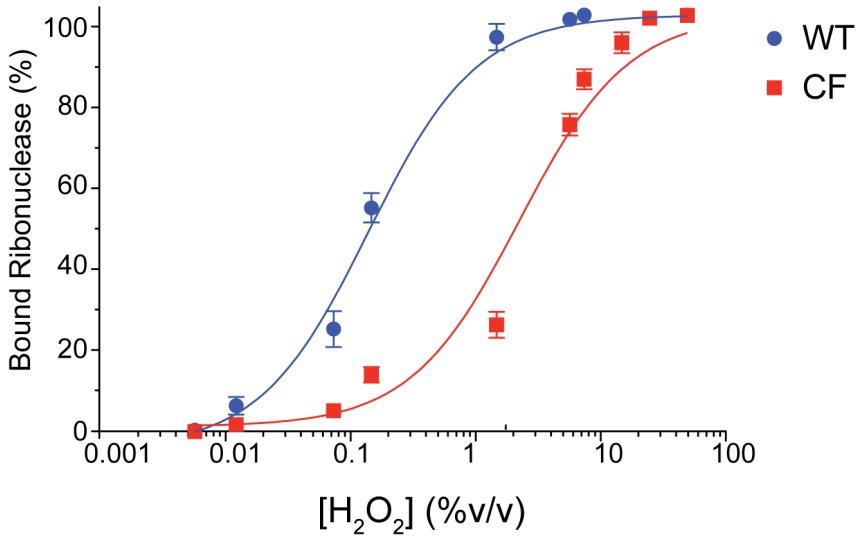
Bound Ribonuclease (%)
100
80
60
40
20
0
0.001
0.01
0.1
1
10
100
[H2O2] (%v/v)
WT
CF

Figure A1.6 CF–RI is more resistant to oxidation than wild-type RI

RI•RNase dissociation curves upon titration with H_2O_2. CF–RI displays an IC_{50} for H_2O_2 approximately 10-fold higher than wild-type RI. This surprisingly small difference might be attributable to the lower stability of the CFRI molecule as compared to WT.

Figure A1.7

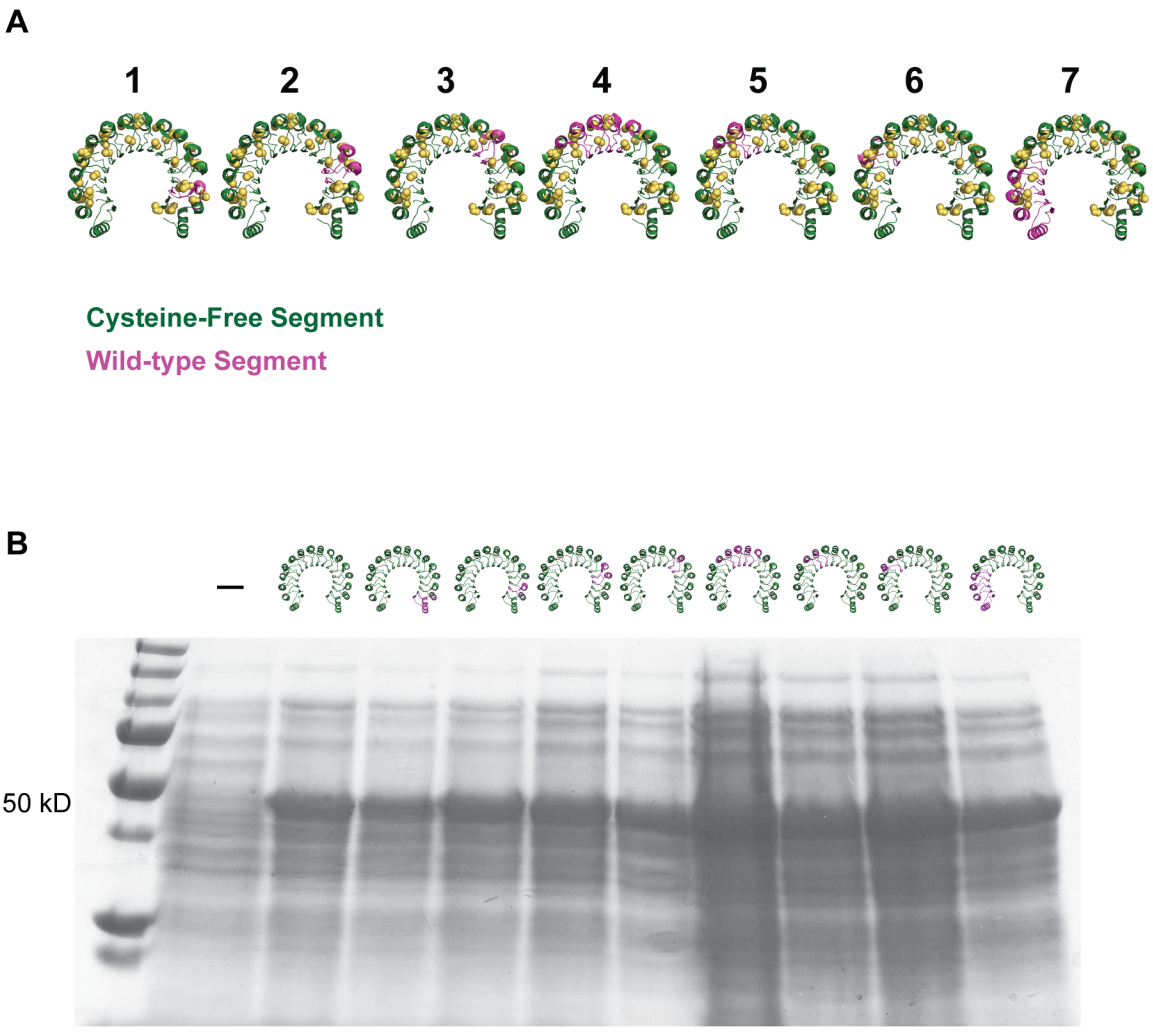

Figure A1.7 Generation and expression of chimeric CF/WT proteins

A. Structural depictions of the seven chimeric proteins that incorporate segments of both WT and CF-RI sequence. *B*. SDS–PAGE expression gel of total cell lysate showing production of each chimeric protein upon induction with IPTG. Lane 1 is the uninduced control.

APPENDIX II

Establishment of a Robust Production Strategy for Three Fluorescent Proteins

A2.1 Abstract

Successful cytosolic delivery of exogenous molecules represents a key hurdle in drug design. Improved targeting and delivery strategies are needed to expedite passage of materials across the cell membrane. Green fluorescent protein (GFP) is a useful model protein scaffold to aid in the development of such technologies. It is stable, genetically tractable, and possesses a direct biological readout for cellular internalization. Previously, recombinant forms of GFP were not readily available, given the insolubility of GFP in bacterial hosts. Recent efforts in directed evolution have yielded variants of multiple fluorescent proteins that are readily produced in *E. coli* and have enhanced spectral properties. Here, robust expression and purification systems were established for protein variants of GFP, RFP, and BFP. These proteins are now poised to become extremely useful tools for the testing of various chemical modifications to facilitate intracellular cargo transport.

A2.2 Introduction

One of the biggest barriers to the development of novel therapeutics and diagnostic tools is the cellular plasma membrane. This natural hydrophobic barrier is critical for life because it allows cells to regulate their internal environment apart from the extracellular space. Not surprisingly, it is evolutionarily designed to exclude most molecules. This barrier drastically limits the delivery of polar molecules—like peptides, proteins, nucleic acids, and small molecule drugs—to intracellular targets.[401] Thus, new techniques are necessary to enhance the cytosolic delivery of biological cargoes, without causing deleterious off-target effects.

For over ten years, the Raines group has focused on designing new strategies to endow proteins and small molecules with cellular permeability. Not only have we carefully studied the mechanisms of translocation for pancreatic-type RNases, which are endogenously imbued with the ability to translocate,[128,132,338] but we have also attempted to enhance this uptake through various means.[248,249,402] We are now seeking to expand our arsenal of strategies to include biocompatible chemical modifications to proteins. Specifically, we are probing the use of boronate-containing groups, as boron are known to bind sugars and can facilitate interactions with cell-surface proteoglycans. The ensuing moieties can be removed by cellular esterases that reside in the endosomes and cytosol. Ultimately, we seek "bioreversible" modifications that will deliver native cargo into the cytosol of cells.[403,404]

In order to test the efficacy of novel chemical modifications that enhance cellular uptake, amenable protein scaffolds (*i.e.,* cargoes) are needed. Previously, we have utilized RNase A as our model protein scaffold.[403] This protein is ostensibly ideally suited as a scaffold, given its high thermostability, acid stability, and relatively high tolerance for organic solvents.[15] RNase A can tolerate the harsh reaction conditions that are often necessary for chemical labeling.

However, as most proteins do not possess the legendary stability of RNase A, these modifications might not be extendable to other proteins, precluding their utility. Further, the biological readout of RNase A internalization—cytotoxicity—is indirect. Cytotoxicity can be affected by multiple factors, including cellular uptake, evasion of the cytosolic ribonuclease inhibitor protein, as well as catalytic activity against RNA substrates. Therefore, assessing the specific causes of increased RNase A-induced cytotoxicity can be confounded by multiple properties and is difficult to interpret.

The ideal protein cargo scaffold would exhibit high stability as well as a direct biological readout for cellular internalization. One candidate for this ideal protein is Green Fluorescent Protein (GFP). GFP is a compact protein of 238 amino acids consisting of a chromophore core composed of three post-translationally modified amino acids (–Ser^{65}–Tyr^{66}–Gly^{67}). Owing to its autofluorescence both *in vitro* and *in vivo*, as well as its remarkable stability, it is widely used for numerous cell biology and molecular biology applications. Because the fluorescence of GFP is linked to its properly folded structure, it is possible to use the fluorescence of GFP as an indication of its stability; indeed, GFP has been shown to be stable to proteases, heat treatment, and denaturing agents, including urea and SDS.[405] Importantly, wild-type GFP does not readily internalize into mammalian cells, mostly due to its overall negative charge. Also important, GFP can tolerate multiple mutations, including N- and C-terminal fusions, as evidenced by the plethora of variants that have been created over the years.[406] Previously, the Raines lab utilized a GFP variant, enhanced GFP (eGFP), to demonstrate that genetic incorporation of five arginine residues could imbue GFP with cell-permeating ability.[407] Still, the eGFP protein was very insoluble in bacteria, requiring long induction periods at low temperatures to produce

unimpressive yields. Empirically testing chemical compounds often requires large amounts of protein; hence, a better purification strategy for GFP was needed.

Recently, new variants of GFP have been created that are much more soluble in *E. coli*. Directed evolution experiments in bacteria have yielded modified GFP proteins that are readily produced at 37°C in soluble form. These experiments, performed in multiple rounds by multiple investigators, have lead to finely honed, extremely soluble forms of GFP that maintain high quantum yield and protein stability (Table A2.1). By recapitulating these mutations through site-directed mutagenesis, I have been able to create my own superfolding GFP protein. Further, I have combined these solubility-enhancing mutations with the permeability-inducing arginine mutations ("arginine graft") to achieve a superfolding, cell-penetrating GFP.

Similar to green fluorescent protein, red fluorescent protein (RFP) has also undergone multiple rounds of directed evolution to produce especially useful variants. RFP, originally derived from the red *Discosoma* coral, exists in nature as a tetramer. However, it has been modified to be not only monomeric, but to also have enhanced brightness, stability, and protein folding.[408] A particularly bright, stable variant of monomeric RFP is mCherry (Figures A2.4 and A2.5). This protein is much more inherently soluble than GFP and can be readily produced recombinantly in *E. coli*. Similarly, Azurite is an evolved variant of blue fluorescent protein (BFP; derived from GFP) that possesses enhanced photostability, fluorescence and protein folding ability.[409] This protein is also fairly soluble in *E. coli* and can be recombinantly produced in large scale (Figures A2.4 and A2.5).

The ability to utilize three distinct fluorescent proteins opens new doors in terms of experimental design and functionality. As these three proteins each exhibit a different emission

spectrum, they can be imaged simultaneously with confocal microscopy, or measured simultaneously with flow cytometry, with minimal spectral overlap.

A2.3 Materials and Methods

A2.3.1 Cloning and mutagenesis of fluorescent protein vectors

Genes encoding eGFP and mCherry RFP were amplified from mammalian expression vectors (Promega) and inserted into a novel vector derived from a pET vector (Novagen). This vector, subsequently referred to as the "HisTEV" vector, contained an N-terminal 6X His tag, followed by a spacer region and finally a TEV protease recognition sequence (Figure A2.1). The vector also contained a T7 promoter, was ampicillin resistant and did not contain *LacI*; however, as fluorescent protein expression is not toxic to *E. coli*, leaky expression is not a large concern. The vector was modified to contain an *StuI* cloning site right after the TEV cleavage sequence, allowing for easy blunt cloning of target genes with an N-terminal tag. The gene encoding Azurite BFP was obtained from a reporter plasmid (Addgene) and also inserted into the HisTEV vector. All eGFP mutations were created via site-directed mutagenesis with the reported primers (Table A2.1) using the high-fidelity Phusion polymerase (New England BioLabs).

A2.3.2 Recombinant expression of fluorescent proteins

Plasmids were transformed into electrocompetent BL21(DE3) *E. coli* cells (New England BioLabs) and plated on LB-agar containing ampicillin. The following day, a single colony was used to inoculate 50 mL of LB and grown overnight at 37 °C in a shaking incubator. The following day, 5 mL of starter culture was used to inoculate 1 L of Terrific Broth medium (Research Products International, RPI) previously prepared in a 3.8–L glass flask. Ampicillin was also added to each flask to a final concentration of 200 μg/mL. Flasks were allowed to shake

at 200 rpm at 37 °C in a large shaking incubator until cells reached an optical density of 0.6–0.8 (log phase of growth). Once at optimal density, the incubator temperature was switched to 20 °C and cells were equilibrated at the new temperature for 20 min. Cells were then induced to a final concentration of 1 mM IPTG (RPI) and were grown overnight at 20 °C in a shaking incubator.[1]

Cells were harvested by centrifugation for 20 min at 5,000 rpm at 4 °C. Cell pellets appeared brightly colored for GFP and RFP (green and magenta, respectively); conversely BFP pellets did not appear blue—as the wavelength of ambient light did not excite the fluorescence—and instead appeared uncolored. Cell pellets were collected and resuspended in a 1X lysis buffer containing 50 mM Tris-HCl pH 7.0, 100 mM NaCl, 30 mM imidazole, 1% Triton X-100, and 20% w/v sucrose. The buffer was filter-sterilized, but not autoclaved. 15 mL of buffer was used for every 2 L of liquid growth. The cell pellets were vortexed until resuspended and frozen at –20 °C overnight.[2]

Cells were lysed with mechanical disruption using a cell disrupter (Constant Systems) and the lysate was immediately cleared by centrifugation for 1 h at 11,000 rpm at 4 °C. Supernatants were collected and filtered using either 5–μM syringe filters (Millipore) or glass fiber pre-filters (Sartorius). Solid pelleted material was discarded. Filtered supernatants were stored on ice and protected from light prior to FPLC purification.

Filtered cell lysates were purified using a nickel column (GE healthcare or Fisher) and eluted over a linear gradient of imidazole. The 1X binding (wash) buffer (*i.e.*, Buffer A) was composed as follows: 20 mM sodium phosphate, 0.5 M NaCl, 30 mM imidazole, pH 7.4. The 1X elution buffer (*i.e.*, Buffer B) was composed as follows: 20 mM sodium phosphate, 0.5 M NaCl, 500 mM imidazole, pH 7.4. Eluted fractions were collected, pooled, and dialyzed against 4 L of 20

[1] sfGFP can be induced at 37°C or 20°C; however, cpGFP, mCherry RFP and Azurite BFP require reduced

[2] It is critical that the lysis buffer does not contain EDTA or reducing agents, as these will ruin the nickel column used in downstream purification.

mM Tris-HCl, 1 mM EDTA, pH 7.0. Dialyzed material was then purified again using ion-exchange chromatography. For sfGFP, mCherry RFP, and Azurite BFP (*i.e.*, negatively charged proteins), an anion-exchange [hiTrap Q] column was used. For cpGFP (*i.e.*, positively charged protein), a cation-exchange [hiTrap SPHP] column was used. For both columns, proteins were eluted over a linear gradient of NaCl. Buffers used were as follows: (Buffer A) 20 mM Tris–HCl, 1 mM EDTA, pH 7.0. (Buffer B) 20 mM Tris–HCl, 1 mM EDTA, 1.0 M NaCl, pH 7.0. Upon elution, colored fractions were pooled and concentrated as needed.[3]

A2.3.3 Visualization of cellular internalization

HeLa cells and Chinese hamster ovary cells (CHO-K1) were obtained from the American Type Culture Collection (ATCC) and maintained according to recommended instructions. The day before protein incubation, cells were seeded onto 8-well chambered coverglass tissue culture dishes (Ibidi) to yield 75% confluency on the next day. The following day, protein solutions (in PBS) were added to 200 μL cells to a final concentration of 10 μM protein. Protein was incubated with cells for 3 h at 37 °C and the cells were then washed with PBS containing magnesium and calcium three times prior to visualization. Cell nuclei were stained by the addition of Hoechst 33342 (2 μg/mL) for the final 5 min of incubation. Internalization was visualized by imaging cells with a Nikon Eclipse TE2000-U laser scanning confocal microscope equipped with a Zeiss AxioCam digital camera. A blue-diode laser provided excitation at 408 nm, and emission at 450 nm was passed through a 35–nm band-pass filter. An argon-ion laser provided excitation at 488 nm and emission at 515 nm was passed through a 40–nm band-pass filter.

[3] The N-terminal His tag can be removed if desired by incubating protein with TEV protease.

A2.3.4 Measuring protein molecular weight

The molecular mass of each fluorescent protein was determined by matrix-assisted laser desorption/ionization-time-of-flight (MALDI–TOF) mass spectrometry using a Voyager-DE-PRO Biospectrometry Workstation (Applied Biosystems). Protein samples were desalted using ZipTip pipette tips (Pierce) prior to analysis. Sinapinic acid was used as a matrix. MALDI–TOF mass spectrometry experiments were performed at the campus Biophysics Instrumentation Facility.

A2.3.5 Measuring fluorescent protein stability

The conformational stability of fluorescent proteins was determined by following the change in fluorescence as a function of pH and organic solvent concentration. Fluorescent proteins (200 nM) were incubated in 96-well black, flat-bottom plates (Corning) in various buffers and conditions. pH titration assays were carried out at 23 °C in various buffers: 0.1 M NaOAc, 0.1 M NaCl (pH 3.5–5.5); 0.1 M BisTris, 0.1 M NaCl (pH 6.0–6.5); 0.1 M Tris, 0.1 M NaCl (pH 7.0–9.0). Organic solvents were mixed with ddH_2O to final concentrations of 0–50% acetonitrile (ACN), dimethyl sulfoxide (DMSO), dimethylformamide (DMF), ethanol (ETOH), or methanol (MEOH). Proteins were incubated at 37 °C for 6 h; fluorescent measurements were taken every hour at the appropriate excitation/emission spectra for each protein (Table A2.3). All fluorescence measurements were made using a Tecan M1000 fluorimeter plate reader and data were analyzed using the graphing software package Prism 5 (GraphPad).

A2.4 Results

A2.4.1 Engineering a superfolding, cell-penetrating GFP

Based on previous reports of mutations that enhance GFP solubility and folding in *E. coli*, 17 mutations were selected to engineer into the original eGFP plasmid (Table A2.1 and Figure A2.2). eGFP already contained the substitutions F64L and S65T. Other substitutions were successfully conferred via site-directed mutagenesis and confirmed by sequencing. Further substitutions that enhance cellular permeability were also engineered, resulting in two versions of "superfolding" GFP: sfGFP (wild-type) and cell-penetrating (cp)sfGFP.

A2.4.2 Establishing a high yield, recombinant purification system

Proteins were expressed recombinantly in *E. coli*, purified, and concentrated. Each recombinant protein also possessed an N-terminal purification tag that could be cleaved by TEV protease. Average protein yields between batches were as follows: sfGFP, ~120 mg protein/L growth; cpsfGFP, ~20 mg/L; mCherry RFP, ~55 mg/L; Azurite BFP, ~53 mg/L. Purified proteins ran as a single band on a denaturing SDS–PAGE gel (data not shown). cp-sfGFP had a significantly reduced yield as compared to sfGFP. The five arginine residues in cpGFP could reduce the overall stability of the protein and limit its folding during purification. Alternatively, the cationic "arginine graft" could cause the protein to aggregate and precipitate upon purification.

A2.4.3 cp-sfGFP can internalize into mammalian cells

The cell-penetrating, superfolding GFP variant was able to internalize readily into mammalian cells, whereas wild-type superfolding GFP was not (Figure A2.3). GFP protein was visualized in both endosomes (*i.e.*, punctate staining) as well as the cytosol (*i.e.*, diffuse staining)

for both human and rodent cells. CHOK1 cells appeared to have more diffuse staining than do HeLa cells. After incubation for 3 h with GFP proteins, cells appeared completely healthy and presented normal morphology. Cells remained adhered to the dish surface, and nuclei were unchanged from PBS controls (data not shown). Lower concentrations of GFP were also tested, and yielded internalization to a lesser extent (data not shown).

A2.4.4 Characterization of fluorescent proteins

Fluorescent proteins were analyzed for maximal excitation and emission using the wave–scan function of a NanoVue small-volume spectrophotometer. Values were found to match closely to those reported in the literature (Table A2.3). The molecular mass of each protein was calculated using MALDI–TOF mass spectrometry, and values were found to be close to expected values (Figure 6). Proteins appeared to fluoresce under long-wave UV light (Figure A2.7).

Proteins were assayed for stability across a wide pH range. sfGFP was found to lose 50% fluorescence (where fluorescence represents stability and proper folding) at ~pH 5.4. mCherry RFP was found to lose 50% fluorescence at ~pH 4.4. Azurite BFP was found to lose 50% fluorescence at ~pH 4.9. All proteins maintained 100% fluorescence at pH 6.5–9.0, implying that they are stable at those pH values. Proteins were also assayed for stability across a range of various solvent conditions at 37 °C. sfGFP was found to be most stable overall in various solvents. It was most sensitive to ACN and least sensitive to DMSO. mCherry RFP was also most sensitive to ACN and least sensitive to DMSO. Azurite BFP demonstrated the least stability overall, with extreme sensitivity to ACN, ETOH, MEOH, and DMF. BFP was least sensitive to DMSO.

A2.5 Discussion

Fluorescent proteins have great potential as useful scaffolds for designing cell-permeating moieties. They are relatively stable, genetically tractable, and have a direct visual readout for cellular internalization. Yet, until recently, many fluorescent proteins were not readily produced in bacterial hosts due to issues of solubility and folding. Recent efforts in directed evolution have achieved variant proteins that not only can be recombinantly produced, but that also have increased brightness and photostability. This new class of proteins is poised to be extremely relevant to chemical biologists.

Prior to the work outlined in this Appendix, the Raines group had only ever worked with eGFP, an insoluble GFP variant that was extremely hard to purify. The group now has access to three different recombinant proteins that can be purified in high yield and purity from *E. coli*. These three proteins, sfGFP, mCherry RFP, and Azurite BFP, have distinct excitation and emission spectra that do not overlap. They can therefore be used simultaneously in both confocal microscopy and flow cytometry experiments. Up to three different compounds or chemical modifications can be studied at one time, and competition experiments can be designed to measure and compare internalization rates. Further, cell-penetrating GFP can now also be produced readily. cp-sfGFP can serve as a useful positive control for testing various compounds that enhance cellular internalization.

The N-terminal His tag present on each protein offers additional options for experimental design. This tag is optimized for specific and efficient cleavage by TEV protease. TEV protease is the common name for the 27–kDa catalytic domain of the Nuclear Inclusion a (NIa) protein encoded by the tobacco etch virus (TEV). It is easy to purify in large scale, and is widely available commercially.[322] The N-terminal tags on each fluorescent protein can be cleaved prior

to chemical labeling. Alternatively, the tag can remain intact during chemical modification and subsequent cell treatment. The tag can then be used to pull delivered protein cargo out of cell lysates to assess the presence or absence of various moieties. The bi-functionality of the N-terminal tag is especially useful when monitoring the "bioreversibility" of cleavable chemical modifications.

The addition of chemical modifications to proteins often requires harsh reaction conditions. Therefore, screening the stability of fluorescent proteins in various buffers and pH ranges can yield extremely valuable information for chemical biologists. The results outlined in this Appendix revealed that fluorescent proteins are most stable in a pH range of 6.5–9.0, and that they lose approximately half of their fluorescence (indicating a folded state) in more acidic conditions. sfGFP appears to be most sensitive to low pH, whereas mCherry RFP appears least sensitive. These results agree with previous studies that report eGFP loses 50% of fluorescence at pH 5.5[410] and that under pH 6.5, GFP is much more sensitive to denaturing conditions, including SDS, urea, and heat.[411] Taken together, these results imply that to achieve maximum protein retention during chemical modification, the reaction pH should be at least 6.0. Additionally, based on screens of various organic solvents, it is apparent that all three fluorescent proteins have the highest stability and tolerance to DMSO. Therefore, DMSO is the optimal solvent for use in chemical reactions involving fluorescent proteins.

The protein characterization results presented in this Appendix represent preliminary studies only. In order to maximize the efficiency of chemical modifications to fluorescent proteins, reaction conditions and protein tolerances must be determined empirically. Nevertheless, the data herein will provide a useful starting point for the establishment of fluorescent proteins as model protein scaffolds for the Raines group.

Table A2.1 List of mutations for enhanced solubility and stability of fluorescent proteins

Protein	**Mutations**	**Ref.**
eGFP	F64L, S65T	[410]
"folding reporter" GFP	*F64L, S65T*, F99S, M153T, V163A	[412,413]
"Superfolder" GFP (sfGFP)	*F64L, S65T, F99S, M153T, V163A*, S30R, Y39N, N105T, Y145F, I171V, A206V	[414]
"GFP 1–10 OPT" (optimized for self-assembly *in vivo*)	*F64L, S65T*, *F99S, M153T, V163A, S30R, Y145F, I171V, A206V,* N39I, T105K, E111V, I128T, K166T, I167V, S205T, L221H, F223Y, T225N	[381]
Cell Penetrating (cp)GFP	E17R, D19R, D21R, V111R, E124R	[407]
J.E.L. Superfolder GFP	F64L, S65T, F99S, M153T, V163A, S30R, Y145F, I171V, A106V, Y39I, N105K, E111V, I128T, K166T, I167V, S205T, L221H, F223Y, T225N	
J.E.L. Superfolder cpGFP	F64L, S65T, F99S, M153T, V163A, S30R, Y145F, I171V, A106V, Y39I, N105K, I128T, K166T, I167V, S205T, L221H, F223Y, T225N, E17R, D19R, D21R, V111R, E124R	
"Azurite" BFP	*F64L, S65T, Y66H, Y145F*, V163A, V150I, V224R	[409]
mCherry RFP	V7I, M182K, M163Q, N6aD, R17H, M182K, K194N, T195V, D196N	[408]

Table A2.2 List of oligonucleotides used in cloning of fluorescent proteins vector

Protein	Primer Name	Function	Sequence
eCFP	eCFP pet22b forward	Cloning into pet22b vector (NdeI)	ATTAAATAATCATATGGTGAGCAAGGGCGAGGAGC
	eCFP pet22b reverse	Cloning into pet22b vector (SalI)	ATTATTATATGTCGACCTACTTGTACAGCTCGTCCATG
eGFP	eGFP pet22b forward	Cloning into pet22b vector (NdeI)	ATTAAATAATCATATGGTGAGCAAGGGCGAGGAGC
	eGFP pet22b reverse	Cloning into pet22b vector (SalI)	ATTATTATATGTCGACCTACTTGTACAGCTCGTCCATG
eGFP	Y39I forward	Quikchange; Y39I	GAGGGCGAGGGCGATGCCACCTACGGCAAGCTGACC CTGAAGTTCATC
	Y39I reverse	Quikchange; Y39I	GAGGGCGAGGGCGATGCCACCATCGGCAAGCTGACC CTGAAGTTCATC
	F99S forward	Quikchange; F99S	GTTGCCGTCGTCCTTGAAGCTGATGG
	F99S reverse	Quikchange; F99S	GTCCAGGAGCGCACCATCAGCTTC
	N105K/E111V forward	Quikchange; N105K/E111V	TTCAAGGACGACGGCAACTACAAGACCCGCGCCGAG GTGAAGTTCGAGGGCGACACC
	N105K/E111V reverse	Quikchange; N105K/E111V	TTCAAGGACGACGGCAAATACAAGACCCGCGCCGTG GTGAAGTTCGAGGGCGACACC
	I128T forward	Quikchange; I128T	AACCGCATCGAGCTGAAGGGCATCGACTTCAAGGAG GACGGCAACATC
	I128T reverse	Quikchange; I128T	AACCGCATCGAGCTGAAGGGCACCGACTTCAAGGAG GACGGCAACATC
	Y145F/M153T forward	Quikchange; Y145F/M153T	GGGCACAAGCTGGAGTACAACTACAACAGCCACAAC GTCTATATCATGGCCGACAAGCAGAAGAAC
	Y145F/M153T reverse	Quikchange; Y145F/M153T	GGGCACAAGCTGGAGTACAACTTCAACAGCCACAAC GTCTATATCACCGCCGACAAGCAGAAGAAC
	S205T/A206V forward	Quikchange; S205T/A206V	AACCACTACCTGAGCACCCAGTCCGCCCTGAGCAAAG ACCCCAAC
	S205T/A206V reverse	Quikchange; S205T/A206V	AACCACTACCTGAGCACCCAGACCGTGCTGAGCAAA GACCCCAAC
	L221H/F223Y/T225N forward	Quikchange; HYN	CGCGATCACATGGTCCTGCTGGAGTTCGTGACCGCCG CCGGGATCACTCTCGGCATGGAC
	L221H/F223Y/T225N reverse	Quikchange; HYN	CGCGATCACATGGTCCTGCATGAGTACGTGAACGCCG CCGGGATCACTCTCGGCATGGAC
	GFP HisTEV forward	Cloning into HisTEV vector (blunt)	CATGGTGAGCAAGGGCGAGGAGCTGTTCA
	GFP HisTEV reverse	Cloning into HisTEV vector (SalI)	ATTATAATA GTCGAC CTACTTGTACAGCTCGTCCATGCCG
	GFP E17R/D19R/D21R forward	Quikchange; Install Arg Graft	GTGGTGCCCATCCTGGTCGAGCTGGACGGCGACGTAA ACGGCCACAAGTTCAGC
	GFP E17R/D19R/D21R reverse	Quikchange; Install Arg Graft	GTGGTGCCCATCCTGGTCCGTCTGCGTGGCCGTGTAA ACGGCCACAAGTTCAGC
	GFP E111R forward	Quikchange; Install Arg Graft	AAATACAAGACCCGCGCCGTGGTGAAGTTCGAGGGC GAC
	GFP E111R reverse	Quikchange; Install Arg Graft	AAATACAAGACCCGCGCCCGTGTGAAGTTCGAGGGC GAC
	GFP 124R forward	Quikchange; Install Arg Graft	ACCCTGGTGAACCGCATCGAGCTGAAGGGCACCGACT TC
	GFP 124 reverse	Quikchange; Install Arg Graft	ACCCTGGTGAACCGCATCCGTCTGAAGGGCACCGACT TC
mCherry	mCherry HisTEV forward	Cloning into HisTEV vector (blunt)	CATGGTGAGCAAGGGCGAGGAGGATA
	mCherry HisTEV reverse	Cloning into HisTEV vector (SalI)	ATTATATATGTCGACCTACTTGTACAGCTCGTCCATGC CGC
Azurite	Azurite HisTEV forward	Cloning into HisTEV vector (blunt)	CATGTCTAAAGGTGAAGAATTATTCAC
	Azurite HisTEV reverse	Cloning into HisTEV vector (SalI)	ATTATATATGTCGACCTATTTGTACAATTCATCCATAC CATGGGT

Figure A2.1

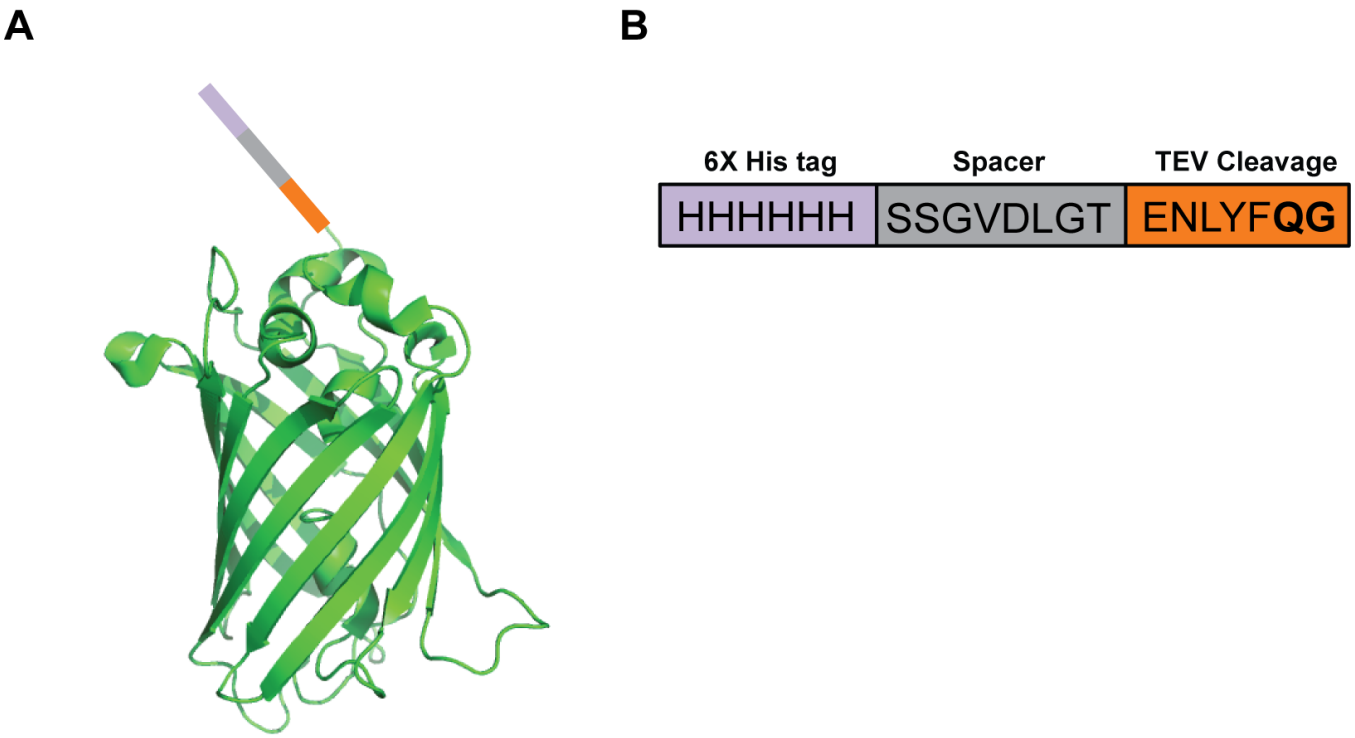

Figure A2.1 Expression strategy for fluorescent proteins

Expression strategy for fluorescent proteins from the HisTEV vector.

A. Fluorescent proteins contain an N-terminal purification tag (GFP shown as representative protein). B. Sequence of N-terminal tag. The tag contains a 6X histidine sequence for purification, followed by a spacer region, and also contains a recognition site for TEV protease. Bold residues (**QG**) represent the exact cleavage site of TEV protease.

Figure A2.2

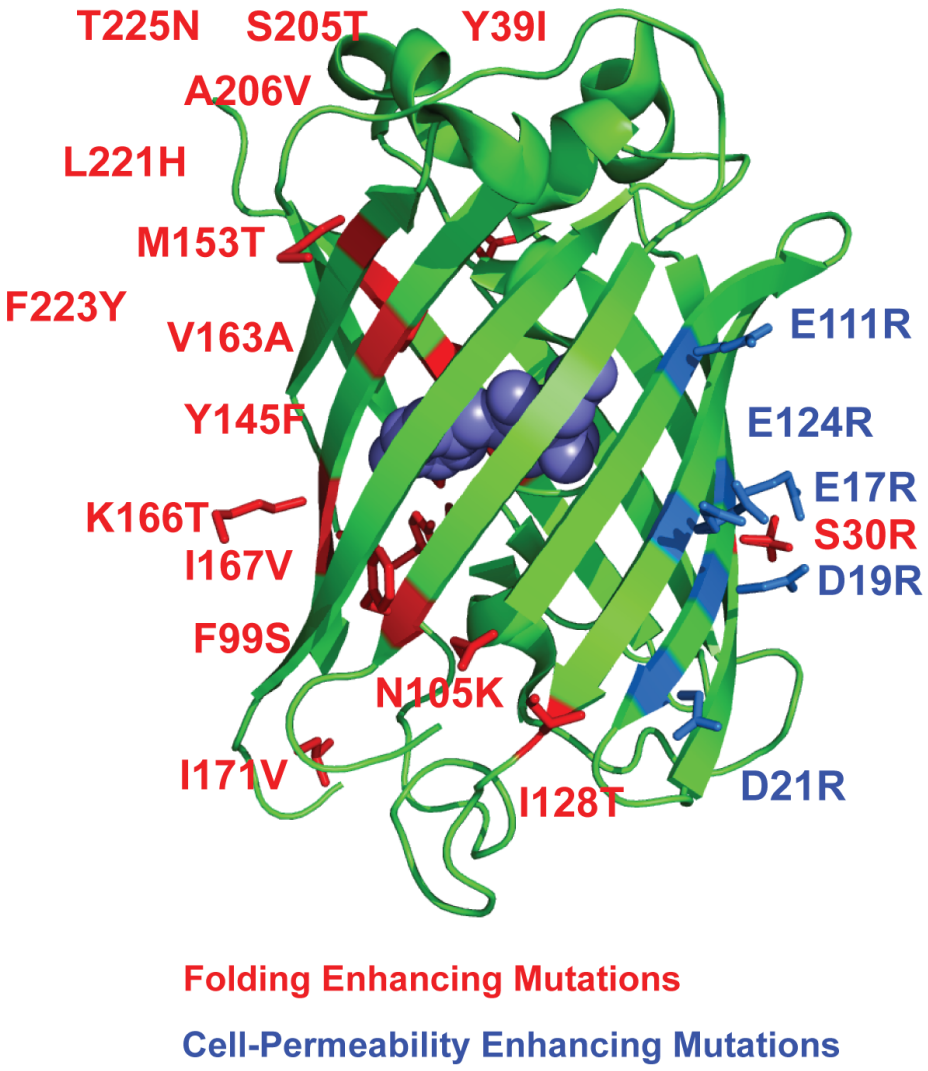
T225N
S205T
Y39I
A206V
L221H
M153T
F223Y
V163A
Y145F
K166T
I167V
F99S
N105K
I171V
I128T
E111R
E124R
E17R
S30R
D19R
D21R
Folding Enhancing Mutations
Cell-Permeability Enhancing Mutations

Figure A2.2 Efficacious residue substitutions for improved GFP variants

Crystal structure of superfolder GFP (PDB code 2Q6P) showing the position of various engineered mutations. Red: mutations that enhance solubility and folding in *E. coli*; Blue: mutations that endow cellular permeability (*i.e.*, "arginine grafts").

Figure A2.3

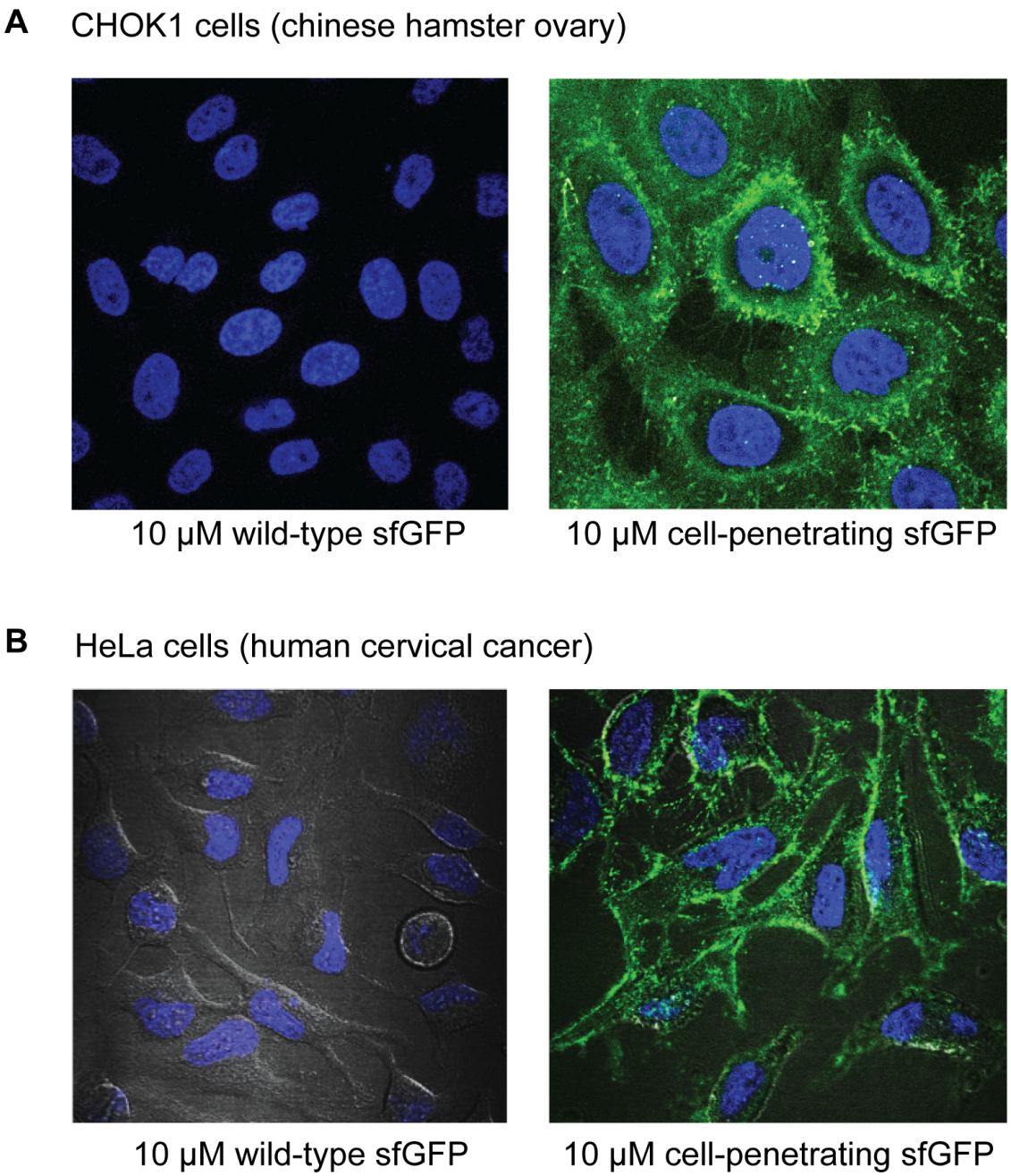
A
CHOK1 cells (chinese hamster ovary)
10 μM wild-type sfGFP
10 μM cell-penetrating sfGFP
B
HeLa cells (human cervical cancer)
10 μM wild-type sfGFP
10 μM cell-penetrating sfGFP

Figure A2.3 Cellular internalization of cell-penetrating GFP

Confocal microscopy images showing cellular internalization of modified GFP. *A*. Rodent CHOK1 cells with both wild-type and cell-penetrating (cp)GFP. *B*. Human HeLa cells with both wild-type and cpGFP.

Figure A2.4

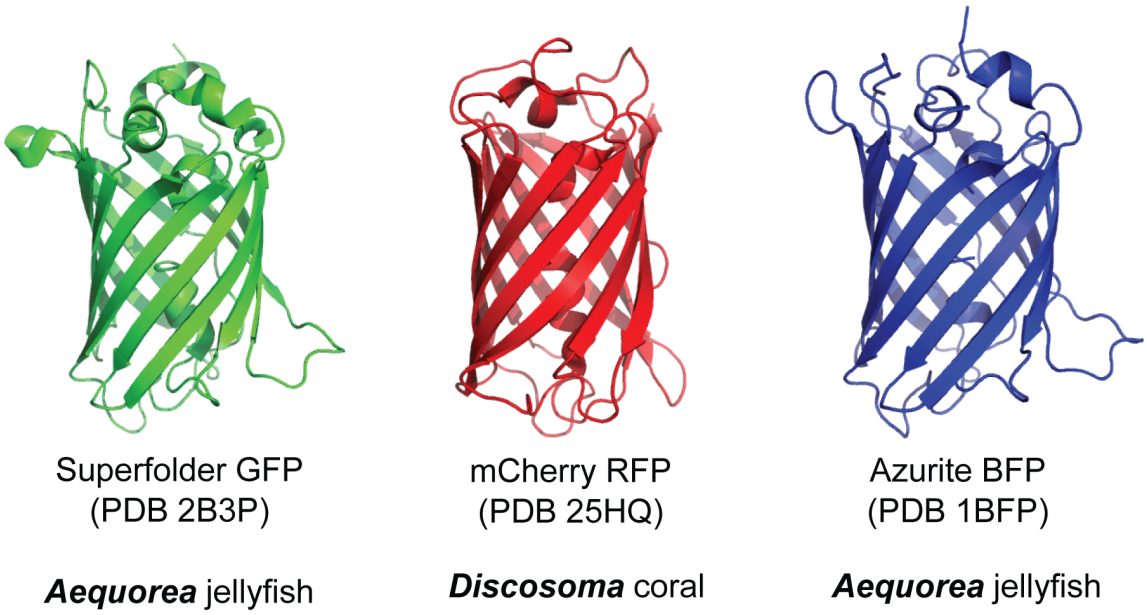
Superfolder GFP
(PDB 2B3P)
Aequorea jellyfish
mCherry RFP
(PDB 25HQ)
Discosoma coral
Azurite BFP
(PDB 1BFP)
Aequorea jellyfish

Figure A2.4 Structural comparisons of fluorescent proteins

Table A2.3 Biophysical properties of fluorescent proteins

Protein	MW (w/ tag)	*z*	MW (cleaved)	*z*	Excitation	Emission	ε_{max}	Ref.
sfGFP	29361	-8	26923.3	-6	485 nm	510 nm	83,300	[414]
cp-sfGFP	29554.4	+1	27106.7	+3	485 nm	510 nm	83,300	[407]
RFP (mcherry)	29244.8	-8	26797.1	-6	587 nm	610 nm	72,000	[408]
BFP (azurite)	29404	-9	26956.3	-7	383 nm	450 nm	26,200	[409]

Figure A2.5

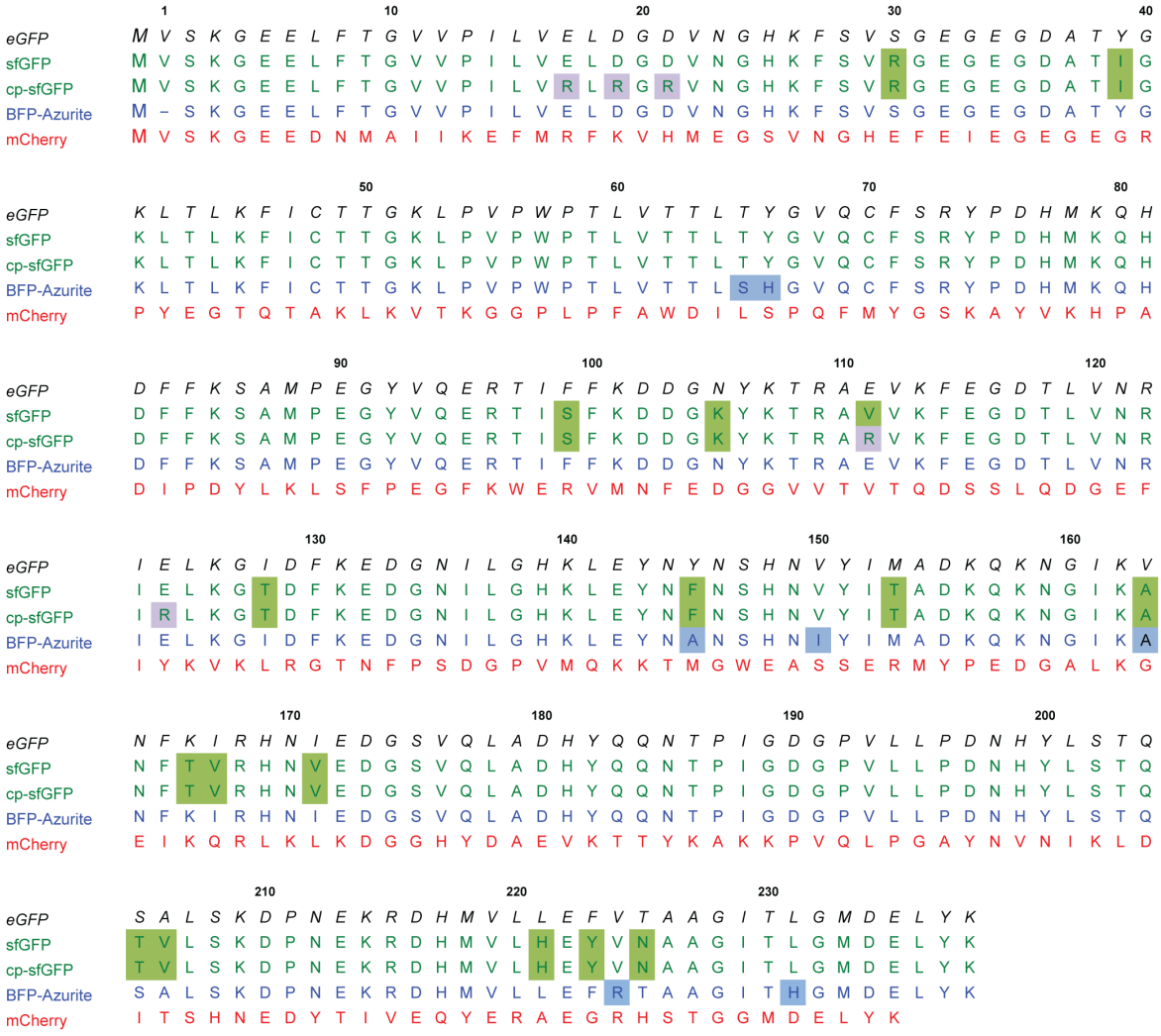
1 10 20 30 40
eGFP M V S K G E E L F T G V V P I L V E L D G D V N G H K F S V S G E G E G D A T Y G
sfGFP M V S K G E E L F T G V V P I L V E L D G D V N G H K F S V R G E G E G D A T I G
cp-sfGFP M V S K G E E L F T G V V P I L V R L R G R V N G H K F S V R G E G E G D A T I G
BFP-Azurite M - S K G E E L F T G V V P I L V E L D G D V N G H K F S V S G E G E G D A T Y G
mCherry M V S K G E E D N M A I I K E F M R F K V H M E G S V N G H E F E I E G E G E G R
50 60 70 80
eGFP K L T L K F I C T T G K L P V P W P T L V T T L T Y G V Q C F S R Y P D H M K Q H
sfGFP K L T L K F I C T T G K L P V P W P T L V T T L T Y G V Q C F S R Y P D H M K Q H
cp-sfGFP K L T L K F I C T T G K L P V P W P T L V T T L T Y G V Q C F S R Y P D H M K Q H
BFP-Azurite K L T L K F I C T T G K L P V P W P T L V T T L S H G V Q C F S R Y P D H M K Q H
mCherry P Y E G T Q T A K L K V T K G G P L P F A W D I L S P Q F M Y G S K A Y V K H P A
90 100 110 120
eGFP D F F K S A M P E G Y V Q E R T I F F K D D G N Y K T R A E V K F E G D T L V N R
sfGFP D F F K S A M P E G Y V Q E R T I S F K D D G K Y K T R A V V K F E G D T L V N R
cp-sfGFP D F F K S A M P E G Y V Q E R T I S F K D D G K Y K T R A R V K F E G D T L V N R
BFP-Azurite D F F K S A M P E G Y V Q E R T I F F K D D G N Y K T R A E V K F E G D T L V N R
mCherry D I P D Y L K L S F P E G F K W E R V M N F E D G G V V T V T Q D S S L Q D G E F
130 140 150 160
eGFP I E L K G I D F K E D G N I L G H K L E Y N Y N S H N V Y I M A D K Q K N G I K V
sfGFP I E L K G T D F K E D G N I L G H K L E Y N F N S H N V Y I T A D K Q K N G I K A
cp-sfGFP I R L K G T D F K E D G N I L G H K L E Y N F N S H N V Y I T A D K Q K N G I K A
BFP-Azurite I E L K G I D F K E D G N I L G H K L E Y N A N S H N I Y I M A D K Q K N G I K A
mCherry I Y K V K L R G T N F P S D G P V M Q K K T M G W E A S S E R M Y P E D G A L K G
170 180 190 200
eGFP N F K I R H N I E D G S V Q L A D H Y Q Q N T P I G D G P V L L P D N H Y L S T Q
sfGFP N F T V R H N V E D G S V Q L A D H Y Q Q N T P I G D G P V L L P D N H Y L S T Q
cp-sfGFP N F T V R H N V E D G S V Q L A D H Y Q Q N T P I G D G P V L L P D N H Y L S T Q
BFP-Azurite N F K I R H N I E D G S V Q L A D H Y Q Q N T P I G D G P V L L P D N H Y L S T Q
mCherry E I K Q R L K L K D G G H Y D A E V K T T Y K A K K P V Q L P G A Y N V N I K L D
210 220 230
eGFP S A L S K D P N E K R D H M V L L E F V T A A G I T L G M D E L Y K
sfGFP T V L S K D P N E K R D H M V L H E Y V N A A G I T L G M D E L Y K
cp-sfGFP T V L S K D P N E K R D H M V L H E Y V N A A G I T L G M D E L Y K
BFP-Azurite S A L S K D P N E K R D H M V L L E F R T A A G I T H G M D E L Y K
mCherry I T S H N E D Y T I V E Q Y E R A E G R H S T G G M D E L Y K

Figure A2.5 Sequence alignment of fluorescent proteins

Shaded residues indicate engineered mutations. Alignment was made using the program MUSCLE[211] with manual adjustments.

Figure A2.6

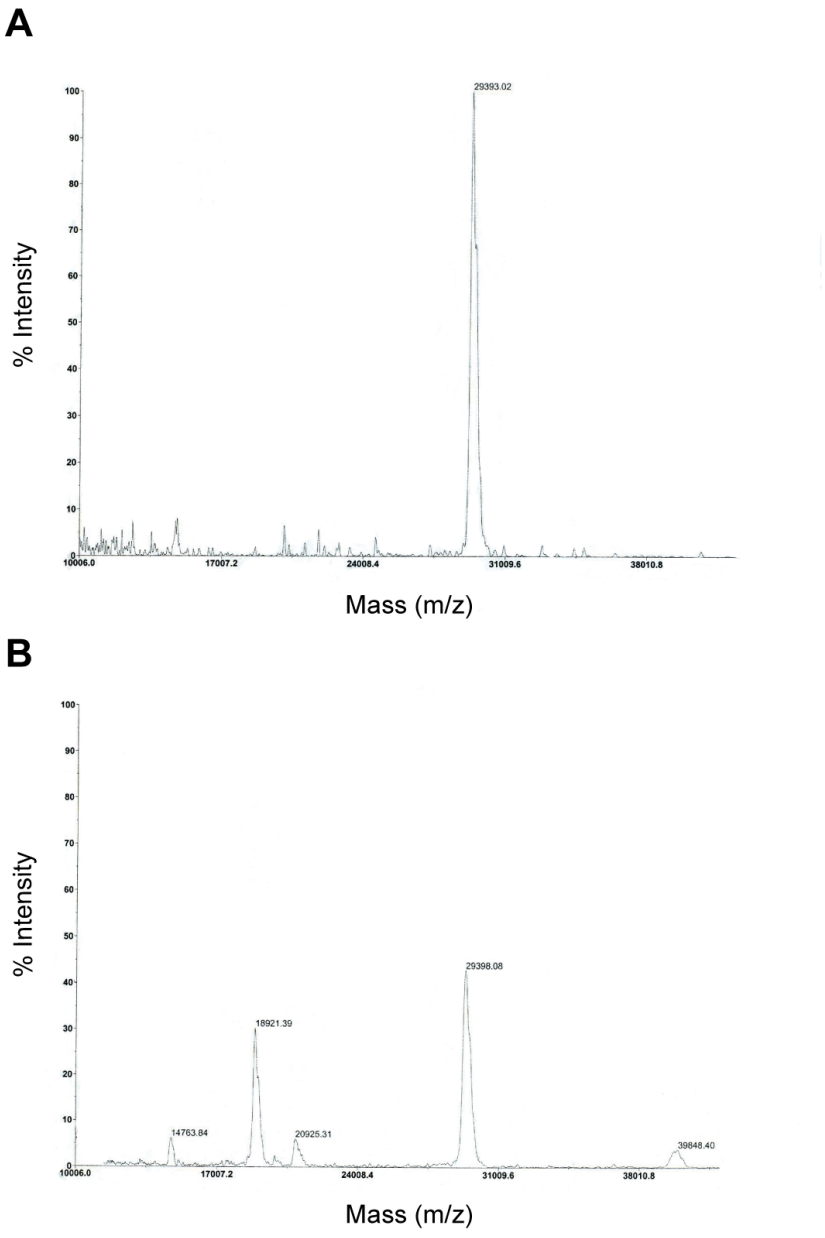
A
% Intensity
29393.02
Mass (m/z)
B
% Intensity
29398.08
18921.39
14763.84
20925.31
39648.40
Mass (m/z)

Figure A2.6 MALDI spectra for two fluorescent proteins

A. Spectra for sfGFP with a His tag. *Expected MW*: 29,361 Da; *Calculated MW*: 29,393.02 Da.

B. Spectra for mCherry with a His tag. *Expected MW*: 29244.8; *Calculated MW*: 29398.08.

Figure A2.7

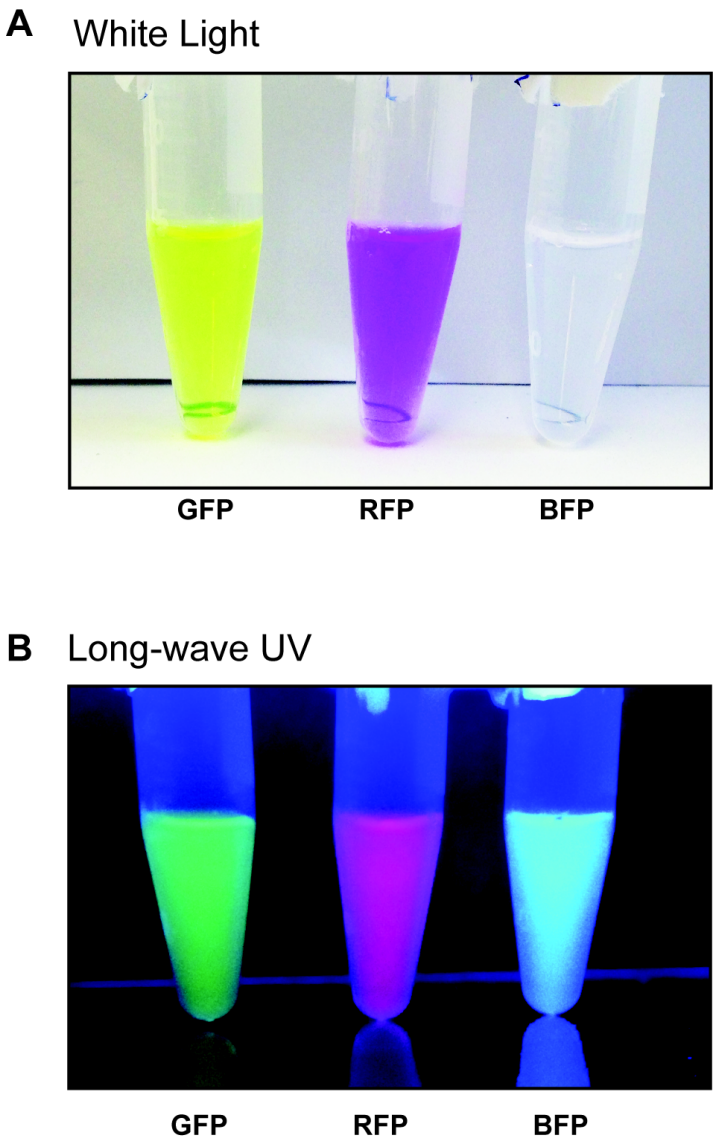

Figure A2.7 Recombinant fluorescent proteins

Photographs of solutions of recombinant fluorescent proteins. A. sfGFP, mCherry, and Azurite, visualized in white (ambient) light. B. sfGFP, mCherry, and Azurite, visualized in long-wave UV light.

Figure A2.8

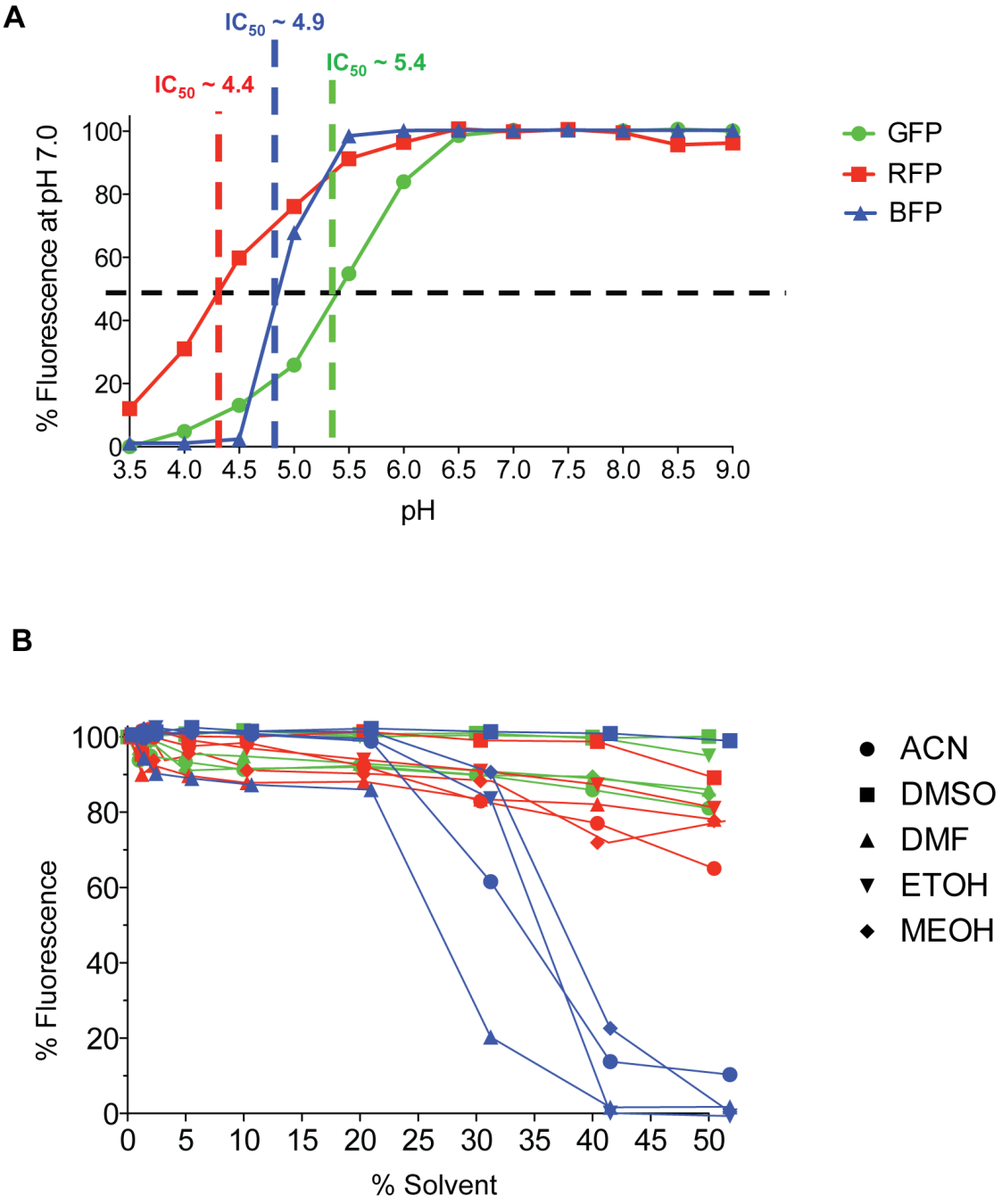
A
IC50 ~ 4.9
IC50 ~ 5.4
IC50 ~ 4.4
% Fluorescence at pH 7.0
100
80
60
40
20
0
3.5 4.0 4.5 5.0 5.5 6.0 6.5 7.0 7.5 8.0 8.5 9.0
pH
GFP
RFP
BFP
B
% Fluorescence
100
80
60
40
20
0
0 5 10 15 20 25 30 35 40 45 50
% Solvent
ACN
DMSO
DMF
ETOH
MEOH

Figure A2.8 Fluorescent protein stability in heat and solvent

Analyses of fluorescent protein stability after 3 h at 37 °C under various conditions. A. Fluorescent protein stability (as measured by fluorescence) across a range of pH values. IC_{50} values were fitted by eye and represent estimates only. B. Fluorescent protein stability (as measured by fluorescence) across a range of various organic solvent concentrations. Solvents were dissolved in ddH_2O, and pH was not adjusted.

REFERENCES

1. The noncoding RNA revolution: trashing old rules to forge new ones. Cech, T. R.; Steitz, J. A. *Cell* **2014**, *157*, 77-94.

2. Characterization of extracellular circulating microRNA. Turchinovich, A.; Weiz, L.; Langheinz, A.; Burwinkel, B. *Nucleic Acids Res.* **2011**, *39*, 7223-33.

3. MicroRNAs and other non-coding RNAs as targets for anticancer drug development. Ling, H.; Fabbri, M.; Calin, G. A. *Nat. Rev. Drug Discov.* **2013**, *12*, 847-65.

4. Exoribonucleases and their multiple roles in RNA metabolism. Deutscher, M. P.; Li, Z. *Prog. Nucleic Acid Res. Mol. Biol.* **2001**, *66*, 67-105.

5. 3' processing of eukaryotic precursor tRNAs. Maraia, R. J.; Lamichhane, T. N. *Wiley Interdiscip. Rev. RNA* **2011**, *2*, 362-75.

6. Ribonucleases P/MRP and the expanding ribonucleoprotein world. Hernandez-Cid, A.; Aguirre-Sampieri, S.; Diaz-Vilchis, A.; Torres-Larios, A. *IUBMB Life* **2012**, *64*, 521-8.

7. The eukaryotic RNA exosome. Januszyk, K.; Lima, C. D. *Curr. Opin. Struct. Biol.* **2014**, *24c*, 132-40.

8. MicroRNA-independent roles of the RNase III enzymes Drosha and Dicer. Johanson, T. M.; Lew, A. M.; Chong, M. M. *Open Biol.* **2013**, *3*, 130-44.

9. T2 Family ribonucleases: ancient enzymes with diverse roles. Luhtala, N.; Parker, R. *Trends Biochem. Sci.* **2010**, *35*, 253-9.

10. Ribonuclease H: the enzymes in eukaryotes. Cerritelli, S. M.; Crouch, R. J. *FEBS J.* **2009**, *276*, 1494-505.

11. RNase-L control of cellular mRNAs: roles in biologic functions and mechanisms of substrate targeting. Brennan-Laun, S. E.; Ezelle, H. J.; Li, X. L.; Hassel, B. A. *J. Interferon Cytokine Res.* **2014**, *34*, 275-88.

12. Function, mechanism and regulation of bacterial ribonucleases. Nicholson, A. W. *FEMS Microbiol. Rev.* **1999**, *23*, 371-90.

13. RNase T_1/RNase T_2 family RNases. Irie, M. In *Ribonucleases: Structures and Functions*; D'Alessio, G., Riordan, J. F., Eds.; Academic Press: New York, 1997.

14. RNS2: A senescence-associated RNase of *Arabidopsis* that diverged from the S-RNases before speciation. Taylor, C. B.; Bariola, P. A.; delCardayré, S. B.; Raines, R. T.; Green, P. J. *Proc. Natl. Acad. Sci. U.S.A.* **1993**, *90*, 5118-22.

15. Ribonuclease A. Raines, R. T. *Chem. Rev.* **1998**, *98*, 1045-65.

16. Isolation from beef pancreas of a crystalline protein possessing ribonuclease activity. Kunitz, M. *Science* **1939**, *90*, 112-13.

17. The action of boiled pancreas extract on yeast nucleic acid. Jones, W. *J. Am. Physiol.* **1920**, *52*, 203-7.

18. The golden years of protein science. Neurath, H. *Protein Sci.* **1995**, *4*, 1939-43.

19. Biological function of pancreatic ribonuclease. Barnard, E. A. *Nature* **1969**, *221*, 340-4.

20. Elevated serum ribonuclease in patients with pancreatic cancer. Reddi, K. K.; Holland, J. F. *Proc. Natl. Acad. Sci. U.S.A.* **1976**, *73*, 2308-10.

21. Ribonuclease as a tumour marker for pancreatic carcinoma. Doran, G.; Allen-Mersh, T. G.; Reynolds, K. W. *J. Clin. Pathol.* **1980**, *33*, 1212-3.

22. Evolutionary rate at the molecular level. Kimura, M. *Nature* **1968**, *217*, 624-6.

23. Serum RNase in the diagnosis of pancreatic carcinoma. Peterson, L. M. *Proc. Natl. Acad. Sci. U.S.A.* **1979**, *76*, 2630-4.

24. "Plasma"-type ribonuclease in pancreatic cancer diagnosis: a critical appraisal. Fabris, C.; Farini, R.; del Favero, G.; Piccoli, A.; Naccarato, R. *Hepatogastroenterology* **1981**, *28*, 316-8.

25. Sequences related to the ox pancreatic ribonuclease coding region in the genomic DNA of mammalian species. Breukelman, H. J.; Beintema, J. J.; Confalone, E.; Costanzo, C.; Sasso, M. P.; Carsana, A.; Palmieri, M.; Furia, A. *J. Mol. Evol.* **1993**, *37*, 29-35.

26. Tissue-specific expression of pancreatic-type RNases and RNase inhibitor in humans. Futami, J.; Tsushima, Y.; Murato, Y.; Tada, H.; Sasaki, J.; Seno, M.; Yamada, H. *DNA Cell Biol.* **1997**, *16*, 413-9.

27. Ribonuclease inhibitor: structure and function. Dickson, K. A.; Haigis, M. C.; Raines, R. T. *Prog. Nucleic Acid Res. Mol. Biol.* **2005**, *80*, 349-74.

28. Structure and action of mammalian ribonuclease (angiogenin) inhibitor. Lee, F. S.; Vallee, B. L. *Prog. Nucleic Acid Res. Mol. Biol.* **1993**, *44*, 1-30.

29. Ribonuclease inhibitor. Hofsteenge, J. In *Ribonucleases: Structures and Functions*; D'Alessio, G., Riordan, J. F., Eds.; Academic Press: New York, 1997, p 621-58.

30. Molecular evolution of the ribonuclease superfamily. Beintema, J. J.; Schüller, C.; Irie, M.; Carsana, A. *Prog. Biophys. Molec. Biol.* **1988**, *51*, 165-92.

31. The eight human "canonical" ribonucleases: molecular diversity, catalytic properties, and special biological actions of the enzyme proteins. Sorrentino, S. *FEBS Lett.* **2010**, *584*, 2194-200.

32. The RNase A superfamily: generation of diversity and innate host defense. Dyer, K. D.; Rosenberg, H. F. *Mol. Divers.* **2006**, *10*, 585-97.

33. Evasion of ribonuclease inhibitor as a determinant of ribonuclease cytotoxicity. Rutkoski, T. J.; Raines, R. T. *Curr. Pharm. Biotechnol.* **2008**, *9*, 185-9.

34. The ribonuclease A superfamily of mammals and birds: identifying new members and tracing evolutionary histories. Cho, S.; Beintema, J. J.; Zhang, J. *Genomics* **2005**, *85*, 208-20.

35. Mapping, phylogenetic and expression analysis of the RNase (RNaseA) locus in cattle. Wheeler, T. T.; Maqbool, N. J.; Gupta, S. K. *J. Mol. Evol.* **2012**, *74*, 237-48.

36. Characterization of ribonucleases and ribonuclease inhibitor in subcellular fractions from rat adrenals. Girija, N. S.; Sreenivasan, A. *Biochem J.* **1966**, *98*, 562-6.

37. Living and dying for inflammation: neutrophils, eosinophils, basophils. Geering, B.; Stoeckle, C.; Conus, S.; Simon, H. U. *Trends Immunol.* **2013**, *34*, 398-409.

38. Eosinophils: changing perspectives in health and disease. Rosenberg, H. F.; Dyer, K. D.; Foster, P. S. *Nat. Rev. Immunol.* **2013**, *13*, 9-22.

39. Human ribonuclease A superfamily members, eosinophil-derived neurotoxin and pancreatic ribonuclease, induce dendritic cell maturation and activation. Yang, D.; Chen, Q.; Rosenberg, H. F.; Rybak, S. M.; Newton, D. L.; Wang, Z. Y.; Fu, Q.; Tchernev, V. T.; Wang, M.; Schweitzer, B.; Kingsmore, S. F.; Patel, D. D.; Oppenheim, J. J.; Howard, O. M. *J. Immunol.* **2004**, *173*, 6134-42.

40. Eosinophil-derived neurotoxin / RNase 2: connecting the past, the present and the future. Rosenberg, H. F. *Curr. Pharm. Biotechnol.* **2008**, *9*, 135-40.

41. The antipathogen activities of eosinophil cationic protein. Boix, E.; Torrent, M.; Sanchez, D.; Nogues, M. V. *Curr. Pharm. Biotechnol.* **2008**, *9*, 141-52.

42. Eosinophil cationic protein: overview of biological and genetic features. de Oliveira, P. C.; de Lima, P. O.; Oliveira, D. T.; Pereira, M. C. *DNA Cell Biol.* **2012**, *31*, 1442-6.

43. Eosinophil cationic protein and eosinophil-derived neurotoxin. Rosenberg, H. F.; Dyer, K. D. *J. Biol. Chem.* **1995**, *270*, 21539-44.

44. Rapid evolution of a unique family of primate ribonuclease genes. Rosenberg, H. F.; Dyer, K. D.; Tiffany, H. L.; Gonzalez, M. *Nature Genet.* **1995**, *10*, 219-23.

45. Of mice and not men: differences between mouse and human immunology. Mestas, J.; Hughes, C. C. *J. Immunol.* **2004**, *172*, 2731-8.

46. The amino acid sequence of human ribonuclease 4, a highly conserved ribonuclease that cleaves specifically on the 3' side of uridine. Zhou, H.-M.; Strydom, D. J. *Eur. J. Biochem.* **1993**, *217*, 401-10.

47. Ribonuclease 4, an evolutionarily highly conserved member of the superfamily. Hofsteenge, J.; Vicentini, A.; Zelenko, O. *Cell. Mol. Life Sci.* **1998**, *54*, 804-10.

48. Ribonuclease 4 protects neuron degeneration by promoting angiogenesis, neurogenesis, and neuronal survival under stress. Li, S.; Sheng, J.; Hu, J. K.; Yu, W.; Kishikawa, H.; Hu, M. G.; Shima, K.; Wu, D.; Xu, Z.; Xin, W.; Sims, K. B.; Landers, J. E.; Brown, R. H., Jr.; Hu, G. F. *Angiogenesis* **2013**, *16*, 387-404.

49. The angiogenins. Strydom, D. J. *Cell. Mol. Life Sci.* **1998**, *54*, 811-24.

50. Ribonuclease inhibitor regulates neovascularization by human angiogenin. Dickson, K. A.; Kang, D. K.; Kwon, Y. S.; Kim, J. C.; Leland, P. A.; Kim, B. M.; Chang, S. I.; Raines, R. T. *Biochemistry* **2009**, *48*, 3804-6.

51. Targeting angiogenin in therapy of amyotropic lateral sclerosis. Kishikawa, H.; Wu, D.; Hu, G. F. *Expert Opin. Ther. Targets* **2008**, *12*, 1229-42.

52. Angiogenin induces modifications in the astrocyte secretome: relevance to amyotrophic lateral sclerosis. Skorupa, A.; Urbach, S.; Vigy, O.; King, M. A.; Chaumont-Dubel, S.; Prehn, J. H.; Marin, P. *J. Proteomics* **2013**, *91*, 274-85.

53. Angiogenin variants in Parkinson disease and amyotrophic lateral sclerosis. van Es, M. A.; Schelhaas, H. J.; van Vught, P. W.; Ticozzi, N.; Andersen, P. M.; Groen, E. J.; Schulte, C.; Blauw, H. M.; Koppers, M.; Diekstra, F. P.; Fumoto, K.; LeClerc, A. L.; Keagle, P.; Bloem, B. R.; Scheffer, H.; van Nuenen, B. F.; van Blitterswijk, M.; van Rheenen, W.; Wills, A. M.; Lowe, P. P.; Hu, G. F.; Yu, W.; Kishikawa, H.; Wu, D.; Folkerth, R. D.; Mariani, C.; Goldwurm, S.; Pezzoli, G.; Van Damme, P.; Lemmens, R.; Dahlberg, C.; Birve, A.; Fernandez-Santiago, R.; Waibel, S.; Klein, C.; Weber, M.; van der Kooi, A. J.; de Visser, M.; Verbaan, D.; van Hilten, J. J.; Heutink, P.; Hennekam, E. A.; Cuppen, E.; Berg, D.; Brown, R. H., Jr.; Silani, V.; Gasser, T.; Ludolph, A. C.; Robberecht, W.; Ophoff, R. A.; Veldink, J. H.; Pasterkamp, R. J.; de Bakker, P. I.; Landers, J. E.; van de Warrenburg, B. P.; van den Berg, L. H. *Ann. Neurol.* **2011**, *70*, 964-73.

54. Angiogenin enhances cell migration by regulating stress fiber assembly and focal adhesion dynamics. Wei, S.; Gao, X.; Du, J.; Su, J.; Xu, Z. *PLoS One* **2011**, *6*, e28797.

55. Degradation by stratum corneum proteases prevents endogenous RNase inhibitor from blocking antimicrobial activities of RNase 5 and RNase 7. Abtin, A.; Eckhart, L.; Mildner,

M.; Ghannadan, M.; Harder, J.; Schroder, J. M.; Tschachler, E. *J. Invest. Dermatol.* **2009**, *129*, 2193-201.

56. Molecular cloning and characterization of a novel human ribonuclease (RNase k6): increasing diversity in the enlarging ribonuclease gene family. Rosenberg, H. F.; Dyer, K. D. *Nucleic Acids Res.* **1996**, *24*, 3507-13.

57. Signalling pathways involved in ribonuclease-7 expression. Mohammed, I.; Yeung, A.; Abedin, A.; Hopkinson, A.; Dua, H. S. *Cell Mol Life Sci* **2011**, *68*, 1941-52.

58. Ribonuclease 7, an antimicrobial peptide upregulated during infection, contributes to microbial defense of the human urinary tract. Spencer, J. D.; Schwaderer, A. L.; Wang, H.; Bartz, J.; Kline, J.; Eichler, T.; DeSouza, K. R.; Sims-Lucas, S.; Baker, P.; Hains, D. S. *Kidney Int.* **2013**, *83*, 615-25.

59. Human hair follicle epithelium has an antimicrobial defence system that includes the inducible antimicrobial peptide psoriasin (S100A7) and RNase 7. Reithmayer, K.; Meyer, K. C.; Kleditzsch, P.; Tiede, S.; Uppalapati, S. K.; Glaser, R.; Harder, J.; Schroder, J. M.; Paus, R. *Br. J. Dermatol.* **2009**, *161*, 78-89.

60. An endogenous ribonuclease inhibitor regulates the antimicrobial activity of ribonuclease 7 in the human urinary tract. Spencer, J. D.; Schwaderer, A. L.; Eichler, T.; Wang, H.; Kline, J.; Justice, S. S.; Cohen, D. M.; Hains, D. S. *Kidney Int.* **2013**, *85*, 1179-91.

61. RNase 8, a novel RNase A superfamily ribonuclease expressed uniquely in placenta. Zhang, J.; Dyer, K. D.; Rosenberg, H. F. *Nucleic Acids Res.* **2002**, *30*, 1169-75.

62. Genetic diversity of human RNase 8. Chan, C. C.; Moser, J. M.; Dyer, K. D.; Percopo, C. M.; Rosenberg, H. F. *BMC Genomics* **2012**, *13*, 40.

63. Human ribonuclease 9, a member of ribonuclease A superfamily, specifically expressed in epididymis, is a novel sperm-binding protein. Cheng, G. Z.; Li, J. Y.; Li, F.; Wang, H. Y.; Shi, G. X. *Asian J. Androl.* **2009**, *11*, 240-51.

64. Cloning, expression and location of RNase9 in human epididymis. Liu, J.; Li, J.; Wang, H.; Zhang, C.; Li, N.; Lin, Y.; Liu, J.; Wang, W. *BMC Res. Notes* **2008**, *1*, 111.

65. Impaired sperm maturation in Rnase9 knockout mice. Westmuckett, A. D.; Nguyen, E. B.; Herlea-Pana, O. M.; Alvau, A.; Salicioni, A. M.; Moore, K. L. *Biol. Reprod.* **2014**. Advance online publication. doi: 10.1095/biolreprod.113.116863

66. Epididymal protein Rnase10 is required for post-testicular sperm maturation and male fertility. Krutskikh, A.; Poliandri, A.; Cabrera-Sharp, V.; Dacheux, J. L.; Poutanen, M.; Huhtaniemi, I. *FASEB J.* **2012**, *26*, 4198-209.

67. Ribonucleases: structural and biochemical insights into cytotoxic activity. Johnson, R. J. *Ph.D. Thesis, University of Wisconsin–Madison* **2007**.

68. Genetic architecture of resilience of executive functioning. Mukherjee, S.; Kim, S.; Gibbons, L. E.; Nho, K.; Risacher, S. L.; Glymour, M. M.; Habeck, C.; Lee, G. J.; Mormino, E.; Ertekin-Taner, N.; Montine, T. J.; Decarli, C.; Saykin, A. J.; Crane, P. K. *Brain Imaging Behav.* **2012**, *6*, 621-33.

69. Purification and properties of an alkaline ribonuclease from the hepatic cytosol fraction of bullfrog, *Rana catesbeiana*. Nagano, H.; Kiuchi, H.; Abe, Y.; Shukuya, R. *J. Biochem.* **1976**, *80*, 19-26.

70. Onconase and Amphinase, the antitumor ribonucleases from *Rana pipiens* oocytes. Ardelt, W.; Shogen, K.; Darzynkiewicz, Z. *Curr. Pharm. Biotechnol.* **2008**, *9*, 215-25.

71. Inhibition of cell proliferation by *Rana catesbeiana* and *Rana japonica* lectins belonging to the ribonuclease superfamily. Nitta, K.; Ozaki, K.; Ishikawa, M.; Furusawa, S.; Hosono, M.; Kawauchi, H.; Sasaki, K.; Takayanagi, Y.; Tsuiki, S.; Hakomori, S. *Cancer Res.* **1994**, *54*, 920-7.

72. Comprehensive comparison of the cytotoxic activities of onconase and bovine seminal ribonuclease. Matoušek, J.; Souček, J.; Slavík, T.; Tománek, M.; Lee, J. E.; Raines, R. T. *Comp. Biochem. Physiol.* **2003**, *136C*, 343-56.

73. Characterization of a ribonuclease gene and encoded protein from the reptile, Iguana iguana. Nitto, T.; Lin, C.; Dyer, K. D.; Wagner, R. A.; Rosenberg, H. F. *Gene* **2005**, *352*, 36-44.

74. Evolution and function of leukocyte RNase A ribonucleases of the avian species, Gallus gallus. Nitto, T.; Dyer, K. D.; Czapiga, M.; Rosenberg, H. F. *J. Biol. Chem.* **2006**, *281*, 25622-34.

75. Ribonucleases and angiogenins from fish. Pizzo, E.; Buonanno, P.; Di Maro, A.; Ponticelli, S.; De Falco, S.; Quarto, N.; Cubellis, M. V.; D'Alessio, G. *J. Biol. Chem.* **2006**, *281*, 27454-60.

76. Ribonucleases with angiogenic and bactericidal activities from the Atlantic salmon. Pizzo, E.; Varcamonti, M.; Di Maro, A.; Zanfardino, A.; Giancola, C.; D'Alessio, G. *FEBS J.* **2008**, *275*, 1283-95.

77. A new RNase sheds light on the RNase/angiogenin subfamily from zebrafish. Pizzo, E.; Merlino, A.; Turano, M.; Russo Krauss, I.; Coscia, F.; Zanfardino, A.; Varcamonti, M.; Furia, A.; Giancola, C.; Mazzarella, L.; Sica, F.; D'Alessio, G. *Biochem J.* **2011**, *433*, 345-55.

78. Zebrafish ribonucleases are bactericidal: implications for the origin of the vertebrate RNase A superfamily. Cho, S.; Zhang, J. *Mol. Biol. Evol.* **2007**, *24*, 1259-68.

79. A gene atlas of the mouse and human protein-encoding transcriptomes. Su, A. I.; Wiltshire, T.; Batalov, S.; Lapp, H.; Ching, K. A.; Block, D.; Zhang, J.; Soden, R.; Hayakawa, M.; Kreiman, G.; Cooke, M. P.; Walker, J. R.; Hogenesch, J. B. *Proc. Natl. Acad. Sci. U.S.A.* **2004**, *101*, 6062-7.

80. Evolution of mammalian pancreatic ribonucleases. Beintema, J. J.; Lenstra, J. A. In *Macromolecular Sequences in Systematic and Evolutionary Biology*; Goodman, M., Ed.; Plenum: New York, 1982, p 43-73.

81. Evolutionary reconstructions in the ribonuclease family. Benner, S. A.; Ciglic, M. I.; Haugg, M.; Jermann, T. M.; Opitz, J. G.; Raillard-Yoon, S.-A.; Souček, J.; Stackhouse, J.; Trabesinger-Rüf, N.; Trautwein, K.; Zankel, T. R. In *Ribonucleases: Structures and Functions*; D'Alessio, G., Riordan, J. F., Eds.; Academic Press: New York, 1997, p 213-43.

82. Adaptive evolution of a duplicated pancreatic ribonuclease gene in a leaf-eating monkey. Zhang, J.; Zhang, Y. P.; Rosenberg, H. F. *Nat. Genet.* **2002**, *30*, 411-5.

83. Human pancreatic-type and nonpancreatic-type ribonucleases: a direct side-by-side comparison of their catalytic properties. Sorrentino, S.; Libonati, M. *Arch. Biochem. Biophys.* **1994**, *312*, 340-8.

84. Degradation of double-stranded RNA by mammalian pancreatic-type ribonucleases. Libonati, M.; Sorrentino, S. *Methods Enzymol.* **2001**, *341*, 234-48.

85. Hybridase activity of human ribonuclease-1 revealed by a real-time fluorometric assay. Potenza, N.; Salvatore, V.; Migliozzi, A.; Martone, V.; Nobile, V.; Russo, A. *Nucleic Acids Res.* **2006**, *34*, 2906-13.

86. Degradation of double-stranded RNA by human pancreatic ribonuclease: crucial role of noncatalytic basic amino acid residues. Sorrentino, S.; Naddeo, M.; Russo, A.; D'Alessio, G. *Biochemistry* **2003**, *42*, 10182-90.

87. Distribution of two urinary ribonuclease-like enzymes in human organs and body fluids. Morita, T.; Niwata, Y.; Ohgi, K.; Ogawa, M.; Irie, M. *J. Biochem.* **1986**, *99*, 17-25.

88. Immunological assay of pancreatic ribonuclease in serum as an indicator of pancreatic cancer. Weickmann, J. L.; Olson, E. M.; Glitz, D. G. *Cancer Res.* **1984**, *44*, 1682-7.

89. Expression and localisation of vascular ribonucleases in endothelial cells. Fischer, S.; Nishio, M.; Dadkhahi, S.; Gansler, J.; Saffarzadeh, M.; Shibamiyama, A.; Kral, N.; Baal, N.; Koyama, T.; Deindl, E.; Preissner, K. T. *Thromb. Haemost.* **2011**, *105*, 345-55.

90. The amino acid sequence of human pancreatic ribonuclease. Beintema, J. J.; Wietzes, P.; Weickmann, J. L.; Glitz, D. G. *Anal. Biochem.* **1984**, *136*, 48-64.

91. Lysozyme and RNases as anti-HIV components in beta-core preparations of human chorionic gonadotropin. Lee-Huang, S.; Huang, P. L.; Sun, Y.; Kung, H. F.; Blithe, D. L.; Chen, H. C. *Proc. Natl. Acad. Sci. U.S.A.* **1999**, *96*, 2678-81.

92. Serum alkaline ribonuclease derived from vascular endothelial cells is raised in patients with rheumatoid vasculitis. Oribe, M.; Shingu, M.; Nobunaga, M. *Ann. Rheum. Dis.* **1986**, *45*, 937-40.

93. Heterogeneity in the glycosylation pattern of human pancreatic ribonuclease. Ribó, M.; Beintema, J. J.; Osset, M.; Fernández, E.; Bravo, J.; de Llorens, R.; Cuchillo, C. M. *Biol. Chem. Hoppe-Seyler* **1994**, *375*, 357-63.

94. Glycosylation of serum ribonuclease 1 indicates a major endothelial origian and reveals an increase in core fucosylation in pancreatic cancer. Barrabés, S.; Pagès-Pons, L.; Radcliffe, C. M.; Tabarés, G.; Fort, E.; Royle, L.; Harvey, D. J.; Moenner, M.; Dwek, R. A.; Rudd, P. M.; De Llorens, R.; Peracaula, R. *Glycobiology* **2007**, *17*, 388-400.

95. Human endothelial cells selectively express large amounts of pancreatic-type ribonuclease (RNase 1). Landre, J. B.; Hewett, P. W.; Olivot, J. M.; Friedl, P.; Ko, Y.; Sachinidis, A.; Moenner, M. *J. Cell. Biochem.* **2002**, *86*, 540-52.

96. Immune regulation by microvascular endothelial cells: directing innate and adaptive immunity, coagulation, and inflammation. Danese, S.; Dejana, E.; Fiocchi, C. *J. Immunol.* **2007**, *178*, 6017-22.

97. Cell biology of endothelial cells. Jaffe, E. A. *Hum. Pathol.* **1987**, *18*, 234-9.

98. Endothelial function in different organs. Bassenge, E. *Prog. Cardiovasc. Dis.* **1996**, *39*, 209-28.

99. Functional architecture of Weibel-Palade bodies. Valentijn, K. M.; Sadler, J. E.; Valentijn, J. A.; Voorberg, J.; Eikenboom, J. *Blood* **2011**, *117*, 5033-43.

100. Extracellular 'communicator RNA'. Benner, S. A. *FEBS Lett.* **1988**, *233*, 225-8.

101. Extracellular RNA: a new player in blood coagulation and vascular permeability. Preissner, K. T. *Hamostaseologie* **2007**, *27*, 373-7.

102. Extracellular RNA mediates endothelial-cell permeability via vascular endothelial growth factor. Fischer, S.; Gerriets, T.; Wessels, C.; Walberer, M.; Kostin, S.; Stolz, E.; Zheleva, K.; Hocke, A.; Hippenstiel, S.; Preissner, K. T. *Blood* **2007**, *110*, 2457-65.

103. Host-derived extracellular nucleic acids enhance innate immune responses, induce coagulation, and prolong survival upon infection in insects. Altincicek, B.; Stotzel, S.; Wygrecka, M.; Preissner, K. T.; Vilcinskas, A. *J. Immunol.* **2008**, *181*, 2705-12.

104. Circulating microRNAs as stable blood-based markers for cancer detection. Mitchell, P. S.; Parkin, R. K.; Kroh, E. M.; Fritz, B. R.; Wyman, S. K.; Pogosova-Agadjanyan, E. L.; Peterson, A.; Noteboom, J.; O'Briant, K. C.; Allen, A.; Lin, D. W.; Urban, N.; Drescher, C. W.; Knudsen, B. S.; Stirewalt, D. L.; Gentleman, R.; Vessella, R. L.; Nelson, P. S.; Martin, D. B.; Tewari, M. *Proc. Natl. Acad. Sci. U.S.A.* **2008**, *105*, 10513-8.

105. Extracellular RNA liberates tumor necrosis factor-alpha to promote tumor cell trafficking and progression. Fischer, S.; Gesierich, S.; Griemert, B.; Schanzer, A.; Acker, T.; Augustin, H. G.; Olsson, A. K.; Preissner, K. T. *Cancer Res.* **2013**, *73*, 5080-9.

106. Extracellular RNA promotes leukocyte recruitment in the vascular system by mobilising proinflammatory cytokines. Fischer, S.; Grantzow, T.; Pagel, J. I.; Tschernatsch, M.; Sperandio, M.; Preissner, K. T.; Deindl, E. *Thromb. Haemost.* **2012**, *108*, 730-41.

107. Extracellular plasma RNA from colon cancer patients is confined in a vesicle-like structure and is mRNA-enriched. Garcia, J. M.; Garcia, V.; Pena, C.; Dominguez, G.; Silva, J.; Diaz, R.; Espinosa, P.; Citores, M. J.; Collado, M.; Bonilla, F. *RNA* **2008**, *14*, 1424-32.

108. Argonaute2 complexes carry a population of circulating microRNAs independent of vesicles in human plasma. Arroyo, J. D.; Chevillet, J. R.; Kroh, E. M.; Ruf, I. K.; Pritchard, C. C.; Gibson, D. F.; Mitchell, P. S.; Bennett, C. F.; Pogosova-Agadjanyan, E. L.; Stirewalt, D. L.; Tait, J. F.; Tewari, M. *Proc. Natl. Acad. Sci. U.S.A.* **2011**, *108*, 5003-8.

109. Extracellular RNA constitutes a natural procoagulant cofactor in blood coagulation. Kannemeier, C.; Shibamiya, A.; Nakazawa, F.; Trusheim, H.; Ruppert, C.; Markart, P.; Song, Y.; Tzima, E.; Kennerknecht, E.; Niepmann, M.; von Bruehl, M. L.; Sedding, D.; Massberg, S.; Gunther, A.; Engelmann, B.; Preissner, K. T. *Proc. Natl. Acad. Sci. U.S.A.* **2007**, *104*, 6388-93.

110. Extracellular RNA is a natural cofactor for the (auto-)activation of Factor VII-activating protease (FSAP). Nakazawa, F.; Kannemeier, C.; Shibamiya, A.; Song, Y.; Tzima, E.; Schubert, U.; Koyama, T.; Niepmann, M.; Trusheim, H.; Engelmann, B.; Preissner, K. T. *Biochem. J.* **2005**, *385*, 831-8.

111. Toll-like receptors in antiviral innate immunity. Lester, S. N.; Li, K. *J. Mol. Biol.* **2014**, *426*, 1246-64.

112. Structural basis of toll-like receptor 3 signaling with double-stranded RNA. Liu, L.; Botos, I.; Wang, Y.; Leonard, J. N.; Shiloach, J.; Segal, D. M.; Davies, D. R. *Science* **2008**, *320*, 379-81.

113. When two strands are better than one: the mediators and modulators of the cellular responses to double-stranded RNA. Jacobs, B. L.; Langland, J. O. *Virology* **1996**, *219*, 339-49.

114. RNase therapy assessed by magnetic resonance imaging reduces cerebral edema and infarction size in acute stroke. Walberer, M.; Tschernatsch, M.; Fischer, S.; Ritschel, N.; Volk, K.; Friedrich, C.; Bachmann, G.; Mueller, C.; Kaps, M.; Nedelmann, M.; Blaes, F.; Preissner, K. T.; Gerriets, T. *Curr. Neurovasc. Res.* **2009**, *6*, 12-9.

115. Glycosylation of human pancreatic ribonuclease: differences between normal and tumor states. Peracaula, R.; Royle, L.; Tabares, G.; Mallorqui-Fernandez, G.; Barrabes, S.; Harvey, D. J.; Dwek, R. A.; Rudd, P. M.; de Llorens, R. *Glycobiology* **2003**, *13*, 227-44.

116. Glycosylation of serum ribonuclease 1 indicates a major endothelial origin and reveals an increase in core fucosylation in pancreatic cancer. Barrabés, S.; Pagès-Pons, L.; Radcliffe, C. M.; Tabarés, G.; Fort, E.; Royle, L.; Harvey, D. J.; Moenner, M.; Dwek, R. A.; Rudd, P. M.; De Llorens, R.; Peracaula, R. *Glycobiology* **2007**, *17*, 388-400.

117. Differences in glycosylation pattern of human secretory ribonucleases. Beintema, J. J.; Blank, A.; Schieven, G. L.; Dekker, C. A.; Sorrentino, S.; Libonati, M. *Biochem. J.* **1988**, *255*, 501-5.

118. Glycans in cancer and inflammation--potential for therapeutics and diagnostics. Dube, D. H.; Bertozzi, C. R. *Nat. Rev. Drug Discov.* **2005**, *4*, 477-88.

119. Effect of glycosylation on the in vivo circulating half-life of ribonuclease. Baynes, J. W.; Wold, F. *J. Biol. Chem.* **1976**, *251*, 6016-24.

120. Glycosylation protects proteins against free radicals generated from toxic xenobiotics. Martinek, V.; Sklenar, J.; Dracinsky, M.; Sulc, M.; Hofbauerova, K.; Bezouska, K.; Frei, E.; Stiborova, M. *Toxicol. Sci.* **2010**, *117*, 359-74.

121. Kinetic and thermodynamic thermal stabilities of ribonuclease A and ribonuclease B. Arnold, U.; Ulbrich-Hofmann, R. *Biochemistry* **1997**, *36*, 2166-72.

122. Glycosylation of onconase increases it conformational stability and toxicity for cancer cells. Kim, B.-M.; Kim, H.; Raines, R. T.; Lee, Y. *Biochem. Biophys. Res. Commun.* **2004**, *315*, 976-83.

123. Strong, L. E.; Kink, J. A.; Pensinger, D; Mei, B.; Shahan, M.; Raines, R. T. (2012) Efficacy of ribonuclease QBI-139 in combination with standard of care therapies. *Cancer Res.* **72** (Suppl. 1), 1838

124. Strong, L. E.; Kink, J. A.; Mei, B.; Shahan, M. N.; Raines, R. T. (2012) First in human phase I clinical trial of QBI-139, a human ribonuclease variant, in solid tumors. *J. Clin. Oncol.* **30** (Suppl.), TPS3113.

125. First-in-human phase I trial of human ribonuclease variant QBI-139 in solid tumors. Strong, L. E.; Kink, J. A.; Mei, B.; Shahan, M. N.; Raines, R. T. Abstract 116629 for the 2013 ACSO Annual Meeting (May 31–June 4, 2013).

126. Longer action means better drug: tuning up protein therapeutics. Szlachcic, A.; Zakrzewska, M.; Otlewski, J. *Biotechnol. Adv.* **2011**.

127. Rational design and evaluation of mammalian ribonuclease cytotoxins. Lomax, J. E.; Eller, C. H.; Raines, R. T. *Methods Enzymol.* **2012**, *502*, 273-90.

128. Secretory ribonucleases are internalized by a dynamin-independent endocytic pathway. Haigis, M. C.; Raines, R. T. *J. Cell Sci.* **2003**, *116*, 313-24.

129. Disruption of shape-complementarity markers to create cytotoxic variants of ribonuclease A. Rutkoski, T. J.; Kurten, E. L.; Mitchell, J. C.; Raines, R. T. *J. Mol. Biol.* **2005**, *354*, 41-54.

130. Natural and engineered cytotoxic ribonucleases: therapeutic potential. Rybak, S. M.; Newton, D. L. *Exp. Cell Res.* **1999**, *253*, 325-35.

131. Cytotoxic ribonucleases: The dichotomy of Coulombic forces. Johnson, R. J.; Chao, T.-Y.; Lavis, L. D.; Raines, R. T. *Biochemistry* **2007**, *46*, 10308-16.

132. Cellular uptake of ribonuclease A relies on anionic glycans. Chao, T. Y.; Lavis, L. D.; Raines, R. T. *Biochemistry* **2010**, *49*, 10666-73.

133. Endocytotic internalization as a crucial factor for the cytotoxicity of ribonucleases. Leich, F.; Stohr, N.; Rietz, A.; Ulbrich-Hofmann, R.; Arnold, U. *J. Biol. Chem.* **2007**, *282*, 27640-6.

134. Ribonucleases as novel chemotherapeutics: the ranpirnase example. Lee, J. E.; Raines, R. T. *BioDrugs* **2008**, *22*, 53-8.

135. A cytotoxic ribonuclease: study of the mechanism of onconase cytotoxicity. Wu, Y.; Mikulski, S. M.; Ardelt, W.; Rybak, S. M.; Youle, R. J. *J. Biol. Chem.* **1993**, *268*, 10686-93.

136. Phase I human clinical trial of ONCONASE (P-30 Protein) administered intravenously on a weekly schedule in cancer patients with solid tumors. Mikulski, S. M.; Grossman, A. M.; Carter, P. W.; Shogen, K.; Costanzi, J. J. *Int. J. Oncol.* **1993**, *3*, 57-64.

137. Alfacell starts phase III of RNase drug onconase. Shrine, J. In *BioWorld Today* 1995, p 1,4.

138. Ribonucleases as a novel pro-apoptotic anticancer strategy: review of the preclinical and clinical data for ranpirnase. Costanzi, J.; Sidransky, D.; Navon, A.; Goldsweig, H. *Cancer Invest.* **2005**, *23*, 643-50.

139. Reversible nephrotoxicity of onconase and effect of lysine pH on renal onconase uptake. Vasandani, V. M.; Burris, J. A.; Sung, C. *Cancer Themother. Pharmacol.* **1999**, *44*, 164-9.
140. Molecular determinants in the plasma clearance and tissue distribution of ribonucleases of the ribonuclease A superfamily. Vasandani, V. M.; Wu, Y.-N.; Mikulski, S. M.; Youle, R. J.; Sung, C. *Cancer Res.* **1996**, *56*, 4180-6.

141. Contribution of active-site residues to the function of onconase, a ribonuclease with antitumoral activity. Lee, J. E.; Raines, R. T. *Biochemistry* **2003**, *42*, 11443-50.

142. Structural basis for catalysis by onconase. Lee, J. E.; Bae, E.; Bingman, C. A.; Phillips, G. N., Jr.; Raines, R. T. *J. Mol. Biol.* **2008**, *374*, 165-77.

143. Intraspecies regulation of ribonucleolytic activity. Johnson, R. J.; Lavis, L. D.; Raines, R. T. *Biochemistry* **2007**, *46*, 13131-140.

144. A structural basis of the interactions between leucine-rich repeats and protein ligands. Kobe, B.; Deisenhofer, J. *Nature* **1995**, *374*, 183-6.

145. Ribonuclease inhibitor as an intracellular sentry. Haigis, M. C.; Kurten, E. L.; Raines, R. T. *Nucleic Acids Res.* **2003**, *31*, 1024-32.

146. Ribonuclease A variants with potent cytotoxic activity. Leland, P. A.; Schultz, L. W.; Kim, B.-M.; Raines, R. T. *Proc. Natl. Acad. Sci. U.S.A.* **1998**, *95*, 10407-12.

147. Cytotoxic potential of ribonuclease and ribonuclease hybrid proteins. Rybak, S. M.; Saxena, S. K.; Ackerman, E. J.; Youle, R. J. *J. Biol. Chem.* **1991**, *266*, 21202-7.

148. Ribonuclease inhibitor regulations neovascularization by human angiogenin. Dickson, K. A.; Kang, D.-K.; Kwon, Y. S.; Kim, J. C.; Leland, P. A.; Kim, B.-M.; Chang, S.-I.; Raines, R. T. *Biochemistry* **2009**, *48*, 3804-6.

149. Human placental ribonuclease inhibitor abolishes both angiogenic and ribonucleolytic activities of angiogenin. Shapiro, R.; Vallee, B. L. *Proc. Natl. Acad. Sci. U.S.A.* **1987**, *84*, 2238-41.

150. *Ribonucleases: Structures and Functions*; D'Alessio, G.; Riordan, J. F., Eds.; Academic Press: New York, 1997.

151. Ribonuclease/angiogenin inhibitor 1 regulates stress-induced subcellular localization of angiogenin to control growth and survival. Pizzo, E.; Sarcinelli, C.; Sheng, J.; Fusco, S.; Formiggini, F.; Netti, P.; Yu, W.; D'Alessio, G.; Hu, G. F. *J. Cell Sci.* **2013**, *126*, 4308-19.

152. Oxidation of sulfhydryl groups of ribonuclease inhibitor in epithelial cells is sufficient for its intracellular degradation. Blázquez, M.; Fominaya, J. M.; Hofsteenge, J. *J. Biol. Chem.* **1996**, *271*, 18638-42.

153. Radical scavenging activity of ribonuclease inhibitor from cow placenta. Wang, S.; Li, H. *Biochemistry (Mosc.)* **2006**, *71*, 520-4.

154. The cytosolic ribonuclease inhibitor contributes to intracellular redox homeostasis. Monti, D. M.; Montesano Gesualdi, N.; Matoušek, J.; Esposito, F.; D'Alessio, G. *FEBS Lett.* **2007**, *581*, 930-4.

155. The antioxidant effects of ribonuclease inhibitor. Cui, X. Y.; Fu, P. F.; Pan, D. N.; Zhao, Y.; Zhao, J.; Zhao, B. C. *Free Radic. Res.* **2003**, *37*, 1079-85.

156. Ribonuclease inhibitors in human blood: comparative studies on the inhibitors detected in erythrocytes, platelets, mononuclear leukocytes and granulocytes. Nadano, D.; Yasuda, T.; Takeshita, H.; Kishi, K. *Int. J. Biochem. Cell Biol.* **1995**, *27*, 971-9.

157. Ribonuclease inhibitor protein of human erythrocytes: characterization, loss of activity in response to oxidative stress, and association with Heinz bodies. Moenner, M.; Vosoghi, M.; Ryazantsev, S.; Glitz, D. *Blood Cells Mol. Dis.* **1998**, *24*, 149-64.

158. Isozymes of ribonuclease in human serum and urine: a survey of patients with cystic fibrosis. Thomas, J. M.; Eigen, H.; Hodes, M. E. *Clin. Chim. Acta* **1981**, *111*, 199-209.

159. Effect of endotoxin on the serum ribonuclease activity in rats. Kutas, V.; Bertok, L.; Szabo, L. D. *J. Bacteriol.* **1969**, *100*, 550-1.

160. Muscle protein catabolism in the septic patient as measured by 3-methylhistidine excretion. Long, C. L.; Schiller, W. R.; Blakemore, W. S.; Geiger, J. W.; O'Dell, M.; Henderson, K. *Am. J. Clin. Nutr.* **1977**, *30*, 1349-52.

161. Endotoxin induces rat lung ribonuclease activity. Clerch, L. B.; Wright, A.; Massaro, D. *FEBS Lett.* **1993**, *328*, 250-2.

162. Effect of disease states on the ribonuclease concentration of body fluids. Levy, A. L.; Rottino, A. *Clin. Chem.* **1960**, *6*, 43-51.

163. Serum ribonuclease in patients with malignant disease. Zytko, J.; Cantero, A. *Can. Med. Assoc. J.* **1962**, *86*, 482-5.

164. Age and sex related reference values for serum ribonuclease. Coombes, E. J.; Shakespeare, P. G.; Batstone, G. F. *Clin. Chim. Acta* **1977**, *79*, 271-5.

165. Evidence of age-dependent activity increase of poly(C)-avid-serum ribonuclease in man. Francesconi, M.; Meryn, S.; Moser, K.; Bauer, K. *J. Clin. Chem. Clin. Biochem.* **1981**, *19*, 17-20.

166. Changes in serum and urinary ribonuclease activity in surgically treated cases of digestive organ tumors and various other diseases. Hisada, T. *Iryo* **1969**, *23*, 613-25.

167. Intrathecal origin of CSF ribonuclease: differences between infectious processes of the nervous system and multiple sclerosis. Allinquant, B.; Musenger, C.; Schuller, E. *Acta Neurol. Scand.* **1984**, *70*, 12-9.

168. Immune-complex vasculitis: role of complement and IgG-Fc receptor functions. Smiley, J. D.; Moore, S. E., Jr. *Am. J. Med. Sci.* **1989**, *298*, 267-77.

169. Observations on serum and urine alkaline ribonuclease activity and urate after burn injury in man. Coombes, E. J.; Shakespeare, P. G.; Batstone, G. F. *Clin. Chim. Acta* **1978**, *86*, 279-90.

170. Urinary alkaline ribonuclease activity in children with burns and scalds. Barlow, G. B.; Withear, S. H. *Clin. Chim. Acta* **1977**, *78*, 331-4.

171. Ribonuclease-inhibitor system abnormality in dystrophic mouse skeletal muscle. Little, B. W.; Meyer, W. L. *Science* **1970**, *170*, 747-9.

172. Effects of recombinant leukocyte interferon on ribonuclease activities in serum in chronic hepatitis B. Tsuji, H.; Murai, K.; Akagi, K.; Fujishima, M. *Clin. Chem.* **1990**, *36*, 913-6.

173. Serum ribonuclease in rheumatic disease: serum alkaline ribonuclease activities in rheumatic diseases, especially in malignant rheumatoid arthritis. Oribe, M. *Fukuoka Igaku Zasshi* **1984**, *75*, 524-33.

174. Serum ribonuclease in patients with lung carcinoma. Marabella, P. C.; Tritsch, G. L.; Moore, R. H.; Takita, H. *J. Surg. Oncol.* **1976**, *8*, 501-5.

175. Carcinoma of the lung and cigarette smoking: effect on serum ribonuclease activity. Maor, D.; Klein, M. E.; Kenady, D. E.; Chretien, P. B.; Mardiney, M. R., Jr. *J. Am. Med. Assoc.* **1978**, *239*, 2766-8.

176. Increase in serum ribonuclease activity after bilateral nephrectomy. Rabinovitch, M.; Dohi, S. R. *Am. J. Physiol.* **1956**, *187*, 525-8.

177. Serum ribonuclease activity in acute myocardial infarction. Sznajd, J.; Magdon, M.; Naskalski, J. W.; Uracz, R.; Wojcikiewicz, O. *Cor. Vasa.* **1981**, *23*, 241-7.

178. Fluctuations of ribonucleinase activity in the blood and urine of leukemia patients. Aleksandrowicz, J.; Spirer, L. *Sang* **1955**, *26*, 212-5.

179. Serum ribonuclease activity. Houck, J. C.; Berman, L. B. *J. Appl. Physiol.* **1958**, *12*, 473-6.

180. Serum nucleases as nonspecific antiviral factors and their role in artificial anti-influenza immunity. Maksimovich, M. B. *Vopr. Virusol.* **1984**, *29*, 682-7.

181. Serum ribonuclease activities and body weight loss. Karawya, E. M. *Bahrain Medical Bulletin* **1995**, *17*, 1-8.

182. Alteration of human serum ribonuclease activity in malignancy. Maor, D.; Mardiney, M. R., Jr. *CRC Crit. Rev. Clin. Lab. Sci.* **1978**, *10*, 89-111.

183. Serum ribonuclease activity in patients with simple or toxic goiter. Malolepszy, E.; Malolepszy, A.; Pawlik, L. *Przegl. Lek.* **1969**, *25*, 742-5.

184. Serum ribonuclease in urologic cancer: relation to host immunocompetence. Catalona, W. J.; Chretien, P. B.; Matthews, W. J.; Tarpley, J. L. *Urology* **1973**, *2*, 577-81.

185. A long-term effect of adult thymectomy on cortisone sensitivity and alkaline RNAse activity of murine lymphoid cells. Maor, D.; Bar-Eyal, A.; Eylan, E.; Alexander, P. *Biomedicine* **1976**, *25*, 45-7.

186. Alzheimer's disease brain: alterations in RNA levels and in a ribonuclease-inhibitor complex. Sajdel-Sulkowska, E. M.; Marotta, C. A. *Science* **1984**, *225*, 947-9.

187. Ribonuclease treatment of tick-borne encephalitis. Glukhov, B. N.; Jerusalimsky, A. P.; Canter, V. M.; Salganik, R. I. *Arch. Neurol.* **1976**, *33*, 598-603.

188. Serum ribonuclease activity in cancer patients. Kottel, R. H.; Hoch, S. O.; Parsons, R. G.; Hoch, J. A. *Br. J. Cancer* **1978**, *38*, 280-6.

189. Nucleases in the cerebrospinal fluid: ribonuclease in normal, neurologically normal, and in pathological CSF. Kovacs, E. *Can. J. Med. Sci.* **1953**, *31*, 437-46.

190. Nucleases in the cerebrospinal fluid: simultaneous determination of ribo- and desoxyribonuclease in the CSF of patients with poliomyelitis. Kovacs, E. *J. Pediatr.* **1955**, *46*, 691-8.

191. Alkaline ribonuclease activity is increased in rat sympathetic ganglia after nerve injury. Bates, D. J.; Good, R. T.; Austin, L. *Neurochem. Res.* **1985**, *10*, 953-67.

192. Purification and properties of human acid-thermostable ribonucleases, and diagnosis of childhood pancreatic fibrosis. Bardon, A.; Slerakowska, H.; Shugar, D. *Clin. Chim. Acta* **1976**, *67*, 231-43.

193. Serum deoxyribonuclease and ribonuclease in pancreatic cancer and chronic pancreatitis. Basso, D.; Fabris, C.; Meani, A.; Del Favero, G.; Panucci, A.; Vianello, D.; Piccoli, A.; Naccarato, R. *Tumori* **1985**, *71*, 529-32.

194. Some physical and chemical properties of Coxsackie viruses A9 and A10. Mattern, C. F. *Virology* **1962**, *17*, 520-32.

195. Serum ribonuclease in multiple myeloma. Fink, K.; Adams, W. S.; Skoog, W. A. *Am. J. Med.* **1971**, *50*, 450-7.

196. Salivary acid and alkaline ribonuclease in the different types of tumors. AL-Smaisim, M. F. *Medical Journal of Babylon* **2005**, *2*, 283-7.

197. Effect of hemodialysis on acid leukocyte-type ribonuclease, alkaline ribonuclease and polymorphonuclear elastase serum levels in patients with end-stage renal disease. Naskalski, J. W.; Kapusta, M.; Fedak, D.; Dumnicka, P.; Kusnierz-Cabala, B.; Kuzniewski, M.; Sulowicz, W. *Nephron Clin. Pract.* **2009**, *112*, c248-54.

198. Studies on infectious RNA of Japanese B encephalitis virus: change of RNase activity in mouse brains during virus and RNA infections. Liu, Y. Y.; Liu, H. C. *Sci. Sin.* **1963**, *12*, 1553-61.

199. Variations of ribonuclease in the blood and in urine in various types of leukemia. Aleksandrowicz, J.; Spirer, L. *Arch. Immunol. Ther. Exp. (Warsz)* **1954**, *2*, 31-6.

200. Effect on prolonged use of oral contraceptive pills on the activity of serum and vaginal ribonuclease. El-dardiry, N.; El-kabarity, H.; Maarei, S.; El-sahwi, S.; Kira, L.; Rizk, M.; El-sewedy, S. M.; Mostafa, M. H.; Saad, A. A.; El-zoghby, S. M. *Bull. Alexandria Fac.* **1980**, *16*, 359-65.

201. Increasing human serum ribonuclease activity is a concomitant phenomenon of ovarian carcinoma. Schleich, H. G.; Wiest, W. *J. Cancer Res. Clin. Oncol.* **1980**, *97*, 307-14.

202. Plasma ribonuclease: a marker for the detection of ovarian cancer. Sheid, B.; Lu, T.; Pedrinan, L.; Nelson, J. H., Jr. *Cancer* **1977**, *39*, 2204-8.

203. Alkaline ribonuclease activity in plasma and leucocytes of malnourished women. Reddy, V.; Mohanram, M.; Prabhavathi, P. *Nutr. Metab.* **1978**, *22*, 357-61.

204. Plasma and urine ribonuclease as a measure of nutritional status in children. Sigulem, D. M.; Brasel, J. A.; Velasco, E. G.; Rosso, P.; Winick, M. *Am. J. Clin. Nutr.* **1973**, *26*, 793-7.

205. The excretion of alkaline ribonuclease by children undergoing surgery. Barlow, G. B.; Whitear, S. H.; Wilkinson, A. W. *Br. J. Surg.* **1979**, *66*, 412-4.

206. Hormones as modulators of ribonuclease activity in lymphoid organs of immunized rats. Maor, D.; Eylan, E.; Alexander, P. *Biomedicine* **1974**, *21*, 107-9.

207. Epinephrine blockade of ribonuclease activity stimulation in lymphoid organs by cortisone and prostaglandin. Maor, D.; Niviy, S.; Eylan, E. *Biomedicine* **1973**, *19*, 374-8.

208. The hormonal control of ribonuclease activity in the lymphatic tissue of mice. Maor, D.; Eylan, E.; Alexander, P. *Acta Endocrinol. (Copenh.)* **1973**, *74*, 201-8.

209. Concerning the mechanism of the increased RNAse activity in lymphatic cells following whole-body irradiation. Maor, D.; Alexander, P. *Int. J. Radiat. Biol.* **1963**, *6*, 93-103.

210. Abnormal profile of human nucleolytic activity as a test for cancer. Drake, W. P.; Schmukler, M.; Pendergrast, W. J., Jr.; Davis, A. S.; Lichtenfeld, J. L.; Mardiney, M. R., Jr. *J. Natl. Cancer Inst.* **1975**, *55*, 1055-9.

211. MUSCLE: multiple sequence alignment with high accuracy and high throughput. Edgar, R. C. *Nucleic Acids Res.* **2004**, *32*, 1792-7.

212. MEGA5: molecular evolutionary genetics analysis using maximum likelihood, evolutionary distance, and maximum parsimony methods. Tamura, K.; Peterson, D.; Peterson, N.; Stecher, G.; Nei, M.; Kumar, S. *Mol. Biol. Evol.* **2011**, *28*, 2731-9.

213. A general empirical model of protein evolution derived from multiple protein families using a maximum-likelihood approach. Whelan, S.; Goldman, N. *Mol. Biol. Evol.* **2001**, *18*, 691-9.

214. Maximum likelihood phylogenetic estimation from DNA sequences with variable rates over sites: approximate methods. Yang, Z. *J. Mol. Evol.* **1994**, *39*, 306-14.

215. Inhibition of metastasis development by daily administration of ultralow doses of RNase A and DNase I. Patutina, O.; Mironova, N.; Ryabchikova, E.; Popova, N.; Nikolin, V.; Kaledin, V.; Vlassov, V.; Zenkova, M. *Biochimie* **2011**, *93*, 689-96.

216. Increased ribonuclease expression reduces inflammation and prolongs survival in TLR7 transgenic mice. Sun, X.; Wiedeman, A.; Agrawal, N.; Teal, T. H.; Tanaka, L.; Hudkins, K. L.; Alpers, C. E.; Bolland, S.; Buechler, M. B.; Hamerman, J. A.; Ledbetter, J. A.; Liggitt, D.; Elkon, K. B. *J. Immunol.* **2013**, *190*, 2536-43.

217. Role of extracellular RNA in atherosclerotic plaque formation in mice. Simsekyilmaz, S.; Cabrera-Fuentes, H. A.; Meiler, S.; Kostin, S.; Baumer, Y.; Liehn, E. A.; Weber, C.; Boisvert, W. A.; Preissner, K. T.; Zernecke, A. *Circulation* **2014**, *129*, 598-606.

218. Role of extracellular RNA and TLR3-Trif signaling in myocardial ischemia-reperfusion injury. Chen, C.; Feng, Y.; Zou, L.; Wang, L.; Chen, H. H.; Cai, J. Y.; Xu, J. M.; Sosnovik, D. E.; Chao, W. *J. Am. Heart Assoc.* **2014**, *3*, e000683.

219. Ribonuclease inhibits Kaposi's sarcoma. Griffiths, S. J.; Adams, D. J.; Talbot, S. J. *Nature* **1997**, *390*, 568.

220. Endowing human pancreatic ribonuclease with toxicity for cancer cells. Leland, P. A.; Staniszewski, K. E.; Kim, B.-M.; Raines, R. T. *J. Biol. Chem.* **2001**, *276*, 43095-102.

221. Inhibition of human pancreatic ribonuclease by the human ribonuclease inhibitor protein. Johnson, R. J.; McCoy, J. G.; Bingman, C. A.; Phillips, G. N., Jr.; Raines, R. T. *J. Mol. Biol.* **2007**, *367*, 434-49.

222. Antitumor activity of ribonuclease multimers created by site-specific covalent tethering. Rutkoski, T. J.; Kink, J. A.; Strong, L. E.; Schilling, C. I.; Raines, R. T. *Bioconjug. Chem.* **2010**, *21*, 1691-702.

223. Human ribonuclease with a pendant poly(ethylene glycol) inhibits tumor growth in mice. Rutkoski, T. J.; Kink, J. A.; Strong, L. E.; Raines, R. T. *Transl. Oncol.* **2013**, *6*, 392-7.

224. A fully human antitumor immunoRNase selective for ErbB-2-positive carcinomas. De Lorenzo, C.; Arciello, A.; Cozzolino, R.; Palmer, D. B.; Laccetti, P.; Piccoli, R.; D'Alessio, G. *Cancer Res.* **2004**, *64*, 4870-4.

225. Effects of a second-generation human anti-ErbB2 ImmunoRNase on trastuzumab-resistant tumors and cardiac cells. D'Avino, C.; Paciello, R.; Riccio, G.; Coppola, M.; Laccetti, P.; Maurea, N.; Raines, R. T.; De Lorenzo, C. *Protein Eng. Des. Sel.* **2014**, *27*, 83-8.

226. Preparation of potent cytotoxic ribonucleases by cationization: enhanced cellular uptake and decreased interaction with ribonuclease inhibitor by chemical modification of carboxyl groups. Futami, J.; Maeda, T.; Kitazoe, M.; Nukui, E.; Tada, H.; Seno, M.; Kosaka, M.; Yamada, H. *Biochemistry* **2001**, *26*, 7518-24.

227. Design of cytotoxic ribonucleases by cationization to enhance intracellular protein delivery. Futami, J.; Yamada, H. *Curr. Pharm. Biotechnol.* **2008**, *9*, 180-4.

228. Introduction to current and future protein therapeutics: a protein engineering perspective. Carter, P. J. *Exp. Cell Res.* **2011**, *317*, 1261-9.

229. Phase II trial of a single weekly intravenous dose of ranpirnase in patients with unresectable malignant mesothelioma. Mikulski, S. M.; Costanzi, J. J.; Vogelzang, N. J.; McCachren, S.; Taub, R. N.; Chun, H.; Mittelman, A.; Panella, T.; Puccio, C.; Fine, R.; Shogen, K. *J. Clin. Oncol.* **2002**, *20*, 274-81.

230. Ranpirnase—an antitumour ribonuclease: its potential role in malignant mesothelioma. Pavlakis, N.; Vogelzang, N. J. *Expert Opin. Biol. Ther.* **2006**, *6*, 391-99.

231. Ribonucleases as potential modalities in anticancer therapy. Ardelt, W.; Ardelt, B.; Darzynkiewicz, Z. *Eur. J. Pharmacol.* **2009**, *625*, 181-9.

232. Ribonucleases of different origins with a wide spectrum of medicinal applications. Fang, E. F.; Ng, T. B. *Biochim. Biophys. Acta* **2011**, *1815*, 65-74.

233. Cancer chemotherapy—ribonucleases to the rescue. Leland, P. A.; Raines, R. T. *Chem. Biol.* **2001**, *8*, 405-13.

234. Quantitative analysis of the effect of salt concentration on enzymatic catalysis. Park, C.; Raines, R. T. *J. Am. Chem. Soc.* **2001**, *123*, 11472-9.

235. A ribonuclease A variant with low catalytic activity but high cytotoxicity. Bretscher, L. E.; Abel, R. L.; Raines, R. T. *J. Biol. Chem.* **2000**, *275*, 9893-96.

236. Catalytic activity of bovine seminal ribonuclease is essential for its immunosuppressive and other biological activities. Kim, J.-S.; Souček, J.; Matoušek, J.; Raines, R. T. *Biochem. J.* **1995**, *308*, 547-50.

237. The structural stability of a protein is an important determinant of its proteolytic susceptibilityin *Escherichia coli*. Parsell, D. A.; Sauer, R. T. *J. Biol. Chem.* **1989**, *264*, 7590-5.

238. Conformational stability is a determinant of ribonuclease A cytotoxicity. Klink, T. A.; Raines, R. T. *J. Biol. Chem.* **2000**, *275*, 17463-7.

239. Genetic selection for critical residues in ribonucleases. Smith, B. D.; Raines, R. T. *J. Mol. Biol.* **2006**, *362*, 459-78.

240. Contribution of disulfide bonds to the conformational stability and catalytic activity of ribonuclease A. Klink, T. A.; Woycechowsky, K. J.; Taylor, K. M.; Raines, R. T. *Eur. J. Biochem.* **2000**, *267*, 566-72.

241. A synapomorphic disulfide bond is critical for the conformational stability and cytotoxicity of an amphibian ribonuclease. Leland, P. A.; Staniszewski, K. E.; Kim, B.-M.; Raines, R. T. *FEBS Lett.* **2000**, *477*, 203-7.

242. Hypersensitive substrate for ribonucleases. Kelemen, B. R.; Klink, T. A.; Behlke, M. A.; Eubanks, S. R.; Leland, P. A.; Raines, R. T. *Nucleic Acids Res.* **1999**, *27*, 3696-701.

243. Fast, facile, hypersensitive assays for ribonucleolytic activity. Park, C.; Kelemen, B. R.; Klink, T. A.; Sweeney, R. Y.; Behlke, M. A.; Eubanks, S. R.; Raines, R. T. *Methods Enzymol.* **2001**, *341*, 81-94.

244. The use of differential scanning fluorimetry to detect ligand interactions that promote protein stability. Niesen, F. H.; Berglund, H.; Vedadi, M. *Nat. Protoc.* **2007**, *2*, 2212-21.

245. Onconase cytotoxicity relies on the distribution of its positive charge. Turcotte, R. F.; Lavis, L. D.; Raines, R. T. *FEBS J.* **2009**, *276*, 3846-57.

246. Increasing the potency of a cytotoxin with an arginine graft. Fuchs, S. M.; Rutkoski, T. J.; Kung, V. M.; Groeschl, R. T.; Raines, R. T. *Protein Eng. Des. Sel.* **2007**, *20*, 505-9.

247. Polyarginine as a multifunctional fusion tag. Fuchs, S. M.; Raines, R. T. *Protein Sci.* **2005**, *14*, 1538-44.

248. Potentiation of ribonuclease cytotoxicity by a poly(amidoamine) dendrimer. Ellis, G. A.; Hornung, M. L.; Raines, R. T. *Bioorg. Med. Chem. Lett.* **2010**.

249. Site-specific folate conjugation to a cytotoxic protein. Smith, B. D.; Higgin, J. J.; Raines, R. T. *Bioorg. Med. Chem. Lett.* **2011**, *21*, 5029-32.

250. The nuclear transport capacity of a human-pancreatic ribonuclease variant is critical for its cytotoxicity. Tubert, P.; Rodriguez, M.; Ribo, M.; Benito, A.; Vilanova, M. *Invest. New Drugs* **2011**, *29*, 811-7.

251. Cytotoxicity of bovine seminal ribonuclease: Monomer versus dimer. Lee, J. E.; Raines, R. T. *Biochemistry* **2005**, *44*, 15760-7.

252. Tandemization endows bovine pancreatic ribonuclease with cytotoxic activity. Leich, F.; Köditz, J.; Ulbrich-Hofman, R.; Arnold, U. *J. Mol. Biol.* **2006**, *358*, 1305-13.

253. Crystal structure of RNase A tandem enzymes and their interaction with the cytosolic ribonuclease inhibitor. Arnold, U.; Leich, F.; Neumann, P.; Lilie, H.; Ulbrich-Hofmann, R. *FEBS J.* **2011**, *278*, 331-40.

254. Fluorogenic label for biomolecular imaging. Lavis, L. D.; Chao, T.-Y.; Raines, R. T. *ACS Chem. Biol.* **2006**, *1*, 252-60.

255. Fluorescence assay for the binding of ribonuclease A to the ribonuclease inhibitor protein. Abel, R. L.; Haigis, M. C.; Park, C.; Raines, R. T. *Anal. Biochem.* **2002**, *306*, 100-7.

256. Tuning the pK_a of fluorescein to optimize binding assays. Lavis, L. D.; Rutkoski, T. J.; Raines, R. T. *Anal. Chem.* **2007**, *79*, 6775-82.

257. Ribonuclease A: revealing structure–function relationships with semisynthesis. Messmore, J. M.; Fuchs, D. N.; Raines, R. T. *J. Am. Chem. Soc.* **1995**, *117*, 8057-60.

258. Tryptophan fluorescence as a probe of placental ribonuclease inhibitor binding to angiogenin. Lee, F. S.; Auld, D. S.; Vallee, B. L. *Biochemistry* **1989**, *28*, 219-24.

259. Creation of a zymogen. Plainkum, P.; Fuchs, S. M.; Wiyakrutta, S.; Raines, R. T. *Nat. Struct. Biol.* **2003**, *10*, 115-19.

260. A ribonuclease zymogen activated by the NS3 protease of the hepatitis C virus. Johnson, R. J.; Lin, S. R.; Raines, R. T. *FEBS J.* **2006**, *273*, 5457-65.

261. Design and characterization of an HIV-specific ribonuclease zymogen. Turcotte, R. F.; Raines, R. T. *AIDS Res. Hum. Retroviruses* **2008**, *24*, 1357-63.

262. Ruminal temperature may aid in the detection of subacute ruminal acidosis. AlZahal, O.; Kebreab, E.; France, J.; Froetschel, M.; McBride, B. *J. Dairy Sci.* **2008**, *91*, 202-7.

263. Dietary regulation of pancreatic enzyme synthesis, secretion and inactivation in the rat. Snook, J. T. *J. Nutr.* **1965**, *87*, 297-305.

264. Serum RNase in the diagnosis of pancreatic carcinoma. Peterson, L. M. *Proc. Natl. Acad. Sci. U.S.A.* **1979**, *76*, 2630-4.

265. Increased ribonuclease expression reduces inflammation and prolongs survival in TLR7 transgenic mice. Sun, X.; Wiedeman, A.; Agrawal, N.; Teal, T. H.; Tanaka, L.; Hudkins, K. L.; Alpers, C. E.; Bolland, S.; Buechler, M. B.; Hamerman, J. A.; Ledbetter, J. A.; Liggitt, D.; Elkon, K. B. *J. Immunol.* **2013**, *190*, 2536-43.

266. Extracellular RNA liberates tumor necrosis factor-alpha to promote tumor cell trafficking and progression. Fischer, S.; Gesierich, S.; Griemert, B.; Schanzer, A.; Acker, T.; Augustin, H. G.; Olsson, A. K.; Preissner, K. T. *Cancer Res.* **2013**, *73*, 5080-9.

267. Effects of a second-generation human anti-ErbB2 immunoRNase on trastuzumab-resistant tumors and cardiac cells. D'Avino, C.; Paciello, R.; Riccio, G.; Coppola, M.; Laccetti, P.; Maurea, N.; Raines, R. T.; De Lorenzo, C. *Protein Eng. Des. Select.* **2014**, *27*, 83-8.

268. Inclusion of cetaceans within the order Artiodactyla based on phylogenetic analysis of pancreatic ribonuclease genes. Kleineidam, R. G.; Pesole, G.; Breukelman, H. J.; Beintema, J. J.; Kastelein, R. A. *J. Mol. Evol.* **1999**, *48*, 360-8.

269. Molecular evolution of genes encoding ribonucleases in ruminant species. Confalone, E.; Beintema, J. J.; Sasso, M. P.; Carsana, A.; Palmieri, M.; Vento, M. T.; Furia, A. *J. Mol. Evol.* **1995**, *41*, 850-8.

270. Ribonucleases in ruminants. Beintema, J. J. *Science* **2002**, *297*, 1121-2.

271. Seminal RNase: a unique member of the ribonuclease superfamily. D'Alessio, G.; Di Donato, A.; Parente, A.; Piccoli, R. *Trends Biochem. Sci.* **1991**, *16*, 106-8.

272. Ribonucleases and their antitumor activity. Matoušek, J. *Comp. Biochem. Physiol.* **2001**, *129C*, 175-91.

273. Primary structure of a ribonuclease from bovine brain. Watanabe, H.; Katoh, H.; Ishii, M.; Komoda, Y.; Sanda, A.; Takizawa, Y.; Ohgi, K.; Irie, M. *J. Biochem.* **1988**, *104*, 939-45.

274. Characterization of a ribonuclease from bovine brain. Elson, M.; Glitz, D. G. *Biochemistry* **1975**, *14*, 1471-6.

275. Parallel functional changes in the digestive RNases of ruminants and colobines by divergent amino acid substitutions. Zhang, J. *Mol. Biol. Evol.* **2003**, *20*, 1310-7.

276. Cytotoxicity of bovine seminal ribonuclease: monomer versus dimer. Lee, J. E.; Raines, R. T. *Biochemistry* **2005**, *44*, 15760-7.

277. Contribution of electrostatics to the binding of pancreatic-type ribonucleases to membranes. Sundlass, N. K.; Eller, C. H.; Cui, Q.; Raines, R. T. *Biochemistry* **2013**, *52*, 6304-12.

278. High-throughput melting-temperature analysis of a monoclonal antibody by differential scanning fluorimetry in the presence of surfactants. Menzen, T.; Friess, W. *J. Pharm. Sci.* **2013**, *102*, 415-28.

279. The use of differential scanning fluorimetry to detect ligand interactions that promote protein stability. Niesen, F. H.; Berglund, H.; Vedadi, M. *Nat. Protoc.* **2007**, *2*, 2212-21.

280. Membrane binding of pH-sensitive influenza fusion peptides. Positioning, configuration, and induced leakage in a lipid vesicle model. Esbjorner, E. K.; Oglecka, K.; Lincoln, P.; Graslund, A.; Norden, B. *Biochemistry* **2007**, *46*, 13490-504.

281. Mechanism of leakage of contents of membrane vesicles determined by fluorescence requenching. Ladokhin, A. S.; Wimley, W. C.; Hristova, K.; White, S. H. *Methods Enzymol.* **1997**, *278*, 474-86.

282. MUSCLE: Multiple sequence alignment with high accuracy and high throughput. Edgar, R. C. *Nucleic Acids Res.* **2004**, *32*, 1792-7.

283. The rapid generation of mutation data matrices from protein sequences. Jones, D. T.; Taylor, W. R.; Thornton, J. M. *Comput. Appl. Biosci.* **1992**, *8*, 275-82.

284. Molecular cloning of the gene encoding the bovine brain ribonuclease and its expression in different regions of the brain. Sasso, M. P.; Carsana, A.; Confalone, E.; Cosi, C.; Sorrentino, S.; Viola, M.; Palmieri, M.; Russo, E.; Furia, A. *Nucleic Acids Res.* **1991**, *19*, 6469-74.

285. Ruminant brain ribonucleases: Expression and evolution. Zhao, W.; Confalone, E.; Breukelman, H. J.; Sasso, M. P.; Jekel, P. A.; Hodge, E.; Furia, A.; Beintema, J. J. *Biochim. Biophys. Acta* **2001**, *1547*, 95-103.

286. Antitumor action of seminal ribonuclease, its dimeric structure, and its resistance to the cytosolic ribonuclease inhibitor. Antignani, A.; Naddeo, M.; Cubellis, M. V.; Russo, A.; D'Alessio, G. *Biochemistry* **2001**, *40*, 3492-6.

287. Adaptive evolution of a duplicated pancreatic ribonuclease gene in a leaf-eating monkey. Zhang, J.; Zhang, Y. P.; Rosenberg, H. F. *Nat. Genet.* **2002**, *30*, 411-5.

288. Role of unique basic residues of human pancreatic ribonuclease in its catalysis and structural stability. Dey, P.; Islam, A.; Ahmad, F.; Batra, J. K. *Biochem. Biophys. Res. Commun.* **2007**, *360*, 809-14.

289. Degradation of double-stranded RNA by human pancreatic ribonuclease: crucial role of noncatalytic basic amino acid residue. Sorrentino, S.; Naddeo, M.; Russo, A.; D'Alessio, G. *Biochemistry* **2003**, *42*, 10182-90.

290. Bovine pancreatic ribonuclease: fifty years of the first enzymatic reaction mechanism. Cuchillo, C. M.; Nogués, M. V.; Raines, R. T. *Biochemistry* **2011**, *50*, 7835-41.

291. Back to the future: ribonuclease A. Marshall, G. R.; Feng, J. A.; Kuster, D. J. *Biopolymers* **2008**, *90*, 259-77.

292. Reconstructing the evolutionary history of the artiodactyl ribonuclease superfamily. Jermann, T. M.; Opitz, J. G.; Stackhouse, J.; Benner, S. A. *Nature* **1995**, *374*, 57-9.

293. Planetary biology—paleontological, geological, and molecular histories of life. Benner, S. A.; Caraco, M. D.; Thomson, J. M.; Gaucher, E. A. *Science* **2002**, *296*, 864-8.

294. The interferon response circuit: Induction and suppression by pathogenic viruses. Haller, O.; Kochs, G.; Weber, F. *Virology* **2006**, *344*, 119-30.

295. Pathogen recognition and innate immunity. Akira, S.; Uematsu, S.; Takeuchi, O. *Cell* **2006**, *124*, 5598-603.

296. Recognition of double-stranded RNA and activation of NF-kappaB by Toll-like receptor 3. Alexopoulou, L.; Holt, A. C.; Medzhitov, R.; Flavell, R. A. *Nature* **2001**, *413*, 732-8.

297. Recognition of single-stranded RNA viruses by Toll-like receptor 7. Lund, J. M.; Alexopoulou, L.; Sato, A.; Karow, M.; Adams, N. C.; Gale, N. W.; Iwasaki, A.; Flavel, R. A. *Proc. Natl. Acad. Sci. U.S.A.* **2004**, *101*, 5598-603.

298. Mechanism of ribonuclease A endocytosis: Analogies to cell-penetrating peptides. Chao, T.-Y.; Raines, R. T. *Biochemistry* **2011**, *50*, 8374-82.

299. Molecular modeling of protein–glycosaminoglycan interactions. Cardin, A. D.; Weintraub, H. J. *Arteriosclerosis* **1989**, *9*, 21-32.

300. Glycosaminoglycan–protein interactions: Definition of consensus sites in glycosaminoglycan binding proteins. Hileman, R. E.; Fromm, J. R.; Weiler, J. M.; Linhardt, R. J. *Bioessays* **1998**, *20*, 156-67.

301. The BBXB motif of RANTES is the principal site for heparin binding and controls receptor selectivity. Proudfoot, A. E.; Fritchley, S.; Borlat, F.; Shaw, J. P.; Vilbois, F.; Zwahlen, C.; Trkola, A.; Marchant, D.; Clapham, P. R.; Wells, T. N. *J. Biol. Chem.* **2001**, *276*, 10620-6.

302. Kinetic and equilibrium studies of the ribonuclease-catalyzed hydrolysis of uridine 2′,3′-cyclic phosphate. del Rosario, E. J.; Hammes, G. G. *Biochemistry* **1969**, *8*, 1884-9.

303. Composite active sites in bovine seminal ribonuclease. Mazzarella, L.; Mattia, C. A.; Capasso, S.; Di Lorenzo, G. *Gaz. Chim. Ital.* **1987**, *117*, 91-7.

304. The dual-mode quaternary structure of seminal RNase. Piccoli, R.; Tamburrini, M.; Piccialli, G.; Di Donato, A.; Parente, A.; D'Alessio, G. *Proc. Natl. Acad. Sci. U.S.A.* **1992**, *89*, 1870-4.

305. The influence of management, breed and season upon the pH of bull semen. Raps, G.; Cannon, C. Y. *J. Dairy Sci.* **1947**, *30*, 933-8.

306. The structure of the asparagine-linked sugar chains of bovine brain ribonuclease. Katoh, H.; Ohgi, K.; Irie, M.; Endo, T.; Kobata, A. *Carbohydr. Res.* **1990**, *195*, 273-93.

307. The importance of being proline: The interaction of proline-rich motifs in signaling proteins with their cognate domains. Kay, B. K.; Williamson, M. P.; Sudol, M. *FASEB J.* **2000**, *14*, 231-41.

308. Enforcing the positive charge of N-termini enhances membrane interaction and antitumor activity of bovine seminal ribonuclease. D'Errico, G.; Ercole, C.; Lista, M.; Pizzo, E.; Falanga, A.; Galdiero, S.; Spadaccini, R.; Picone, D. *Biochim. Biophys. Acta* **2011**, *1808*, 3007-15.

309. Structural diversity of leucine-rich repeat proteins. Kajava, A. V. *J. Mol. Biol.* **1998**, *277*, 519-27.

310. Crystal structure of porcine ribonuclease inhibitor, a protein with leucine-rich repeats. Kobe, B.; Deisenhofer, J. *Nature* **1993**, *366*, 751-6.

311. Mechanism of ribonuclease inhibition by ribonuclease inhibitor protein based on the crystal structure of its complex with ribonuclease A. Kobe, B.; Deisenhofer, J. *J. Mol. Biol.* **1996**, *264*, 1028-43.

312. Molecular recognition of human angiogenin by placental ribonuclease inhibitor—an X-ray crystallographic study at 2.0 Å resolution. Papageorgiou, A.; Shapiro, R.; Acharya, K.R. *EMBO J.* **1997**, *16*, 5162-77.

313. Rhodamine B and Rhodamine 101 as reference substances for fluorescence quantum yield measurements. Karstens, T.; Kobe, K. *J. Phys. Chem.* **1980**, *84*, 1871-2.

314. Variants of ribonuclease inhibitor that resist oxidation. Kim, B.-M.; Schultz, L. W.; Raines, R. T. *Protein Sci.* **1999**, *8*, 430-4.

315. Inactivation of ribonuclease inhibitor by thiol–disulfide exchange. Fominaya, J. M.; Hofsteenge, J. *J. Biol. Chem.* **1992**, *267*, 24655-60.

316. The ribonuclease/angiogenin inhibitor is also present in mitochondria and nuclei. Furia, A.; Moscato, M.; Cali, G.; Pizzo, E.; Confalone, E.; Amoroso, M. R.; Esposito, F.; Nitsch, L.; D'Alessio, G. *FEBS Lett.* **2011**, *585*, 613-7.

317. Oxidants, oxidative stress and the biology of ageing. Finkel, T.; Holbrook, N. J. *Nature* **2000**, *408*, 239-47.

318. Oxidative stress, inflammation, and cancer: how are they linked? Reuter, S.; Gupta, S. C.; Chaturvedi, M. M.; Aggarwal, B. B. *Free Radic. Biol. Med.* **2010**, *49*, 1603-16.

319. Disulfide stress: a novel type of oxidative stress in acute pancreatitis. Moreno, M. L.; Escobar, J.; Izquierdo-Alvarez, A.; Gil, A.; Perez, S.; Pereda, J.; Zapico, I.; Vento, M.; Sabater, L.; Marina, A.; Martinez-Ruiz, A.; Sastre, J. *Free Radic. Biol. Med.* **2014**. Advance online publication. doi: 10.1016/j.freeradbiomed.2014.01.009

320. RNH1 regulation of reactive oxygen species contributes to histone deacetylase inhibitor resistance in gastric cancer cells. Zhu, Y.; Das, K.; Wu, J.; Lee, M. H.; Tan, P. *Oncogene* **2013**, *33*, 1527-37.

321. Evolution of vertebrate ribonucleases: ribonuclease A superfamily. Beintema, J. J.; Breukelman, H. J.; Carsana, A.; Furia, A. In *Ribonucleases: Structures and Functions*; D'Alessio, G., Riordan, J. F., Eds.; Academic Press: New York, 1997, p 245-69.

322. A new tagged-TEV protease: construction, optimisation of production, purification and test activity. Miladi, B.; Bouallagui, H.; Dridi, C.; El Marjou, A.; Boeuf, G.; Di Martino, P.; Dufour, F.; Elm'Selmi, A. *Protein Expr. Purif.* **2011**, *75*, 75-82.

323. Contribution of electrostatics to the binding of pancreatic-type ribonucleases to membranes. Sundlass, N. K.; Eller, C. H.; Cui, Q.; Raines, R. T. *Biochemistry* **2013**, *52*, 6304-12.

324. High-throughput melting-temperature analysis of a monoclonal antibody by differential scanning fluorimetry in the presence of surfactants. Menzen, T.; Friess, W. *J. Pharm. Sci.* **2013**, *102*, 415-28.

325. Towards rationalization of crystallization screening for small- to medium-sized academic laboratories: the PACT/JCSG+ strategy. Newman, J.; Egan, D.; Walter, T. S.; Meged, R.;

Berry, I.; Ben Jelloul, M.; Sussman, J. L.; Stuart, D. I.; Perrakis, A. *Acta Crystallogr. D Biol. Crystallogr.* **2005**, *61*, 1426-31.

326. Phaser crystallographic software. McCoy, A. J.; Grosse-Kunstleve, R. W.; Adams, P. D.; Winn, M. D.; Storoni, L. C.; Read, R. J. *J. Appl. Crystallogr.* **2007**, *40*, 658-74.

327. Features and development of Coot. Emsley, P.; Lohkamp, B.; Scott, W. G.; Cowtan, K. *Acta Crystallogr. D Biol. Crystallogr.* **2010**, *66*, 486-501.

328. PHENIX: a comprehensive Python-based system for macromolecular structure solution. Adams, P. D.; Afonine, P. V.; Bunkoczi, G.; Chen, V. B.; Davis, I. W.; Echols, N.; Headd, J. J.; Hung, L. W.; Kapral, G. J.; Grosse-Kunstleve, R. W.; McCoy, A. J.; Moriarty, N. W.; Oeffner, R.; Read, R. J.; Richardson, D. C.; Richardson, J. S.; Terwilliger, T. C.; Zwart, P. H. *Acta Crystallogr. D Biol. Crystallogr.* **2010**, *66*, 213-21.

329. MolProbity: all-atom structure validation for macromolecular crystallography. Chen, V. B.; Arendall, W. B., 3rd; Headd, J. J.; Keedy, D. A.; Immormino, R. M.; Kapral, G. J.; Murray, L. W.; Richardson, J. S.; Richardson, D. C. *Acta Crystallogr. D Biol. Crystallogr.* **2010**, *66*, 12-21.

330. PDBsum: summaries and analyses of PDB structures. Laskowski, R. A. *Nucleic Acids Res.* **2001**, *29*, 221-2.

331. Satisfying hydrogen bonding potential in proteins. McDonald, I. K.; Thornton, J. M. *J. Mol. Biol.* **1994**, *238*, 777-93.

332. KFC Server: interactive forecasting of protein interaction hot spots. Darnell, S. J.; LeGault, L.; Mitchell, J. C. *Nucleic Acids Res.* **2008**, *36*, W265-9.

333. KFC2: a knowledge-based hot spot prediction method based on interface solvation, atomic density, and plasticity features. Zhu, X.; Mitchell, J. C. *Proteins* **2011**, *79*, 2671-83.

334. The accessible surface area and stability of oligomeric proteins. Miller, S.; Lesk, A. M.; Janin, J.; Chothia, C. *Nature* **1987**, *328*, 834-6.

335. The rapid generation of mutation data matrices from protein sequences. Jones, D. T.; Taylor, W. R.; Thornton, J. M. *Comput. Appl. Biosci.* **1992**, *8*, 275-82.

336. Hot spots--a review of the protein-protein interface determinant amino-acid residues. Moreira, I. S.; Fernandes, P. A.; Ramos, M. J. *Proteins* **2007**, *68*, 803-12.

337. RNase A ribonucleases and host defense: an evolving story. Rosenberg, H. F. *J. Leukoc. Biol.* **2008**, *83*, 1079-87.

338. Mechanism of ribonuclease A endocytosis: analogies to cell-penetrating peptides. Chao, T. Y.; Raines, R. T. *Biochemistry* **2011**, *50*, 8374-82.

339. Further studies on ribonuclease inhibitor. Roth, J. S. *Biochim. Biophys. Acta.* **1962**, *61*, 903-15.

340. Protein-protein interactions: general trends in the relationship between binding affinity and interfacial buried surface area. Chen, J.; Sawyer, N.; Regan, L. *Protein Sci.* **2013**, *22*, 510-5.

341. Analysis of the interactions of human ribonuclease inhibitor with angiogenin and ribonuclease A by mutagenesis: importance of inhibitor residues inside versus outside the C-terminal "Hot Spot". Shapiro, R.; Ruiz-Gutierrez, M.; Chen, C.-Z. *J. Mol. Biol.* **2000**, *302*, 497-519.

342. Protein co-evolution: how do we combine bioinformatics and experimental approaches? Sandler, I.; Abu-Qarn, M.; Aharoni, A. *Mol. Biosyst.* **2013**, *9*, 175-81.

343. An integrated view of molecular coevolution in protein-protein interactions. Lovell, S. C.; Robertson, D. L. *Mol. Biol. Evol.* **2010**, *27*, 2567-75.

344. The RNAse-RNAse inhibitor system in the liver of the frog Rana esculenta: subcellular distribution and differential binding of inhibitor with multiple RNAses. Malicka-Blaszkiewicz, M.; Kubicz, A. *Acta Physiol. Pol.* **1981**, *32*, 317-26.

345. Thiol-disulfide exchange of ribonuclease inhibitor bound to ribonuclease A. Ferreras, M.; Gavilanes, J. G.; Lopéz-Otín, C.; García-Segura, J. M. *J. Biol. Chem.* **1995**, *270*, 28570-8.

346. Shape complementarity at protein/protein interfaces. Lawrence, M. C.; Colman, P. M. *J. Mol. Biol.* **1993**, *234*, 946-50.

347. Tight-binding inhibition of angiogenin and ribonuclease A by placental ribonuclease inhibitor. Lee, F. S.; Shapiro, R.; Vallee, B. L. *Biochemistry* **1989**, *28*, 225-30.

348. Natural and engineered ribonucleases as potential cancer therapeutics. Arnold, U.; Ulbrich-Hofmann, R. *Biotechnol. Lett.* **2006**, *28*, 1615-22.

349. Characteristics of rat and guinea pig serum ribonuclease. Rabinovitch, M.; Dohi, S. R. *Arch. Biochem. Biophys.* **1957**, *70*, 239-47.

350. Purification and properties of alkaline ribonuclease from human serum. Akagi, K.; Murai, K.; Hirao, N.; Yamanaka, M. *Biochim. Biophys. Acta* **1976**, *442*, 368-78.

351. Purification and characterization of human brain ribonuclease inhibitor. Nadano, D.; Yasuda, T.; Takeshita, H.; Uchide, K.; Kishi, K. *Arch. Biochem. Biophys.* **1994**, *312*, 421-8.

352. Two distinct secretory ribonucleases from human cerebrum: Purification, characterization and relationships to other ribonucleases. Yasuda, T.; Nadano, D.; Takeshita, H.; Kishi, K. *Biochem. J.* **1993**, *296*, 617-25.

353. Changes in serum RNase activities in chronic phase and acute crisis of chronic myelocytic leukemia. Maruoka, K.; Yamanaka, M.; Misago, M.; Nakata, K.; Tsukada, J.; Nagata, K.; Sato, T.; Mori, N.; Oda, S.; Chiba, S.; et al. *Rinsho Ketsueki* **1989**, *30*, 988-93.

354. Ribonucleases and neoplasia. Daoust, R.; de Lamirande, G. *Subcell. Biochem.* **1975**, *4*, 185-211.

355. Changes in alkaline ribonuclease activity during compensatory renal growth. Rosso, P.; Diggs, J.; Winick, M. *Proc. Natl. Acad. Sci. U.S.A.* **1973**, *70*, 169-72.

356. Differential regulation of endothelial exocytosis of P-selectin and von Willebrand factor by protease-activated receptors and cAMP. Cleator, J. H.; Zhu, W. Q.; Vaughan, D. E.; Hamm, H. E. *Blood* **2006**, *107*, 2736-44.

357. Cancers as wounds that do not heal: differences and similarities between renal regeneration/repair and renal cell carcinoma. Riss, J.; Khanna, C.; Koo, S.; Chandramouli, G. V.; Yang, H. H.; Hu, Y.; Kleiner, D. E.; Rosenwald, A.; Schaefer, C. F.; Ben-Sasson, S. A.; Yang, L.; Powell, J.; Kane, D. W.; Star, R. A.; Aprelikova, O.; Bauer, K.; Vasselli, J. R.; Maranchie, J. K.; Kohn, K. W.; Buetow, K. H.; Linehan, W. M.; Weinstein, J. N.; Lee, M. P.; Klausner, R. D.; Barrett, J. C. *Cancer Res.* **2006**, *66*, 7216-24.

358. The role of extracellular RNA in atherosclerotic plaque formation in mice. Simsekyilmaz, S.; Cabrera-Fuentes, H. A.; Meiler, S.; Kostin, S.; Baumer, Y.; Liehn, E. A.; Weber, C.; Boisvert, W. A.; Preissner, K. T.; Zernecke, A. *Circulation* **2013**, *129*, 598-606.

359. Isolation of the murine ribonuclease gene Rib-1: structure and tissue specific expression in pancreas and parotid gland. Samuelson, L. C.; Wiebauer, K.; Howard, G.; Schmid, R. M.; Koeplin, D.; Meisler, M. H. *Nucleic Acids Res.* **1991**, *19*, 6935-41.

360. A highly efficient recombineering-based method for generating conditional knockout mutations. Liu, P.; Jenkins, N. A.; Copeland, N. G. *Genome Res.* **2003**, *13*, 476-84.

361. Potent inhibition of ribonuclease A by oligo(vinylsulfonic acid). Smith, B. D.; Soellner, M. B.; Raines, R. T. *J. Biol. Chem.* **2003**, *278*, 20934-8.

362. Mouse eosinophil-associated ribonucleases: a unique subfamily expressed during hematopoiesis. Cormier, S. A.; Larson, K. A.; Yuan, S.; Mitchell, T. L.; Lindenberger, K.; Carrigan, P.; Lee, N. A.; Lee, J. J. *Mamm. Genome* **2001**, *12*, 352-61.

363. Tissue-specific hemostasis in mice. Mackman, N. *Arterioscler. Thromb. Vasc. Biol.* **2005**, *25*, 2273-81.

364. The role of tissue factor pathway inhibitor in atherosclerosis and arterial thrombosis. Winckers, K.; ten Cate, H.; Hackeng, T. M. *Blood Rev.* **2013**, *27*, 119-32.

365. Biology of tissue factor pathway inhibitor. Wood, J. P.; Ellery, P. E.; Maroney, S. A.; Mast, A. E. *Blood* **2014**. Advance online publication. doi: 10.1182/blood-2013-11-512764

366. Targeting toll-like receptors: emerging therapeutics? Hennessy, E. J.; Parker, A. E.; O'Neill, L. A. *Nat. Rev. Drug Discov.* **2010**, *9*, 293-307.

367. Inflammatory mechanisms in obesity. Gregor, M. F.; Hotamisligil, G. S. *Annu. Rev. Immunol.* **2011**, *29*, 415-45.

368. Inflammation, obesity, and thrombosis. Samad, F.; Ruf, W. *Blood* **2013**, *122*, 3415-22.

369. Inflammation-sensitive plasma proteins are associated with future weight gain. Engstrom, G.; Hedblad, B.; Stavenow, L.; Lind, P.; Janzon, L.; Lindgarde, F. *Diabetes* **2003**, *52*, 2097-101.

370. Blood pressure increase and incidence of hypertension in relation to inflammation-sensitive plasma proteins. Engstrom, G.; Janzon, L.; Berglund, G.; Lind, P.; Stavenow, L.; Hedblad, B.; Lindgarde, F. *Arterioscler. Thromb. Vasc. Biol.* **2002**, *22*, 2054-8.

371. Effects of cholesterol and inflammation-sensitive plasma proteins on incidence of myocardial infarction and stroke in men. Engstrom, G.; Lind, P.; Hedblad, B.; Stavenow, L.; Janzon, L.; Lindgarde, F. *Circulation* **2002**, *105*, 2632-7.

372. Inflammation-sensitive proteins and erythrocyte aggregation in atherothrombosis. Assayag, E. B.; Bornstein, N.; Shapira, I.; Mardi, T.; Goldin, Y.; Tolshinski, T.; Vered, Y.; Zakuth, V.; Burke, M.; Berliner, S.; Bonet, D. S. *Int. J. Cardiol.* **2005**, *98*, 271-6.

373. Inflammation-sensitive plasma proteins, diabetes, and mortality and incidence of myocardial infarction and stroke: a population-based study. Engstrom, G.; Stavenow, L.; Hedblad, B.; Lind, P.; Eriksson, K. F.; Janzon, L.; Lindgarde, F. *Diabetes* **2003**, *52*, 442-7.

374. Risk of treatment of peripheral arterial disease is related to inflammation-sensitive plasma proteins: a prospective cohort study. Engstrom, G.; Site-Flondell, D.; Lindblad, B.; Janzon, L.; Lindgarde, F. *J. Vasc. Surg.* **2004**, *40*, 1101-5.

375. Coagulation and inflammation: molecular insights and diagnostic implications. Lipinski, S.; Bremer, L.; Lammers, T.; Thieme, F.; Schreiber, S.; Rosenstiel, P. *Hamostaseologie* **2011**, *31*, 94-102, 4.

376. Innate sensors of pathogen and stress: linking inflammation to obesity. Jin, C.; Flavell, R. A. *J. Allergy Clin. Immunol.* **2013**, *132*, 287-94.

377. The complexity, function and applications of RNA in circulation. Etheridge, A.; Gomes, C. P.; Pereira, R. W.; Galas, D.; Wang, K. *Front. Genet.* **2013**, *4*, 115.

378. The complex exogenous RNA spectra in human plasma: an interface with human gut biota? Wang, K.; Li, H.; Yuan, Y.; Etheridge, A.; Zhou, Y.; Huang, D.; Wilmes, P.; Galas, D. *PLoS One* **2012**, *7*, e51009.

379. Bimolecular fluorescence complementation (BiFC): a 5-year update and future perspectives. Kodama, Y.; Hu, C. D. *BioTechniques* **2012**, *53*, 285-98.

380. Improvement of a Venus-based bimolecular fluorescence complementation assay to visualize bFos-bJun interaction in living cells. Nakagawa, C.; Inahata, K.; Nishimura, S.; Sugimoto, K. *Biosci. Biotechnol. Biochem.* **2011**, *75*, 1399-401.

381. Protein tagging and detection with engineered self-assembling fragments of green fluorescent protein. Cabantous, S.; Terwilliger, T. C.; Waldo, G. S. *Nat. Biotechnol.* **2005**, *23*, 102-7.

382. Preparation of the membrane-permeant biarsenicals FlAsH-EDT2 and ReAsH-EDT2 for fluorescent labeling of tetracysteine-tagged proteins. Adams, S. R.; Tsien, R. Y. *Nat. Protoc.* **2008**, *3*, 1527-34.

383. Fluorescent labeling of tetracysteine-tagged proteins in intact cells. Hoffmann, C.; Gaietta, G.; Zurn, A.; Adams, S. R.; Terrillon, S.; Ellisman, M. H.; Tsien, R. Y.; Lohse, M. J. *Nat. Protoc.* **2010**, *5*, 1666-77.

384. Mammalian cell-based optimization of the biarsenical-binding tetracysteine motif for improved fluorescence and affinity. Martin, B. R.; Giepmans, B. N.; Adams, S. R.; Tsien, R. Y. *Nat. Biotechnol.* **2005**, *23*, 1308-14.

385. Arterial thrombus formation in cardiovascular disease. Lippi, G.; Franchini, M.; Targher, G. *Nat. Rev. Cardiol.* **2011**, *8*, 502-12.

386. Triggers, targets, and treatments for thrombosis. Mackman, N. *Nature* **2008**, *451*, 914-8.

387. Coagulation and innate immune responses: can we view them separately? Delvaeye, M.; Conway, E. M. *Blood* **2009**, *114*, 2367-74.

388. Overview of anticoagulant drugs for the future. Moll, S.; Roberts, H. R. *Semin. Hematol.* **2002**, *39*, 145-57.

389. Peptides selected for binding to clotted plasma accumulate in tumor stroma and wounds. Pilch, J.; Brown, D. M.; Komatsu, M.; Jarvinen, T. A.; Yang, M.; Peters, D.; Hoffman, R. M.; Ruoslahti, E. *Proc. Natl. Acad. Sci. U.S.A.* **2006**, *103*, 2800-4.

390. Targeting atherosclerosis by using modular, multifunctional micelles. Peters, D.; Kastantin, M.; Kotamraju, V. R.; Karmali, P. P.; Gujraty, K.; Tirrell, M.; Ruoslahti, E. *Proc. Natl. Acad. Sci. U.S.A.* **2009**, *106*, 9815-9.

391. Specific penetration and accumulation of a homing peptide within atherosclerotic plaques of apolipoprotein E-deficient mice. Hamzah, J.; Kotamraju, V. R.; Seo, J. W.; Agemy, L.; Fogal, V.; Mahakian, L. M.; Peters, D.; Roth, L.; Gagnon, M. K.; Ferrara, K. W.; Ruoslahti, E. *Proc. Natl. Acad. Sci. U.S.A.* **2011**, *108*, 7154-9.

392. Construction of thrombus-targeted microbubbles carrying tissue plasminogen activator and their in vitro thrombolysis efficacy: a primary research. Hua, X.; Liu, P.; Gao, Y. H.; Tan, K. B.; Zhou, L. N.; Liu, Z.; Li, X.; Zhou, S. W.; Gao, Y. J. *J. Thromb. Thrombolysis* **2010**, *30*, 29-35.

393. Effects of the ribonuclease inhibitor on the biological activity of pancreatic-type ribonucleases. Dickson, K. A. *Ph.D. Thesis, University of Wisconsin–Madison* **2006**.

394. Designing repeat proteins: modular leucine-rich repeat protein libraries based on the mammalian ribonuclease inhibitor family. Stumpp, M. T.; Forrer, P.; Binz, H. K.; Plückthun, A. *J. Mol. Biol.* **2003**, *332*, 471-87.

395. Evaluation of structural and evolutionary contributions to deleterious mutation prediction. Saunders, C. T.; Baker, D. *J. Mol. Biol.* **2002**, *322*, 891-901.

396. SIFT: predicting amino acid changes that affect protein function. Ng, P. C.; Henikoff, S. *Nucleic Acids Res.* **2003**, *31*, 3812-4.

397. Predicting the effects of coding non-synonymous variants on protein function using the SIFT algorithm. Kumar, P.; Henikoff, S.; Ng, P. C. *Nat. Protoc.* **2009**, *4*, 1073-81.

398. SIFT web server: predicting effects of amino acid substitutions on proteins. Sim, N. L.; Kumar, P.; Hu, J.; Henikoff, S.; Schneider, G.; Ng, P. C. *Nucleic Acids Res.* **2012**, *40*, W452-7.

399. RosettaDesign server for protein design. Liu, Y.; Kuhlman, B. *Nucleic Acids Res.* **2006**, *34*, W235-8.

400. Macromolecular modeling with Rosetta. Das, R.; Baker, D. *Annu. Rev. Biochem.* **2008**, *77*, 363-82.

401. Recent approaches to intracellular delivery of drugs and DNA and organelle targeting. Torchilin, V. P. *Annu. Rev. Biomed. Eng.* **2006**, *8*, 343-75.

402. Pathway for polyarginine entry into mammalian cells. Fuchs, S. M.; Raines, R. T. *Biochemistry* **2004**, *43*, 2438-44.

403. Boronate-mediated biologic delivery. Ellis, G. A.; Palte, M. J.; Raines, R. T. *J. Am. Chem. Soc.* **2012**, *134*, 3631-4.

404. Trimethyl lock: a trigger for molecular release in chemistry, biology, and pharmacology. Levine, M. N.; Raines, R. T. *Chem. Sci.* **2012**, *3*, 2412-20.

405. The green fluorescent protein. Tsien, R. Y. *Annu. Rev. Biochem.* **1998**, *67*, 509-44.

406. The fluorescent toolbox for assessing protein location and function. Giepmans, B. N.; Adams, S. R.; Ellisman, M. H.; Tsien, R. Y. *Science* **2006**, *312*, 217-24.

407. Arginine grafting to endow cell permeability. Fuchs, S. M.; Raines, R. T. *ACS Chem. Biol.* **2007**, *2*, 167-70.

408. Improved monomeric red, orange and yellow fluorescent proteins derived from Discosoma sp. red fluorescent protein. Shaner, N. C.; Campbell, R. E.; Steinbach, P. A.; Giepmans, B. N.; Palmer, A. E.; Tsien, R. Y. *Nat. Biotechnol.* **2004**, *22*, 1567-72.

409. Blue fluorescent proteins with enhanced brightness and photostability from a structurally targeted library. Mena, M. A.; Treynor, T. P.; Mayo, S. L.; Daugherty, P. S. *Nat. Biotechnol.* **2006**, *24*, 1569-71.

410. Use of the green fluorescent protein and its mutants in quantitative fluorescence microscopy. Patterson, G. H.; Knobel, S. M.; Sharif, W. D.; Kain, S. R.; Piston, D. W. *Biophys. J.* **1997**, *73*, 2782-90.

411. Effect of pH on thermal- and chemical-induced denaturation of GFP. Alkaabi, K. M.; Yafea, A.; Ashraf, S. S. *Appl. Biochem. Biotechnol.* **2005**, *126*, 149-56.

412. Improved green fluorescent protein by molecular evolution using DNA shuffling. Crameri, A.; Whitehorn, E. A.; Tate, E.; Stemmer, W. P. *Nat. Biotechnol.* **1996**, *14*, 315-9.

413. Rapid protein-folding assay using green fluorescent protein. Waldo, G. S.; Standish, B. M.; Berendzen, J.; Terwilliger, T. C. *Nat. Biotechnol.* **1999**, *17*, 691-5.

414. Engineering and characterization of a superfolder green fluorescent protein. Pedelacq, J. D.; Cabantous, S.; Tran, T.; Terwilliger, T. C.; Waldo, G. S. *Nat. Biotechnol.* **2006**, *24*, 79-88.